MECHANICS OF ROLLING CONTINUOUSLY CAST STOCK

PAUL JAMES GREENING

Submitted for the degree of

DOCTOR OF PHILOSOPHY

THE UNIVERSITY OF ASTON IN BIRMINGHAM

DEPARTMENT OF MECHANICAL AND PRODUCTION ENGINEERING

JULY 1987

THE UNIVERSITY OF ASTON IN BIRMINGHAM

MECHANICS OF ROLLING CONTINUOUSLY CAST STOCK

PAUL JAMES GREENING

PhD THESIS 1987

SUMMARY

A review of published literature was made to establish the fundamental aspects of rolling and allow an experimental programme to be planned. Simulated hot rolling tests, using pure lead as a model material, were performed on a laboratory mill to obtain data on load and torque when rolling square section stock. Billet metallurgy and consolidation of representative defects was studied when modelling the rolling of continuously cast square stock with a view to determining optimal reduction schedules that would result in a product having properties to the high level found in fully wrought billets manufactured from large ingots.

It is difficult to characterize sufficiently the complexity of the porous central region in a continuously cast billet for accurate modelling. However, holes drilled into a lead billet prior to rolling was found to be a good means of assessing central void consolidation in the laboratory.

A rolling schedule of 30% (1.429:1) per pass to a total of 60% (2.5:1) will give a homogeneous, fully recrystallized product. To achieve central consolidation, a total reduction of approximately 70% (3.333:1) is necessary. At the reduction necessary to achieve consolidation, full recrystallization is assured.

A theoretical analysis using a simplified variational principle with experimentally derived spread data has been developed for a homogeneous material. An upper bound analysis of a single, centrally situated void has been shown to give good predictions of void closure with reduction and the reduction required for void closure for initial void area fractions $\leq$ 0.45%.

A limited number of tests in the works has indicated compliance with the results for void closure obtained in the laboratory.

Key Words: Rolling
Continuously cast stock
Void consolidation
Recrystallization
Variational - Upper bound analysis

ACKNOWLEDGEMENTS

The author wishes to express his sincere thanks to his supervisor Mr L W Crane and his associate supervisor Dr K Baines. Mr Crane's help, guidance and patience in taking over the supervision of this project in mid-term is well appreciated.

I also wish to express my thanks to Professor D H Sansome for his help and guidance during the first half of this project.

Thank you also to Mr M C Gleave, Dr D Dulieu, Dr A P Hirst, and Mr P W Morris of the British Steel Corporation, Swinden Research Laboratories for their involvement and discussions throughout the project and for organizing the works' trials.

The author also wishes to thank:
The technical staff of The University of Aston, especially Mr D Farmer for his help with the casting of test billets.
The Department of Mechanical and Production Engineering of The University of Aston in Birmingham for the facilities provided.
The Science and Engineering Research Council and the British Steel Corporation for the financial support during the course of this project.

Finally, but by no means least, thanks Mum and Dad for your help and encouragement at all times.

CONTENTS

CHAPTER THREE

THE ANALYSIS OF THE ROLLING PROCESS

Page

CHAPTER FOUR

THEORETICAL ANALYSIS

CHAPTER FIVE

DESCRIPTION OF EXPERIMENTAL EQUIPMENT

CHAPTER SIX

MATERIAL TESTING

CHAPTER SEVEN

EXPERIMENTAL TEST PROGRAMME AND PROCEDURES

Page

Page

CHAPTER NINE

DISCUSSION OF RESULTS

CHAPTER TEN

CONCLUSIONS AND SUGGESTIONS FOR FUTURE WORK

APPENDICES

Page

Page

LIST OF FIGURES

CHAPTER SIX

CHAPTER SEVEN

CHAPTER EIGHT

APPENDIX J

LIST OF TABLES

CHAPTER TWO

CHAPTER SEVEN

CHAPTER ONE

INTRODUCTION

1.1. The Mechanical Working Of Metals.

Modern shaping processes can be divided into two distinct groups, hot working and cold working operations.

A hot working process is one which is carried out at a temperature above that of recrystallization for the workpiece. Deformation and recrystallization takes place at the same time so that the material remains malleable during the working process. Intermediate annealing processes are not required and thus working may take place quickly.

Cold work is applied to most products as a final stage in manufacture and as a means of obtaining the required material mechanical properties and surface quality. By varying the degree of cold work, the degree of hardness and strength can be controlled.

Some cold forming operations can only be carried out on metals and alloys, notably those involving drawing or pulling of the metal. Ductility is usually less at high temperatures due to a decrease in tensile strength, so the material may tear apart when hot worked. While malleability is increased by a rise in temperature, ductility is generally reduced. Hence, there are more cold working operations than there are hot working processes, because of the large number of different final shapes which are produced in metals of varying ductility.

Finally, cold working allows much greater accuracy of

dimensions to be obtained in the finished product.

1.2. Rolled Products.

Blooms and large slabs are the products of the primary rolling process to which an ingot is subjected. Their uses and sizes are given in the chart, Figure 1.1.

The function of the blooming (cogging) and slabbing mill is to produce blooms and slabs, for further rolling or forging, from the cast ingot. In some plants the cogging mill may produce billet sizes from smaller ingots.

The ingots may be square, rectangular or polygonal, the size and shape controlled not only by physical and economical considerations involving casting practice, mill size and product size, but also by metallurgical considerations.

A square ingot is frequently used for rolling to blooms while a rectangular ingot lends itself to the rolling of slabs. Polygonal ingots are frequently used for tube rolling.

1.3. Rolling Production.

Traditionally steel is cast into the form of large tapered ingots approximately 630 mm square, up to 3 meters in length and typically weighing several metric tonnes.

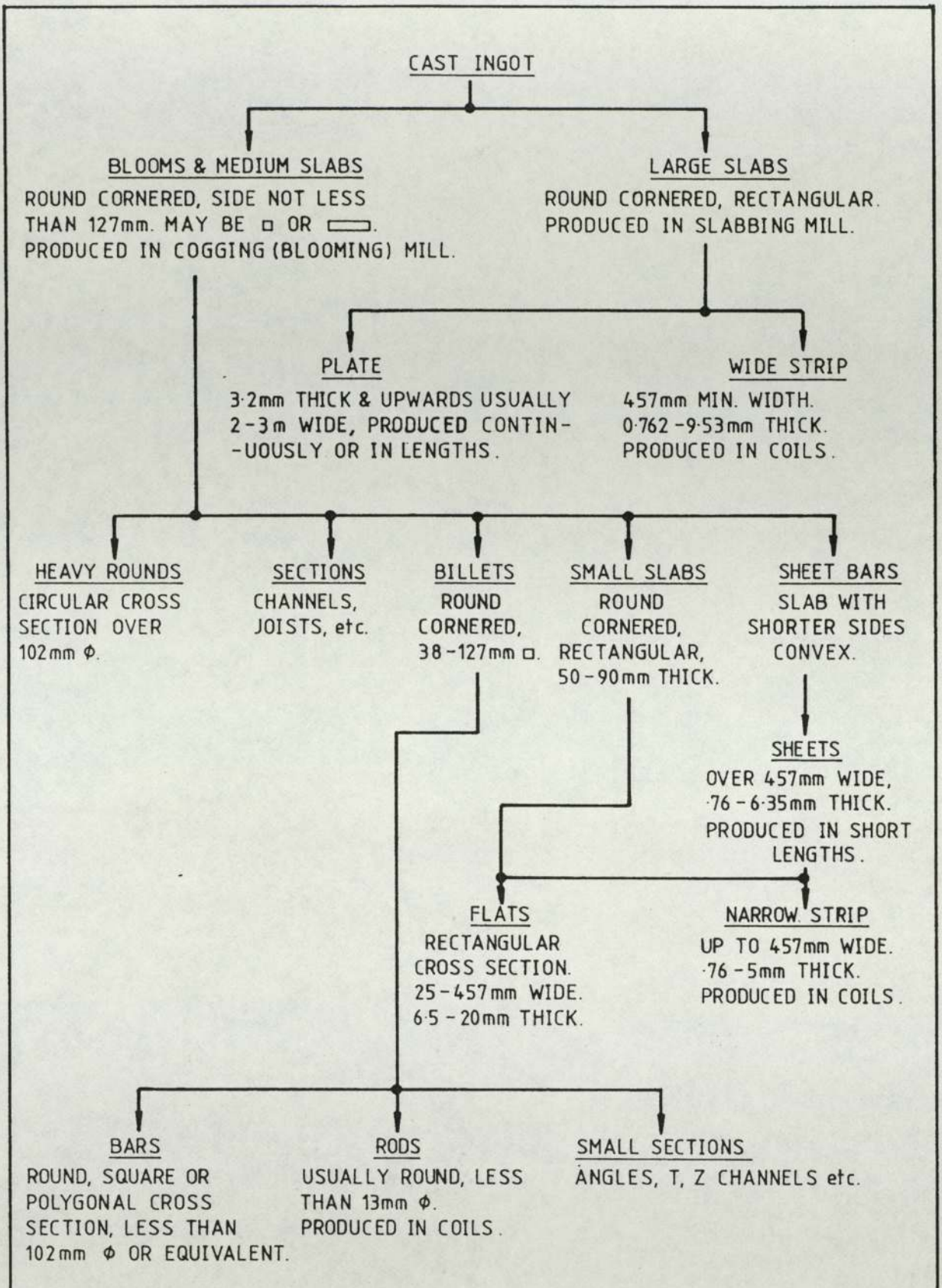

FIG. 1.1.

PRODUCTION CHART - ROLLED PRODUCTS.

(REF. 147)

These ingots are transferred from the casting plant to the primary rolling plant in a cold or semi-heated state and left to soak in a furnace for several hours at a temperature of the order of 1250 deg.C.

The length of the soak, determined by the ingot size and composition, ensures even heat distribution throughout the ingot section, ie. no temperature gradients. When ready, the ingot is transferred to the blooming or cogging mill for breakdown rolling.

The rolls used on the blooming mill are typically made up of two distinct sections, the bullhead pass and the box or hole passes which are machined into the roll barrel across its width.

The bullhead is that part of the roll barrel which is flat and plain and of a width greater than the stock to be rolled in it. Though it may have end collars they are not used to restrict the spread of the stock, so the bullhead gives parallel vertical draughting with unrestricted spread.

The general rolling technique is to break down the cast ingot in the bullhead pass with progressively increasing reductions, after which the stock is alternatively edged in a grooved pass and reduced in the bullhead until the required dimensions are reached. Alternatively, after breakdown and entering the grooved passes, the stock is not returned to the bullhead if sufficient grooves are available for completion

of the sequence.

A typical breakdown sequence is shown in Figure 1.2. for the rolling of a 533 mm tapered ingot down to a 203 mm square bloom.

Strip, produced from cast slabs in the slabbing hot mill, is often cold rolled as a subsequent operation to improve the surface finish and increase the accuracy of the gauge of the strip.

The hot strip is pickled, for example in hot hydrochloric acid, to remove the hard oxide scale before cold rolling. This is now increasingly performed on tandem mills, that is a three, four or five stand mill connected together in harmony. The stands are close together so that the strip is reduced in all the stands simultaneously.

In cold rolling, tension is applied to the strip between the stands and between the final coiler and the last stand. Strip tension reduces the rolling force and causes a redistribution of power from one stand to another because each stand provides the tension for the stands lying behind and ahead.

Tension applied so as to pull back on strip entering a stand is termed back tension while that applied to strip leaving a stand is termed front tension.

Cold rolling is normally undertaken on strip of

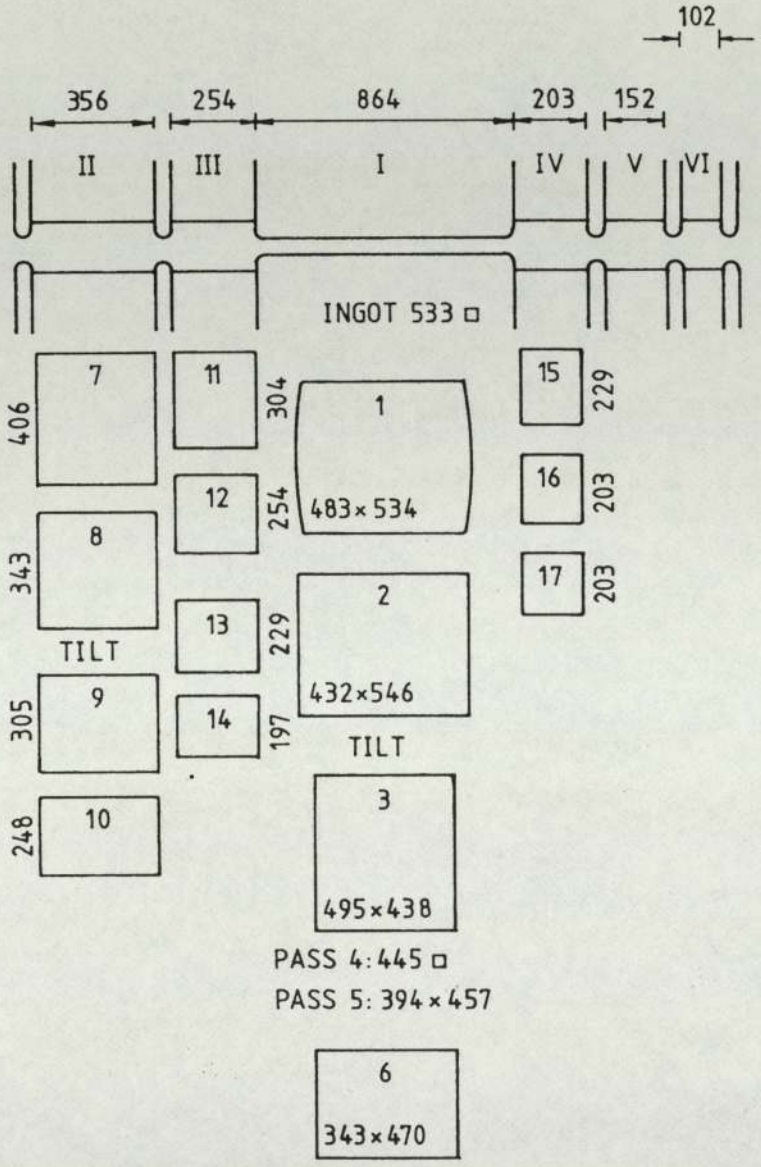

FIG. 1.2.

ADJUSTABLE TWO-HIGH BLOOMING ROLLS AND ROLLING SEQUENCE USING BULLHEAD PASS.

(REF. 147)

approximately 2.54 mm (0.10 in) thickness or less. Most common metals can be cold rolled down to 0.17 mm (0.007 in) economically and without difficulty while aluminium can be cold rolled to foil of 0.0254 mm (0.001 in) or even less.

Special precautions and sometimes special mills are used to roll harder metals to thicknesses less than 0.17 mm, for example intermediate annealing of the strip or use of cluster mills with small diameter work rolls.

Types of mill used in the rolling of foil are shown in Figure 1.3.

To roll very thin strip, small diameter rolls are necessary, and, if the material is of a large width, the work rolls must be supported by back-up rolls. If this is not done, they may bend to such an extent that accurate reduction in thickness of a very thin material becomes impossible. For rolling thicker strip, ordinary two-high mills are generally used.

The production of a mirror finish metal foil necessitates the use of rolls with a highly polished surface. Only by working in perfectly clean surroundings can high-grade foil be produced.

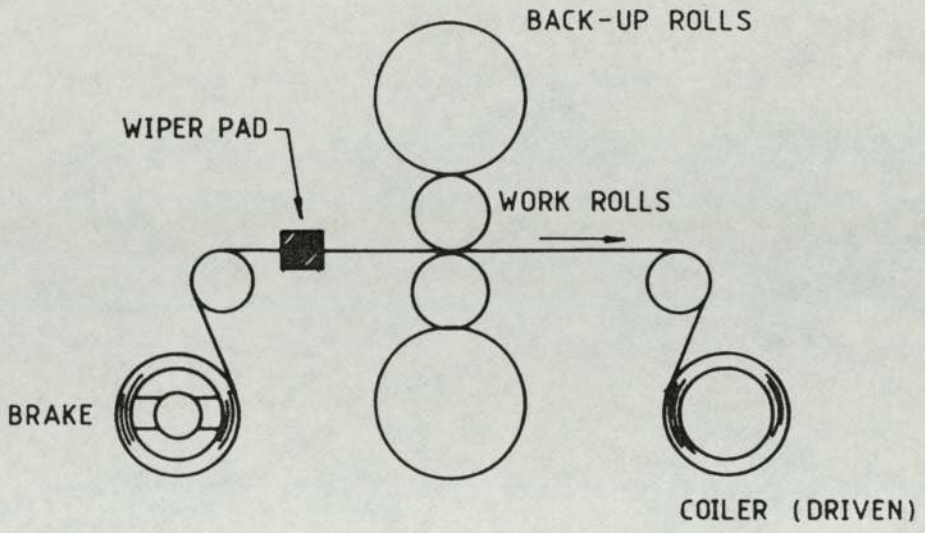

a. FOUR-HIGH MILL.

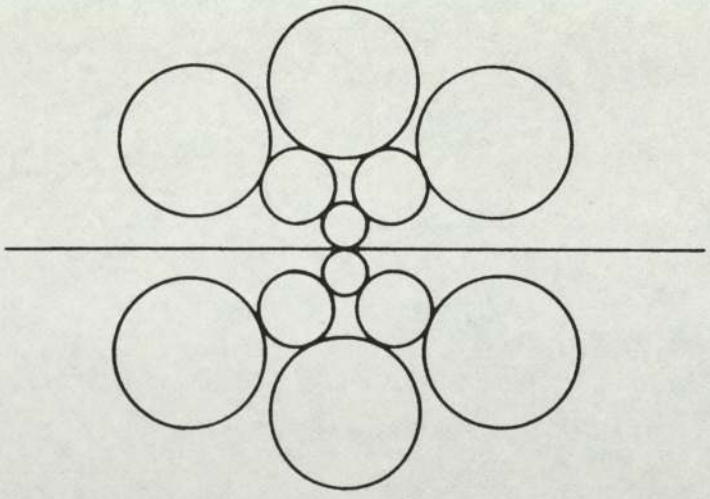

b. CLUSTER MILL.

FIG. 1.3.

ROLL ARRANGEMENT FOR PRODUCTION OF THIN METAL FOIL.

1.4. Project Outline.

Poor metallurgical quality can be exhibited in hot rolled products in a number of forms, some of which are associated with the structural inhomogeneity introduced at the casting stage, for example segregation and central porosity, and some of which are associated with subsequent processing, for example surface spread.

In general, a statically cast ingot, typically several metric tonnes in weight, has sufficient deformation work carried out on it to ensure a homogeneous, fully wrought product. This has been the traditional process route for rolled products since the last century.

Over the past twenty to thirty years, interest has focused on an alternative production route for rolled products, namely continuous casting.

The savings in plant, operational costs and energy in casting a bar close to its required finish dimensions are attractive, provided that subsequent working produces a fully wrought structure.

The function of the deformation process in this case is to do the minimum work necessary to achieve the required mechanical and metallurgical properties consonant with dimensional accuracy.

This research project, carried out in conjunction with

British Steel Research Laboratories, Swinden House, Rotherham studies the deformation of square section continuously cast stock.

By use of a model material in the laboratory and steel in the hot mill at British Steel, the effect of various rolling schedules on material metallurgy and inherent defects are assessed in terms of grain refinement and closure of representative defects.

In addition, a theoretical analysis of the rolling of square stock is made using an upper bound type approach in order to predict material behaviour and rolling parameters for effective working.

CHAPTER TWO

THE DEVELOPMENT OF THE CONTINUOUS CASTING PROCESS

2.1. The Development of the Continuous Casting Process.

2.1.1. Historical Developments.

Thirty five years after the development of his steel making process, Henry Bessemer (1) described a method of handling liquid steel which was in principle similar to the modern day process of continuous casting.

Referring to Figure 2.1, liquid steel was poured from a ladel into a tundish from which it flowed between two water cooled rotating rolls acting as a mould. The gap between the rolls was adjustable allowing a casting variation in slab thickness. The steel thus formed was allowed to settle on a support table and cut to length.

The economic implications were clear to Bessemer, the production of slabs and ingots being commercially viable. The idea was certainly ahead of its time.

Forty years or so passed before active process development was initiated and seventy before any significant plant installation and production of any special steels in quantity.

The cost advantages of the process were immediately apparent, the main obstacle to its implementation being the control of the casting conditions at the liquid metal/mould interface to prevent breakout of the liquid core. This was achieved in the early 1930's with the development of a

FIG. 2.1. ILLUSTRATING BESSEMER'S METHOD OF CONTINUOUS CASTING.

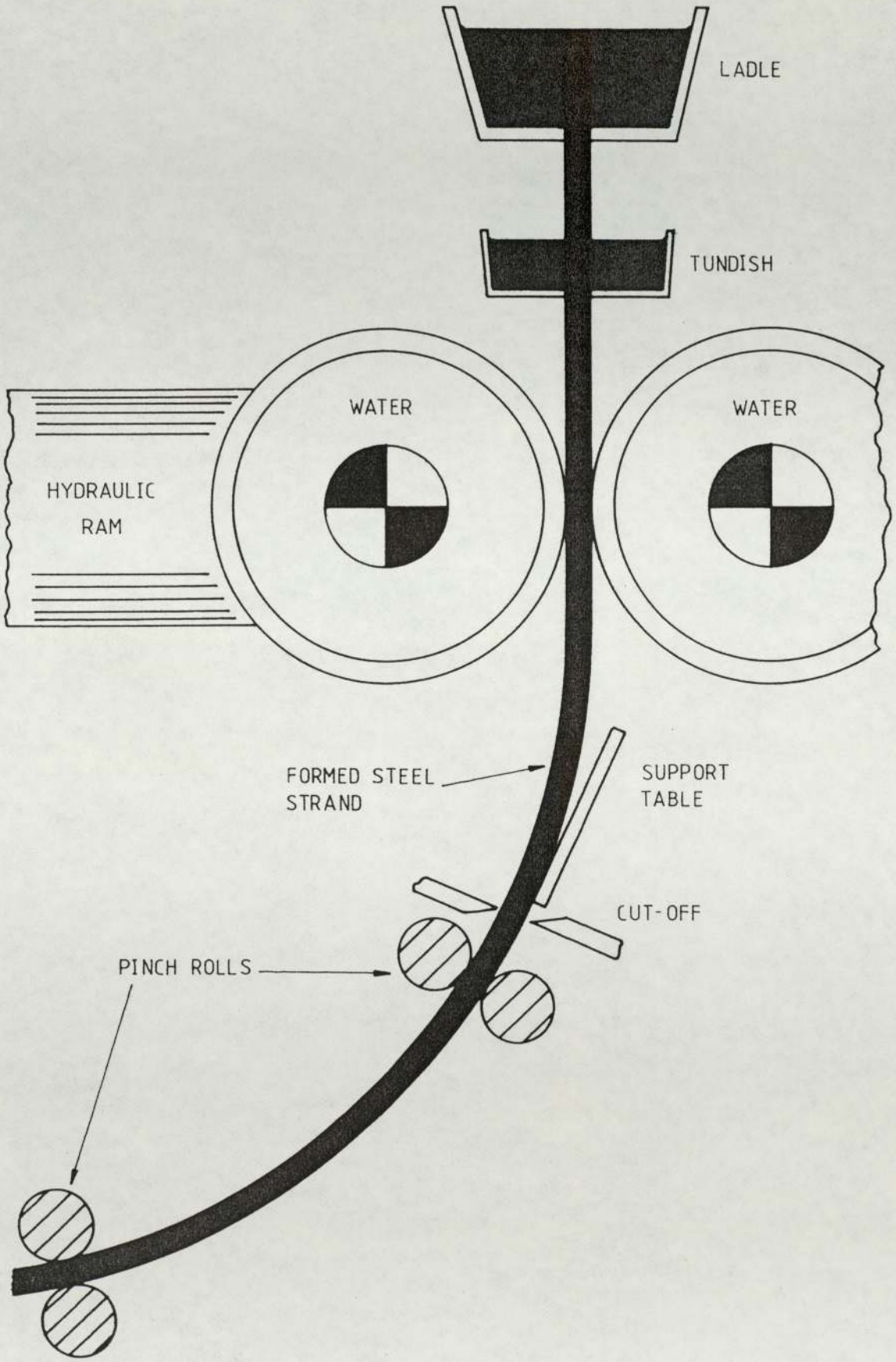

reciprocating enclosed water-cooled mould.

During World War II trials were made by the Ministry of Defence and in the 1950's development continued, particularly in Europe.

In 1952 a twin strand continuous caster was erected at Bohler Bros. & Co. Ltd, Kapfenberg and soon afterwards at the Ironworks Breitenfeld GmbH, Wartberg, both in Austria. Breitenfeld was the first steelworks to commit its entire production to the continuous casting process.

Also in 1952 the continuous casting machine at The United Steel Companies works at Barrow in the UK went on stream where the possibility of high casting speeds for the casting of small sections was soon proven.

A number of years later, Halliday (2) demonstrated that in practice, the bending of continuously cast strands into a horizontal position prior to cutting could be done, leading to the development of the vertical bending machine.

The first high performance plant was commissioned in 1958 at Terni, Societe par l'industria e elettricita in Italy. This eight strand plant was served by heats of seventy tons and proved that the distribution of liquid steel into eight strands was possible with adequate through-put and that large heats would maintain temperature over a prolonged period of casting.

In 1960, S.A.F.A. (Societe des aciers fins de l'est), Hargondange in France commissioned a four strand billet caster for production of steel specifically for use in the automotive industry. With a monthly production of 13000 tonnes of five and eight inch squares, it was shown that high quality steel could be made from continuously cast heats.

Up to this point in the history of the continuous casting process, plant had been designed to operate in a vertical mode.

In 1963 a new type of machine which featured a curved mould was used at the Von Moorsschen Ironworks at Luzerne in Switzerland. However, problems with maintenance, adjustment and additional metallurgical problems such as reduced heat transfer, impaired skin growth and accumulation of impurities at the inner skin radius led to a new direction of development.

A bow type casting machine featuring a straight mould was commissioned in 1964 at Bohler Bros. & Co. Ltd, Kapfenberg, Austria. The strand was cast vertically but bent into a bowed arc starting about 2.03 metres below the mould, its core still being liquid.

Figure 2.2. shows this type of plant installed at the Indiana Harbour Works in the USA for the casting of 178 mm squares.

The first high production application of the bow type

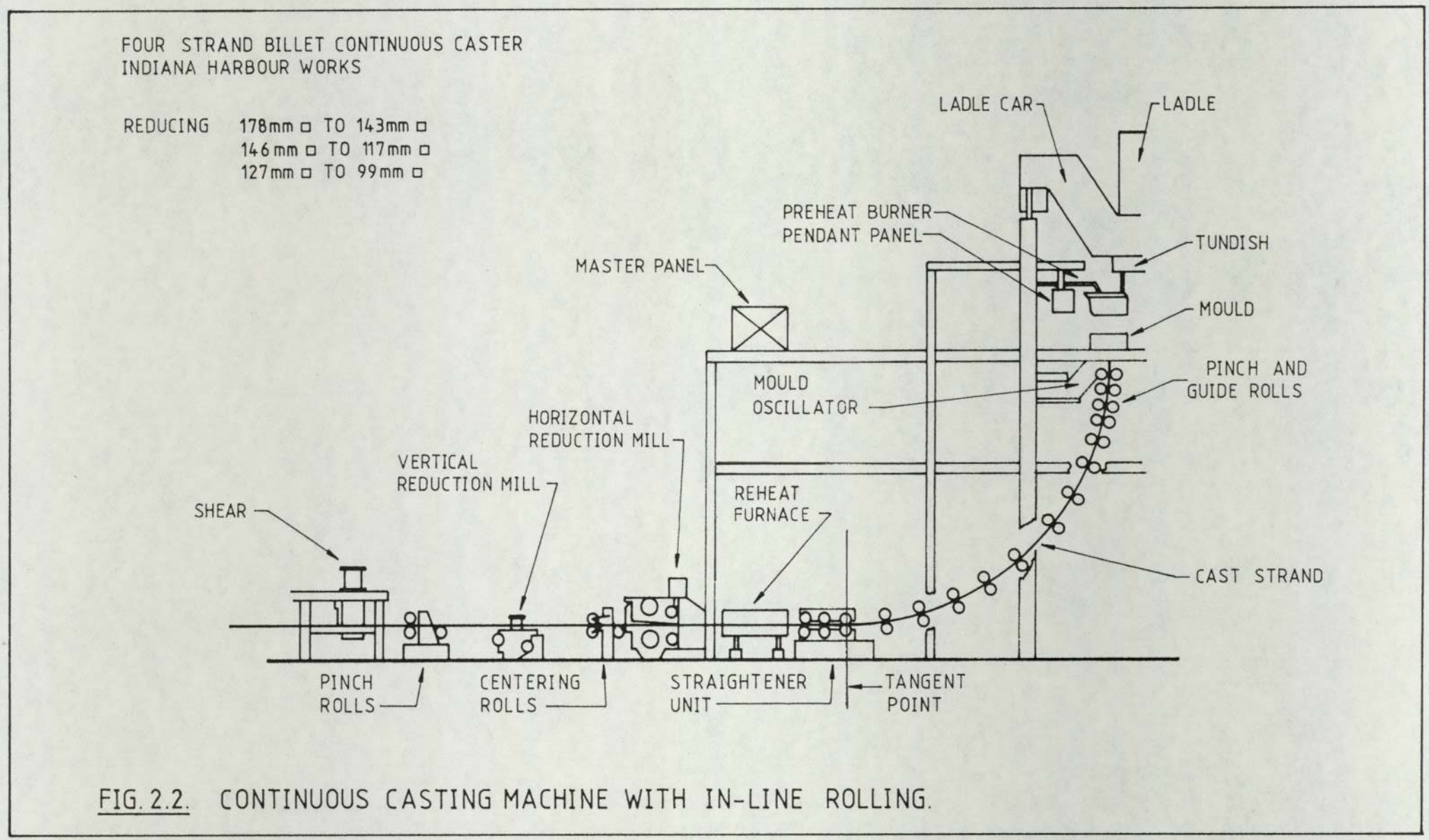

FIG. 2.2. CONTINUOUS CASTING MACHINE WITH IN-LINE ROLLING.

plant was initiated in 1965 when the six strand casting machine at Armco Steel Corp, Sand Springs, Texas, USA was installed and was followed by a large number of billet casters throughout the world.

By the end of 1974 the following continuous casting capacity was on stream:

290 Billet casters with 820 strands.
110 Bloom casters with 400 strands.
130 Slab casters with 200 strands.

In the last decade there has been a steady growth in the percentage of steel produced by the continuous casting process.

Continuous casting as a new technology grew as a result of it having a number of financial and technological advantages over the traditional ingot route of steel production and its future growth will depend on a combination of the following factors:

a. Fewer processing steps.
b. Reduced investment costs.
c. Reduced manning and labour costs.
d. Reduced energy consumption and related costs.
e. Improved yield and improved quality in certain products.

Table 2.1. shows the production of continuously cast steel as a percentage of total steel production in a number

of countries.

Country	Total Crude Steel			Of Which Con-Cast			Con-Cast As % Of Total		
	1970	1980	1984	1970	1980	1984	1970	1980	1984
Japan	93.3	111.4	105.6	5.3	66.3	94.1	5.7	59.5	89.1
W.Germany	45.0	43.8	39.4	3.7	20.2	30.3	8.2	46.1	76.9
Italy	17.3	26.5	24.0	0.7	13.2	17.6	4.0	49.8	73.3
France	23.8	23.2	19.0	0.2	9.6	12.7	0.8	41.4	66.8
S.Korea	0.5	8.6	13.0	*	2.8	7.9	*	32.4	60.8
U.K.	28.3	11.3	15.2	0.5	3.1	7.9	1.8	27.4	52.0
Spain	7.4	12.6	13.5	0.9	4.6	6.6	12.2	36.5	48.9
Belgium	12.6	12.3	11.3	*	3.2	5.6	*	26.0	49.6
Canada	11.1	15.9	14.7	1.3	4.7	5.6	11.7	29.6	38.1
Brazil	5.4	15.3	18.4	0.04	5.1	7.6	0.8	33.3	41.7
U.S.A.	119.3	101.5	84.5	4.5	20.6	33.3	3.8	20.3	39.4
Romania	6.5	13.2	13.8	*	2.4	4.0	*	18.1	29.8
Poland	11.8	19.5	16.3	0.3	0.8	1.5	2.5	4.1	9.2
India	6.3	9.5	10.5	*	0.3	0.4	*	3.2	3.8

[x Million Tons]

Table 2.1. Production of continuously cast steel by selected countries.

Source: Steel Times, July 1985.

It is interesting to note the figures for the USA where there was heavy investment in rolling plant in the mid-1960's. The proportion of continuously cast steel is low but is expected to rise moderately. The cost of replacing an existing ingot production plant is the primary factor controlling the growth of continuous casting rather than any limitations in technology.

Improvements in existing continuous casting plant design and operation have been the use of larger tundishes, shrouding of the liquid steel stream, top loading of dummy

bars, increased casting speed, development of mould powders, variable width moulds, electromagnetic stirring, automatic pouring control, cooling spray control and automatic control of the cut-off shears.

A detailed description of these improvements is not necessary here but of interest is a brief summary of electromagnetic stirring as this has a significant effect on the solidification of continuously cast steels.

Electromagnetic stirring can be used to influence the steel within the mould or to influence the solidified cast below the mould after primary solidification, when the core of the strand is still liquid.

Applied within the mould it is possible to achieve very clean surface conditions in the cast product and applied to the strand in the latter stages of solidification it is possible to influence segregation, structure and central porosity.

Recently the trend has been towards the design and installation of simpler continuous casting machines and the 'Rokop' design of billet caster, by use of a special solid dummy bar, eliminates the need for roll supports immediately below the mould giving freedom for arrangement of the cooling sprays in the spray chamber, Figure 2.3.

Further developments in reducing plant size have been made by Hitachi (3) who introduced a belt-wheel caster having

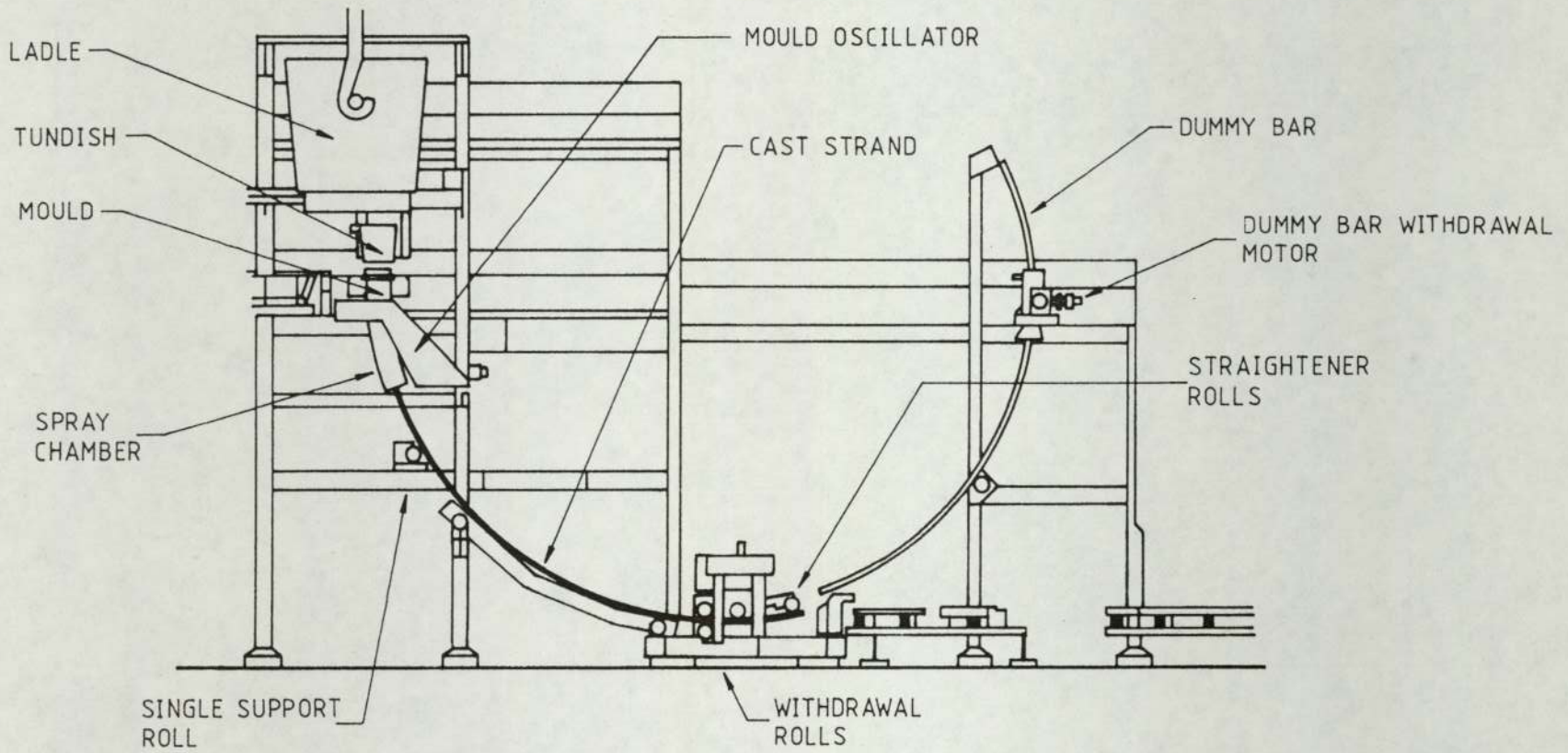

FIG. 2.3. 'ROKOP' DESIGN BILLET CONTINUOUS CASTING MACHINE.

double the cast rate per strand of a conventional billet caster. The facility was designed to operate at a casting speed of 3.05 to 7 metres per minute with a casting rate of thirty to sixty tonnes per hour per strand for the production of 130 mm squares. Figure 2.4. illustrates the basic design of this type of machine.

Other machines for the production of continuously cast stock are the rotary caster of the Vallourec design for seamless products and the Hazlett process with its ability to cast thin sections at very high speed. These developments all have the aim of increasing casting speed, reducing plant size and lowering costs.

Horizontal continuous casting is the ultimate in the search for plant size reduction. The General Motors (USA) horizontal caster operated for most of the 1970's at the Lansing, Michigan plant, turning out billet to be forged into connecting rods, but was shut down in 1980 due to the recession in the motor industry.

The general mode of operation of the horizontal caster is shown in Figure 2.5.

Since the metal is flowing horizontally, there can be no gap between the tundish and the mould, and so it is more difficult to have the mould oscillation which prevents sticking as in the conventional vertical continuous casting machine.

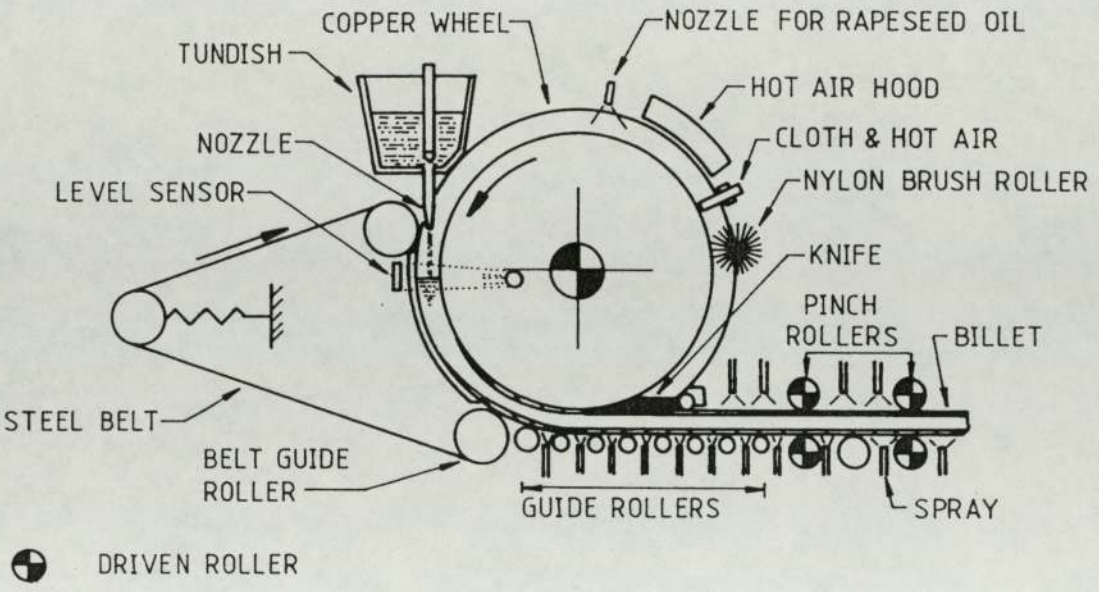

FIG. 2.4. BELT-WHEEL TYPE BILLET CON-CASTER.

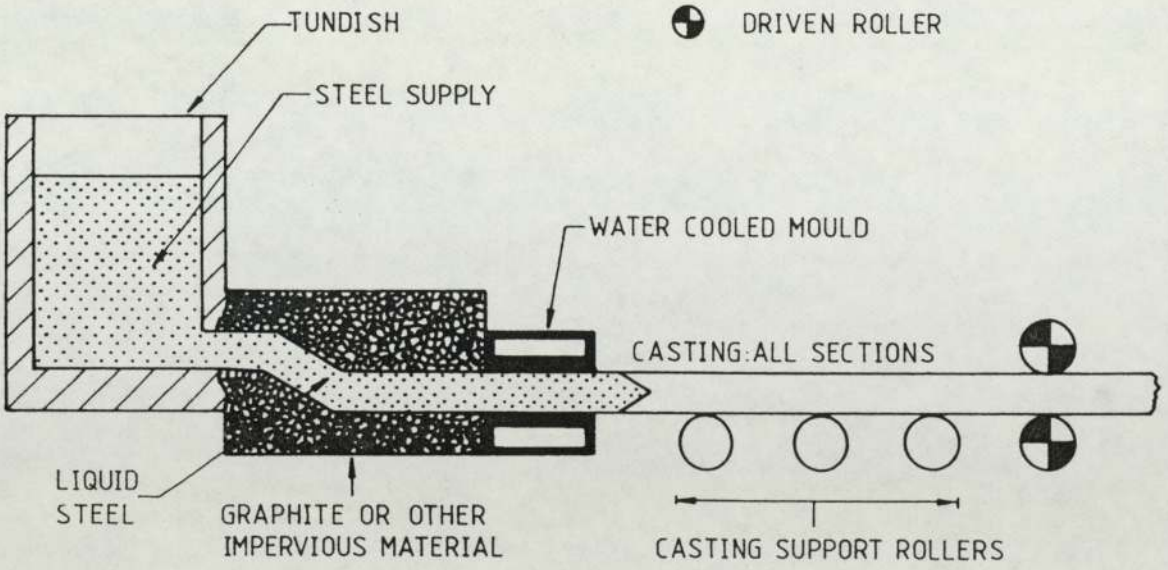

FIG. 2.5. OUTLINE OF HORIZONTAL CONTINUOUS CASTING MACHINE.

As a substitute for mould oscillation some operational plant has the cast billet travel intermittently. The billet is pulled steadily for an interval then stopped, for example, a withdrawal pattern of 30 cycles a minute (0.5 seconds pull and 1.5 seconds stop).

2.1.2. Summary.

Continuous casting of steel is now firmly established as a major production route. Initial doubts as to the process reliability and apprehension on the part of the end user in using steel that had been continuously cast for engineering products and applications have now been quashed.

Future trends in machine design and operating practice will be concerned mainly with the improvement of product quality, machine flexibility, increasing through-put and decreasing machine down time.

Developments downstream of the casting machine (outlined in Section 2.3) enabling a wide range of products to be produced from a limited range of cast section size will also be important. In general, worldwide commercial pressures are coinciding with technical development which favours the continued growth of continuous casting leading to increased productivity and greater competition in the world market for steel products.

2.2. Quality of Continuously Cast Steel.

2.2.1. Introduction.

The metallurgical aspects of statically cast and continuously cast steel products is well documented.
It is not intended to detail extensively the metallurgical features, however a resumé of the major features found in cast products is included here as a necessary part of the introduction to continuous casting.

The reader is advised to consult the literature, for example publications by The Metals Society (4),(5) for more detailed information on this topic.

The quality of steel produced by continuous casting, as compared to static ingot casting, is a function of the defects present in the cast structure and the change in the size and distribution of these defects with subsequent hot working.

Due to the mechanism of solidification, statically cast top poured ingots tend to exhibit coarse dendritic structures in the centre with macrosegregation and porosity confined to the upper third of the solidifying ingot.

Continuously cast steel, which solidifies more rapidly than static ingot castings, exhibits a finer dendritic structure with less macrosegregation. Normally, with a static ingot, the structure is refined and rendered more

homogeneous by subsequent hot working. Since statically cast ingots are originally large in size, the hot working operation is successful because of the large degree of reduction required to obtain a product section size. However, a continuously cast billet, having a smaller cast cross section, is subjected to less hot working to obtain the same product size.

Some of the major metallurgical characteristics of a continuously cast billet are outlined here.

2.2.2. Cast Structure.

For a continuously cast billet, heat is extracted rapidly over a short distance and time with a tendancy to strong columnar growth towards the billet centre becoming less directional and infilled with equiaxial growth to a degree depending on the teeming conditions, particularly the degree of superheat.

The degree of central porosity is relatively low in the case of a continuously cast billet since there is always hot metal available from above at a steady temperature to feed the central region where the 'pipe' may form. This feed is of fresh not solute enriched liquid metal.

Unlike statically cast ingots where the porosity is confined to the upper part of the ingot (top poured), porosity may appear at points along the whole length of a

continuously cast billet. No opportunity exists for major segregation of the type in which equi-axed crystals settle from subsequently solute-enriched liquid and take with them primary deoxidation products. Where there is strong columnar growth there is the tendancy for bridging similar to that found in big-end-down ingots when feed metal can no longer penetrate the shrinkage below and when separations in porosity develop down the billet axis.

In order to avoid this bridging and thus minimize shrinkage or central porosity, a minimum superheat giving a maximum equi-axial growth is desired. This is achieved by control of the tundish temperature and the casting speed.

Figure 2.6. shows a transverse section of a typical continuously cast billet, an SAE 8620 steel of the following composition:

0.18-0.23% C	0.70-0.90% Mn	0.20-0.35% Si
0.40-0.70% Ni	0.40-0.60% Cr	0.15-0.55% Mo
0.04% P (max)	0.04% S (max)	

Three distinct zones are clearly visible, the outer zone of chill crystals (small equi-axed), the dendritic zone and the central equi-axed zone. Note also the inclination of the dendrites due to the swirl pattern induced by the electromagnetic stirring and the white band at the equi-axed/dendritic interface.

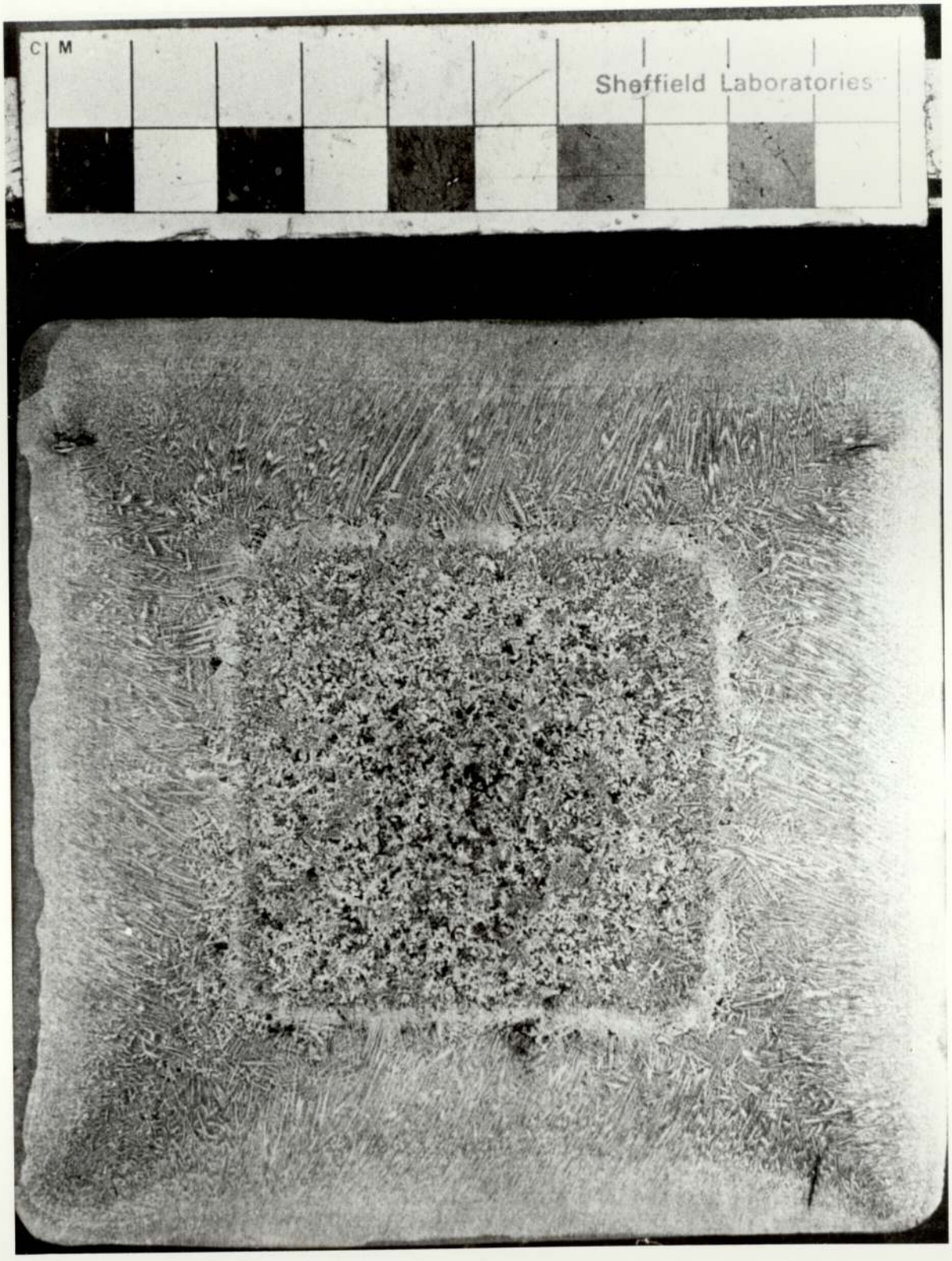

FIG. 2.6.

TRANSVERSE SECTION OF SAE 8620 CONTINUOUSLY CAST STEEL BILLET.

It has been postulated that formation of the white band depends upon the material flow pattern during solidification. The white band, a negative segregation line, is located in the last millimetres of the dendritic zone. Sulphide levels have been measured to be up to 20% lower here than in the remainder of the structure. The likely interpretation is that a local macrosegregation effect is caused by the difference in velocity between the solidification front just starting and the solidification front just ending which appears when the dendrites are eroded away.

White band formation can be suppressed by selecting optimised electromagnetic stirring parameters, Figure 2.7. See also Lipton (6) and Alberny et al (7).

2.2.3. Segregation.

It is generally accepted that segregation in continuously cast products is both lower and more uniform than in statically cast ingots. Work on segregation in slabs has confirmed the view that superheat and strand stability, particularly in the region of total solidification, are the main factors influencing segregation and central unsoundness (porosity).

The essential issue of macrosegregation is concerned with what occurs at the advancing solidification front. The nature of the segregation depends on three factors:

a. LONGITUDINAL CROSS SECTION THROUGH SOLIDIFIED SLAB WITH NON-OPTIMISED E.M.S.

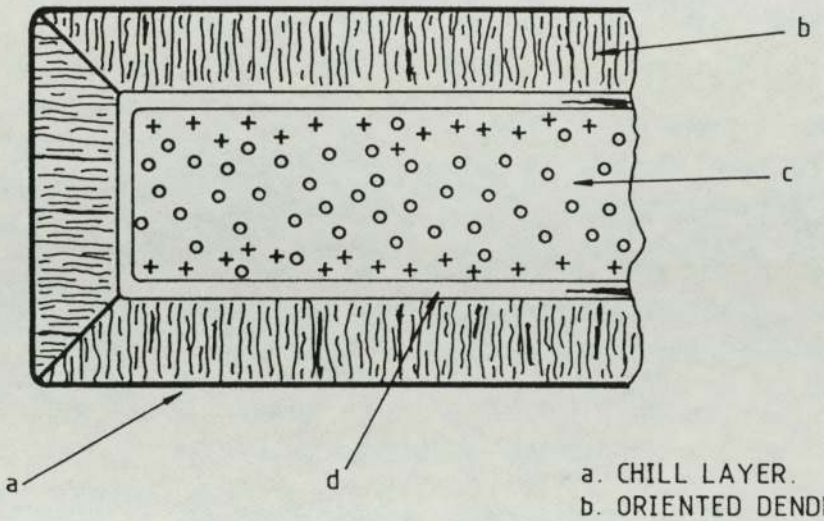

a. CHILL LAYER.
b. ORIENTED DENDRITIC SOLIDIFICATION.
c. UNORIENTED EQUI-AXED SOLIDIFICATION.
d. WHITE BAND.

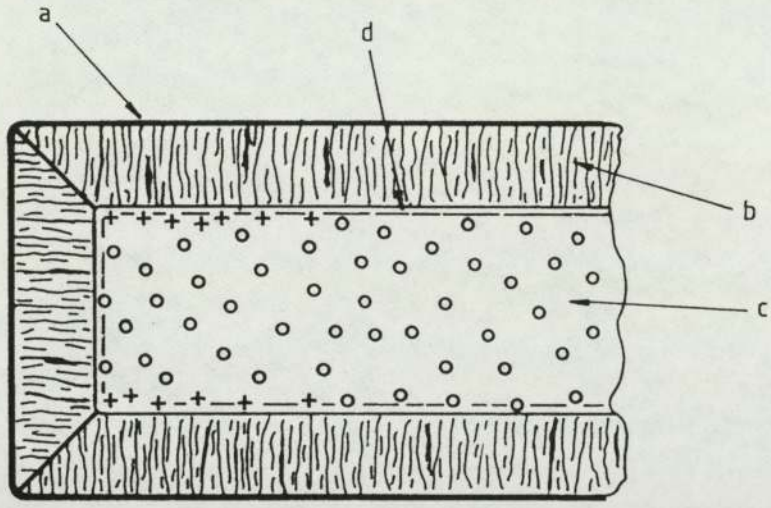

b. LONGITUDINAL CROSS SECTION THROUGH SOLIDIFIED SLAB WITH OPTIMISED E.M.S.

FIG. 2.7.

SCHEMATIC EFFECT OF ELECTRO-MAGNETIC--STIRRING ON WHITE BAND FORMATION.

a. The rate of advance of the front.

b. The temperature gradient at the front.

c. The degree of mixing which occurs in the liquid steel ahead of the front.

These factors influence crystal growth at the solidification front and generate a structure that may be equi-axed, trapping small volumes of rejected solute leading to microsegregation when low temperature gradients exist ahead of the solidification front. The low temperature gradient can be caused by low superheat and poor mixing.

When a high temperature gradient exists ahead of the solidification front, a columnar structure develops. This allows solute to be continually rejected and so macrosegregation results. The rate of solidification of the front is determined by the thermal diffusivity of the solidified shell.

A simulation model by Perkins and Irving (8) of the continuous casting process has shown the influence of process variables such as secondary water cooling and casting rate to increase only moderately, by approximately 10%, the rate of solidification. However these variables have an appreciable indirect effect on central unsoundness by affecting the resistance of the solidified shell to bulging forces exerted by the ferrostatic pressure of the liquid core.

When bulging occurs, the shell may be deformed by the

strand support rolls. This may interfere with the crystal structure at the solidification front and allow excess solute to be rejected, promoting macrosegregation.

2.2.4. Non-Metallic Inclusions.

The metallurgical quality of the cast product is largely dependant on the amount and distribution of non-metallic inclusions.

For a continuously cast billet, the increased soldification rate, similar throughout the whole length of a billet, can lead to advantages in producing a more consistent and finer grained structure than that found in statically cast ingots.

The stream of steel entering the mould causes a turbulence and an upward flow which rises near the solidification front. Particles of slag introduced with the metal stream or formed endogeneously by turbulence, rise and are precipitated from the molten metal. If particles during their rise approach the solidification front too closely, they may be retained by the solid shell. This process depends upon the depth of the turbulence and on the irregularity of the solid shell.

Casting with an open jet (open stream teeming) causes heavy turbulence and entrapment of air leading to oxidation. The jet will also force slag into the molten

metal. Air bubbles with oxide particles will be forced against the mould walls and will form macro-inclusions in the shell. Conversely, the rising air bubbles will decrease the depth of penetration of the turbulence.

With immersed casting nozzles (submerged nozzles) or controlled inert atmospheres around the metal stream, air entrapment is avoided and the surface of the liquid steel in the mould can be protected from oxidation by a casting powder. The use of submerged nozzles provide a cast product with much better internal quality than that found in open stream teemed products.

2.2.5. Segregation Cracks.

Segregation cracks pass through sulphides normally located along grain boundaries (open segregation cracks) and usually weld over with deformation work, the inclusions remaining in elongated form.

They occur when strands which are still liquid inside are exposed to tensile stresses in the region of the soldification front. In such cases, the very weak, just solidified structure (dendritic) in the region of the solidification front cracks, and the liquid metal enriched with segregating elements ahead of the front then flows into the resulting cracks.

Depending on the type of stresses originally involved,

segregation cracks may be subdivided into:

2.2.5.1. Bending Cracks.

These may occur on the tension side of the strand during the bending or straightening phase when the strand core is still liquid. This may, for example, occur in bow type continuous casting machines using a straight mould at a position below the mould when straightening the strand.

In bow type plants with curved moulds, these cracks may occur during straightening in the region adjacent to the curve to the horizontal bend point. Bending cracks run perpendicular to the direction of the strand and are visible on longitudinal etched samples or in sulphur prints.

These bending cracks may be avoided by using curved moulds or, when using straight moulds, by having a large bend radius, straightening the strand when in the fully solidified condition.

2.2.5.2. Cooling Stress Cracks.

Occur as a result of non-uniform and/or too abrupt cooling in the primary and/or secondary cooling sections and may occur either close to the surface of the strand or in the core zone. These cracks run preferentially in the direction of the strand axis.

Cooling stress cracks may be avoided by uniform, well

distributed primary and secondary cooling. The quantity of coolant must be modified to suit the quality of the steel and the casting temperature should be kept as low as possible.

2.2.5.3. Compression Cracks.

May occur when a strand which has not fully solidified undergoes deformation with reduction of the strand cross section. This may occur unintentionally if the guide or pinch roll setting is too tight or if there is still a liquid zone at the time of deformation. In this case the cracks will run from the solidification front perpendicular to the strand axis.

Even after complete solidification, cracks may also be caused in the strand core by over tight (pinch) rolls. These are termed pressure cracks. Since, when these occur there is no liquid phase left, pressure cracks are open and not occupied by segregations.

2.2.5.4. Halfway Cracks.

These are intercolumnar cracks occuring in positions approximately midway between the outer and the center of the cast product.

They are caused by thermal stresses attributable to severe or uneven secondary cooling during solidification.

A comprehensive description of the definition and causes of continuous casting defects are given in a publication by The British Iron and Steel Research Association, BISRA (9).

2.2.6. Summary.

The optimum microstructure of a continuously cast product is one of homogeneous equi-axed grains with the minimum of directional interconnected central unsoundness (porosity) and a minimum content of non-metallic inclusions, uniformly distributed and of small particle size.

The full length of a product will not conform to these specifications exactly and so there will be loss of yield from the as-cast material to the wrought product as a consequence of end cropping, surface preparation and rejection in the mill, all due to billet metallurgy.

2.3. Deformation of Continuously Cast Stock.

2.3.1. Introduction.

Since economic operation of continuous casting plant is based on high yield and savings in re-heat and rolling costs, in-line reduction was originally introduced to early continuous casting plant.

The strand being cast would be worked by rolls situated a short distance from the mould, giving a product to accurate

dimensions and possessing good mechanical and metallurgical properties.

In 1964, Bohler Bros. & Co. Ltd at Kapfenberg in Austria began a development programme on in-line reduction of cast steel strands.

Two variants of the method were applied to strand reduction:

2.3.2. Reduction with Liquid Core.

It was postulated that closure of the tip of the liquid core prior to complete solidification, Figure 2.8(a), would produce a sound billet without segregation and porosity in the central zone. The considerable work carried out in regard to this problem determined that reduction with a liquid core actually produced a significantly inferior product. Large internal cracks were formed around the liquid core with no improvement in centre segregation or porosity.

For this reason, the reduction equipment was moved down-line, this being the second variant of the method:

2.3.3. Reduction After Complete Solidification.

Reduction was effected immediately after complete solidification to close voids in the core caused by shrinkage during solidification and to reduce the cross section, Figure 2.8(b). Although the surface temperature

a. REDUCTION WITH LIQUID CORE.

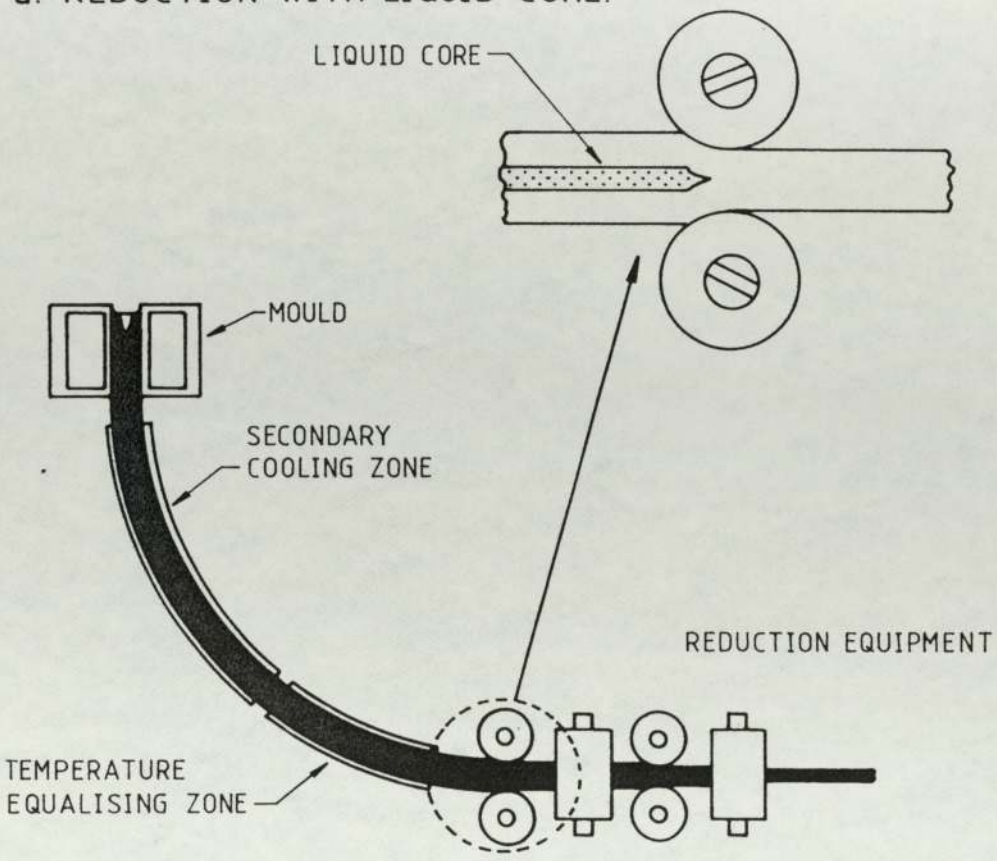

b. REDUCTION AFTER COMPLETE SOLIDIFICATION.

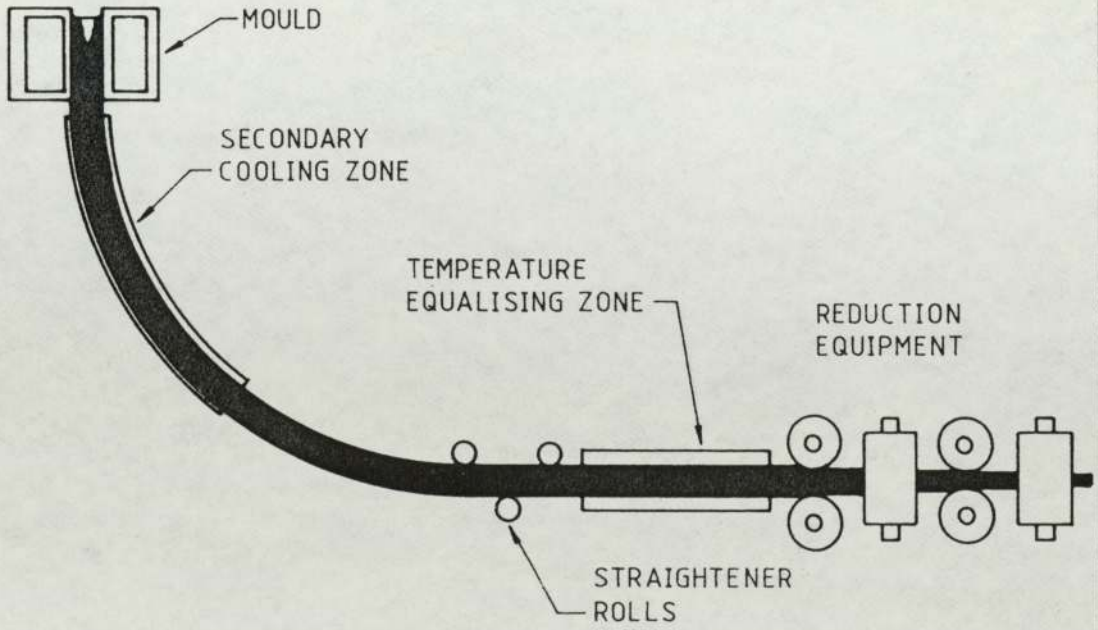

FIG. 2.8. TYPES OF IN-LINE REDUCTION.

was rendered as uniform as possible by a temperature equilization zone, the strand centre was still close to the solidus temperature, that is, within the range of inferior hot workability. Further work on in-line reduction on both sides of the Atlantic, for example by Diehl et al (10), showed in-line reduction to offer no metallurgical advantage over off-line reduction.

Reduction with a liquid core produced a significantly inferior structure and large internal cracks were formed around the liquid core with no improvement in central segregation or porosity.

In-line reduction failed to improve quality and could in fact produce a significant deterioration.

2.3.4. Summary.

At the beginning of continuous casting development it was thought that products and sections could be cast directly without the need for subsequent hot working operations. This was soon proved to be fundamentally incorrect.

Attempts at incorporating in-line reduction plant as a means of producing a product smaller than the as-cast strand at nominal capital expenditure, resulted in added operational complexity and significant production loss. Other shortcomings of in-line reduction were the additional

constraints put on steel making practice and deterioration in surface quality compared to the as-cast strand surface. These penalties determined that other alternatives be considered, one being off-line reduction.

An off-line rolling mill can partially realise the energy savings of in-line reduction but still retain flexibility of product size. In addition, off-line rolling can significantly reduce the aforementioned shortcomings of in-line reduction.

2.4. Conditions for Effective Working.

2.4.1. Objectives and Previous Studies.

The objectives of a hot working process is to weld-up the porosity and shrinkage cavities formed as a consequence of the solidification process and to refine the cast structure over the whole cross section, so that the quality level and required mechanical properties are achieved in the product.

The effect of hot working, be it rolling or forging, on material structure has been extensively studied for statically cast ingots, concentrating on establishing the minimum reduction ratio required to ensure a metallurgically sound and mechanically strong product.

The amount of reduction required has been quoted by

numerous authors in the range 4:1 to 10:1 (75% to 90% reduction in area).

Gorecki (11) related the generation of internal cracks in blooms, ingots and slabs to geometrical factors. His criteria showed that rolling would proceed more efficiently if the ratio of stock height to roll diameter was less than 0.5 ($h1/D < 0.5$). Likewise, the larger the draught the better the condition of the product from the standpoint of freedom from internal cracks expressed by the ratio $h1/L \leq 2$. These criteria were derived empirically on the basis of deciding from works trials the rolling geometries for which unsoundness was not apparent after rolling.

In conclusion, Gorecki deduced that the occurence of internal cracks in stock during rolling was attributable to tearing stresses in the centre layers. He stated that to overcome cracking, heavy draughts should be employed in the initial passes of a rolling schedule and large diameter rolls should be used on not too large ingots that had been sufficiently soaked.

Further experimental work has led to doubts being raised as to Gorecki's results.

Vater (12), without quoting values of reduction, determined that steel of poor workability, with a roll pass sequence of square to oval and employing essentially high reductions per pass, could be rolled free of cracks as

opposed to a pass sequence of square to diamond, all other conditions being equal. A pass sequence of square to trapezoid to square appeared, on the basis of experiment, to be more beneficial with respect to crack-free rolling of steels of poor workability.

Tagawa et al (13) have published results of trials to study the effect of rolling conditions on the elimination of micro-porosities in large steel ingots.

It was found that the perpendicular compressive stress at the centre of a slab during rolling was more important than the effective strains in the elimination of the said defects. In order to increase the compressive stress during rolling the ratio of stock height to roll diameter should be low and the draught taken should be large, suggestions along the same lines as Gorecki.

In cases of rolling not complying to these conditions, if the roll speed and hence strain rate was reduced and the billet centre temperature kept high in relation to the surface temperature, then the elimination of micro-porosities could be effected. The effect of a reduction of 2.7 was shown to be favourable.

Tarmann (14) in an early project looking at continuous cast steels, reported that in-line reduction should proceed to the very centre of a billet. If this was not so then it was possible for tensile stresses in the core region, in

conjunction with the high core temperature, to result in bursting of strands. On the production machine at Bohler Bros. & Co. Ltd, a minimum reduction of 1.25:1 (20% in area) was found to be necessary. As a rule of thumb it was stated that reductions in excess of 1.25:1, preferably of the order of 1.33:1 (25% reduction in area), should be used for the in-line reduction of carbon and alloy steels.

Baumann et al (15),(16) made use of temperature gradients through continuously cast steel billets in order to increase the deformation at the central zone.

When rolling continuously cast billets with a hot inner core and relatively cooler outer layers, the more rigid outer layers give an effect similar to that obtained from an increase in the roll diameter. For a given reduction in cross section, little deformation occurs in the hard outer layers. The core receives preferential deformation so that even relatively small degrees of overall reduction can close-up the solidification cavities and porosity. Industrial tests revealed that a reduction of 1.35:1 gave a sound billet.

Some tests were performed with 8 mm diameter holes drilled along the billet longitudinal axis, in the direction of rolling, at the billet centre and also at the corner region of one billet. The holes were subject to atmosphere during reheating and as such scaled-up. After a 1.52:1 reduction it was found that the centre hole had closed but

the corner hole was still visible.

In conclusion it was stated that 3:1 to 4:1 reductions would weld-up segregation cracks, the segregations remaining in elongated form. Continuous casting with in-line reduction had apparently no adverse effects on the internal quality of the cast product.

Ushijima (17) reported that reduction ratios in the range 6:1 to 10:1 were required to achieve a fully wrought billet when rolling. He also quoted other workers with conflicting results:

Pierce (18) observed the breakdown of the primary crystal structure at 4:1, Kosmider et al (19) at 1.7:1 and diminishing of blow hole occurrence at 3.5:1.

Hofmaier (20) deduced that the reduction ratio should be of the order of 6:1 to 10:1 for billets and 4:1 to 5:1 for plates rolled from slabs.

At 5.5:1 primary crystals diminished and carbide segregations remained, wrote Water et al (21) and Halliday (2) determined columnar crystal breakdown at a 4.8:1 reduction ratio.

Fenton et al (22),(23) quoted general figures of 2:1 up to 6.7:1, Littlewood & Pritchard (24) quoted 9:1 to obtain superior mechanical properties and Cabane (25) determined reduction ratios of 6:1 for carbon and low alloy steels, 8:1

for stainless and 10:1 for tool steels.

Instead of normal flat rolling, Takehara et al (26) produced twin billets from one larger continuously cast billet; two 75 mm squares from one 120 mm square cast billet, rolled in one pass on an in-line reduction facility.

The billets formed in this mill, Figure 2.9(a), were further reduced as shown in the sequence diagram, Figure 2.9(b), by forging or hot rolling.

When the cast billet was rolled into a twin, the centre part of the initial cast billet became the joint area of the twin, as shown in Figure 2.9(c). Blow holes and other defects were squashed but a band of segregation was still present in the joint area, extending into the interior of the two billets.

The joint area exhibited a unique pattern of microstructure which was destroyed as the rolling reduction was raised in the following passes, but was still visible at a reduction of 4.5:1. For reductions in excess of 4.5:1 the difference in structure was negligible resulting in an almost homogeneous structure for low and medium carbon steels.

Saigi et al (27) found shrinkage cavities and porosity to be well sealed by in-line reduction, non-metallic inclusions being elongated in the direction of rolling throughout the billet thickness. The difference between the

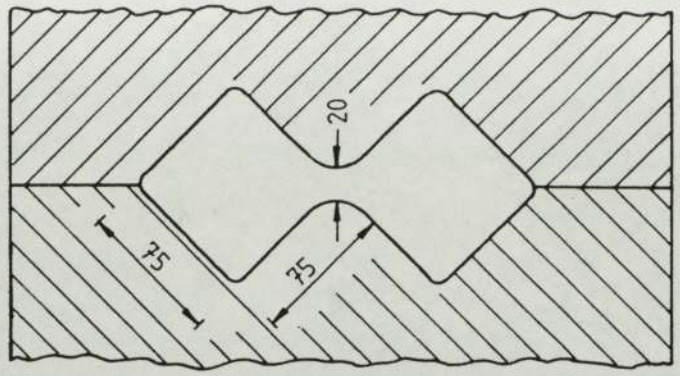

a. SCHEMATIC CROSS SECTION OF REDUCTION ROLLS.

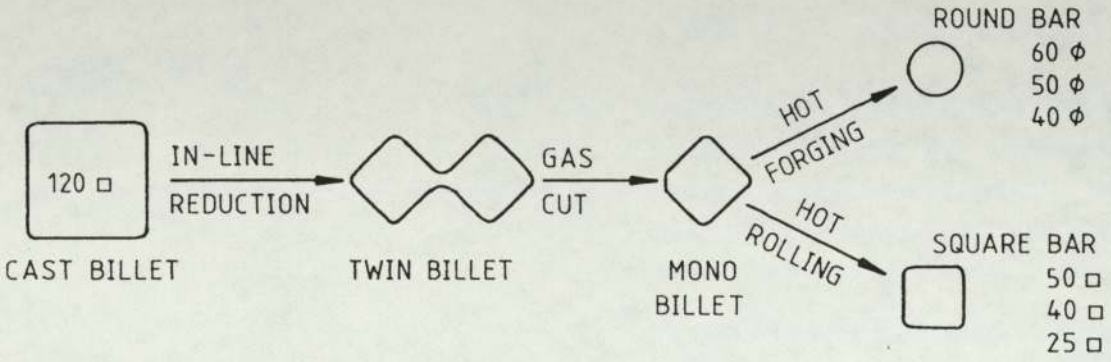

b. BILLET PRODUCTION ROUTES. DIMENSIONS IN mm.

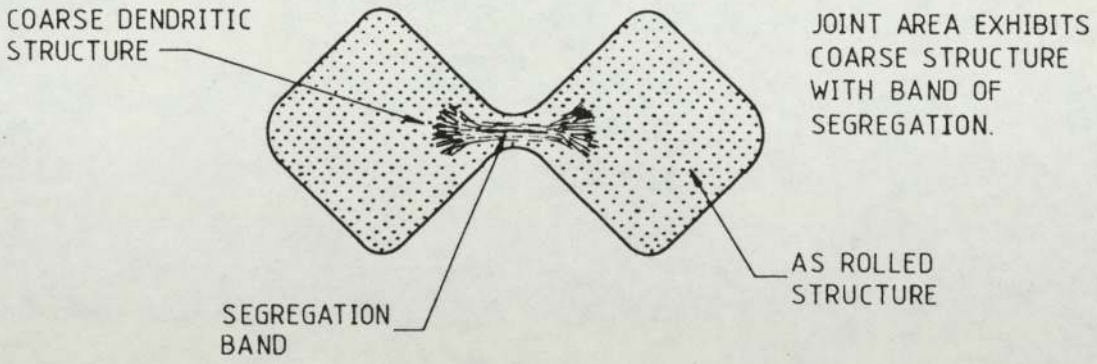

c. SCHEMATIC MACROSTRUCTURE OF TWIN BILLET.

FIG.2.9 TWIN BILLET PRODUCTION (FROM REF. 26).

outer and inner zones with respect to tensile properties was observed to be negligible when rolling 140 mm squares in two passes to 105 mm square, a reduction of 1.78:1. Of interest was the use of inclusion measurement to describe the effectiveness of reduction.

They found that a reduction of only 1.8:1 effected a reduction ratio of 3 at the billet centre on the inclusions present, the reduction ratio in this case being the ratio of inclusion shape index after reduction to inclusion shape index before reduction.

A study of the effect of a temperature gradient across a billet section during reduction was made by Evteev and Listopad (28) in order to assess the effect on axial 'looseness' and the distribution of height deformation with the combination of continuous casting and rolling. They made an effort to evaluate the minimum required reduction to effectively deal with the axial zone. Using pin inserts positioned at points in the billet height, an empirical formula and nomogram were suggested for the calculation of minimum reduction in continuously cast billets.

Hawbolt et al (29) performed trials on continuously cast billets and bars to examine the effect of hot rolling on casting defects, directing their attention primarily to half-way cracks as a representative defect.

They found open defects still present after a 4:1

reduction and laboratory rolling trials showed that a 6:1 reduction was required to close centre-line defects.

Kumazawa and Sato (30) have investigated hot grooved rolling for the elimination of continuous casting defects by analysing grain refinement and microstructure and also by measurement of yield strength, elongation and impact transition temperature.

The complicated deformation mechanism was found to give good results with respect to the material metallurgical and mechanical properties when coupled with finish rolling after air cooling and reheating following on from the grooved roll pass.

Hojas (31) has described a method of hot forming, the continuous forging machine, able to apply large reductions in a single pass.

The GFM, Steyr, Austria, continuous forging machine could effect a reduction of 4:1 in one pass and as a result of trials with continuously cast billets of various sections found that a reduction of 3:1 was sufficient to remove all unsoundness, such as pores or shrinkage cavities. Accordingly the cast structure was refined to a close grained structure.

The following advantages of the forging high reduction unit was claimed by Hojas:

a. Reduced capital outlay and plant size.

b. Large amounts of deformation transferred to the central region of the worked piece with even small total reductions. Reduction ratios of between 3:1 and 3.5:1 would suffice to produce a sound semi-finished product from a continuously cast billet. Hence it is possible to produce a semi-finished product of appreciably larger dimensions than would be possible from an 8:1 reduction ratio by conventional rolling, the amount required for high quality rolled product.

c. Flexibility to a high degree. The machine can produce round or square semi-finished products.

Further, Hojas and Garrett (32) wrote that pipes or shrinkage porosity in continuously cast billets were closed in the continuous forging machine with a reduction of 2.2:1 but, since the reduction was still low, the grain size on a transverse cross-section of the billet still appeared to be uneven.

With a reduction of 3.5:1, absolute core density as well as an even fine grained structure was obtained. The authors stated that such high reduction forming in one pass was comparable to a rolled structure after an 8:1 to 10:1 reduction.

Figure 2.10. compares the forging and rolling processes in terms of an 'effective pressure cone'. For rolling the

DIMENSIONS IN mm

a. CONTINUOUS FORGING.

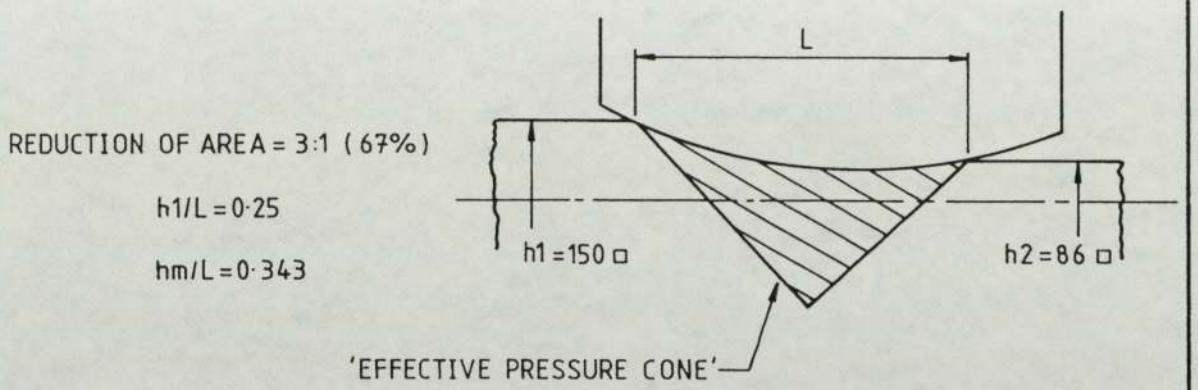

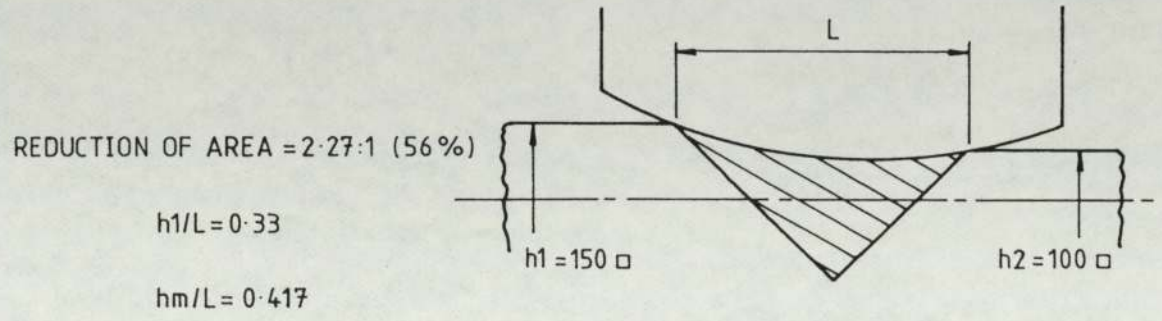

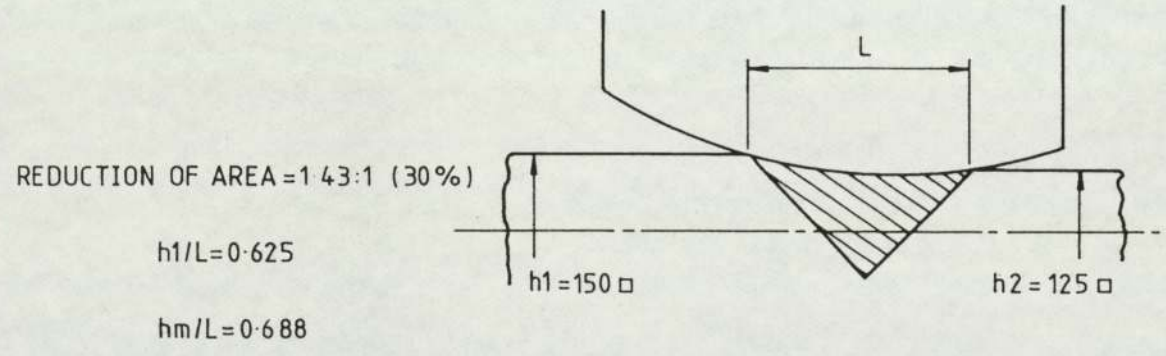

b. ROLLING.

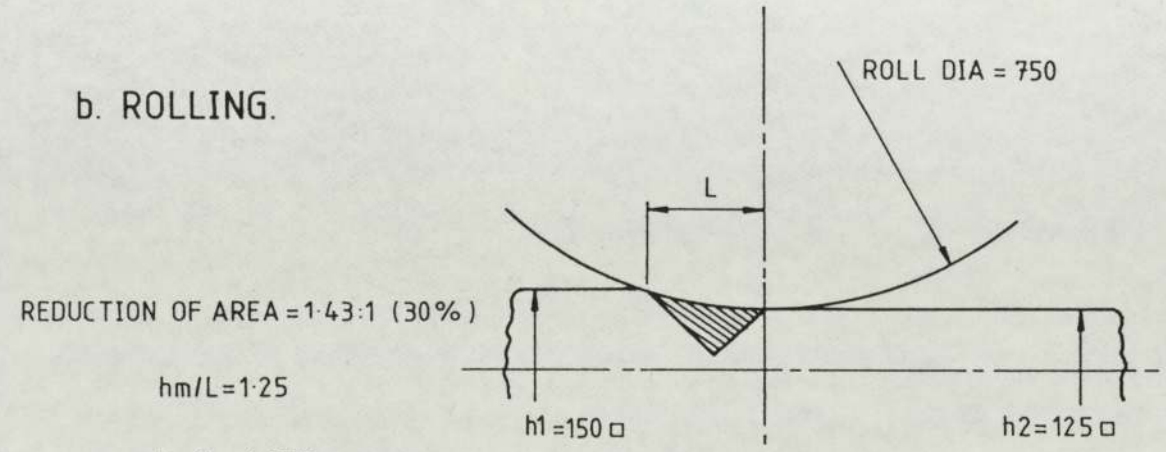

FIG. 2.10. COMPARISON OF FORMING OPERATIONS. (FROM REF. 32)

maximum attainable reduction is limited by the gripping characteristics of the rolls. The forging tool can be used over its entire length because of the constant entry angle.

A direct calculation of this centre-forming is the relationship between the roll contact length, L and the dimension of the existing bar, h2. For rolling, the L/h2 ratio with a reduction of 30% would be 0.8. For the forging tool, with the same reduction, this ratio would be 1.6. For the reduction ratio of 3:1, the L/h2 ratio is 4, five times larger than the maximum value achieved by rolling in one pass. This forging-rolling process has gained popularity in Europe, for example, but has not fully convinced the metal working industry here due to doubts as to its true method of operation and deformation mechanism.

2.4.2. Summary.

The amount of time devoted to the study of the effect of hot working on continuously cast stock is moderate in relation to the problem and further, there are substantial differences in the conclusions drawn from the results obtained by various workers in this field.

Generally, two areas of study have been mounted,

a. To obtain values of reduction and rolling geometry needed to ensure effective working and,
b. To determine alternative process routes to basic rolling

and/or forging.

For the first case, (a), the range of successful processing parameters quoted is extensive, due primarily to the various methods used by the authors to assess effective working. Levels of reduction in the range 2:1 to 10:1 (50% to 90% reduction in cross section area) are quoted. This large difference is substantial implying another three or four passes in a rolling schedule and subsequent plant, energy and direct costs.

For the second case, (b), workers have attempted, with measured success, to develop methods of working whereby the region containing the majority of defects present in continuously cast stock are worked in preference to the remainder of the billet cross section.

Continuous forging, box-pass sequence rolling, split billet rolling and the use of temperature gradients in the stock have all produced results of note.

CHAPTER THREE

THE ANALYSIS OF THE ROLLING PROCESS

3.1. Early Theories.

Over the years the analysis of the rolling process has been tackled by numerous theorists with varying degrees of success and accuracy. Both hot and cold rolling have been extensively covered but there are still certain areas where fundamental knowledge is distinctly lacking. Because, for convenience, thin feed stock has been mainly studied, the rolling of thick slabs or billets where the ratio of the billet width to the billet initial height is less than six ($w/h < 6$), say, is one of these areas.

In order to fully understand the problems associated with this special case it is useful to expand on the limitations of analytical studies and trace the historical development of existing rolling theories.

The early rolling theorists attempted to develop expressions to predict the roll pressure distribution and hence the rolling load and torque from the geometry of the roll gap and the metallurgical and mechanical properties of the material being rolled. The minimum data required was the yield stress and the coefficient of friction between the rolls and the workpiece.

It was necessary to make important assumptions to help simplify the analytical methods, these being;

a. The condition of plane strain deformation - no spread of the material being rolled in the lateral or width

direction.

b. Homogeneous deformation - plane sections perpendicular to the direction of rolling remained plane and perpendicular on passage through the roll gap.

c. The coefficient of friction between the rolls and the workpiece remained constant over the length of the arc of contact.

d. The arc of contact remained circular - no roll flattening.

e. A neutral plane existed within the arc of contact where the workpiece velocity was equal to the roll peripheral velocity.

f. There was negligible elastic deformation of the workpiece in relation to the amount of plastic deformation occuring during rolling.

g. The yield stress of the material remained constant throughout the rolling operation - the material did not work harden.

The most important of these assumptions was the second, in that the material being rolled could be considered to be made up of an infinite number of thin vertical elements with no shear forces acting at their interfaces. Each element was compressed an equal amount as it passed through

the roll gap. The assumed mode of deformation is shown in Figure 3.1.

At some point in the roll gap the roll peripheral velocity and the workpiece longitudinal velocity are equal thus uniquely defining the position of the neutral plane for a given set of geometrical conditions. Material on the inlet side of the neutral plane moved slower than the roll while material on the exit side moved faster. Thus there was slipping friction over the length of the arc of contact with the friction forces directed toward the neutral plane. This mode of deformation gave rise to the characteristic pressure distribution known as the friction-hill, having a maximum value at the neutral plane.

The method of solution for this problem was to equate the horizontal and vertical forces acting on an elemental slice in the roll gap to obtain the governing equations. Since the mode of deformation was pre-defined, the problem was statically determinate.

Stresses were identified by the Levy-Mises flow rule (33, 34) and the horizontal and vertical stresses related by use of a yield criterion to give a third governing equation.

Having determined the roll pressure distribution over the length of the arc of contact and the position of the neutral plane, the velocity of a point within the deformation

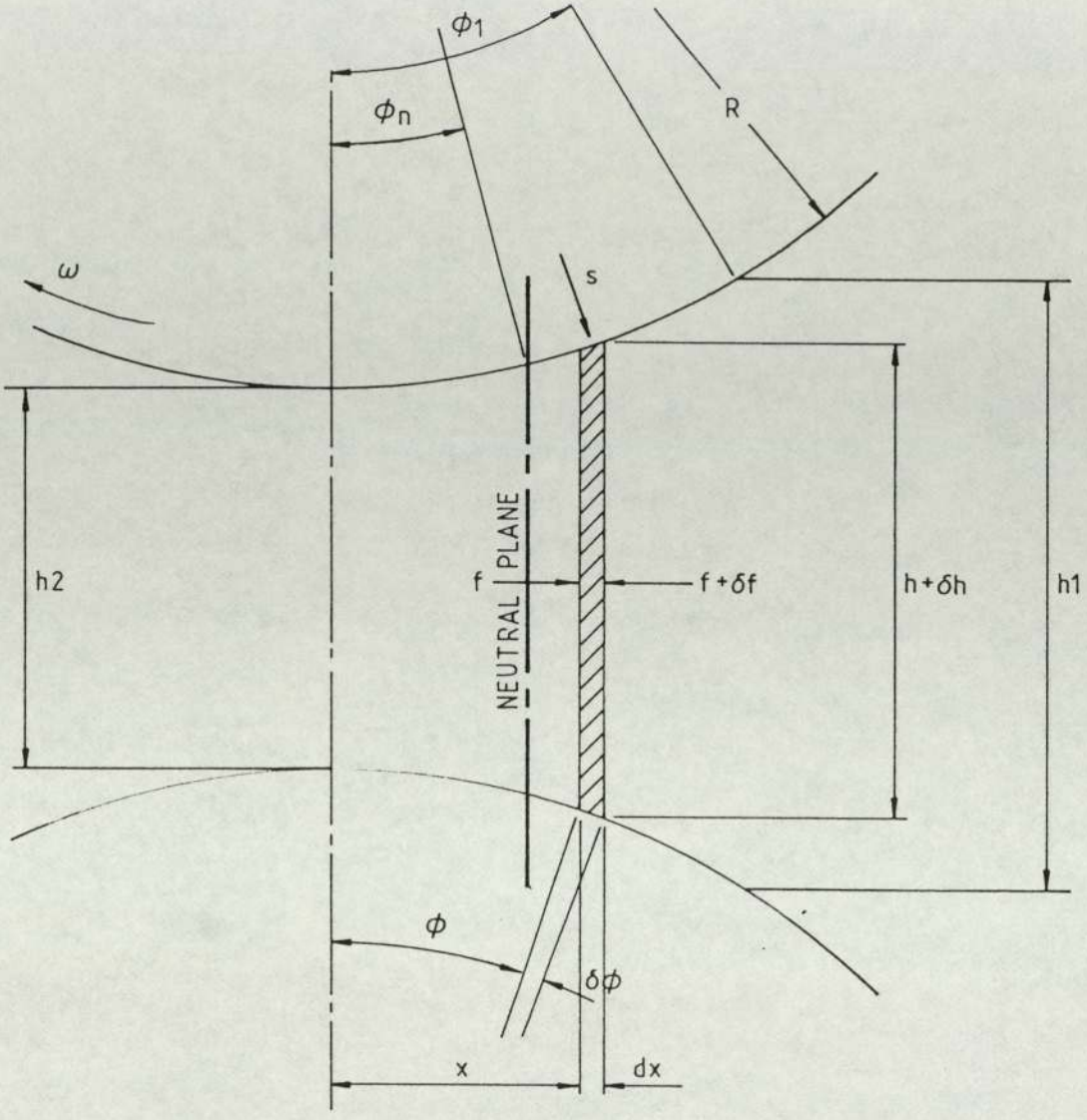

a. ELEMENTAL SLICE IN ROLL GAP.

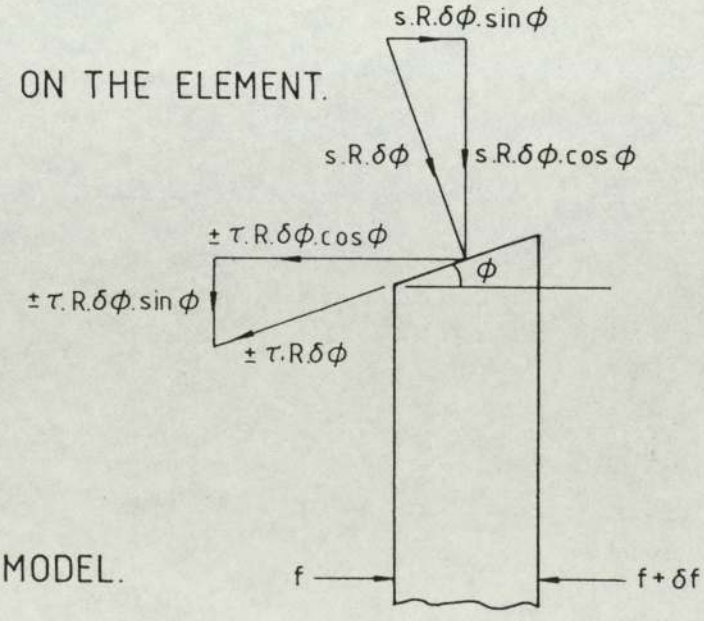

b. FORCES ON THE ELEMENT.

FIG. 3.1.

ROLLING MODEL.

zone could be calculated.

Using this approach, von Karman (35) determined the equations,

$$\frac{d}{d\phi}(h\,\sigma_x) = 2\,R\,s\,(\sin\phi \pm \mu\cos\phi) \quad \ldots\ldots\ldots\ldots \quad 3.1$$

$$\sigma_y = s\,(1 \mp \mu\tan\phi) \quad \ldots\ldots\ldots\ldots\ldots\ldots\ldots\ldots \quad 3.2$$

$$\sigma_x - \sigma_y = 2\,k = 2\,Y/\sqrt{3} \quad \ldots\ldots\ldots\ldots\ldots\ldots \quad 3.3$$

in order to solve the rolling problem for the case of slipping friction. Equations 3.1 and 3.2 were deduced from equating the horizontal and vertical forces respectively on the element. Equation 3.3 was deduced from the von Mises yield criterion.

A number of subsequent rolling theories produced differing results according to the assumptions made in order to solve these equations.

Siebel (36) determined the effect of the coefficient of friction on roll load and torque calculation using simple small angle assumptions and that the vertical stress, σ_y , was constant and equal to 2k. Von Karman made similair assumptions to produce the equation,

$$\frac{d}{d\phi}(h\,\sigma_x) = 2\,R\;\sigma_y\;(\phi \pm \mu) \quad \ldots\ldots\ldots\ldots\ldots\ldots \quad 3.4$$

relating σ_x and σ_y by the von Mises yield criterion to give the differential equation of the friction hill. Nadai (37)

made three different assumptions with regard to the coefficient of friction and obtained solutions for each particular case,

a. $\tau = \mu s$ (Coulomb friction).
b. τ = constant.
c. τ proportional to the relative velocity between the rolls and the worked material.

Siebel and Leug (38) carried out rolling trials to measure the roll pressure distribution by means of a pressure transducer implanted in the roll surface. They succeeded in producing data by which the quantitative reliability of the early theories could be gauged.

Ekelund (39) attempted to account for sticking friction but his analysis was semi-empirical containing many arbitrary approximations. Tselikov (40) simplified the diagramatic representation of the rolling process by replacing the arc of contact by two chords, one between the plane of entry and the neutral plane and the other between the neutral plane and the plane of exit.

In 1943 Orowan (41) put forward a general theory of strip rolling to cover both hot and cold rolling. He recognised that in hot rolling the friction could be high enough to assume that a regime of sticking friction existed where the material would stick to the roll, ie. the

tangential component of stress at the roll surface, μs, would reach the value of the yield stress in shear, k. Orowan produced a means of calculating results for a regime of stick/slip friction. The theoretical analysis is presented here to illustrate the method of solution.

Part I : Assumptions of homogeneous compression and slipping friction.

Consider the equilibrium condition of a thin vertical element between planes situated at angle ϕ and ($\phi + \delta\phi$) as illustrated in Figure 3.1(a). The force exerted on this element by the material on either side of it is determined from,

$$f(x) - f(x + \delta x) = -(df/dx)\, dx \quad \ldots\ldots\ldots\ldots\ldots\ldots \quad 3.5$$

where f = horizontal force per unit width of workpiece.

Equating the horizontal forces on the element, Figure 3.1(b),

$$\frac{df}{dx} = 2\, s\, (\tan\phi \pm \mu) \quad \ldots\ldots\ldots\ldots\ldots\ldots\ldots\ldots \quad 3.6$$

with μ being positive in sense when τ acts in the direction of increasing ϕ, ie. between the exit plane and the neutral plane, and negative in sense between the neutral plane and the plane of entry.

From Equation 3.6,

$$\frac{df}{d\phi} = 2\,R\,s\,\cos\phi\,(\tan\phi \pm \mu) \quad \ldots\ldots\ldots\ldots\ldots\ldots \quad 3.7$$

Under the assumption of homogeneity of deformation, ie. no shear stress between neighbouring elements, the vertical pressure is constant within each element: it is one of the principle stresses, the horizontal pressure being the other.

Equating vertical forces on the element,

$$q = s\,(1 \mp \mu \tan\phi) \quad \ldots\ldots\ldots\ldots\ldots\ldots\ldots\ldots \quad 3.8$$

where q = vertical pressure on the element.

From Equations 3.7 and 3.8,

$$\frac{df}{d\phi} = 2\,R\,q\,\cos\phi\,\tan(\phi \pm \alpha) \quad \ldots\ldots\ldots\ldots\ldots\ldots \quad 3.9$$

where $\alpha = \tan^{-1}(\mu)$, the angle of friction.

The condition of plasticity was used to yield a second relationship between $f(\phi)$ and $q(\phi)$,

$$q = p + k = f/h + k \quad \ldots\ldots\ldots\ldots\ldots\ldots\ldots\ldots \quad 3.10$$

where p = horizontal pressure on the element.

and subsequently,

$$\frac{df}{d\phi} = 2\,R\,(f/h + k)\,\cos\phi\,\tan(\phi \pm \alpha) \quad \ldots\ldots\ldots\ldots \quad 3.11$$

Integration of Equation 3.11 gave $f(\phi)$ for which p and q were obtained in their dependance on angle ϕ.

Part II : Calculation of roll pressure without the assumptions of homogeneous compression and slipping friction.

Orowan made use of Prandtl's Equations (42) for the case of compression between rough parallel platens, Nadai (43) having modified these Equations to apply to platens inclined at a small angle to each other.

Two cases were prevalent depending on whether the flow of material was toward or away from the apex, Figures 3.2(a) and 3.2(b). Expressions for the radial stress, σ_r , and the shear stress, τ , were obtained as,

$$\sigma_r = s - k\,(1 - (\theta/\gamma)^2))^{0.5} \quad \ldots\ldots\ldots\ldots\ldots\ldots \quad 3.12(a)$$

$$\tau = \mp\, k/2\ (\theta/\gamma) \quad \ldots\ldots\ldots\ldots\ldots\ldots\ldots\ldots\ldots \quad 3.12(b)$$

the negative sign in Equation 3.12(b) applying for flow toward the apex only. The azimuthal pressure, s, was independant of angular coordinate θ.

Orowan used Equations 3.12 to determine the horizontal force, f, on an element within the roll gap but with one condition, Nadai's solution to the inclined platen problem applied when material flow was toward the apex of the angle between the platens. In rolling this occurs only on the exit side of the neutral plane. Orowan assumed the

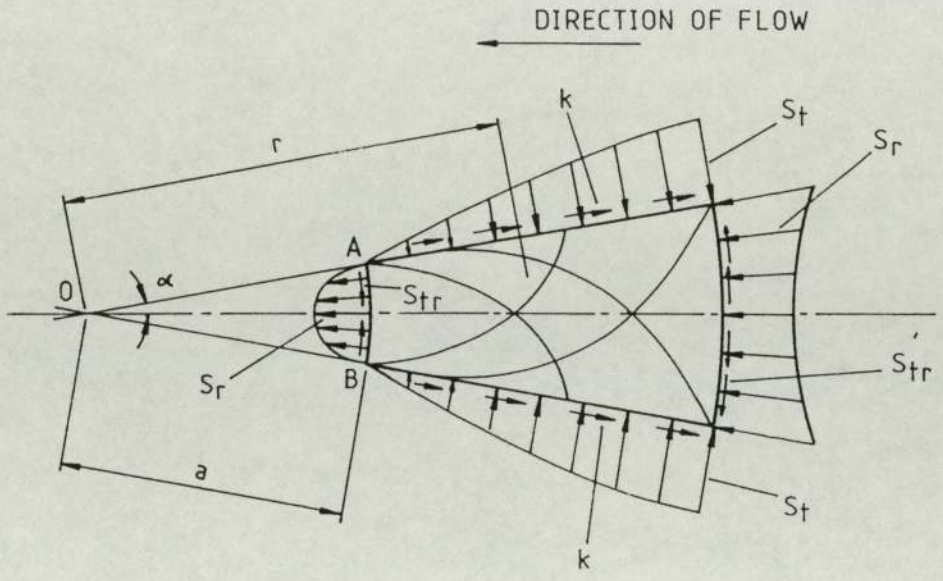

a. EXIT SIDE.

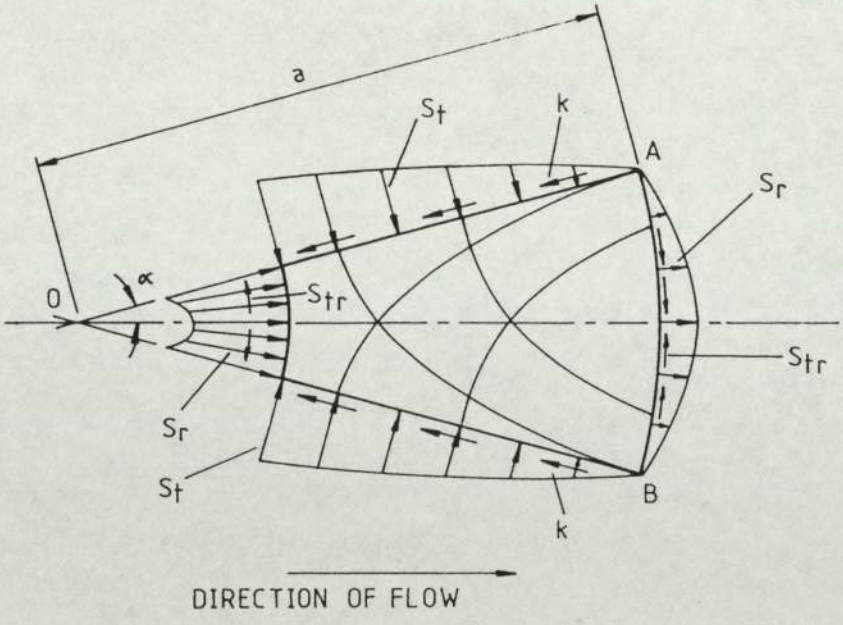

b. ENTRY SIDE.

FIG. 3.2. COMPRESSION BETWEEN INCLINED PLATENS. (FROM REF.43.)

equations would give an accurate approximation on the entry side also.

Equations 3.12 were integrated over the stock thickness to obtain the contribution of σ_r and τ to the horizontal force f. For the radial stress an inhomogeneity factor, $w'(\phi,a)$, was obtained where $a = 2 \mu s/k$.

Orowan showed that $w'(\phi,a)$ was independant of ϕ between zero and $\pi/6$ radians, and for vanishingly small ϕ , $w'(\phi,a)$ tended toward $\pi/4$ when $a = 1$, ie. condition of sticking friction.

Orowan assumed that the contribution of the frictional stress could be neglected in the case of slipping friction which lead to,

$$f = h\,(s - k\,w') \qquad \text{3.13}$$

for the case of slipping friction, and,

$$f = h\left[s - k\left\{w' \mp 0.5\left(\frac{1}{\phi} - \frac{1}{\tan\phi}\right)\right\}\right] \qquad \text{3.14}$$

for the case of sticking friction.

After transforming Equations 3.13 and 3.14 to make s the independant variable, the resultant equations were sustituted into Equation 3.7, the von Karman equation, to obtain the differential equation of the frictional hill for sticking friction,

$$\frac{df}{d\phi} = f\ (2\ R/h)\ \sin\phi + 2\ R\ k\ [\{w' \mp 0.5\ (\frac{1}{\phi} - \frac{1}{\tan\phi})\} \ldots$$

$$\ldots \sin\phi \pm 0.5\ \cos\phi\ ] \ldots\ldots\ 3.15$$

and for slipping friction,

$$\frac{df}{d\phi} = f\ (2\ R/h)\ \sin\phi \pm \mu\ \cos\phi) + \ldots$$

$$\ldots\ 2\ R\ k\ w'\ (\sin\phi \pm \mu\ \cos\phi)\ \ldots\ldots\ 3.16$$

Equations 3.15 and 3.16 were solved graphically after the zones of stick/slip had been identified.

Orowans' aim of providing an accurate theoretical model regardless of mathematical complexity was justified when tested against the experimental data of Siebel and Leug (38). However the requirement for rapid calculation methods for application in rolling mill practice led subsequent workers to make simplifying assumptions. As a result two categories of rolling theory were formulated: hot rolling where sticking friction was assumed for rolling without lubrication and cold rolling where slipping friction was assumed.

3.2. Theories Of Hot And Cold Rolling.

Bland and Ford (44) based a cold rolling theory on similar assumptions to Orowan with the additional assumptions of small contact angle and vertical stress, σ_y , equal to the

normal roll pressure, s.

They established that,

$$\frac{df}{d\phi} = 2\,k\,h\,\frac{d}{d\phi}\,\frac{s}{2\,k} + \left[\frac{s}{2\,k} - 1\right]\frac{d}{d\phi}(2k\,h) \quad \ldots\ldots \quad 3.17$$

and upon substitution into Equation 3.4, von Karmans' equation, a differential equation resulted which, when integrated, yielded expressions for the roll pressure on the inlet and exit sides of the neutral plane. These expressions included terms to account for front and back tension.

Ford, Ellis and Bland (45) devised a graphical method of solution for the (said) expressions using a constant mean yield stress. Orowan and Pascoe (46) suggested that for the case of hot rolling, the roll pressure distribution could be represented by a rectangular base surmounted by a triangular shape representing the friction hill. The position of the neutral plane was related to the geometry of the roll gap and expressions obtained for the roll pressure distribution. The theory also considered the case of medium-narrow stock where the condition of plane strain deformation does not apply. In this case the roll pressure distribution diagram had a three-dimensional friction hill mounted on top of a parallelepiped base of height 0.785k.

For his hot rolling theory, Sims (47) assumed sticking friction over the entire arc of contact and a small arc of

contact angle, to relate the normal roll pressure, s, to the horizontal stress by means of Orowans' equation.

The expression,

$$\frac{f}{h} = s - \frac{\pi}{4} k \quad \ldots\ldots\ldots\ldots\ldots\ldots\ldots\ldots\ldots\ldots \quad 3.18$$

was then substituted into Equation 3.4, von Karmans' equation, and expressions for the normal roll pressure from the entry plane to the exit plane and from the exit plane to the entry plane were obtained. These equations could be manipulated to obtain the position of the neutral plane.

In order to fully utilize the rolling theories developed, reliable data on material yield stress and friction coefficient were very important. Work by Whitton and Ford (48) is notable here as are papers by Watts and Ford (49, 50) who developed the plane strain compression test.

Much effort was directed towards obtaining reliable values of material yield stress over a range of temperatures and relevant strain rates. Work by Alder and Philips (51) produced data for aluminium, copper and mild steel and Cook (52) obtained stress-strain curves for various steel grades at different temperatures and strain rates using a cam plastometer. Consequently, Cook and McCrum (53) developed the industrially popular BISRA (British Iron and Steel

Research Association) method of load and torque calculation, it being a combination of Cook's data and Sims' theory.

More modern methods of solution using a computer are detailed in a paper by Alexander (54). The basic differential equation of von Karman, Equation 3.4, was solved using a similar approach to that used by Orowan.

3.3. Slip Line Field Analysis.

The fundamental assumption of homogeneous deformation to derive the basic differential equations of the friction hill, as indicated in the previous sections, has been shown to be fundamentally incorrect for the rolling of stock which is thick in relation to its width ($w/h < 6$, say).

Consequently, analyses which take account of the variability of deformation through the stock height (variation in strain) are most applicable. One such method is the slip line field approach which enables calculation of stress distribution, metal flow, rolling load and rolling torque.

In 1953 Prager (55) introduced a graphical technique to enable slip line fields to be constructed for various deformation processes and in 1955 Alexander (56) extended a solution by Hill (33) for compression between rough horizontal platens. He produced a slip line field solution

to the problem of hot rolling of strip, ie. stock that was thin in relation to its width.

Due to the complex nature of the solution method, the production of exact solutions for a range of rolling geometries was extremely tedious and so Ford and Alexander (57) constructed approximate slip line field solutions which were adequate for calculating load and torque but could not be used to predict the way in which the workpiece would deform. Crane and Alexander (58) produced slip line field solutions based on Alexander's original method for a range of geometrical configurations, but all for thin stock cases.

The first work to deal with thick stock rolling conditions was that by Druyanov (59). Computational techniques developed by Dewhurst and Collins (60) were used by Dewhurst, Collins and Johnson (61) to present a wide range of solutions in the thick stock range. Potapkin and Bobukh (62) resolved the state of stress in the deformation zone when rolling medium to thick stock in a similair manner to that of Druyanov (59) giving results for values of the parameter Hm/L equal to 0.48 and 2.94. A simple relationship was given for determining the mean hydrostatic pressure at the entry to the plastic zone on the axis of symmetry,

$$Pc = -1.6\ k + 2.8\ lc/hc \quad \ldots\ldots\ldots\ldots\ldots\ldots\ldots\ldots \quad 3.19$$

where Pc = mean hydrostatic pressure at entry point c.

lc, hc = horizontal and vertical projections of the entry plane slip line.

Filipov and Klimenko (63) produced approximate slip line field solutions for thick stock rolling and showed that horizontal stresses were tensile for Hm/L > 1.11.

More recent works have been based on an analogy between rolling and indentation. Pawelski and Neuschütz (64) produced results relating mean roll pressure to the ratio Hm/L in the form of a diagram now referred to as the 'Pawelski curve'. He deduced the general form of the curve by analogy with forging and indentation and carried out rolling trials on hot steel to derive the curve empirically.

Stahlberg (65) considered the analogy between rolling and indentation and discussed the stress state in the centre of the stock with respect to crack formation. He concluded that small Hm/L ratios were preferable but that the corresponding heavy reductions would cause crack formation at the edges of a bloom as a result of greater spread.

Ingham (66) developed a theory based on an indentation analogy for the rolling of thick stock and produced predictions which accurately matched experimentally determined rolling load data over the range $1 \leq Hm/L \leq 8.74$. Figure 3.3 illustrates the analogy. Since the theory was based on the slip line field method, the

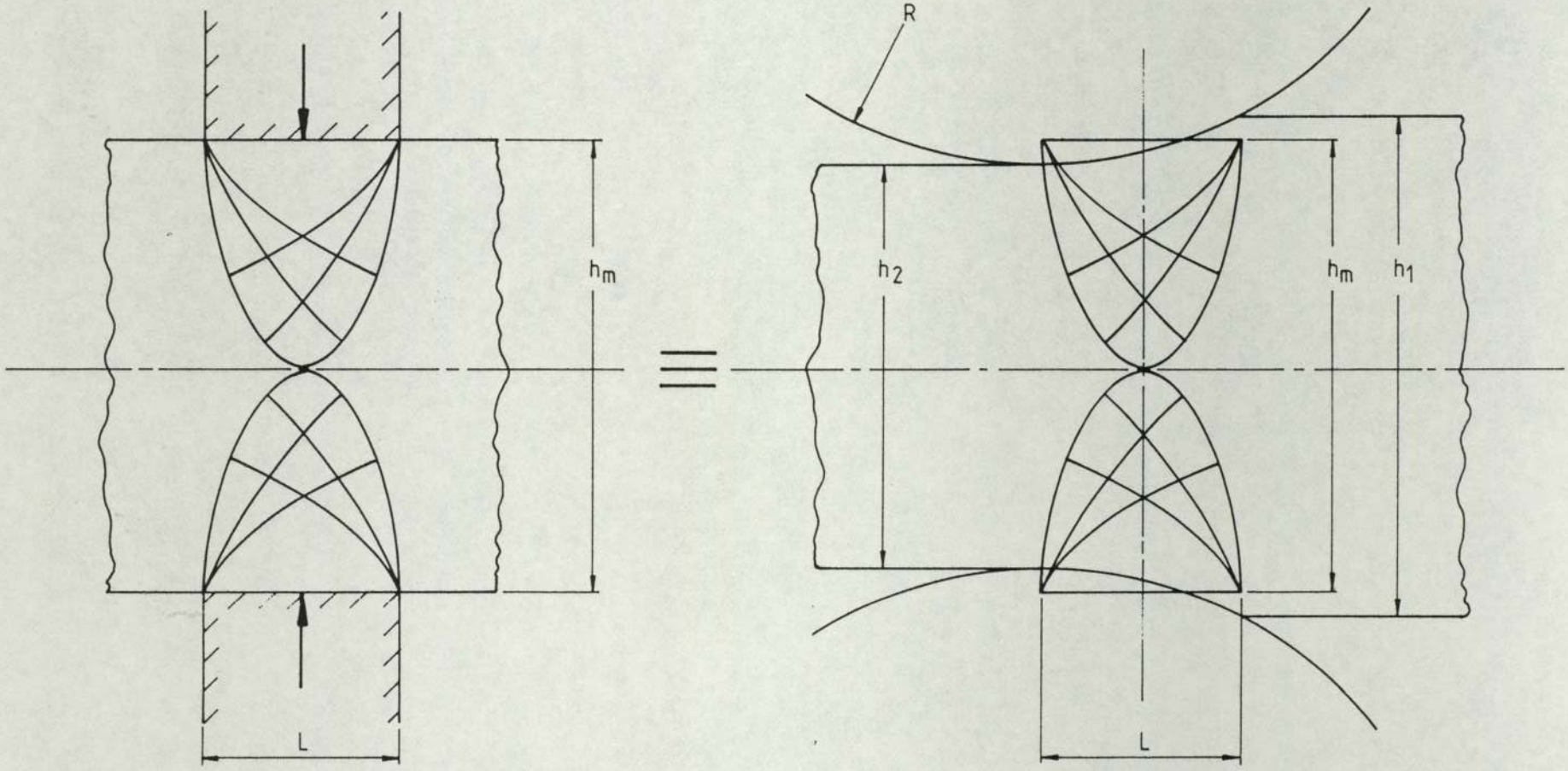

FIG. 3.3. ILLUSTRATING THE ANALOGY BETWEEN ROLLING AND INDENTATION.
(FROM REF.66.)

stress state within the roll gap was definable leading to the identification of conditions causing internal defects such as centre unsoundness, for example, tensile stresses.

Pawelski and Gopinathan (67) compared results of rolling and flat compression tests. They analysed various material properties and proposed a comparison criteria such that when the deformation resistances in rolling and that in the flat compression tests were similar, then the two processes could be considered comparable. When this condition was satisfied, then all the resulting mechanical properties and microstructure resulting from working were also comparable.

More recently, Sparling (68) has produced a computerised evaluation of slip line fields for rolling with a medium arc of contact to thickness ratio, for conditions of sticking friction throughout the arc of contact. Results of load and torque estimation using a computerized version of Prager's geometrical methods were combined with the results of Dewhurst et al (61) for the classes of slip line fields with smaller arc of contact to thickness ratio. The two methods of slip line field evaluation by Prager together with matrix methods gave load and torque functions with smooth transition over the boundary.

Collins (69) has recently presented a review of the state of the art of methods for constructing slip line field solutions in plane strain and axial symmetry. Procedures for constructing and solving the boundary value problems

which arise were developed using series and matrix operator methods for linear problems, and the treatment of non-linear problems using unconstrained non-linear optimization procedures was discussed.

3.4. Variational-Extremum Principle Analysis Methods.

In general, variational methods show that the solutions to a particular problem are those functions which make certain integrals stationary, ie. all or part of the field equations can be obtained by functional differentiation of these integrals.

Several variational principles and corresponding uniqueness theorems are established for certain boundary value problems in plasticity theory. These may be classified into two general groups,

a. For application to an elastic-plastic material.

b. For application to a rigid-plastic material where the component of elastic strain is negligible in comparison with the plastic component.

This general classification does not, of course, mean that the two groups of boundary value problems are unrelated, since a rigid-plastic body may be regarded, in essence, as being elastic-plastic where Youngs' modulus assumes an infinitely large value.

Ilyushin (70) introduced the terms 'deformation' and 'flow' to classify the extremum principles of plasticity theory. Greenberg (71) presented extremum principles for flow pertaining to an isotropic elastic-plastic material obeying the stress-strain laws of Prandtl (72) and Reuss (73). An absolute minimum principle for the stress rates for a general flow theory of a strain hardening elastic-plastic material has been given by Hodge and Prager (74) and a maximum principle for the stresses for a theory of flow has been given by Hill (75) for a rigid-plastic material. Under the assumption that all parts of the body were in the plastic state he deduced, in general, that if the surface velocities were prescribed over only part, S1, of the surface, and the external stresses, $F_i = \sigma_{ij}\, l_j$ over the remainder, S2, then,

$$\int_{S1} F_i\, u_i\, dS \geqslant \int_{S1} F_i^*\, u_i\, dS \quad \ldots\ldots\ldots\ldots\ldots\ldots \quad 3.20$$

where the stress system σ_{ij}^* is such that $F_i^* = \sigma_{ij}^*\, l_j = F_i$ on S2.

u_i = flow velocity.

l_j = direction cosines of outward normal to a surface.

This theorem states an absolute maximum of the plastic work for varying stresses.

The principle of Haar and von Karman (76) bears the same relation to the deformation theory of Hencky (77) as does the

principle of Greenberg (71) to the flow theory of Prandtl (72) and Reuss (73).

Hill (78) extended the variational principle of Markov (79) for velocity distributions in a plastic state to a work hardening material and also took account of more general boundary conditions. Markov's theorem was restricted to a non-work-hardening material obeying the von Mises yield criterion and the plastic stress-strain relationships of Levy and von Mises.

Markov's statement of the principle was:

"If a plastic mass is subjected to continued deformation at all points, under surface velocities u_i , the expression,

$$\int \sqrt{(}\ \varepsilon_{ij}^{*}\ \ \varepsilon_{ij}^{*}\ )\ dV\ ,\qquad \varepsilon_{ij}^{*} = \frac{1}{2}\left(\frac{\partial u_i^{*}}{\partial x} + \frac{\partial u_j^{*}}{\partial x}\right) \quad \ldots\ 3.21$$

makes an absolute minimum value in the actual state".
u_i^{*} is any velocity distribution satisfying the boundary conditions and the equation of incompressibility.

The relationship between Markov's variational principle and that of Hill was shown to be that the work done by the actual surface forces over S1 is the absolute maximum of the expression in the Hill theorem for varying stress, and the absolute minimum of the expression in Markov's theorem for varying velocity. The result provided a means of obtaining upper and lower bounds in the approximate solution of special

problems.

In 1963 Hill (80) proposed a new method of analysis for any metal forming process involving any material which in general was rigid-plastic, whatever the frictional conditions or tool geometry. He systematised the details of procedure and illustrated the method by preliminary anlaysis of inhomogeneous compression, bar drawing and forging. Hill believed that the proposed method was close to the ideal, and indicated that the prospects for implementation of the method were encouraging. However, he wished the final assessement to be based on a longer term and more diverse investigation. This assessement has been incorporated in the analysis of a wide range of metal forming operations, including rolling, by more modern day workers.

An outline of Hill's general method is presented here, for reference, due to its importance in the history of the development of metal working analysis.

3.4.1. On Hill's General Method Of Analysis.

The initial stage of the method is to choose a class of velocity fields from which the best approximation will eventually be taken. The chosen fields must satisfy all kinematic conditions.

The associated stress (given by the material constitutive law) is either also determined uniquely, or at

least to within a hydrostatic pressure if the material is incompressible. The associated stress distribution in the deformation zone of a chosen velocity field will generally not satisfy all the static requirements, so the problem is to select, from the considered class of velocity fields, that one which most nearly satisfies the statical requirements.

Noting the converse of the virtual work-rate principle for a continuum, the final selection criterion is that,

"the statical conditions can be regarded as closely satisfied overall when,

$$\int \sigma_{ij} \frac{\partial w_j}{\partial x_i} \, dV = \int_{Si} \tau_i \, w_j \, dSi - \pi \int_{Sf} n_j \, w_j \, dSf + \begin{cases} \int_{Sc} A \, dSc \\ \int_{Sc} B \, dSc \end{cases} \quad .. \; 3.22$$

where $A = [(n_i \, \tau_i) \, n_j + m \, k \, l_j] \, w_j$ for stiction.

and $B = (n_i \, \tau_i)(n_j - \mu \, l_j) \, w_j$ for friction.

for a sufficient sub-class of virtual orthogonalizing motions, w_j".

The surface, S, of the deforming body consists in general of three distinct parts:

Sc - adjoins a tool or container.

Sf - an unconstrained surface.

Si - suface adjacent to rigid zone.

On surface Sf there is at most a uniform fluid

hydrostatic pressure footnote

pressure, π. The frictional constraint over Sc is represented by a constant frictional stress, m k (where k = shear yield stress of the deforming body).

w_j is the orthogonalizing family to be selected and must be sufficiently wide and extensive enough to select a single approximating field from the particular class constructed to satisfy the kinematic conditions.

If the class were defined by equations involving an unknown function of just one position variable, then the orthogonalizing family must also involve an arbitrary function of just one variable. Once the family is chosen, the calculus of variations technique is applied to Equation 3.22 treating w_j as a variation. Then we obtain a system of equilibrium equations and boundary conditions suited to the particular approximating class and uniquely determining its best member.

Of particular interest here is Hill's analysis of bar drawing, or more accurately 'Steckel rolling' in which a bar of rectangular cross section is pulled through a pair of circular rollers to reduce its thickness.

With axes of reference x in the direction of drawing, y laterally (parallel to the roll axis) and z through the bar thickness, he assumed the zone of deformation to occupy the entire volume between the planes of entry and exit. He further assumed that any line in the z-direction scribed

vertically on the bar side would remain vertical after deformation (homogeneous deformation) and through thickness variation in stress and strain to be negligible.

Of primary interest was the variation in the width direction, in particular curvature of the bar sides and material spread.

Hill wrote down the simplest class of approximating velocity fields within the region bounded by the planes of entry and exit, die faces and the unconstrained surface to be,

$$v_x = \frac{1}{h\,w} \quad , \qquad v_y = -\frac{y}{h}\frac{d}{dx}(1/w) \quad ,$$

$$v_z = -\frac{z}{w}\frac{d}{dx}(1/h) \qquad \ldots\ldots\ldots\ldots\ldots\ldots \quad 3.23$$

and derived the differential equation for the width function, w, leaving the analysis at that point, the solution being clear in principle.

Nagamatsu et al (81) and Murota et al (82) analysed plane strain and axisymmetric compression by Hill's method and computed the bulge profile, compression loads and the stress distribution at the die/material interface due to friction. Baraya and Johnson (83), in a study of flat bar forging, compared Hill's method with experimental results for forging load and spread coefficient. Lahoti and Kobayashi (84) carried out analyses of ring compression with

barreling, thickness change in tube sinking and in particular spread in Steckel rolling neglecting roll/material interface friction in an attempt to explore Hill's general method for the analysis of metal working processes. For the Steckel rolling problem, Hill's differential equation was integrated to obtain a solution for the width function.

With few exceptions, theories of rolling dealing with three-dimensional deformation were not available at this time, studies on deformation being purely experimental.

MacGregor and Coffin (85) evaluated experimentally the complete strain distributions for copper bars rolled in varying numbers of passes. Chitkara and Johnson (86) conducted rolling experiments on lead bars to compare measured values of spread with those calculated from empirical formulae proposed by various authors. These included the following,

Wusatowski (87) collated the results of several researchers with some of his own and suggested a formula of the following kind to describe spread,

$$\frac{w2}{w1} = a'\ b'\ c'\ d'\ (h1/h2)^{p} \quad \ldots\ldots\ldots\ldots\ldots\ldots\ 3.24$$

$$\text{where } p = 0.0538\ (w1/h1)\ (h1/D)^{0.556} \quad \ldots\ldots\ldots\ 3.25$$

and a', b', c' and d' are correction factors allowing for variations in steel composition, rolling temperature, rolling

speed and roll material respectively.

Wusatowski (88) later modified his results after work on higher reduction rolling and altered the constants in Equation 3.25 from 0.0538 and 0.556 to 0.00011 and 0.9676 respectively and further modified a' to be dependant on temperature, composition and reduction.

Sparling's formula (89) was the result of rolling tests on mild steel rolled at approximately 1100 deg.C,

$$\ln(w2/w1) = 0.981 \ln(h1/h2) \; e^{-1.615} (w1/h1)^{0.9} \; \ldots$$

$$\ldots (h1/R)^{0.55} \; (\delta/h1)^{-0.25} \;) \; \ldots\ldots\ldots\ldots\ldots\ldots \; 3.26$$

Other research of note was made by Ekelund (39). The complex formula,

$$w_2^2 - w_1^2 = 8\delta - 4 \ln(w2/w1) \; (h1 + h2) \; (R\,\delta)^{0.5} \; \ldots$$

$$\ldots \; \frac{1.6\,\mu \; (R\,\delta)^{0.5} - 1.2\,\delta}{h1 + h2} \; \ldots\ldots\ldots \; 3.27$$

where μ was a variable for steel or cast iron representing the effect of friction, was stated in the form of a more readily useable nomogram.

For steel rolls, μ was defined by,

$$\mu = 0.55 - 0.0005 \; (T-1000) \; \ldots\ldots\ldots\ldots\ldots\ldots \; 3.28$$

and for cast iron rolls by,

$$\mu = 0.44 - 0.0004\ (T-1000) \quad \ldots\ldots\ldots\ldots\ldots\ldots\ 3.29$$

where T = rolling temperature in degrees centigrade.

More recently Geleji (90) analysed the spread within the roll gap during the rolling of square section stock. Gokyu et al (91) applied the minimum work hypothesis to the rolling problem to derive an expression for the width spread. Simplifying assumptions included uniform stress distribution at the roll-material interface and a parabolic form for the spread profile.

Polukhin (92) has analysed experimentally the spread in rolling certain alloy steels to provide a means of establishing a relationship between spread and microstructure of steel at a hot rolling temperature. He deduced that the amount of spread was proportional to the difference between the hardnesses of the stock and the scale oxides found on the steel outer surfaces at the hot rolling temperature. The harder oxide layers would tend to act as an artificial increase in roll diameter, the principle behind sandwich rolling. However the thickness of the oxides are negligible in relation to the stock thickness and would of course break free from the surface during the rolling operation.

The experimental work by Chitkara and Johnson (86) showed that the various formulae proposed by other researchers predicted too rapid a decrease in spread with

decreasing reduction in thickness. It should be noted however that the experimental relationships were all formed on the basis of rolling trials with steel and not lead as in the work of Chitkara and Johnson.

Oh and Kobayashi (93) produced a theory for the three dimensional analysis of rolling based on the extremum principle for a perfectly rigid-plastic material. In order to apply the extremum principle to a metal working process, the geometry of the deforming material is required at any particular instant (ie. non-steady or steady state operation). Hence, the application of the extremum principle to a three dimensional steady state deformation problem is not straightforward since the flat rolling operation is of an unconstrained nature, ie. spread takes place in the lateral direction, the magnitude of which is unknown.

Oh and Kobayashi's approximate solution method was to assume a class of surface shapes for the deforming body and determine the velocity field, based on those first proposed by Hill (80), which minimized a functional, Φ, for an assumed surface shape as in the usual upper bound method.

The functional was given by,

$$\dot{\Phi} = \dot{E}p + \dot{E}d + \dot{E}f \quad \ldots\ldots\ldots\ldots\ldots\ldots\ldots \quad 3.30$$

where $\dot{E}p$ = plastic deformation energy rate.

$\dot{E}d$ = energy rate dissipated due to the velocity discontinuities along the entry and exit planes.

$\dot{E}f$ = friction energy dissipation rate.

Then, among all the velocity fields thus determined for all the assumed classes of surface shapes, the steady state velocity field and corresponding surface shape was found.

The Rayleigh-Ritz (94) approximation in the direct minimization method was used, reducing the rolling problem to the solution of three complex simultaneous algebraic equations. The solutions for single pass rolling in terms of sideways spread, rolling torque and location of the neutral point were in good agreement with published experimental data (47, 85).

More recently, Saito (95) formulated an upper bound approach to the simulation of three dimensional metal flow in shape rolling. A kinematically admissible velocity field was deduced by assuming the shape of stream lines and the boundaries of the deformation zone. As in previous upper bound approaches the total energy rate was estimated and minimization carried out using the method of Nelder and Mead, a flexible polygon search (96). Theoretical results were compared with experiment in terms of flat, box and diamond roll pass schedules.

3.5. Finite Element Methods Of Analysis.

The methods outlined so far have all been useful in predicting forming loads, overall geometry change of the deforming workpiece, modes of material flow and determining the optimum process conditions in an approximate manner. Accurate determination of the effects of various parameters on metal flow have only been possible with the introduction of the finite element method to the analysis of metal working processes.

The concept of the finite element method is one of discretization in which a number of finite points (nodal points) are identified in the domain of the function (the workpiece) and the values of the function and its derivatives are specified at these nodes. The domain of the function is approximately represented by a finite collection of sub-domains called finite elements, the domain being the assembly of the elements connected together on their boundaries.

The solution of a finite element problem consists, essentially, of five specific steps,

a. The problem.
b. The element.
c. The element equation.
d. The assembly of the element equations.
e. The numerical solution of the global equations.

The formulation of the element equations can be

accomplished in one of four ways,

1. Direct approach.
2. Variational method.
3. Method of weighted residuals.
4. Energy balance approach.

The basis of the variational approach in finite element metal flow modelling is to formulate functionals depending on constitutive relations. The basic mathematical description of the method, as well as solution techniques, are given in several books for example Washizu (94), Zienkiewicz (97) and Huebner (98).

Elastic-plastic, visco-elastic and visco-plastic material models have been applied in simulating various types of rolling and extrusion processes. Elastic-plastic models were first used to determine internal stresses and boundary tractions up to the initiation of unconstrained plastic flow. Elastic-plastic models have been extended to follow material deformation into the fully plastic state by introducing large strains in a convected coordinate formulation.

Lee at al (99) have used elastic-plastic models for the transient analysis of extrusion. Plane strain rolling of an elastic-plastic material was analysed by Rao and Kumar (100), an incremental displacement method being used for the non-linear analysis of the problem. Figure

3.4. illustrates this method.

Recently, Keifer (101) has applied a three dimensional finite element model for an elastic-plastic, isotropic, homogeneous material to the rolling of rectangular billets between flat rolls. The model was capable of handling the extremes of sticking friction in the direction of rolling and either sticking or slipping friction component in the lateral direction. Predictions of metal flow were obtained to study the effect of billet width variation.

An elastic-plastic plane strain rolling analysis taking into account the frictional effect has been made by Yarita et al (102). Sticking and slipping friction were examined at the roll-material boundary using a modification of an original program written by Mallett and Lee (103).

Visco-elastic models have been used by Lynch (104) for predicting the deformation during rolling under steady state conditions and by Batra (105), both using integral forms of the material constitutive law. Webber (106) has used correspondence principles in conjunction with elasticity solutions and time dependant Lagrangian formulations to follow the material through its' deformation history (107).

Lung and Marenholtz (108), Kobayashi (109) and Zienkiewicz et al (110) have all applied various visco-plastic formulations to solve extrusion, rolling and upset

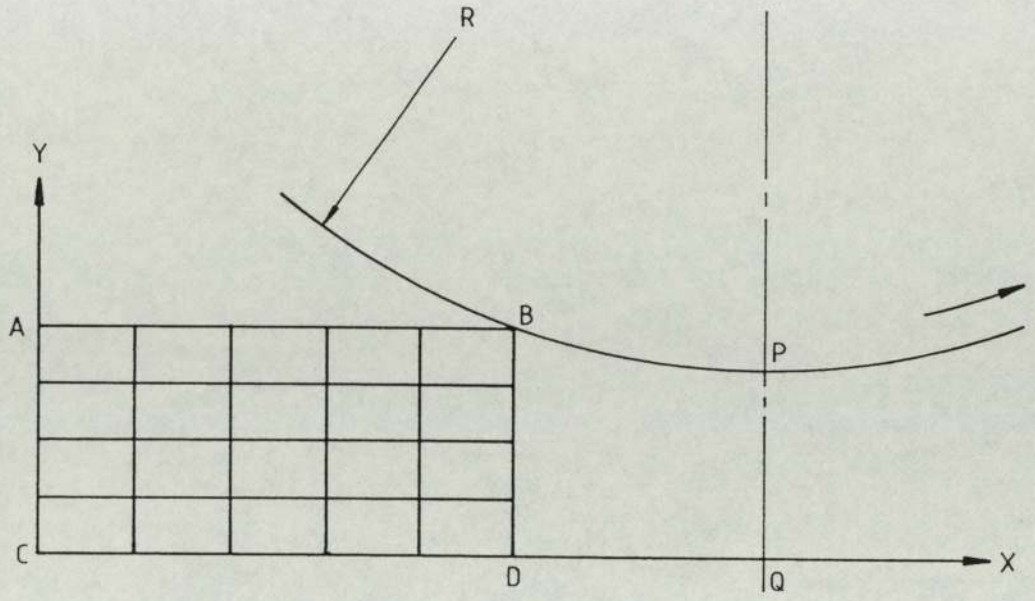

ROLL CENTRE 'O', RADIUS OP.

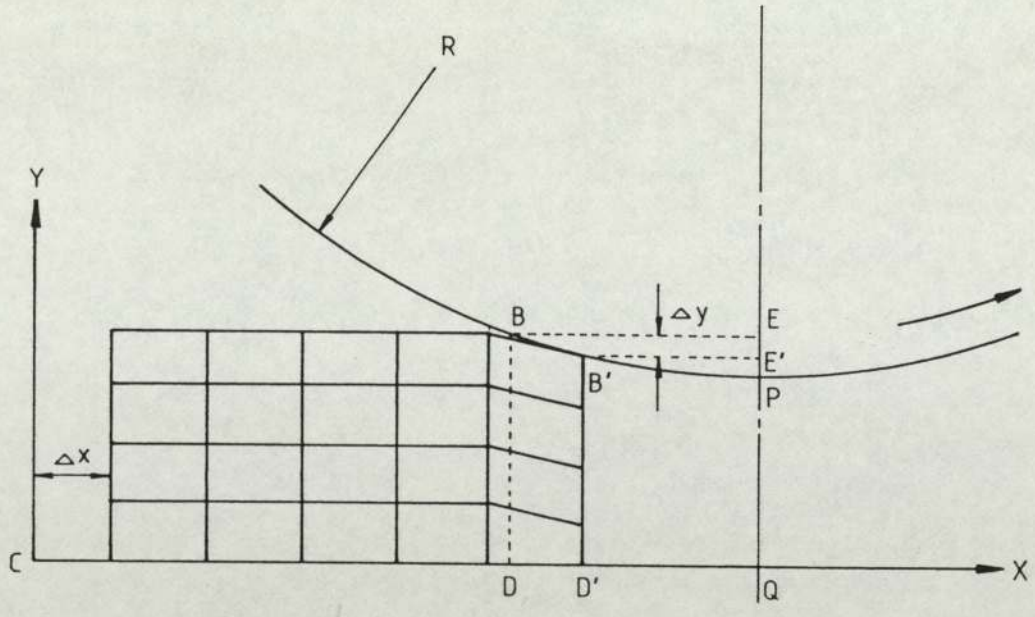

FIG. 3.4. METHOD OF INCREMENTAL DISPLACEMENT. (FROM REF.100.)

forging operations. A visco-plastic formulation using velocity and pressure as the primary variables was extended by Dawson and Thompson (111) to include elastic response.

Dawson (112) presented a method to determine the strain history in an Eularian reference frame and extended a visco-plastic formulation to include strain history dependence. The method was applied to slab rolling.

Altan et al (113) described the features of a rigid visco-plastic finite element method code 'ALPID'. The program could handle the deformation process for arbitrarily shaped dies with constant shear and Coulomb type friction. Greater computational efficiency was achieved by introducing an algorithm for initial guess generation.

The rigid-plastic assumption neglects elastic strains (the elastic strains being negligible when compared with the magnitude of the plastic strains) and so, since the material will then be in a totally plastic state, larger increments of deformation may be made, reducing computational time while retaining reasonable accuracy of solution.

The rigid-plastic finite element method is based on an extremum principle which states that for a plastically deforming body of volume V, under traction F, prescribed on part of the body surface Sf, and the velocity u, prescibed on the remainder of the surface Sc, the actual solution

minimizes the functional,

$$\Phi = \int_V \bar{\sigma}\,\dot{\bar{\varepsilon}}\,dV - \int_{Sf} F\,u\,dS \quad \ldots\ldots\ldots\ldots\ldots\ldots \quad 3.31$$

under the constraint,

$$\dot{\varepsilon}_v = 0 \quad \ldots\ldots\ldots\ldots\ldots\ldots\ldots\ldots \quad 3.32$$

The condition of incompressibility, Equation 3.32, can be removed by introducing either the Lagrange multiplier or a penalty function into the functional Φ. The modified functional becomes,

$$\Phi = \int_V \bar{\sigma}\,\dot{\bar{\varepsilon}}\,dV + \int_V \lambda\,\dot{\varepsilon}_v\,dV - \int_{Sf} F\,u\,dS \quad \ldots\ldots \quad 3.33(a)$$

where is the Lagrange multiplier, or,

$$\Phi = \int_V \bar{\sigma}\,\dot{\bar{\varepsilon}}\,dV + \int_V (\eta/2)\,(\dot{\varepsilon}_v)^2\,dV - \int_{Sf} F\,u\,dS \quad \ldots \quad 3.33(b)$$

where η is a very large positive constant.

The rigid-plastic analysis has been extended to a three-dimensional problem by Kamazawa and Marcal (114) for the determination of spread in rolling using line elements and previously developed software, namely the finite element package 'MARC'. Li and Kobayashi (115), using a simplified element structure, analysed spread in the rolling of flat bars with small initial width to height ratio. A three-dimensional treatment of interface friction was implemented

in the program, taking into account the existence of a neutral flow region in the roll gap.

Li and Kobayashi (116) also solved the plane strain rolling problem by the rigid-plastic finite element method based on the infinitesimal theory of plastic deformation. Non-steady state and steady state solutions, the velocity field in the deformation zone and the external force distribution along the arc of contact were obtained.

Osakada et al (117) produced a finite element anlaysis of metal forming processes based on the equilibrium of nodal forces by assuming the material to be a slightly compressible rigid-plastic material. The method was extended to account for finite deformation derived on the basis of the equilibrium of nodal forces at the end of incremental deformation. The effects of work hardening and shape change of elements during incremental deformation was incorporated into the model.

Mori et al (118) have produced a finite element solution for steady and non-steady state strip rolling for a slightly compressible rigid-plastic material. Stress and strain distributions were calculated for the steady state with a constant coefficient of friction for workhardening and non-workhardening materials. Figure 3.5. gives the general idea of modelling of plane strain rolling.

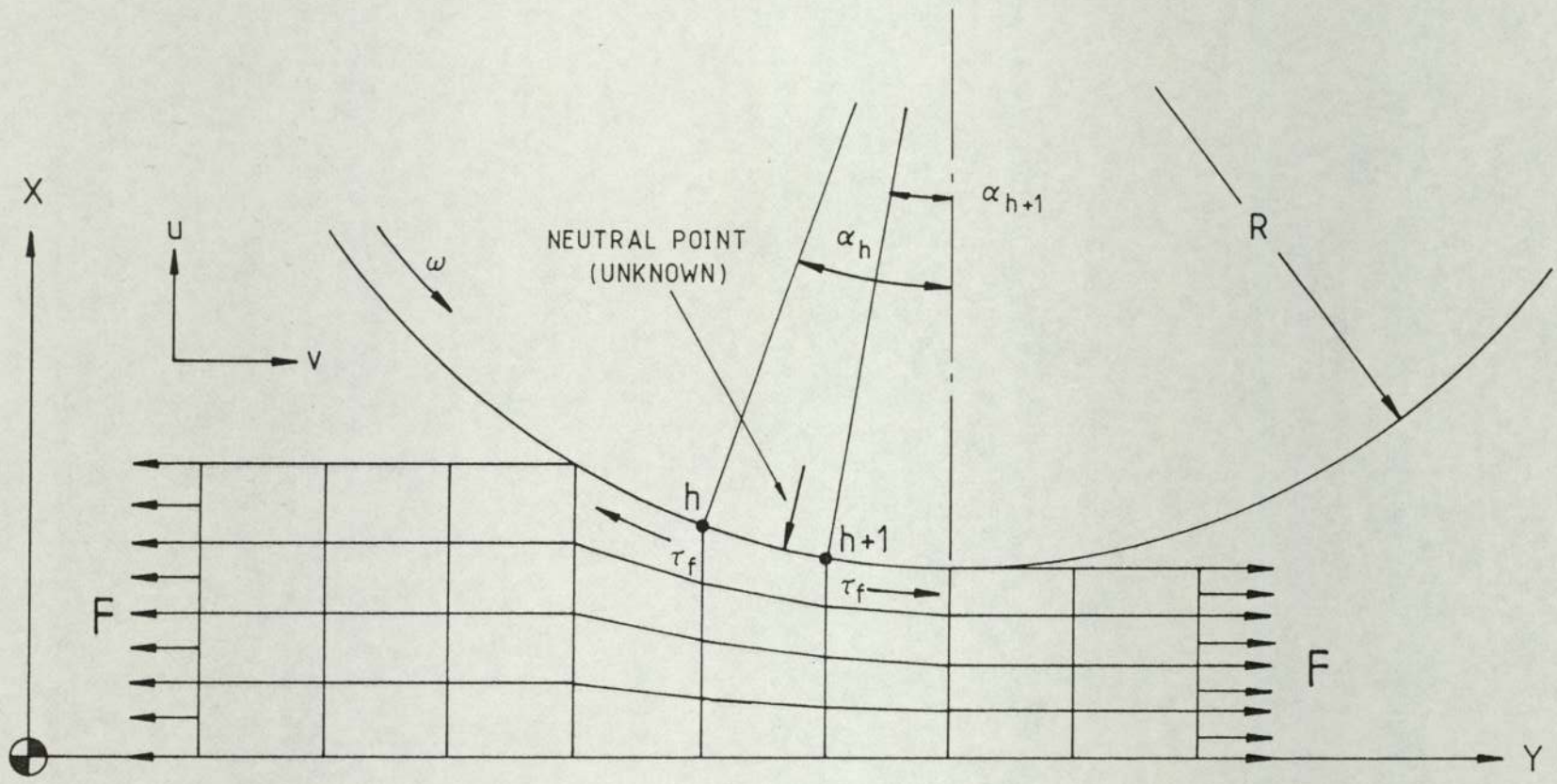

FIG. 3.5.

GENERAL IDEA OF MODELING PLANE STRAIN ROLLING.
(FROM REF.118.)

Further work by Mori et al (119) has produced a simulation of three-dimensional deformation using a rigid-plastic finite element method. Using eight noded isoparametric hexahedral elements, the method could deal with inhomogeneous metal flow in three orthogonal directions by the use of independant velocity components at each node. The metal forming processes considered were side pressing of pipe and upsetting of aluminium pipes and blocks.

Mori and Osakada (120) simulated three-dimensional deformation in plate rolling and edge rolling using a rigid-plastic finite element method. Simplified three-dimensional elements to approximate the deformation were developed, the method being an extension of the approaches made in earlier work (118, 119). The authors showed (121) that simulation of three-dimensional rolling was possible in short computing time by use of a two-dimensional finite element mesh. They re-analysed plate rolling and edge rolling using the rigid-plastic finite element method using simplified elements. Since the plates were divided into only two layers of elements in the thickness direction, the model was only valid when the deformation was fairly uniform through the thickness.

An application of the finite element method to metal forming has been the analysis of overlap at the front and back ends in slab rolling and design of end pre-forms to eliminate crop loss. Stahlberg et al (122) studied the

overlap formed at the front and back ends in slab ingot rolling both theoretically, using a plane strain upper bound solution for a rigid-plastic material, and experimentally.

Hwang and Kobayashi (123) used the finite element method to investigate pre-form end shapes for eliminating crop loss in plane strain rolling of a rigid-plastic material. The formulation of defective overhang of front and back ends in flat ended ingot rolling was shown by simulation for non-workhardening materials and the simulation of plates with pre-form end shapes, obtained by an approximate analysis, was made. The backward tracing scheme by the finite element method was applied to non-workhardening materials to obtain more accurate pre-form end shapes. This scheme is illustrated in Figure 3.6.

Kobayashi (124) presented an approximate solution for design of ingot end shapes using channel flow as a velocity field for non-steady-state deformation end regions and predicted overhang contours and end shapes at the front and back ends.

Inclusion of temperature effects in the analysis is an important step towards extending the finite element analysis to the range of solution of hot working processes. In recent years the practice has been to obtain temperature solutions in uncoupled problems of heat generation.

In order to solve a coupled thermal-plastic deformation

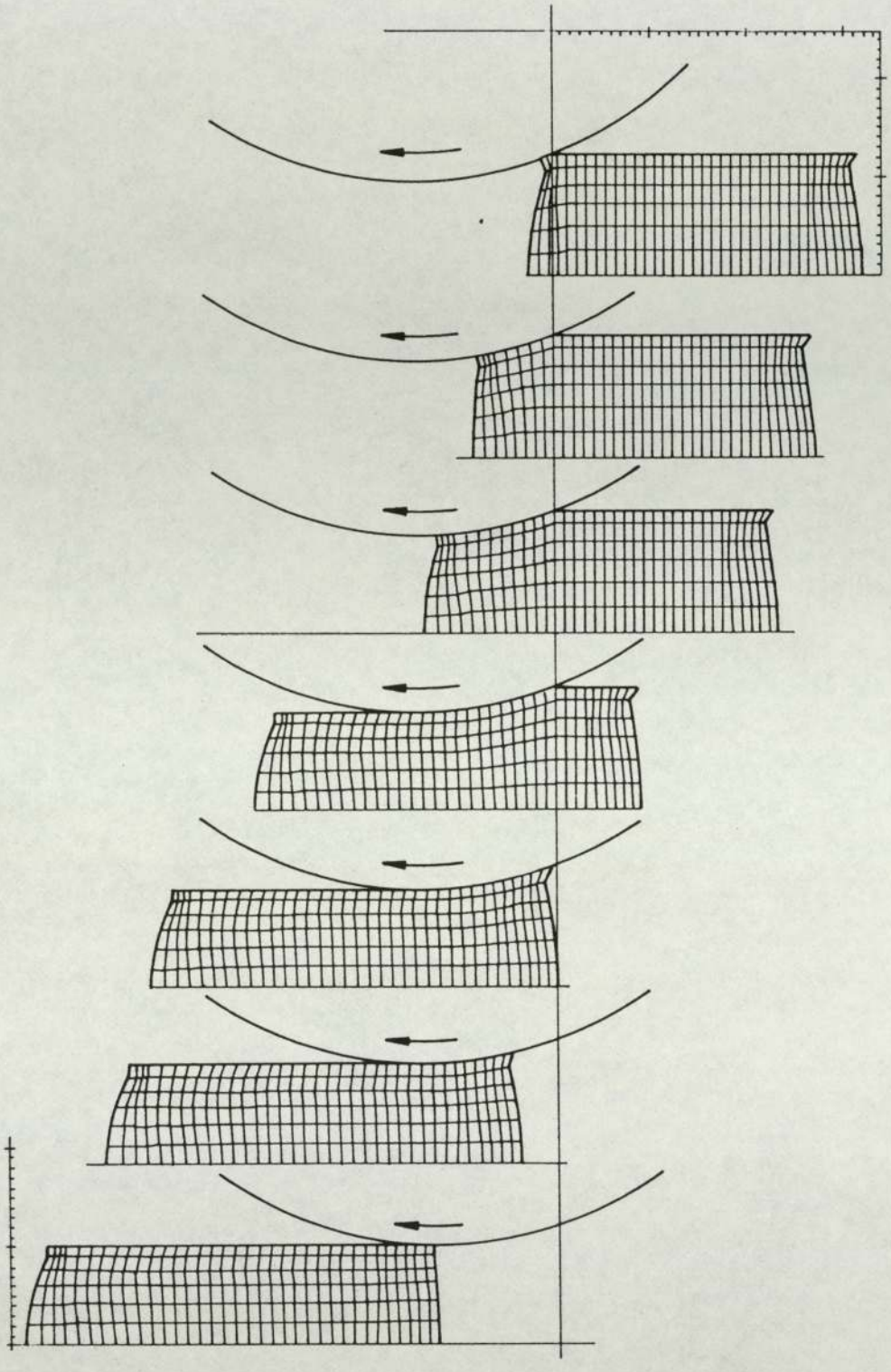

FIG. 3.6. ROLLING SIMULATION WITH PREFORM END SHAPES FOR NON-WORKHARDENING MATERIALS. (FROM REF.123)

problem, it is necessary to solve simultaneously the flow problem for a given temperature distribution and to solve the thermal equations. These aspects of numerical solutions were discussed by Zienkiewicz et al (125) with examples in rolling, extrusion, drawing and some sheet metal forming operations.

Bishop (126) and Altan and Kobayashi (127) predicted the temperature rise for specified velocity fields and Dawson and Thompson (128) have coupled a visco-plastic formulation with equations for conductive heat transfer to obtain fully coupled solutions for several forming processes.

A finite difference model to determine the temperature profiles of the work roll and strip was made by Tseng (129) using an Eulerian formulation in order to minimize the number of grid points required in the numerical analysis. A generalized finite difference scheme was used allowing the use of a non-orthogonal mesh in the deformed strip region and roll-strip interface area.

Abhijit and Subrata (130) recently presented a finite element analysis for warm forming processes. Thermo-mechanical coupling was included and an elastic-visco-plastic material was used. The formulation was capable of using any class of combined creep-plasticity constitutive models with state variables for metal behaviour description.

Further work of interest has been made by Tozawa et

al (131) who produced a theoretical analysis for predicting the three-dimensional distribution of stresses and metal flow in cold strip rolling assuming the material to be rigid-plastic in the deformation zone and an elastic solid out of the zone (see Figure 3.7).

Lahoti et al (132) have developed a comprehensive Computer Aided Design (CAD) system for predicting metal flow and stresses in plate rolling. The CAD system was capable of predicting lateral spread, elongation, deformation zone boundary and location of the neutral plane using a modular upper bound method and the stresses, roll separating force and roll torque using a slab equilibrium method of analysis.

More recently Malinin (133) based an elementary theory of hot rolling on the equation of state of strain-hardening creep using a plane-section hypothesis and assuming stress and strain uniformity across the workpiece height.

In an earlier paper, Kobayashi (134) gave a review of recent developments in the application of the finite element method to metal forming process modelling. The review revealed that almost all of the examples discussed in publications dealt with two-dimensional problems only, more complex problems being treated by an approximate stress analysis or upper bound method. Major developments outlined were the user orientated general purpose program, the rigid-plastic finite element code 'ALPID' by Altan et al (113) and Oh (135) and the coupled analysis of transient viscoplastic

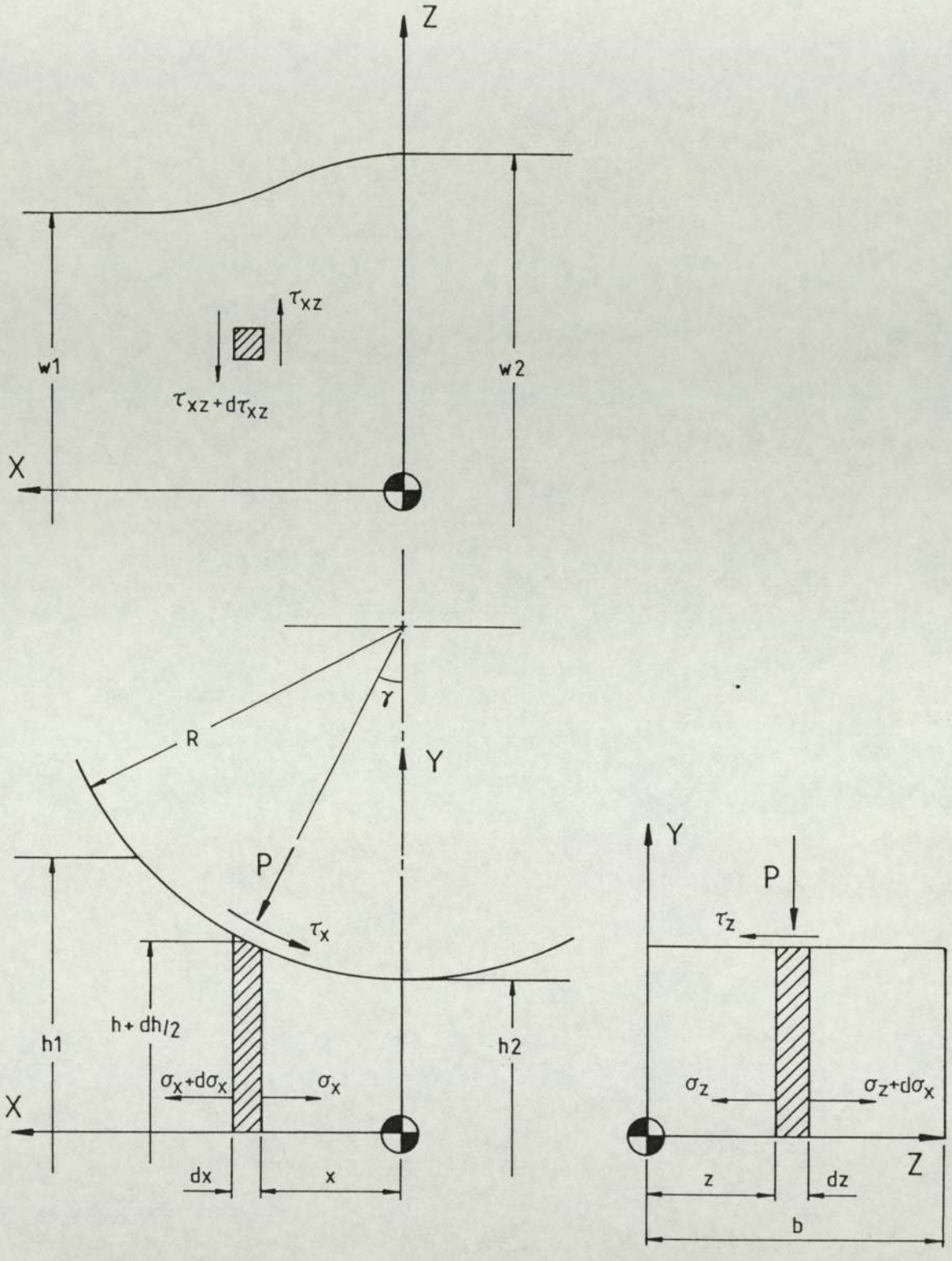

FIG. 3.7.

STRESSES ACTING ON ELEMENT.
(FROM REF. 131)

deformation and heat transfer by Rebelo (136).

More recent developments were described in the upgraded review by Kobayashi (137). The paper reviewed recent developments on the application of the finite element method, particularly the rigid-plastic approach, to the problem of process simulation and pre-form design in metal forming.

In process simulation the developments concerning three-dimensional metal flow analysis were discussed, using examples for block compression with three-dimensional elements and spread analysis in flat tool forging using simplified elements. In the area of pre-form design, a unique application of the finite element method was illustrated by pre-form design in shell nosing.

Kobayashi indicated that for simple deformation patterns in three dimesions, good solutions could be obtained using relatively few elements.

3.6. Summary.

Equilibrium types of analysis are inadequate for the analysis of rolling stock where the ratio of stock width to stock height approaches unity (square section stock). These theories tend to underestimate values of rolling load and torque due to their failure to allow for redundant deformation, overlaid by frictional effects which are still

not easy to assess.

The inhomogeneity of the rolling process can be seen in spread profiles, it being well known that rolling of this size of stock leads to uneven lateral spread, the side faces becoming concave, convex or a combination of both depending on the rolling geometry. This indicates non-uniformity of the stress distribution throughout the stock height as opposed to that assumed in the early equilibrium theories.

In a number of cases, the slip line field method has provided more accurate predictions of roll force and torque. The value of the method is limited by its complex graphical nature and in that it considers the workpiece to be uniform in temperature and properties such as yield stress. More recently, however, the equations of slip line field theory have been solved numerically using computers.

In elasticity, the principles of minimum potential energy and minimum complementary energy are useful tools for obtaining approximate solutions to difficult boundary value problems. In plasticity, exact solutions are harder to obtain than in elasticity and consequently extremum principles play an important role.

The application of extremum principles to the analysis of non-axisymmetric metal forming processes is now well documented and has been successful in predicting forming loads, overall geometrical changes of deforming

workpieces, qualitative modes of metal flow and determining optimum process conditions in an approximate nature.

However, accurate determination of the effects of various parameters involved in the process on the detailed metal flow became possible only recently when the finite element method was introduced into the analysis of metal forming processes. Since then, the method, particularly in the area of process modelling, has assumed steadily increased importance in metal forming technology.

The use of the finite element method for the analysis of three-dimensional metal flow is not straightforward and emphasis must be placed on achieving a balance between computational efficiency (economic constraints) and solution accuracy. This is even more critical when thermal effects, such as those found in hot forming processes, have to be accounted for.

From this review, one can conclude that the finite element method appears to be the most suitable for mathematical modelling of metal flow, especially in view of the recent advantages in computing power and speed. However, economic practice may have the last word.

CHAPTER FOUR

THEORETICAL ANALYSIS

4.1. Introduction.

Rolling of thick stock where the ratio of the billet width to the billet initial height is less than six ($w/h < 6$) usually results in a three dimensional deformation field in the roll gap with subsequent change in the product width. The magnitude of the width change is an unknown factor and is especially important when rolling square section continuously cast stock. If the final product is to have axial symmetry (square or round) then the dimensions of the stock emerging from a pass will dictate the subsequent pass sequence(s) necessary to achieve this objective. A pass sequence that retains some margin of axial symmetry with appropriate internal working will naturally lead to more efficient rolling practice. To control the shape of the product it is necessary to predict the three dimensional behaviour of the material during rolling.

In the analysis of three dimensional deformation (Sections 2.4. and 2.5) most of the analytical methods for rolling which assumed plane strain deformation were extended to the three dimensional case and solved, for example, by the finite difference method (130). When applied to three dimensional deformation this type of solution method becomes extremely complex.

Upper bound methods of analysis (84,93,131) to account for the three dimensional deformation approximated the shape of the material and gave an estimate of the rolling

torque. However, the stress distribution and the rolling load could not be evaluated directly.

Although the finite element method is now a well developed and extremely flexible means of three dimensional elastic deformation, the standard method of three dimensional meshing is not practicable for simulating large plastic deformation since the number of elements and nodes is extremely large. Certainly this is beyond the economic capabilities of a desk top micro computer.

This analysis deals with two aspects of the rolling of continuously cast stock,

a. Billet deformation during rolling.
b. Void closure during rolling.

The objective of this analysis is to produce a means of determining the shape of a rolled billet and hence the velocity field that can be implemented on an office-bound micro-computer system using a common programming language. A simplified upper bound analysis is used in conjunction with experimentally derived data to produce a means of calculating product shape.

Void closure is analysed using a simplified upper bound method based on the compression of a square billet section with appropriate assumptions. The analysis assesses two upper bound solutions and deduces their suitability for

describing the mechanism of void closure.

4.2. Analysis of the Rolling Problem.

4.2.1. Preliminary Considerations.

The analysis of the rolling process by variational principles has been tackled by a number of authors for application to elastic-plastic and rigid-plastic materials. The majority of work since 1963 has been based on Hill's general method of analysis for metal working processes (80). This is described in Section 3.4.1.

In order to apply a variational principle to a metal working process where the deformation field is essentially three dimensional in nature, the geometry of the material being deformed is required at any particular instant. Here, the application of a variational principle to a three dimensional steady state deformation problem is not straightforward since the rolling operation is of an unconstrained nature, ie. spread, the magnitude of which is unknown, takes place in the lateral direction.

In previous upper bound approaches the total energy rate dissipated was estimated and a minimization procedure carried out in order to obtain the steady state velocity field and corresponding surface shape. In this analysis of the rolling of square section stock, the total energy rate is estimated using experimentally derived data on the spread of

square section stock when rolled through plain rolls. This data is then used to form a third order polynomial describing the surface shape of the deformed stock. Since the geometry of the deformed stock is defined, the minimization procedure is superfluous.

4.2.2. Physical Assumptions.

a. Roll flattening does not occur so that along the arc of contact the velocity components normal to it are zero.

b. The geometry and physical condition of both rolls is identical so that the stress and strain fields are symmetrical about the horizontal and vertical planes in the direction of rolling. Consequently only one quarter of the stock in the roll gap need be analysed.

c. Sticking friction is assumed to operate along the length of the arc of contact and hence the velocity components tangential to the arc of contact can be specified arbitrarily. The tangential velocity will be equal to the roll peripheral velocity.

d. The material comprising the workpiece is homogeneous and isotropic. Porosity in the workpiece has been neglected in this part of the work.

e. The material is visco-plastic so that rigid or elastic zones are not included and yielding takes place

throughout the stock.

f. The boundaries of the deformation zone are assumed to be the vertical planes of entry and exit.

g. Deformation takes place under steady state conditions so that inertia and acceleration can be neglected.

h. The deformation is planar in that any vertical lines scribed on the workpiece sides in the lateral direction remain vertical after deformation.

4.2.3. Rolling Model.

A bar of square cross section is rolled through a pair of plain, cylindrical rolls of radius R. The workpiece thickness is reduced from h1 to h2 and the width increased from w1 to a mean value w2. The projected length of the roll-workpiece contact arc is given by L. Coordinate axes are taken with the origin at the midpoint of the entry plane as shown in Figure 4.1. The axes x, y and z are in the directions of length, width and thickness respectively. The workpiece enters the roll gap at velocity V1 and leaves the roll gap at velocity V2 . The roll peripheral velocity is constant and equal to Ur.

From Hill (80), the simplest class of approximating velocity fields is assumed to be,

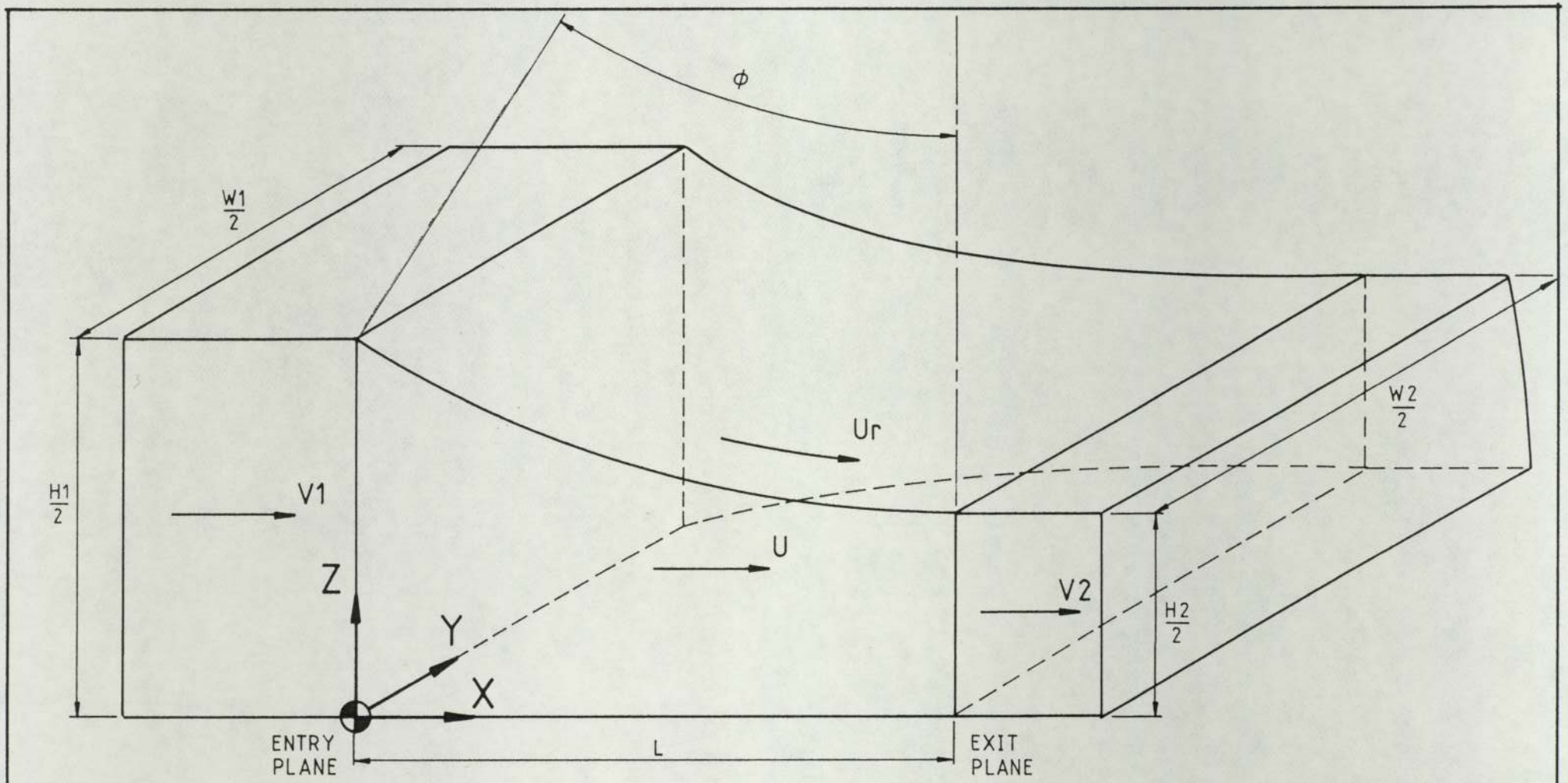

FIG. 4.1.

ROLLING MODEL.

$$v_x = \frac{U}{h\ w(x)} \quad , \quad v_y = -U\,\frac{y}{h}\,\frac{d}{dx}\left\{\frac{1}{w(x)}\right\} \quad , \quad v_z = -U\,\frac{z}{w(x)}\left\{\frac{d}{dx}\ \frac{1}{h}\right\} \qquad \ldots\ldots\ldots\ 4.1$$

within the region bounded by the planes of entry and exit, the roll surfaces and the lateral surfaces $y = \pm w(x)$, where $w(x)$ is a width function to be determined subject to the condition $w(0) = w1$.

Additionally, h is a function of x and $h(x=0) = h1$. U is related to the billet entrance velocity through the condition of constancy of volume flow rate.

It is readily seen that the velocity components given by equation 4.1. satisfy the condition of incompressibility,

$$\dot{\varepsilon}_x + \dot{\varepsilon}_y + \dot{\varepsilon}_z = 0 \qquad \ldots\ldots\ldots\ldots\ 4.2$$

where,

$$\dot{\varepsilon}_x = \frac{\partial v_x}{\partial x} \quad , \quad \dot{\varepsilon}_y = \frac{\partial v_y}{\partial y} \quad , \quad \dot{\varepsilon}_z = \frac{\partial v_z}{\partial z} \qquad \ldots\ldots\ 4.3$$

Substituting (4.1) into (4.3),

$$\dot{\varepsilon}_x = \frac{\partial}{\partial x}\ \frac{U}{h\ w(x)} = \frac{-U}{h\ w(x)}\left\{\frac{h'}{h} + \frac{w'(x)}{w(x)}\right\} \qquad \ldots\ldots\ 4.4a$$

$$\dot{\varepsilon}_y = \frac{\partial}{\partial y}\left\{U\,\frac{y}{h}\,\frac{w'(x)}{(w(x))^2}\right\} = U\left\{\frac{w'(x)}{h\,(w(x))^2}\right\} \qquad \ldots\ldots\ldots\ 4.4b$$

$$\dot{\varepsilon}_z = \frac{\partial}{\partial z}\left\{U \frac{z}{w(x)} \frac{h'}{h}\right\} = U\left\{\frac{h'}{h^2 w(x)}\right\} \quad \ldots\ldots\ldots \quad 4.4c$$

where prime denotes differentiation with respect to x.

Substituting (4.4) into (4.2),

$$\dot{\varepsilon}_x + \dot{\varepsilon}_y + \dot{\varepsilon}_z = -\frac{U\,h'}{h^2 w(x)} - \frac{U\,w'(x)}{h\,(w(x))^2} + \frac{U\,w'(x)}{h\,(w(x))^2} + \frac{U\,h'}{h^2 w(x)} = 0$$

Thus the condition of incompressibility is satisfied.

From the velocity components given in equation 4.1, the strain rate components are obtained as,

$$\dot{\varepsilon}_x = \frac{\partial v_x}{\partial x} = \frac{-U}{h\,w(x)}\left\{\frac{h'}{h} + \frac{w'(x)}{w(x)}\right\} \quad \ldots\ldots\ldots \quad 4.5a$$

$$\dot{\varepsilon}_y = \frac{\partial v_y}{\partial y} = U\left\{\frac{w'(x)}{h\,(w(x))^2}\right\} \quad \ldots\ldots\ldots\ldots\ldots \quad 4.5b$$

$$\dot{\varepsilon}_z = \frac{\partial v_z}{\partial z} = U\left\{\frac{h'}{h^2 w(x)}\right\} \quad \ldots\ldots\ldots\ldots\ldots \quad 4.5c$$

$$\dot{\gamma}_{xy} = \frac{\partial v_x}{\partial y} + \frac{\partial v_y}{\partial x} = \frac{\partial}{\partial y}\left\{\frac{U}{h\,w(x)}\right\} + \frac{\partial}{\partial x}\left\{U \frac{y}{h} \frac{w'(x)}{w\,(x)}\right\}$$

$$\dot{\gamma}_{xy} = U \frac{y}{h\,w(x)}\left\{\frac{w''(x)}{w(x)} - \frac{w'(x)}{w(x)} \frac{h'}{h} - 2\left(\frac{w'(x)}{w(x)}\right)^2\right\} \quad \ldots \quad 4.5d$$

$$\dot{\gamma}_{yz} = \frac{\partial v_y}{\partial z} + \frac{\partial v_z}{\partial y} = \frac{\partial}{\partial z}\left\{U \frac{y}{h} \frac{w'(x)}{w(x)}\right\} + \frac{\partial}{\partial y}\left\{U \frac{z}{w(x)} \frac{h'}{h}\right\}$$

$$\dot{\gamma}_{yz} = 0 \quad \ldots\ldots\ldots\ldots\ldots \quad 4.5e$$

$$\dot{\gamma}_{zx} = \frac{\partial v_x}{\partial z} + \frac{\partial v_z}{\partial x} = \frac{\partial}{\partial z}\left\{\frac{U}{h\ w(x)}\right\} + \frac{\partial}{\partial x}\left\{U\frac{z}{w(x)}\frac{h'}{h}\right\}$$

$$\dot{\gamma}_{zx} = U\frac{z}{h\ w(x)}\left\{\frac{h''}{h} - \frac{h'}{h}\frac{w'(x)}{w(x)} - 2\left(\frac{h'}{h}\right)^2\right\} \ldots\ldots 4.5f$$

The various work components of a functional are determined to give an estimate of the work done. The functional consists of three components,

a. $\dot{E}p$, the plastic work of deformation.

b. $\dot{E}d$, the work done due to velocity discontinuities at the entry and exit planes.

c. $\dot{E}f$, the frictional work done at the roll/material interface.

4.2.3.1. Plastic Work of Deformation.

The incremental plastic work of deformation or the incremental plastic strain energy per unit volume is given by,

$$\delta Up = \sigma_x \delta\varepsilon_x + \sigma_y \delta\varepsilon_y + \sigma_z \delta\varepsilon_z + \tau_{xy} \delta\varepsilon_{xy} + \tau_{yz} \delta\varepsilon_{yz} + \tau_{zx} \delta\varepsilon_{zx}$$

$$= \bar{\sigma}\ \delta\bar{\varepsilon}$$

$$\text{ie.}\quad Up = \int_{\bar{\varepsilon}_1}^{\bar{\varepsilon}_2} \bar{\sigma}\ d\bar{\varepsilon}$$

The power of deformation is then,

$$\dot{U}p = \frac{dUp}{dt} = \bar{\sigma}\ \dot{\bar{\varepsilon}}$$

The total power of deformation is given by,

$$\dot{E}p = \int_V \bar{\sigma}\ \dot{\bar{\varepsilon}}\ \ dV \quad \ldots\ldots\ldots\ldots\ldots\ldots\ 4.6$$

where the effective or mean yield stress, $\bar{\sigma} = K\,\bar{\varepsilon}^{m}$

and the effective strain rate,

$$\dot{\bar{\varepsilon}} = \sqrt{(2/3)\ \{\ \dot{\varepsilon}_x^2 + \dot{\varepsilon}_y^2 + \dot{\varepsilon}_z^2 + 2\ (\ \dot{\gamma}_{xy}^2 + \dot{\gamma}_{yz}^2 + \dot{\gamma}_{zx}^2\ )\}}$$

ie. $$\dot{\bar{\varepsilon}} = \sqrt{(2/3)\ \{\ \dot{\varepsilon}_x^2 + \dot{\varepsilon}_y^2 + \dot{\varepsilon}_z^2 + 2\ (\ \dot{\gamma}_{xy}^2 + \dot{\gamma}_{zx}^2\ )\}} \quad \ldots\ 4.7$$

4.2.3.2. Work Done Due to Velocity Discontinuites at Entry and Exit Planes.

The work done in shear across a velocity jump is given by,

$$\dot{E}d = \frac{\bar{\sigma}}{\sqrt{3}} \int_{Si} |\Delta v| \Big|_{x=0}\ dSi \ + \frac{\bar{\sigma}}{\sqrt{3}} \int_0^{\frac{w2}{2}} \frac{h2}{2}\ v_y \Big|_{x=L}\ dy \ldots\ 4.8$$

The first term on the RHS of equation 4.8. is the work done at the entry plane,

where $|\Delta v|$ = magnitude of the velocity discontinuity at the entry plane.

$$|\Delta v| = \sqrt{v_y^2 + v_z^2} \quad \ldots\ldots\ldots\ldots\ 4.9$$

and Si = area of entry plane over which the discontinuity acts.

The second term on the RHS of equation 4.8. is the work done at the exit plane.

4.2.3.3. Frictional Work Done at the Roll-Workpiece Interface.

In calculating the frictional work done it is assumed that the frictional stress is constant and equal to k, the yield stress in pure shear. There exists a condition of sticking friction on the whole of the roll-workpiece contact surface, that is,

$$\tau = k = \bar{\sigma} / \sqrt{3} \quad \ldots\ldots\ldots\ldots\ldots\ldots \quad 4.10$$

In this analysis it is assumed there to be no relative movement of the workpiece relative to the roll surface in the y-direction throughout the length of the roll gap. Any spread that takes place is purely by migration of material from the layers below the contact surface. The migration spread will result in a proportion of slipping friction acting in the y-direction in these areas but this is neglected in relation to the magnitude of the sticking friction that acts over the remainder of the contact surface.

However, there will be a relative velocity between the roll and the workpiece in the x-direction given by,

$$Vx_r = \{ Ur \cos\phi - v_x (z = h/2) \} \quad \ldots\ldots\ldots\ldots \quad 4.11$$

The frictional work done is therefore given by,

$$\dot{E}f = \int_{Sc} \frac{\bar{\sigma}}{\sqrt{3}} \; Vx_r \; dSc \quad \ldots\ldots\ldots\ldots\ldots \quad 4.12$$

where Sc = area of roll-workpiece contact surface.

The functional,

$$\dot{\Phi} = \dot{E}p + \dot{E}d + \dot{E}f \quad \ldots\ldots\ldots\ldots\ldots\ldots \quad 4.13$$

Hence, from equations 4.6, 4.9 and 4.12,

$$\dot{\Phi} = 4 \int_V \bar{\sigma} \, \dot{\bar{\epsilon}} \; dV + 4 \int_{Si} \frac{\bar{\sigma}}{\sqrt{3}} \sqrt{v_y^2 + v_z^2} \; dSi + \ldots.$$

$$\ldots. + 4 \int_0^{\frac{w2}{2}} \frac{\bar{\sigma}}{\sqrt{3}} \; \frac{h2}{2} \, v_y \Big|_{x=L} dy + 4 \int_{Sc} \frac{\bar{\sigma}}{\sqrt{3}} \; Vx_r \; dSc$$

Thus,

$$\dot{\Phi} = 4 \int_{x=0}^{L} \int_{y=0}^{\frac{w}{2}} \int_{z=0}^{\frac{h}{2}} \bar{\sigma} \, \dot{\bar{\epsilon}} \; dx \, dy \, dz + 4 \int_{y=0}^{\frac{w1}{2}} \int_{z=0}^{\frac{h1}{2}} \frac{\bar{\sigma}}{\sqrt{3}} \sqrt{v_y^2 + v_z^2} \; dy \, dz +$$

$$+ 4 \int_{y=0}^{\frac{w2}{2}} \frac{\bar{\sigma}}{\sqrt{3}} \; \frac{h2}{2} \, v_y \Big|_{x=L} dy + 4 \int_{x=0}^{L} \int_{y=0}^{\frac{w}{2}} \frac{\bar{\sigma}}{\sqrt{3}} \{ Ur \cos\phi - v_x \} \; dx \, dy$$

$$\ldots\ldots\ldots\ldots \quad 4.14$$

This is evidently a complex formula containing the unknown function w, the width of the billet at any point

along the length of the deformation zone. The solution of w will define the steady state deformation.

4.2.4. Method of Solution.

In previous applications of the variational principle to metal deformation problems, the problem was solved by minimization of a functional such that the solution, $\phi(x)$ which minimized the functional Φ for a given w(x) would be equal to w(x).

Oh and Kobayashi (93) used the Ritz approximation (94) by assuming the functions w(x) and $\phi(x)$ to take the form of third order polynomials containing unknown coefficients. The problem was reduced to the solution of three extremely complex simultaneous algebraic equations.

In this analysis the width function w(x) is assumed to take the form of a third order polynomial with coefficients determined from experimental data on width spread.

Square section lead billets were rolled in single passes according to the experimental programme outlined in Section 7.1.3.1. and were measured according to the convention detailed in Figure 7.5. From these measurements a third order polynomial of the following form was fitted to the data to describe the width spread for one quarter of the billet section emerging from the roll gap,

$$w(i) = w1 + 2a1 + 2a2\ h(i) + 2a3\ (h(i)^2) + 2a4\ (h(i)^3) \quad \ldots 4.15$$

In describing the width spread as the billet progresses along the length of the roll gap, the polynomial takes the form,

$$w(i) = w1 + 2\sqrt{x/L}\ \{a1 + a2\ h(i) + a3\ (h(i)^2) + a4\ (h(i)^3)\} \quad \ldots\ 4.16$$

where L = horizontal projection of the length of the arc of contact

and x = length measured from the entry plane.

By assuming the spread to take the form described by equation 4.16, the spread of the billet from x=0 to x=L takes the form of a parabolic arc as illustrated in Figure 4.2. For each rolling trial, a polynomial was fitted to the billet measurements h and w to obtain the coefficients a1, a2, a3 and a4 for rolling geometries in the range $0.6538 \leq Hm/L \leq 2.4142$.

Examination of the coefficients determined that a2 could effectively be set to zero with little difference in rolled shape and that the coefficients could be generalized according to the Hm/L ratio for a particular rolling geometry and rolled shape.

The coefficients according to the rolling geometry are,

for $0.6538 \leq Hm/L \leq 0.9257$

$$a1 = 0.25324$$

$$a3 = -1.25792$$

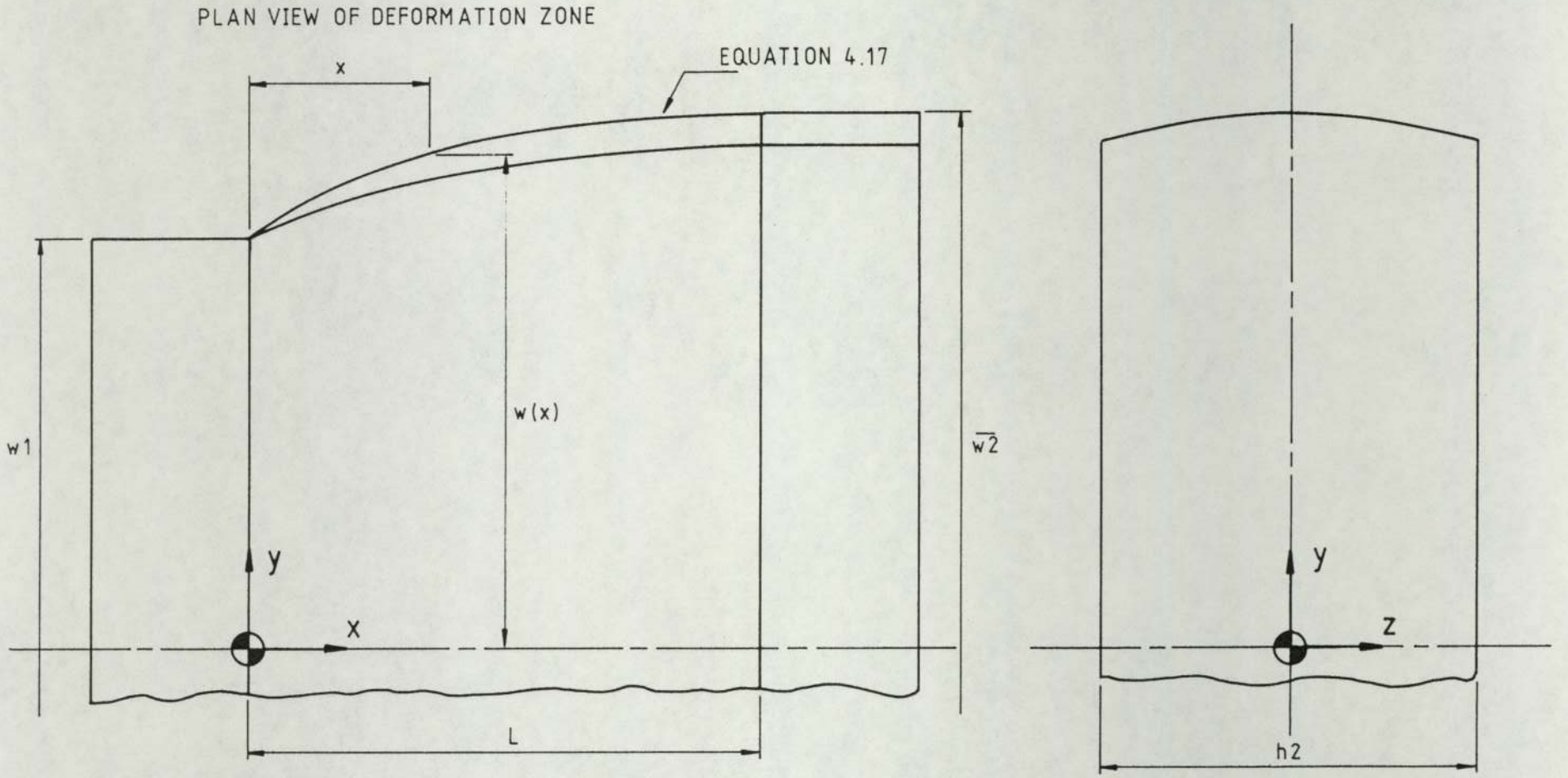

FIG. 4.2.

DEFORMATION ZONE ACCORDING TO EQUATION 4.17.

$$a4 = 1.34251$$

for $0.9257 \leq Hm/L \leq 1.4419$

$$a1 = 0.12114$$

$$a3 = -0.16961$$

$$a4 = 0.00133$$

for $1.4419 \leq Hm/L \leq 2.4142$

$$a1 = 0.04048$$

$$a3 = 0.12269$$

$$a4 = -0.14650$$

and the width function is given as,

$$w(i) = w1 + 2\sqrt{x/L}\ \{a1 + a3\ (h(i)^2) + a4\ (h(i)^3)\} \quad \ldots\ 4.17$$

Having specified the width function using equation 4.17 and the appropriate coefficents a1, a3 and a4, the function may be substituted directly into equations 4.1. to determine the velocity field, equations 4.5 to determine the strain rate fields and equation 4.14 to determine the total work done on the material.

The work done may be equated to the input work per revolution of the rolls to obtain the torque required, assuming the motor is 100% efficient.

$$\frac{2\ \pi\ N\ T}{60} = \Phi \quad \ldots\ 4.18$$

where N = roll speed (rev/min)

T = rolling torque

Analysis and results of the theoretical calculation are given in Appendix J.

4.3. Analysis of Void Closure.*

4.3.1. Assumptions

a. The void is at the billet centre, is circular in cross section and symmetrical about the billet horizontal and vertical axes.

b. In general, voids may be randomly distributed throughout the central 10% by area of the billet cross section. The complement of these voids is represented by one single void, its situation defined in (a).

c. Deformation is non-homogeneous so there will be void volume reduction.

d. When the void has been eliminated, voids that may have been situated at distances from the billet centre will have been eliminated also.

4.3.2. Void Model.

Due to symmetry, the analysis is confined to one quarter of the billet cross section in the y-z plane, as shown in Figure 4.3(a).

According to solution A, Figure 4.3(b), the void height

* Footnote:
This analysis is that of Ståhlberg.U, Melander.A, Keife.H and Lundberg.M. (ref.153), ammended simply by the assumption of a difference in initial void geometry, the latter having a minor effect on the outcome of

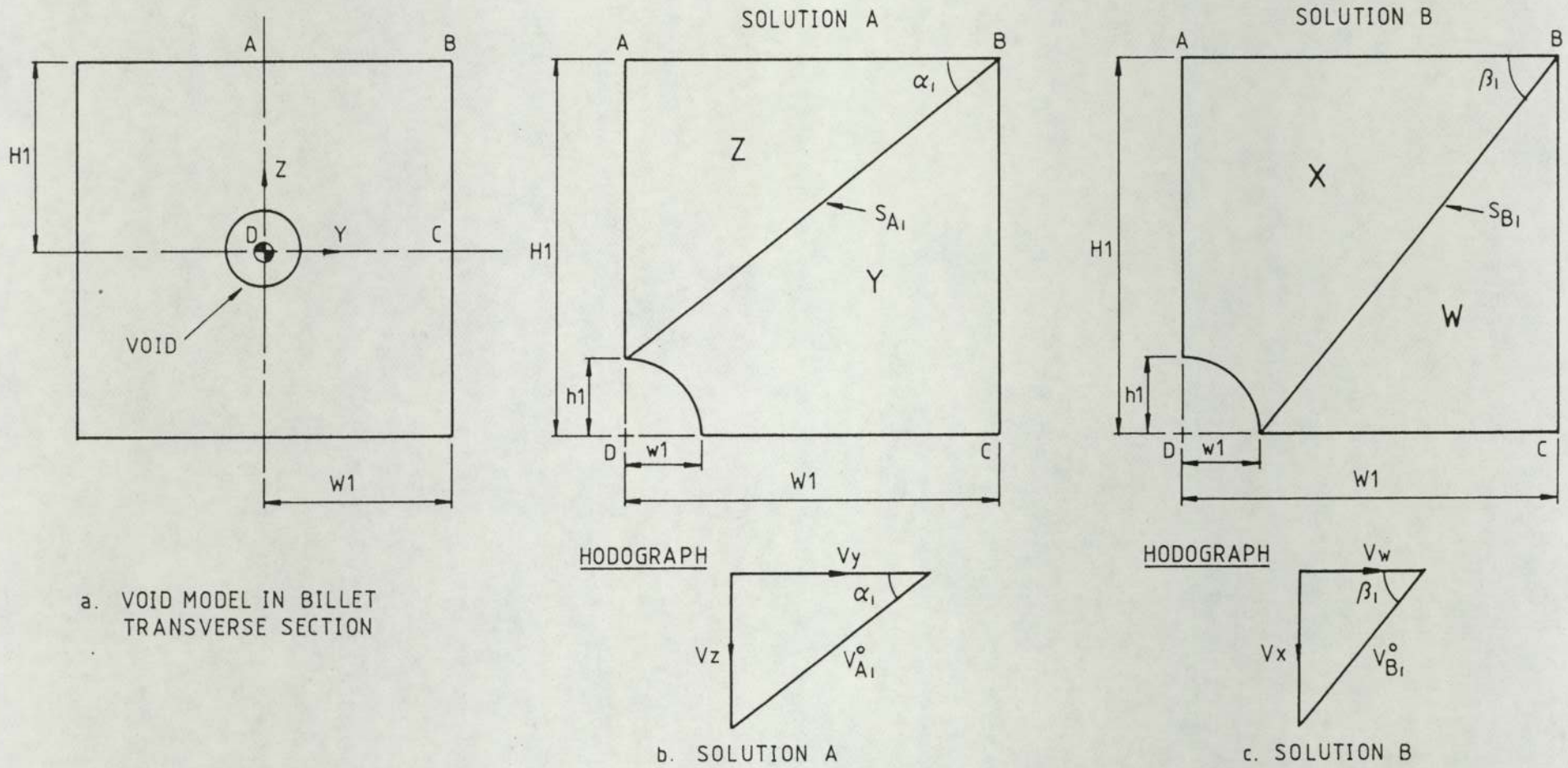

a. VOID MODEL IN BILLET TRANSVERSE SECTION

b. SOLUTION A

c. SOLUTION B

FIG. 4.3.

VOID MODEL AND SOLUTIONS FOR DEFORMATION.

decreases in the direction of the applied stress as all particles on the void surface move outwards in the y-direction.

According to solution B, Figure 4.3(c), the void height decreases in the direction of the applied stress while the void width remains constant.

To determine which solution is the best at the start of deformation, the rates of energy dissipation for the two solutions may be equated. At the start of deformation solution A will be better than solution B if,

$$\dot{W}_{A1} < \dot{W}_{B1} \quad \ldots\ldots\ldots\ldots\ldots\ldots \quad 4.19$$

$$\text{ie. } k\, V^{\circ}_{A1}\, S_{A1} < k\, V^{\circ}_{B1}\, S_{B1} \quad \ldots\ldots\ldots\ldots \quad 4.20$$

from the geometry of Figures 4.3(b) and 4.3(c),

$$V^{\circ}_{A1} = Vz\ S_{A1} / (H1-h1) \quad \ldots\ldots\ldots\ldots\ldots\ldots \quad 4.21$$

$$V^{\circ}_{B1} = Vx\ S_{B1} / H1 \quad \ldots\ldots\ldots\ldots\ldots\ldots \quad 4.22$$

$$S^{2}_{A1} = (H1-h1)^2 + W1^2 \quad \ldots\ldots\ldots\ldots\ldots\ldots \quad 4.23$$

$$S^{2}_{B1} = H1^2 + (W1-w1)^2 \quad \ldots\ldots\ldots\ldots\ldots\ldots \quad 4.24$$

$$H1-h1 = W1-w1 \quad \ldots\ldots\ldots\ldots\ldots\ldots\ldots\ldots \quad 4.25$$

$$Vz = Vx \quad , \quad W1 = H1 \quad , \quad w1 = h1 \quad \ldots\ldots\ldots \quad 4.26$$

Substitution into equation 4.20,

$$Vz \frac{(H1-h1)^2 + W1^2}{H1-h1} < Vx \frac{H1^2 + (W1-w1)^2}{H1} \quad \ldots\ldots 4.27$$

and since Vz = Vx (the vertical velocity),

$$\frac{(H1-h1)^2 + H1^2}{H1-h1} < \frac{H1^2 + (H1-h1)^2}{H1}$$

$$\text{ie.} \qquad h1 > 0 \quad \ldots\ldots\ldots\ldots\ldots\ldots 4.28$$

This inequality is always satisfied and therefore solution A is better than solution B at the onset of the deformation.

It is now necessary to determine whether solution A is still more satisfactory than solution B after some increment of deformation, as shown in Figure 4.4.

In this case the two solutions must have the same rate of energy dissipation at some stage,

$$\dot{W}_A = \dot{W}_B$$

$$\text{ie.} \qquad V_A^\circ \; S_A = V_B^\circ \; S_B \quad \ldots\ldots\ldots\ldots\ldots\ldots 4.29$$

Equation 4.27 is not restricted to the initial stages of deformation and hence for this case it may be written,

$$\frac{(H-h)^2 + W^2}{H-h} = \frac{H^2 + (W-w)^2}{H} \quad \ldots\ldots\ldots\ldots 4.30$$

A feature of solution A is that (H-h) and (W-w) remain constant.

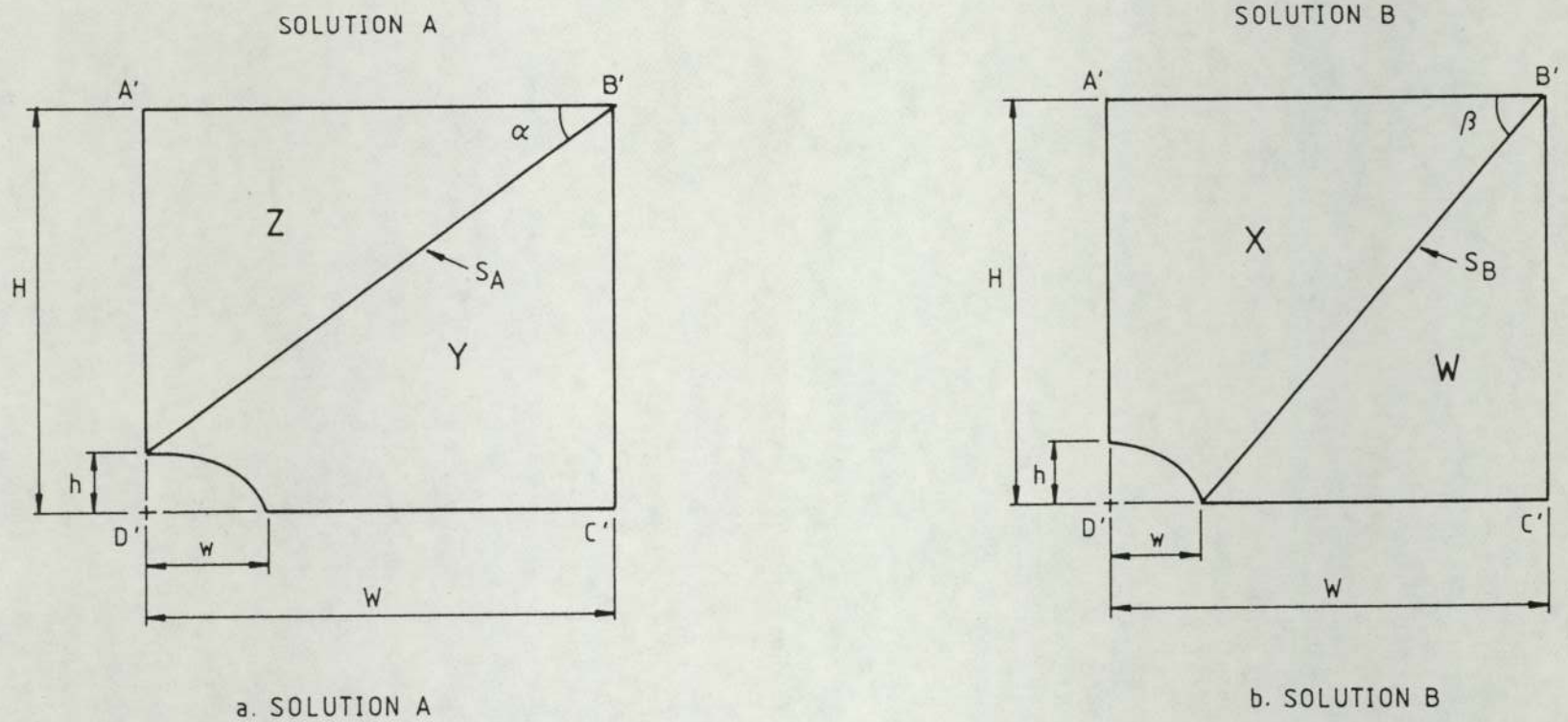

a. SOLUTION A

b. SOLUTION B

FIG. 4.4.

SOLUTION TO VOID MODEL AFTER SOME INCREMENT OF REDUCTION.

Consequently,

$$(W-w) = (W1-w1)$$

and $$(H-h) = (H1-h1)$$

Since, at the start of the deformation $(H1-h1) = (W1-w1)$, we can write down that $(W-w) = (H-h)$.

A feature of solution B is that w remains constant. Consequently $w = w1$.

Hence, from equation 4.30,

$$\frac{(H-h)^2 + (H-h+h)^2}{H-h} = \frac{H^2 + (H-h)^2}{H} \quad \ldots\ldots 4.31$$

ie. $$h = 0 \quad \ldots\ldots\ldots\ldots\ldots\ldots 4.32$$

This equality is not satisfied until the moment of void closure and consequently solution A is better than solution B after some increment of deformation. Solution A is therefore valid for the whole process of void closure.

In order for void closure to take place, the deformation should not be homogeneous. If the deformation at the start is homogeneous, then the rate of energy dissipation for solution A, the preferred solution, can be written as,

$$\dot{W}_{H_A} = 2\,k\,W1\,Vz \quad \ldots\ldots\ldots\ldots\ldots 4.33$$

where $k = Y/\sqrt{3}$, the yield stress in uniaxial compression.

In his analysis of ductile fracture, Thomason (138) deduced a criterion for uniform/homogeneous and non-uniform flow when describing the mechanism of internal necking of cavities.

In order that the deformation is not homogeneous,

$$k\, V^{\circ}_{A1}\, S_{A1} < 2\, k\, W1\, Vz$$

$$V^{\circ}_{A1}\, S_{A1} < 2\, W1\, Vz \quad \ldots\ldots\ldots\ldots\ldots\ldots \quad 4.34$$

using equations 4.21 and 4.23 we can write,

$$Vz\, \frac{(H1-h1)^2 + W1^2}{H1-h1} < 2\, W1\, Vz \quad \ldots\ldots\ldots\ldots \quad 4.35$$

At the start of deformation,

$$\frac{(H1-h1)^2 + H1^2}{H1-h1} < 2\, H1$$

$$2\, H1^2 - 2\, H1\, h1 + h1^2 < 2\, H1^2 - 2\, H1\, h1$$

$$\text{ie.} \qquad h1^2 < 0 \quad \ldots\ldots\ldots\ldots\ldots\ldots \quad 4.36$$

This inequality is never satisfied and consequently deformation at the start of the deformation will be homogeneous.

It is now necessary to determine whether deformation is homogeneous after some increment of deformation.

In this case,

$$V_A^{\circ} \; S_A = 2 \, W \, Vz \quad \ldots\ldots\ldots\ldots\ldots\ldots \quad 4.37$$

using equations 4.21 and 4.23 we can write,

$$V_A^{\circ} \; S_A = Vz \; \frac{(H-h)^2 + W^2}{H-h} \quad \ldots\ldots \; \ldots\ldots\ldots\ldots \quad 4.38$$

Substituting equation 4.38 into 4.37,

$$\frac{(W-w)^2 + W^2}{W-w} = 2 \, W$$

$$2 \, W^2 - 2 \, W \, w + w^2 = 2 \, W^2 - 2 \, W \, w$$

$$\text{ie.} \qquad w^2 = 0 \quad \ldots\ldots\ldots\ldots\ldots\ldots \quad 4.39$$

This equality is never satisfied since the void is always being elongated. Therefore homogeneous deformation does not take place after the start of deformation.

From this analysis it is concluded that solution A presents the most suitable model for closure of a circular void at the billet centre.

4.3.3. Reduction Required for Void Closure.

The reduction is determined under the assumption that material flow and subsequent void closure is independent of the rolling direction (x-direction). Consequently, the deformation model is reduced to the consideration of flow

in the (y,z) coordinate system (Figure 4.3.).

According to the upper bound solution A as defined above, the reduction necessary for the closure of the void is,

$$r_c = \frac{h1}{H1} \quad \ldots\ldots\ldots\ldots\ldots\ldots\ldots \quad 4.40$$

The reduction can be expressed as an equation containing the area fraction of voids. If we assume the circular void to deform into an elliptical shape as shown in Figure 4.4, then,

$$Vf = \frac{\pi\ h\ w}{4\ H\ W} \quad \ldots\ldots\ldots\ldots\ldots\ldots\ldots \quad 4.41$$

From the geometry of the upper bound solution,

$$H = H1 - H1\ r \quad \ldots\ldots\ldots\ldots\ldots\ldots\ldots \quad 4.42$$

$$h = h1 - H1\ r \quad \ldots\ldots\ldots\ldots\ldots\ldots\ldots \quad 4.43$$

$$w = 2\ h1 - h \quad \ldots\ldots\ldots\ldots\ldots\ldots\ldots \quad 4.44$$

combining equations 4.43 and 4.44,

$$w = 2\ h1 - h1 + H1\ r$$

$$w = h1 + H1\ r \quad \ldots\ldots\ldots\ldots\ldots\ldots\ldots \quad 4.45$$

$$W - w = H - h = H1 - h1$$

ie. $W = H1 - h1 + w = H1 - h1 + h1 + H1\ r$

Hence,

$$W = H1 + H1\ r \qquad \ldots\ldots\ldots\ldots\ldots\ldots \quad 4.46$$

Substituting into (4.41),

$$Vf = \frac{\pi}{4} \frac{(h1-H1\ r)}{(H1-H1\ r)} \frac{(h1+H1\ r)}{(H1+H1\ r)}$$

$$Vf = \frac{\pi}{4} \frac{\{(h1/H1)^2 - r^2\}}{1 - r^2} \qquad \ldots\ldots\ldots\ldots \quad 4.47$$

The void area fraction at the start of the deformation is,

$$Vf_i = \frac{\pi}{4} (h1/H1)^2$$

Consequently, equation 4.47 can be re-written as,

$$Vf = \frac{Vf_i - (\pi/4)\ r^2}{1 - r^2} \qquad \ldots\ldots\ldots\ldots \quad 4.48$$

If Vf is set to zero the expression for the reduction required for void closure is obtained as,

$$r_c = 2\sqrt{\frac{Vf}{\pi}} \qquad \ldots\ldots\ldots\ldots\ldots\ldots \quad 4.49$$

CHAPTER FIVE

DESCRIPTION OF EXPERIMENTAL EQUIPMENT

5.1. The Experimental Rolling Mill.

5.1.1. Description of the Mill.

The rolling mill used in the present work was built at Aston University for research work by Quasier (139) and was subsequently modified for work at a later date by Afonja (140).

The mill consists of a four column frame able to accomodate rolls supported in bearing blocks that are a sliding fit in the frame. The rolls are supported in the bearing blocks by double taper roller bearings. The drive side bearing blocks were located axially in the frame while the bearing blocks on the open side of the frame were floating.

The mill could be used as a two-high or four-high unit by the use of smaller diameter friction driven work rolls supported by needle roller bearings in blocks that were a sliding fit between the back-up roll bearing blocks, although in the present work only the two-high set-up was used.

The mill rolls were driven by a 5.6 kW variable speed electric motor giving a speed range of 6 to 54 rpm. The drive to the mill was divided by a Hille 25 pinion gearbox through two double helical 1:1 ratio gears and the final drive was transmitted to the rolls through Hardy Spicer universal shafts. Figures 5.1. and 5.2. show the arrangement of the experimental mill for two-high rolling.

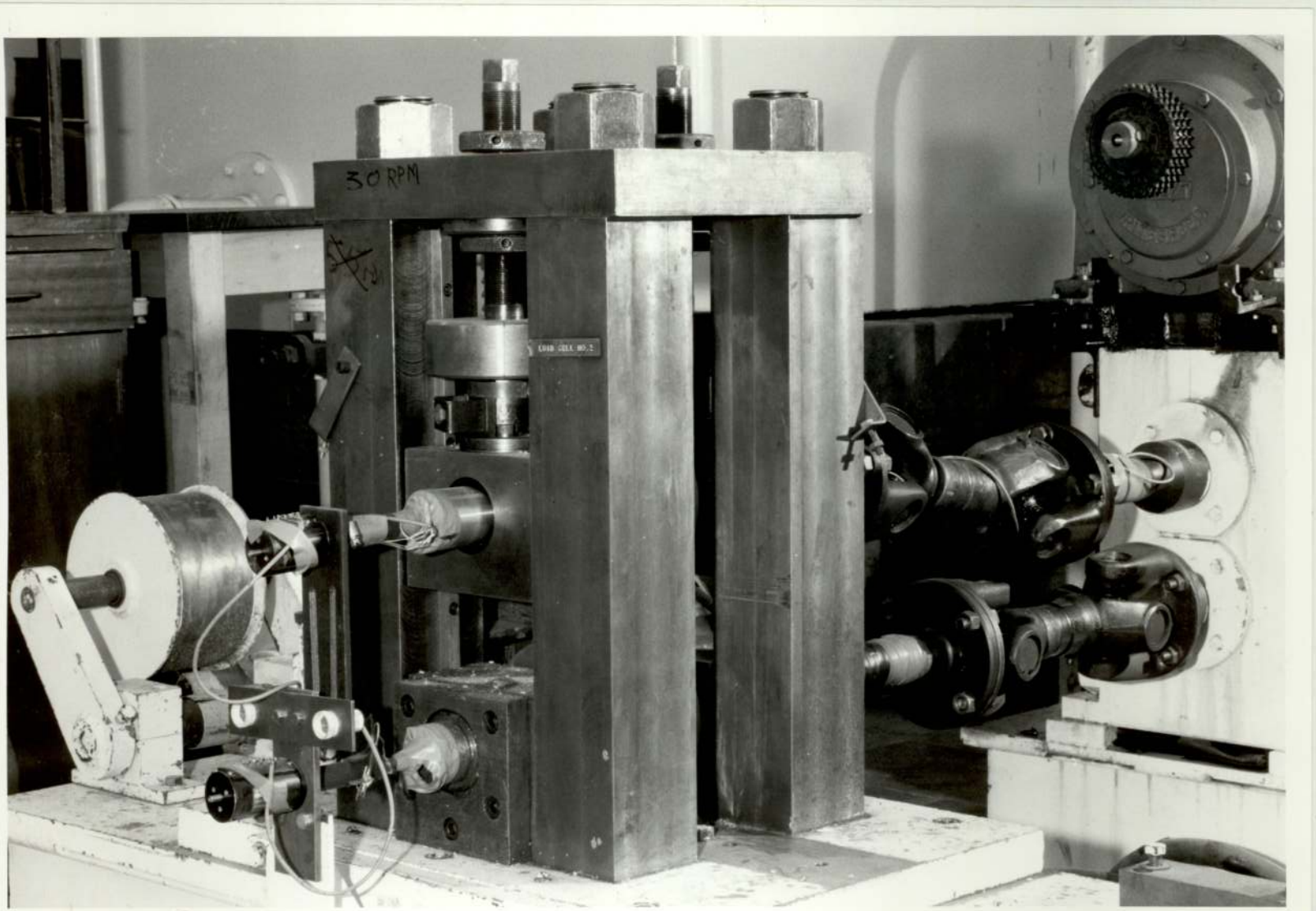

FIG. 5.1. THE EXPERIMENTAL ROLLING MILL.

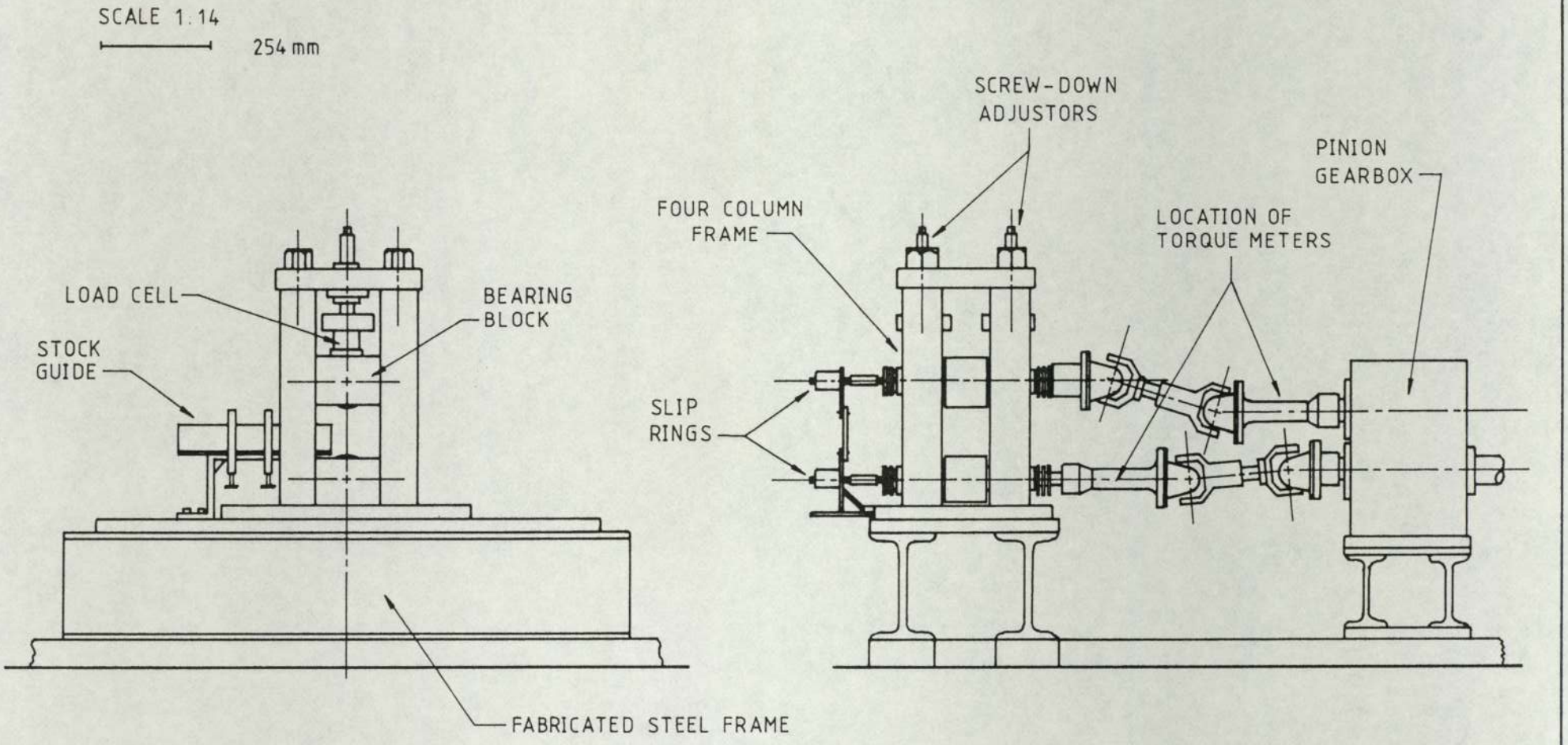

FIG.5.2. DESIGN OF TWO-HIGH EXPERIMENTAL ROLLING MILL.

The upper mill assembly can be adjusted vertically by means of screw-down adjusters on the frame top plate and accurate setting of the roll gap is achieved by applying a pre-load to spacer blocks located between the upper and lower bearing blocks.

Roll separating force is measured by two strain gauge load cells mounted between the upper bearing blocks and the screw-down adjusters. Roll torque is detected by strain gauge torque meters installed on the periphery of the roll drive coupling shafts.

5.1.2. Roll Specification.

Initially the geometry of the rolls used in this work was as follows:

149 mm nominal diameter work rolls.
817 M 40 steel (EN24 steel, British Standard 970, 1955).

Chemical specification:

0.36-0.44% C	0.50-0.70% Mn	0.10-0.35% Si
1.00-1.40% Cr	0.20-0.35% Mo	1.30-1.70% Ni
0.05% S	0.05% P	

Hardened and tempered to 50 Rockwell C Scale.

Roll barrel surface finish:

Top roll (as installed in mill)	0.00667 micron CLA.
Bottom roll (as installed in mill)	0.01096 micron CLA.

After shot blasting, (Section 7.2.1.), the surface finishes of the rolls were:

Top roll (as installed in mill)	0.0544 micron CLA.
Bottom roll (as installed in mill)	0.0495 micron CLA.

5.1.3. Recording Equipment and Calibration.

The experimental rolling mill is equiped with strain gauge bridge circuits to measure roll load/separating force and roll torque. The signals from each bridge circuit are displayed in analogue form on a multi-channel u.v. recorder.

Figure 5.3. shows the circuit diagram of the recording equipment.

Eight strain gauges were mounted on each load cell, four circumferentially and four longitudinally giving a bridge output signal of $2(1+\nu)$ times that of a single active gauge. This arrangement could compensate for temperature variation and flexing of the load cell when in service. Foil type torque gauges were bonded to the roll drive coupling shafts, the bridge connecting leads being routed through the centre of each roll and the signal taken out, through a slip ring arrangement, to the recording equipment.

The strain gauge bridges were supplied with a stabilised d.c. voltage, the individual bridge currents being controlled

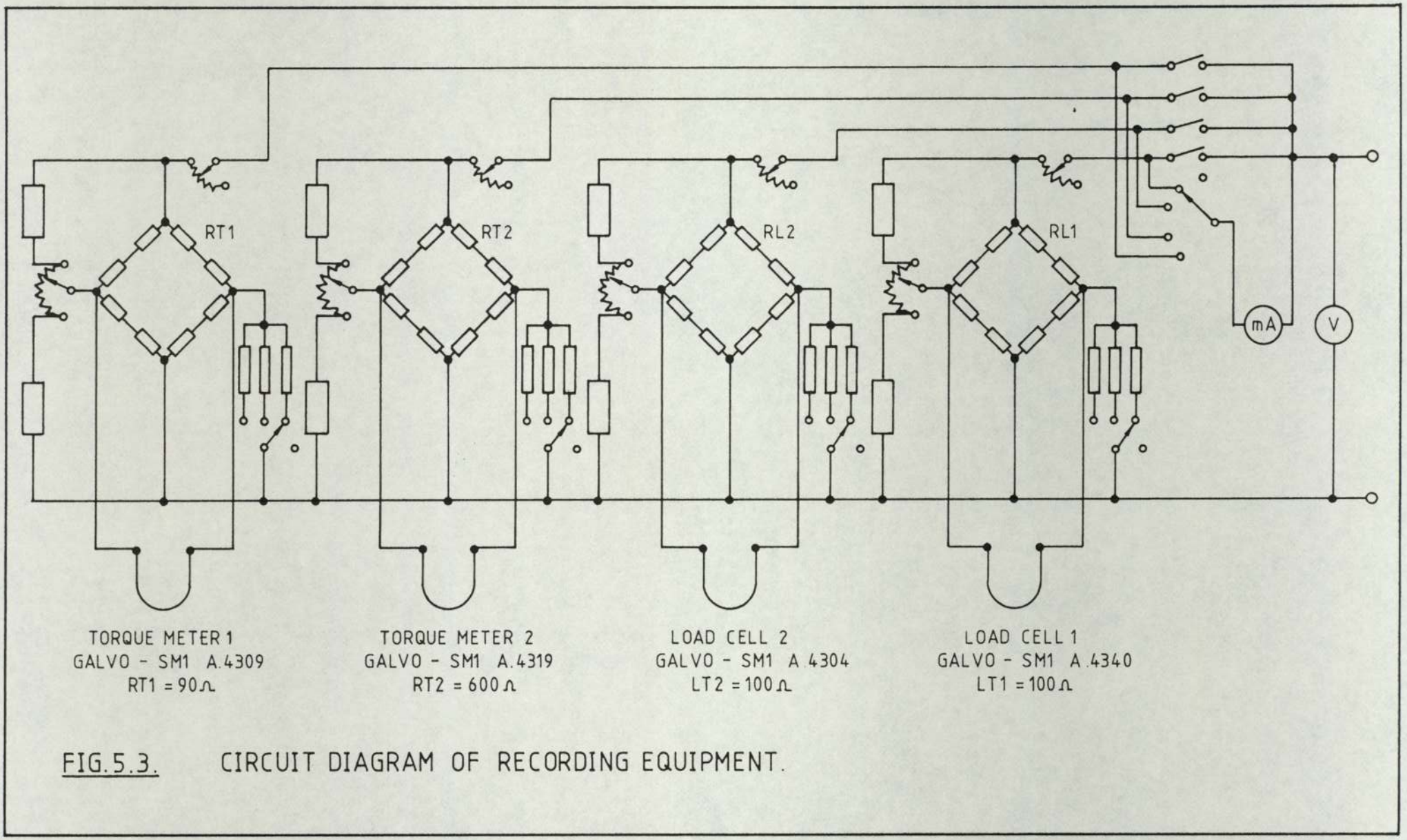

FIG.5.3. CIRCUIT DIAGRAM OF RECORDING EQUIPMENT.

by potentiometers in the recording circuitry.

Calibration resistors to assist in the setting of alternative scales could be switched into each bridge circuit. They could also be switched in at the start of a test to provide a permanant record of the calibration factor used for a particular test.

The load cells were calibrated in an Avery 1000 kN capacity compression testing machine (type 7104 DCJ, No. E62404) and the torque meters in an Avery 1700 N.m capacity torsion testing machine (type 6609 CHG, No. E55703/1).

The calibration procedure is described below.

The bridge output leads were disconnected from the u.v. recorder and the stabilized d.c. power supply set to 20 V. Approximately thirty minutes were allowed for the strain gauge bridge circuits to stabilize.

Each individual bridge circuit was mechanically balanced by adjusting the respective spot galvonometer in the u.v. recorder to a reference point on the displacement scale nominated as zero displacement (zero bridge output). The bridge output leads were reconnected to the u.v. recorder and each individual bridge circuit electrically balanced by adjusting the appropriate potentiometer in the respective bridge circuit to realign the galvonometer spot with the nominated reference point.

Each load cell and torque meter was loaded at various bridge current settings and the values of load and corresponding spot displacement and torque and corresponding spot displacement recorded over the load-unload cycles. For each bridge current setting the calibration resistors were switched in and the spot displacements recorded.

The calibration charts are shown in Figures 5.4, 5.5, 5.6 and 5.7.

5.2. The Steel Rolling Mill.

5.2.1. Description of the Mill.

The three-high rolling mill used in the trials on conventional mould cast and continuously cast steel billets (Section 7.4) is situated at the British Steel Swinden Research Laboratories, Rotherham.

The three-high mill is fitted with rolls having a bullhead pass in the centre of the roll barrel for the rolling of flats and a number of grooved passes on either side for the repeated reduction of rod when the bullhead roll gap is set nominally to zero. The centre of the three rolls is fixed in position, the other two being manually controlled in unison by mechanical d.c. motor drives for the setting of the roll gap with respect to the centre fixed roll.

A bullhead diameter of nominally 300 mm, after dressing

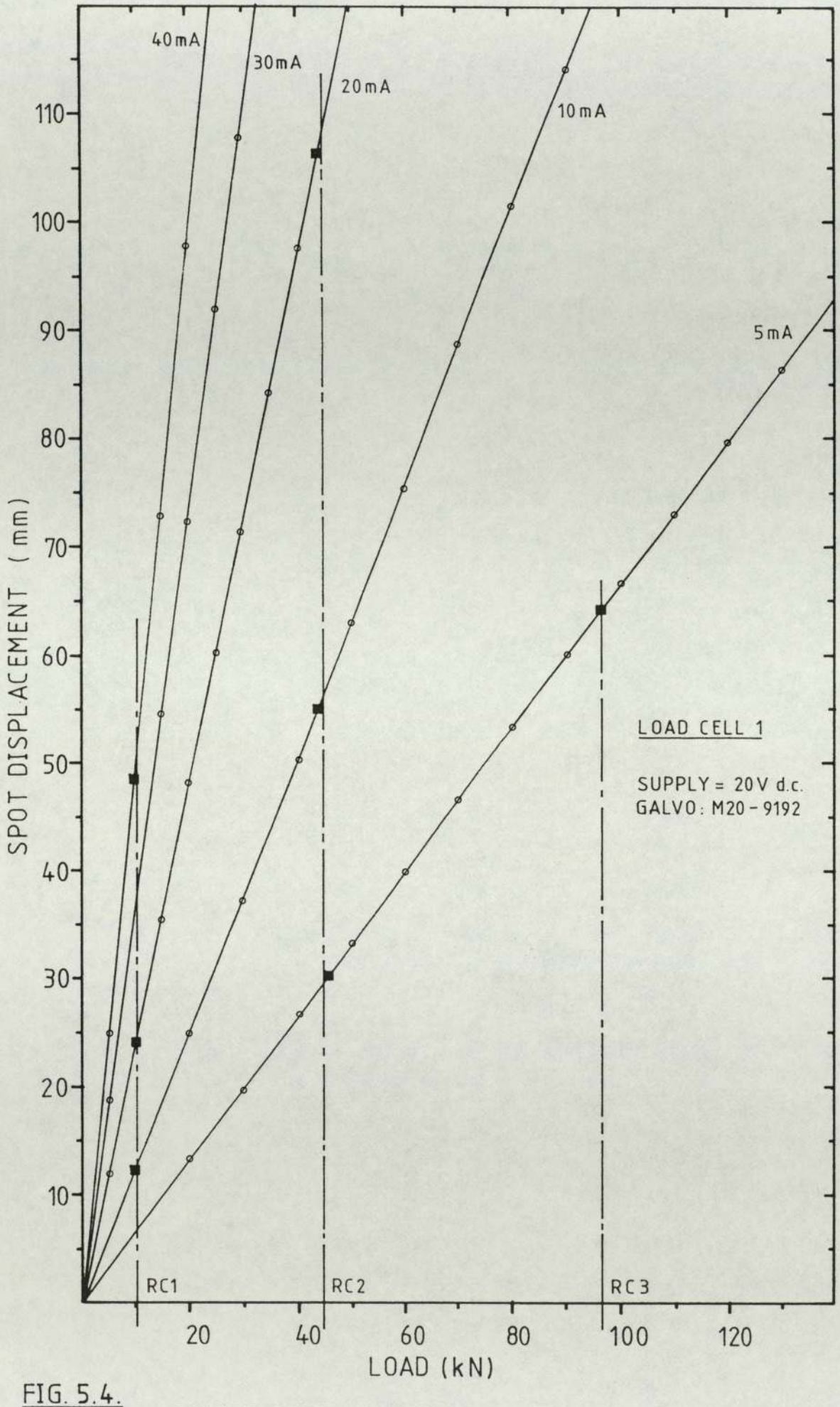

FIG. 5.4.

CALIBRATION CHART LOAD CELL 1.

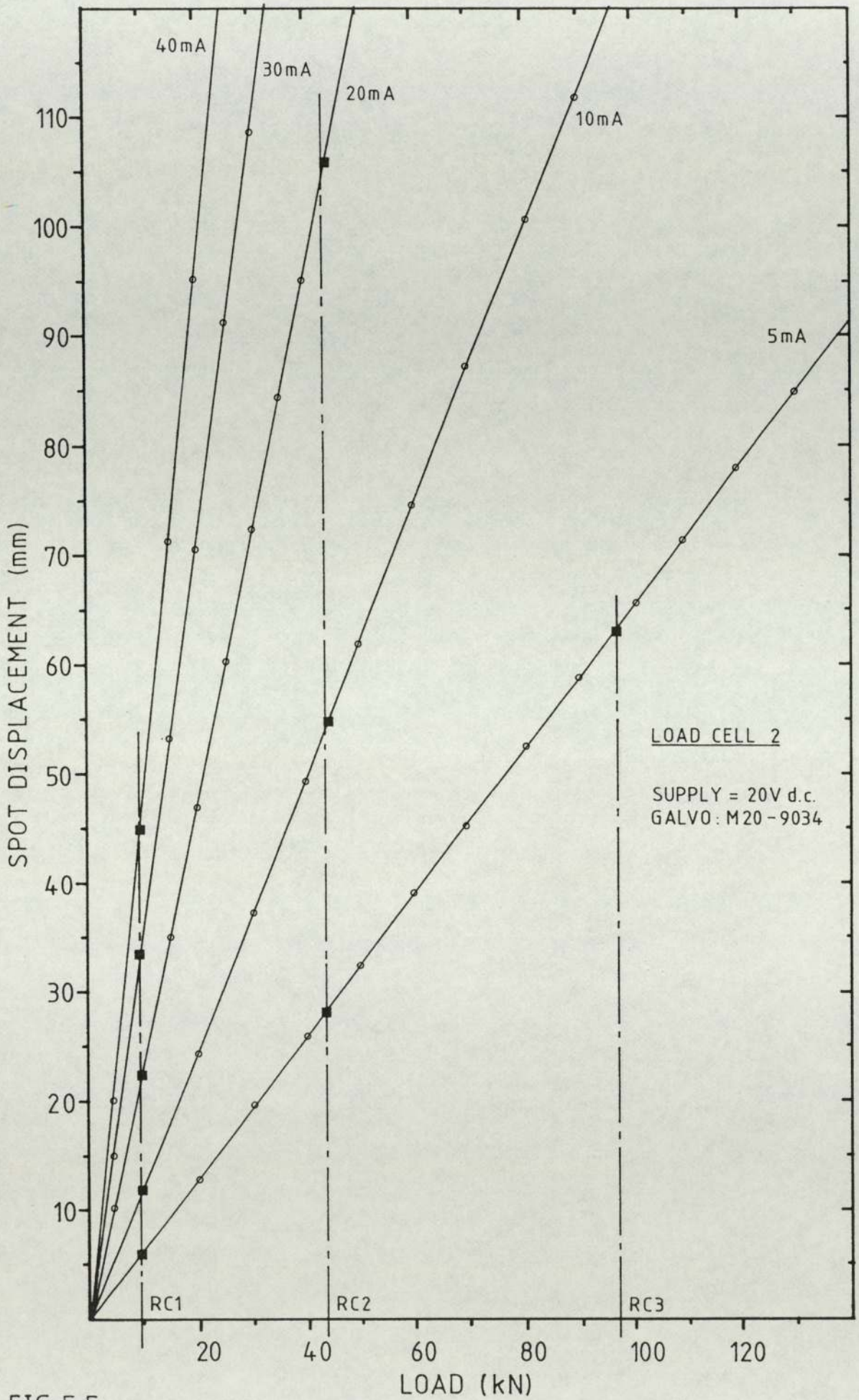

FIG. 5.5.

CALIBRATION CHART LOAD CELL 2.

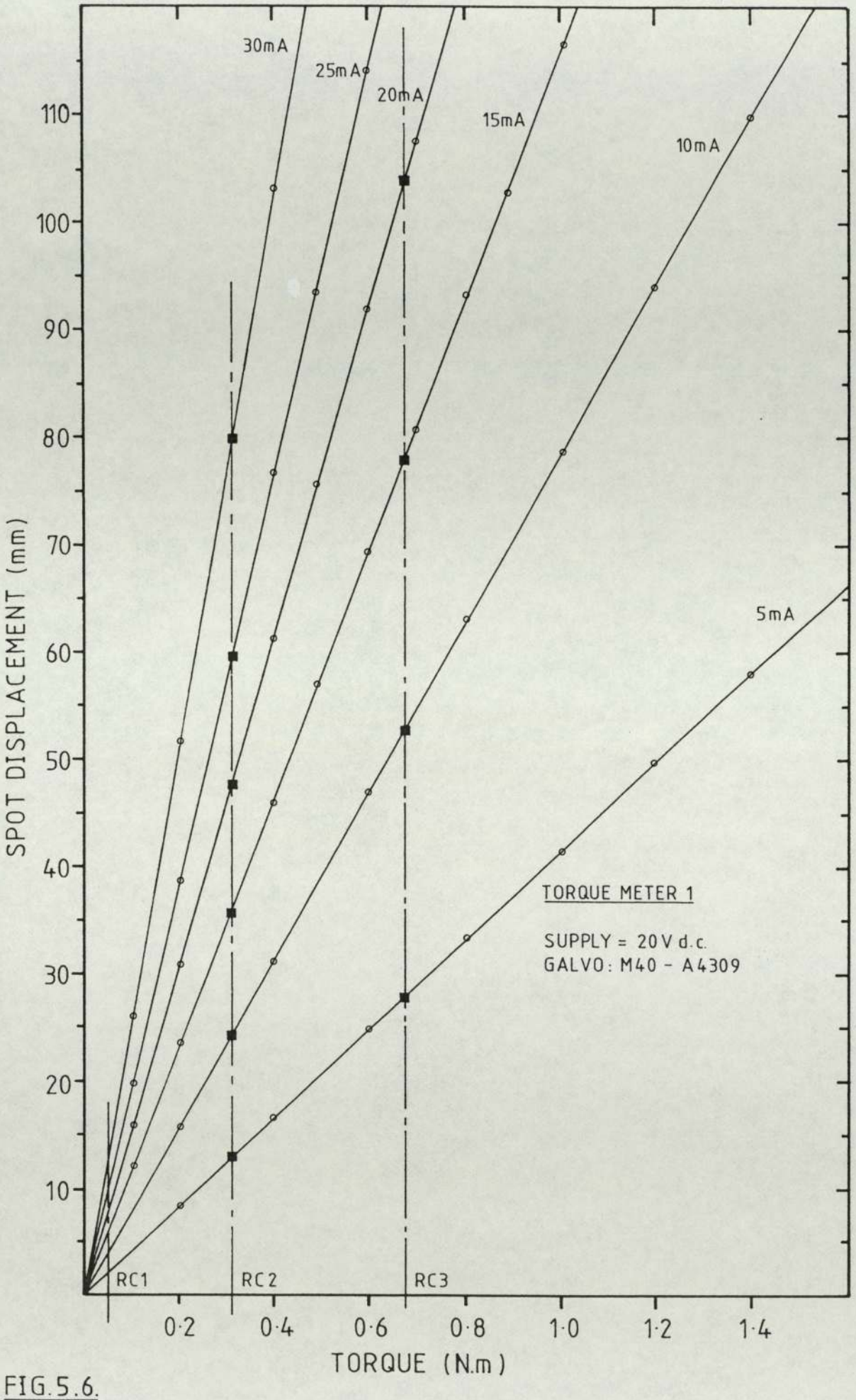

FIG.5.6.

CALIBRATION CHART TORQUE METER 1.

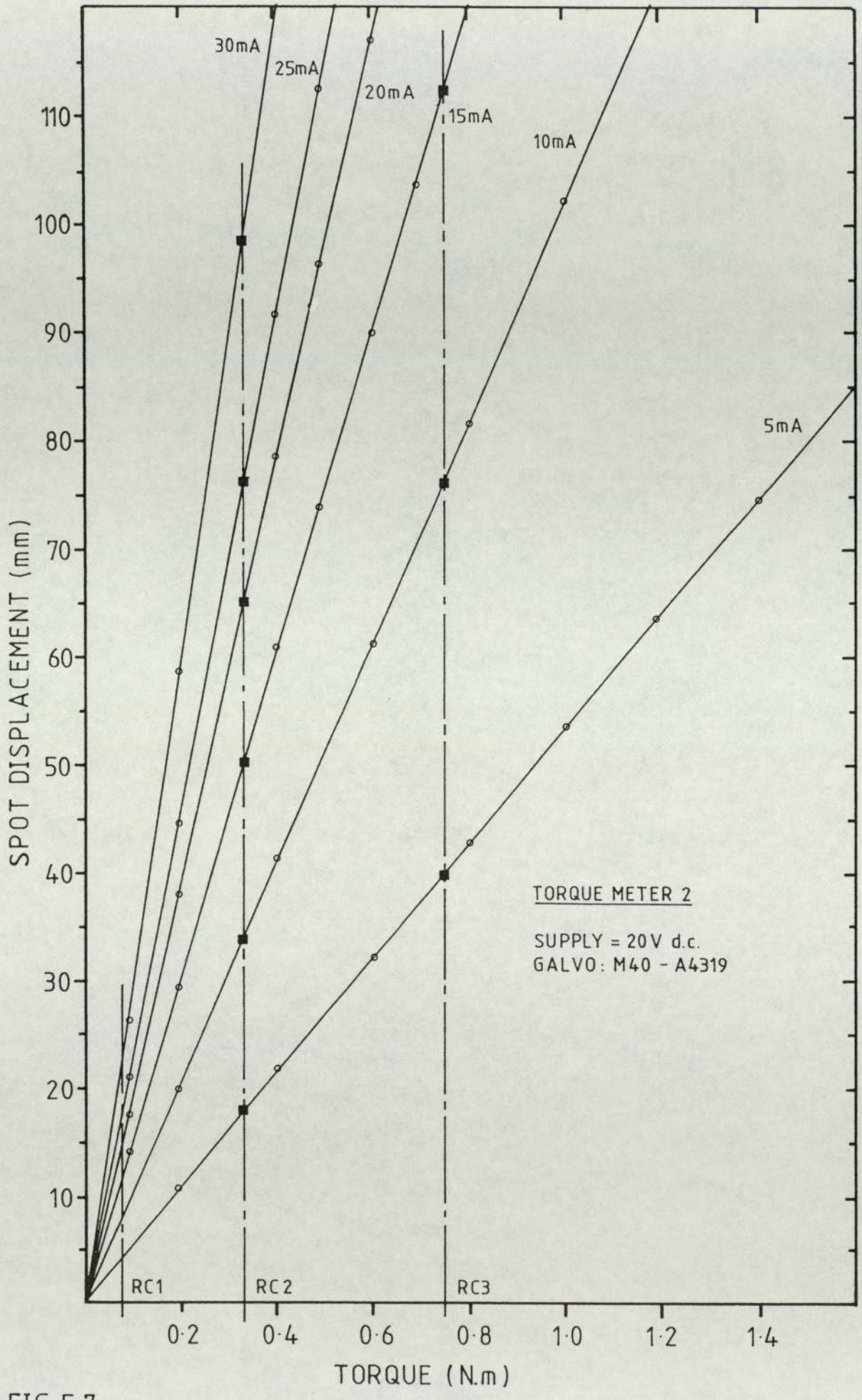

FIG. 5.7

CALIBRATION CHART TORQUE METER 2.

operations, was used in all the tests. The mill is located only a matter of yards from the furnace where the billets used in the test programme were soaked at a temperature of the order of 1320 deg.C. for approximately 50 minutes each.

5.2.2. Load Cell Description and Calibration.

The mill is fitted with two 1 MN load cells installed above the upper roll bearing blocks, one on the drive-side and the other on the non-drive side of the mill.

Each load cell was similar in construction to those used on the Aston University experimental mill, consisting essentially of a central alloy steel column surmounted by a steel bearing pad. The upper surface of the pad is faced with phosphor bronze in the form of a sphere which mated with the end of the mill screw down to give a uniform pressure distribution to the load cell. The cell was covered in a steel casing secured to the base flange and the whole unit was bolted to the mill roll bearing block.

Eight strain gauges, four horizontal and four vertical, were bonded to the central zone of the load cell column, connected together to form a Wheatstone bridge circuit. The gauges were coated in epoxy resin for proofing and connection to the bridge was by a conventional plug and socket arrangement.

The calibration charts for the two load cells are shown

in Figures 5.8. and 5.9. The method of calibration was similair in technique to that described in Section 5.1.3.

Foil type torque gauges were bonded to the centre roll drive coupling shaft. The bridge circuit was powered locally by a d.c. supply and the bridge output routed to the recording equipment by telemetry equipment, the transmitter mounted on the roll shaft.

The torque meter was calibrated to a bridge output of 1V = 5.96 kN.m. The calibration chart is shown in Figure 5.10.

5.2.3. Temperature Measurement.

Since the billet surface temperature was to be measured at three different locations in and around the mill (ex-furnace, pre-roll and post-roll/pre-quench), the temperature measuring equipment had to be portable.

The instrument used was a Minolta-Land Cyclops 33 disappearing filament type hand-held optical pyrometer. For all the tests the emissivity of the steel billets (for setting on the instrument) was assumed to be 0.85, a figure recommended by Land Infrared (141) and used extensively by BSC.

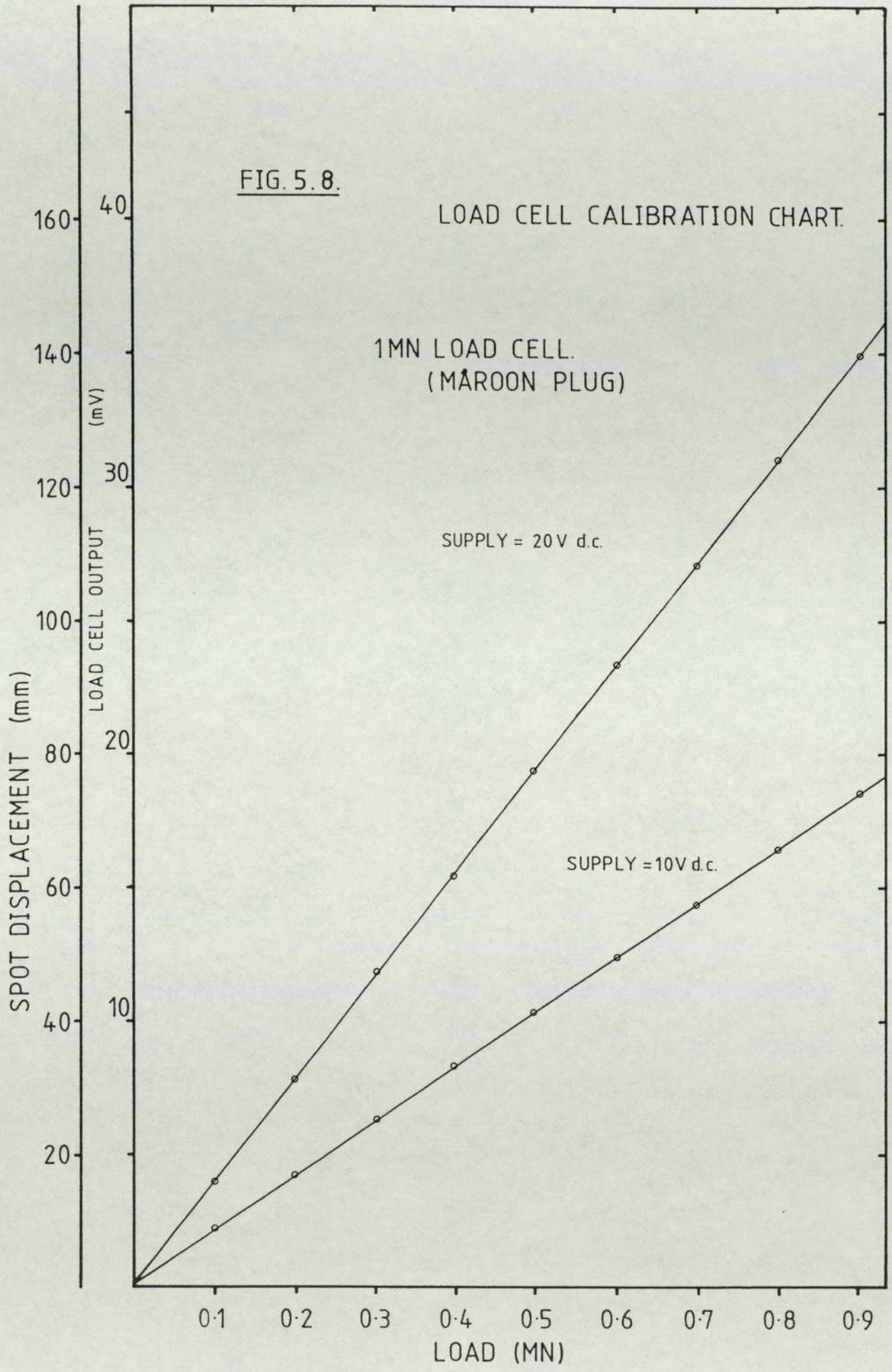
FIG. 5.8.
LOAD CELL CALIBRATION CHART.
1MN LOAD CELL.
(MAROON PLUG)
SUPPLY = 20 V d.c.
SUPPLY = 10V d.c.
SPOT DISPLACEMENT (mm)
LOAD CELL OUTPUT (mV)
160
140
120
100
80
60
40
20
40
30
20
10
0·1
0·2
0·3
0·4
0·5
0·6
0·7
0·8
0·9
LOAD (MN)

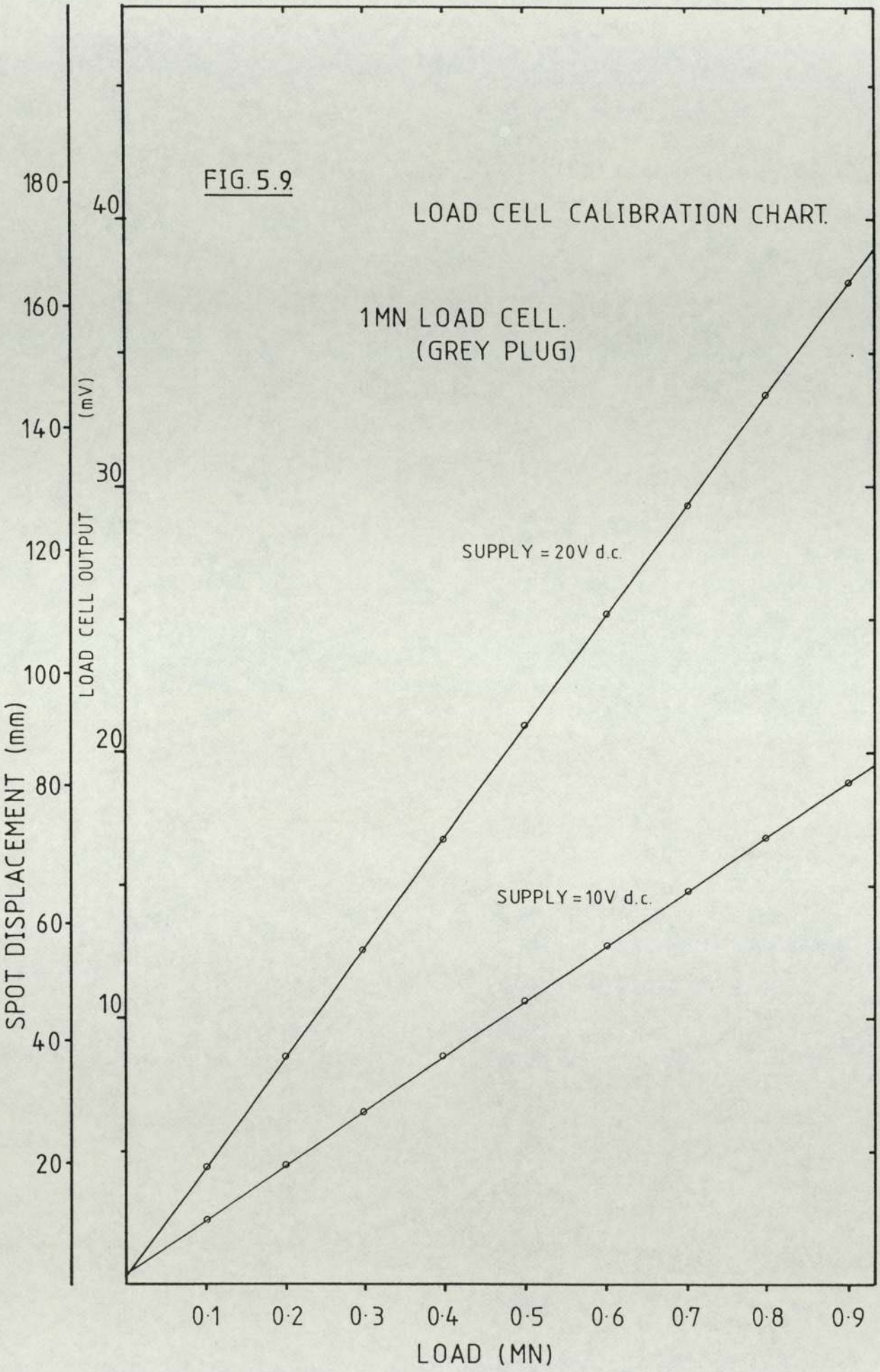
FIG. 5.9
LOAD CELL CALIBRATION CHART.
1MN LOAD CELL.
(GREY PLUG)
SUPPLY = 20V d.c.
SUPPLY = 10V d.c.
SPOT DISPLACEMENT (mm)
LOAD CELL OUTPUT (mV)
LOAD (MN)
180
160
140
120
100
80
60
40
20
40
30
20
10
0·1
0·2
0·3
0·4
0·5
0·6
0·7
0·8
0·9

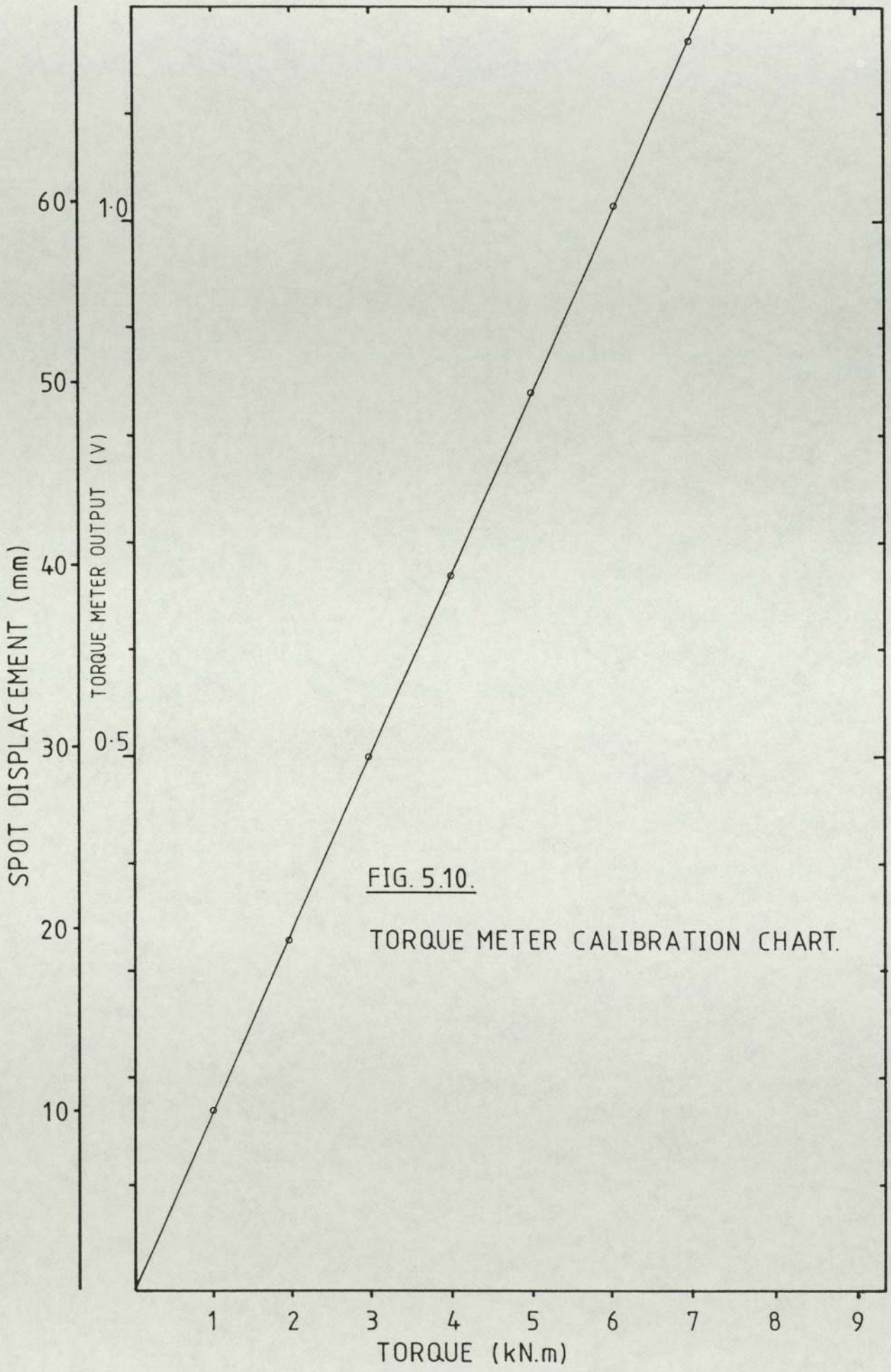

FIG. 5.10.

TORQUE METER CALIBRATION CHART.

5.3. Material Testing Equipment.

5.3.1. Avery-Denison Compression Testing Machine.

Compression tests on pure lead were carried out using an Avery-Denison material testing machine (No.7152/A/30941), having the following specification:

Load Capacity	600 kN.
Load Calibration	British Standard 1610 Grade A.
Ram Stroke	200 mm.
Ram Speed	250 mm/min up to 400 kN.
	180 mm/min at 600 kN.

The machine was controlled by three servo control loops, Figure 5.11, applying to one of the following control modes:

a. Ram control.
b. Load control.
c. Extensometer control.

The feedback signals are derived from load cells in the load system and linear displacement transducers for the ram displacement and extensometer measuring system.

For the determination of lower yield point, B.S. 18 Part 2, 1971 states that the maximum stressing rate in the elastic region should be 30 N.sec/mm^2 , and through yield the straining rate should not exceed 0.0025 s^{-1}.

To enable this to be done automatically, the machine

FIG. 5.11.

AVERY-DENISON
CONTROL CIRCUIT.

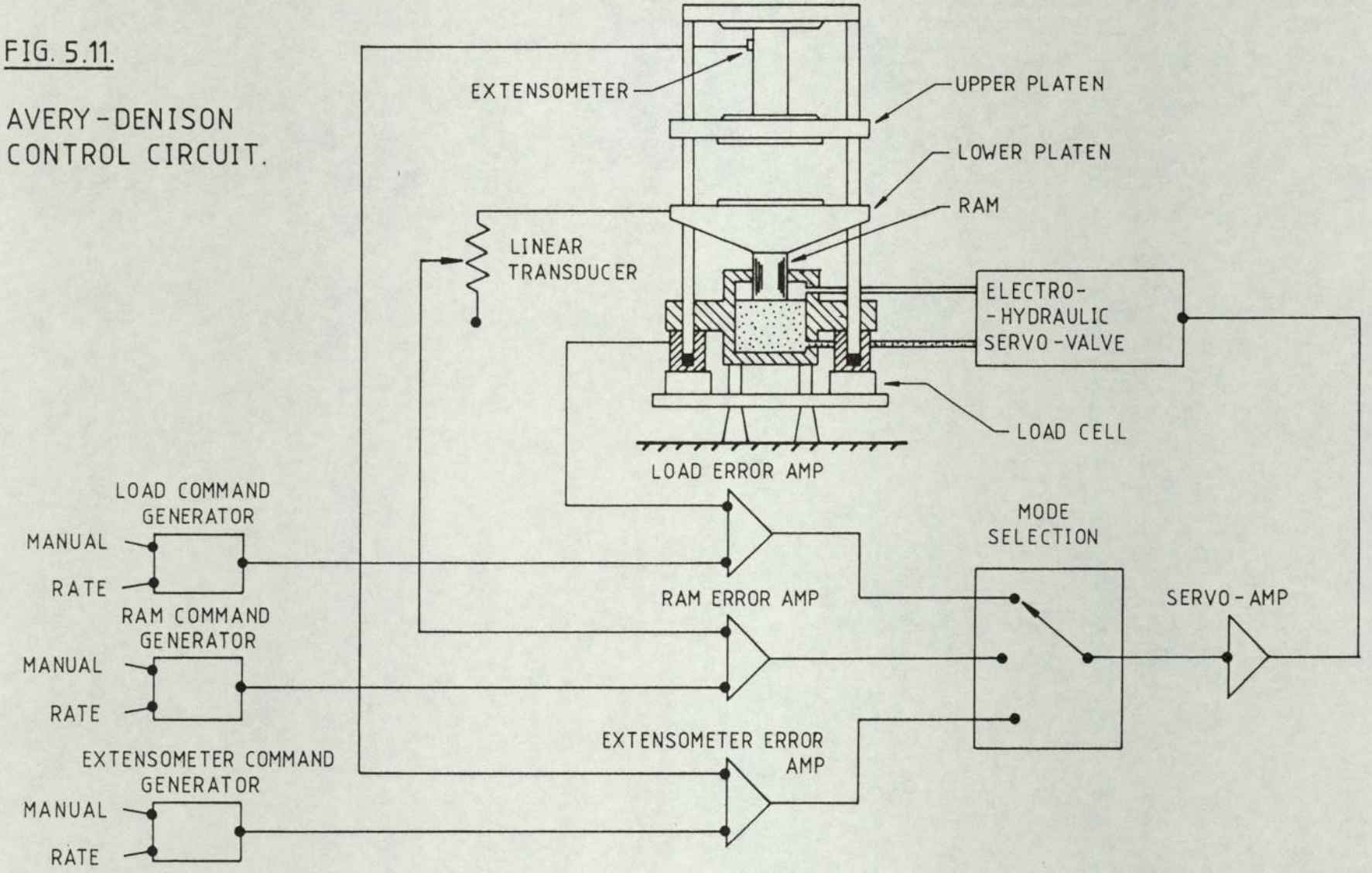

incorporates a pre-program whereby the specimen is strained in the elastic region at a rate of 30 N.sec/mm^2 for a steel with a Youngs Modulus of Elasticity of 207 kN/mm^2. At the point of yield, the machine detects a negative loading rate and switches automatically to the pre-programmed straining rate of 0.0025 s^{-1}.

CHAPTER SIX

MATERIAL TESTING

6.1. Introduction.

In the laboratory, rolling tests were carried out at room temperature using pure lead (99.9999% pure) as a model material to simulate the rolling of hot steel.

Perfect similarity of the two processes is practically impossible to achieve but approximate similarity is easy to obtain and has proved useful in predicting forming loads in previous modelling tests. For example, refer to papers by Altan et al (142) and Wanheim et al (143).

The rolling tests (outlined in Section 7.3) were carried out at approximately 20 deg.C. (ambient temperature), close to the recrystallization temperature of lead. Hence it was felt that the yield stress of the lead could be affected by the strain rate at this temperature.

6.2. Uniaxial Compression Tests on Pure Lead.

6.2.1. Previous Testing.

Compression tests were carried out using the Avery-Denison compression testing machine described in Section 5.3.1. This machine allowed the rate of the deformation to be accurately controlled.

The variation of yield stress of pure lead with temperature, strain and strain rate has been examined by Loizou and Sims (144) using a cam plastometer at strain rates

in the range 1 to 20 per sec at temperatures of 0, 20, 40, 70 and 110 deg.C.

The lead used was cast, hammered down and then cold formed to size prior to final machining. The machined cylinders were then left to anneal at room temperature.

Ingham (66) has provided additional yield stress data for pure lead at ambient temperature using a Mayes testing machine for strain rates in the range 0.0001 to 1 per sec.

Tsukamoto et al (145) recently examined the use of plasticine and lead for simulating the working of hot steel. In particular they determined that by varying the antimony content of the lead, simulation of the working of hot steels having different deformation characteristics, i.e. different steel grades, was possible.

As decribed in Section 7.3.3., the lead used in these rolling trials had a different metallurgy to that used by Ingham and Loizou and Sims, having been annealed. Consequently additional yield stress data is provided here, for comparison, at strain rates between 0.0001 and 1 per sec.

6.2.2. Preparation of Lead Specimens and Test Procedure.

In cold working conditions where strain rate has little effect, a compression test can be carried out incrementaly

with relubrication after each increment of compression.

In these tests, the requirement was for a controlled constant rate of deformation and so concentric grooves were machined into the end faces of the cylindrical specimens to trap lubricant and thus minimize the effects of friction between the specimen and the machine platens.

Loizou and Sims (144) determined by experiment that 32 grooves per inch of radius resulted in elimination of barreling and the ends of the specimens were plane and parallel after compression.

The billets used in the rolling trials were cast in four sizes of square cross section, machined, pre-worked, annealed and then finally machined to size (see Section 7.3.3.). Consequently the compression test specimens were machined from a number of the larger size billets, to the dimensions shown in Figure 6.1.

The test pieces were placed in the laboratory well in advance of the testing to allow their temperatures to stabilize to ambient.

The Denison compression testing machine was switched on and the appropriate settings made for control of the platen speed. The specimen end faces and the compression platens were lubricated with a Castrol brand graphite grease and the specimen was placed in a central position on the lower compression platen.

Dimensions in mm.

16 lubrication grooves in each end face (equi-spaced).

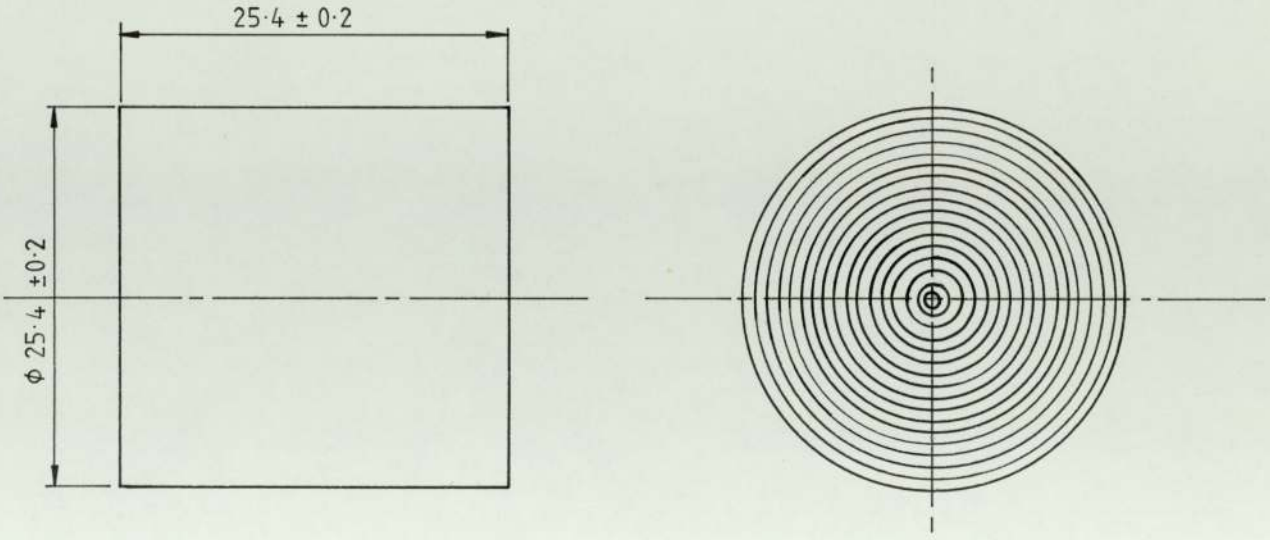

Figure 6.1. Pure lead compression test specimen.

The upper ram was then slowly lowered until the upper platen made contact with the test specimen. The recorder pen on the integral X-Y plotter was set to a suitable datum and the compression stroke initiated.

The specimen was compressed in excess of 50% of its initial height and the compression stroke was terminated manually. All specimens were tested consecutively in this manner.

6.2.3. Test Results and Discussion.

Tabulated results of the compression tests compiled from the charts traced by the machine X-Y recorder are given in Appendix A. and the results are plotted in Figure 6.2.

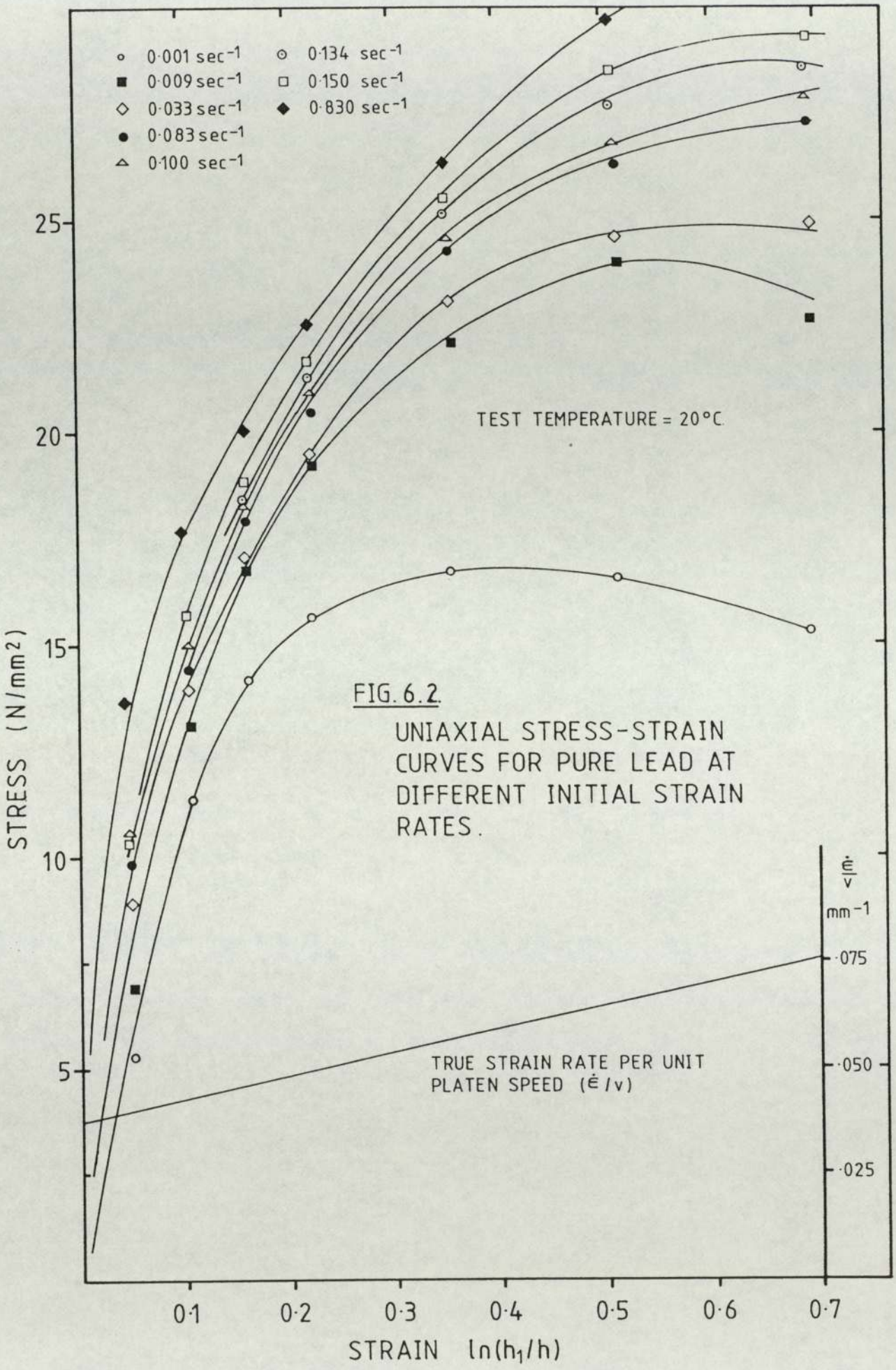

FIG. 6.2.

UNIAXIAL STRESS-STRAIN CURVES FOR PURE LEAD AT DIFFERENT INITIAL STRAIN RATES.

The lower curve in Figure 6.2. shows the variation in strain rate, relative to the true strain per unit platen speed, as the test progressed. These results are replotted in Figure 6.3. as yield stress against strain rate, the values of reduction being indicated on the curves.

With a constant platen speed, the natural strain rate is given by,

$$\dot{\varepsilon} = \frac{1}{h} \frac{dh}{dt} \qquad \ldots\ldots\ldots\ldots\ldots\ldots\ldots\ 6.1$$

where h = specimen height.

dh/dt = platen speed.

At the lower value of initial strain rate ($\dot{\varepsilon}_1$) the work hardening that takes place is balanced by the softening due to dynamic recrystallization. After an initial sharp rise, the yield stress remains essentially constant with increasing strain. At higher levels of initial strain rate where the rate of dynamic softening is no longer sufficient to overcome the work hardening process, the yield stress continues to rise throughout the strain range as in cold working.

This is similair to the behaviour of steels at a hot working temperature of approximately 1000 deg.C, as reported by Cook (52).

After an initial rapid work hardening phase, the yield stress curves go through a maximum associated with the

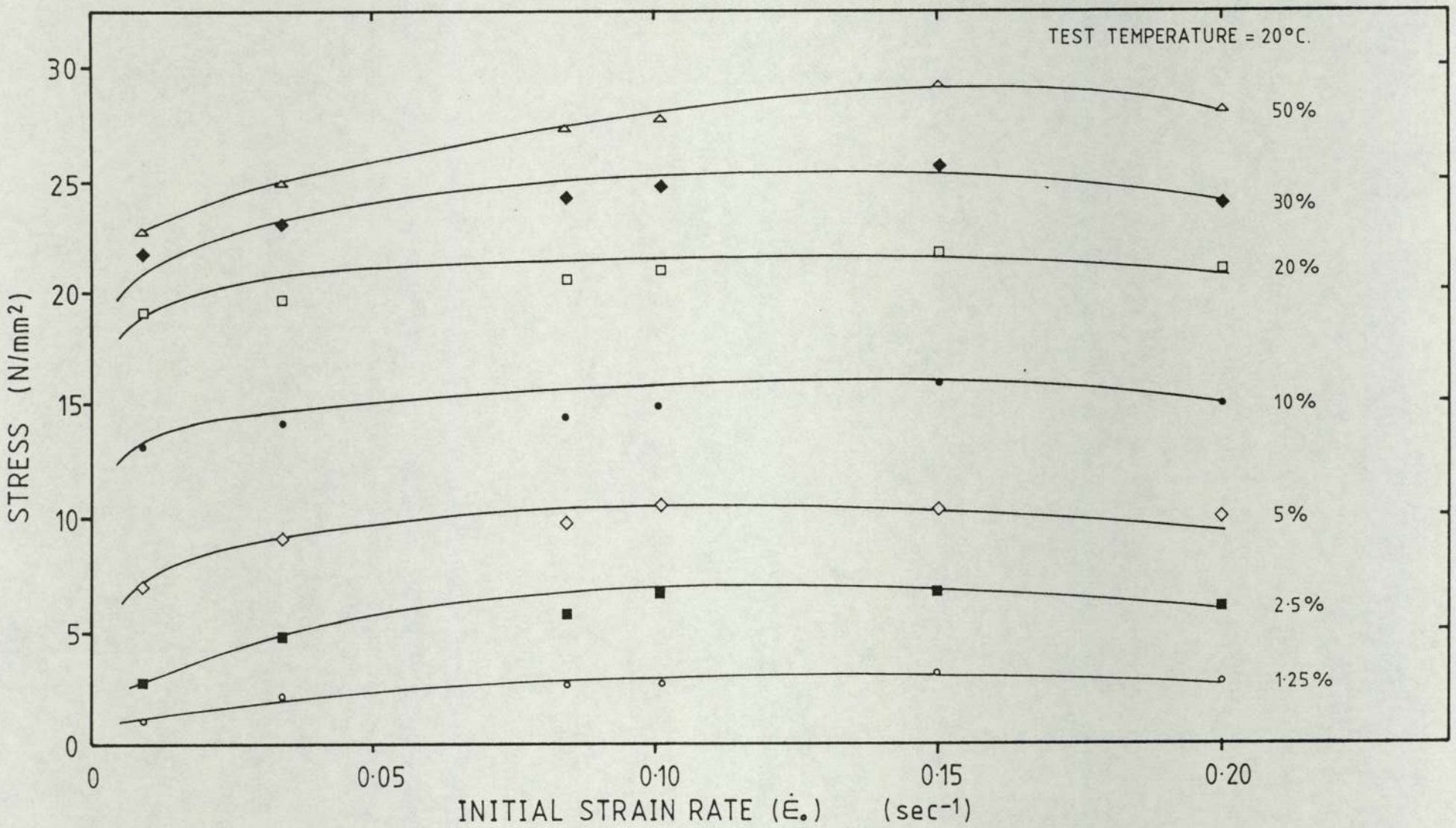

FIG. 6.3. UNIAXIAL YIELD STRESS v INITIAL STRAIN RATE FOR PURE LEAD.

occurence of dynamic recrystallization. The peak in yield stress occurs after some low degree of recrystallization has taken place so that the strain to the peak (ε_p) is always greater than the strain for dynamic recrystallization (ε_c).

The yield stress curves, Figure 6.2, indicate that when considering small strains there is little advantage in obtaining data at constant natural strain rates rather than constant platen speed. The lower curve in Figure 6.2. shows that for a natural strain of 0.6, the strain rate was only approximately twice the initial value and the stress-strain curves referred to above show that such a change in strain rate did not cause a significant change in yield stress.

Probably the largest potential error in the compression test, arises from the friction between the machine platens and the test specimen. This alters the stress distribution near the end faces of the specimen from a uniaxial to a tri-axial stress system inhibiting material flow in a radial direction, resulting in barreling of the specimen.

As mentioned above, friction may be minimized by sufficient lubrication. A pattern of six grooves per centimetre of radius was found to be adequate for the elimination of barreling in these compression tests.

Another possible source of error could be the variation in yield stress with specimen grain size. Loizou and Sims (144) showed the effect to be large between a specimen

in the as cast condition (approximately 12 grains/cm^2) and a specimen in which the grain size had been reduced by working (approximately 3000 grains/cm^2).

This is illustrated in Figure 6.4. where the graph constructed by Loizou and Sims is shown. They deduced, however, that the yield stress was sensitive to grain size only in coarse structured materials. Since all specimens for these compression tests were machined from billets which had undergone similair treatment(s), it was assumed that there was negligible variation in grain size between test specimens.

Tsukamoto (145) has shown the effect of pre-forging on the yield stress for strains less than 0.5. The yield stress of the pre-forged specimen was approximately 15% greater than that of the as-cast specimen, but was little affected by the amount of pre-forging.

The temperature rise during deformation may also have some effect on the material yield stress and it is of interest to calculate approximately the adiabatic temperature rise during compression.

Adiabatic temperature rise,

$$dT = \frac{1}{J\ \rho\ c} \int_{\varepsilon_1}^{\varepsilon_2} \bar{\sigma}\ d\bar{\varepsilon} \quad \ldots\ldots\ldots\ldots\ldots\ldots\ 6.2$$

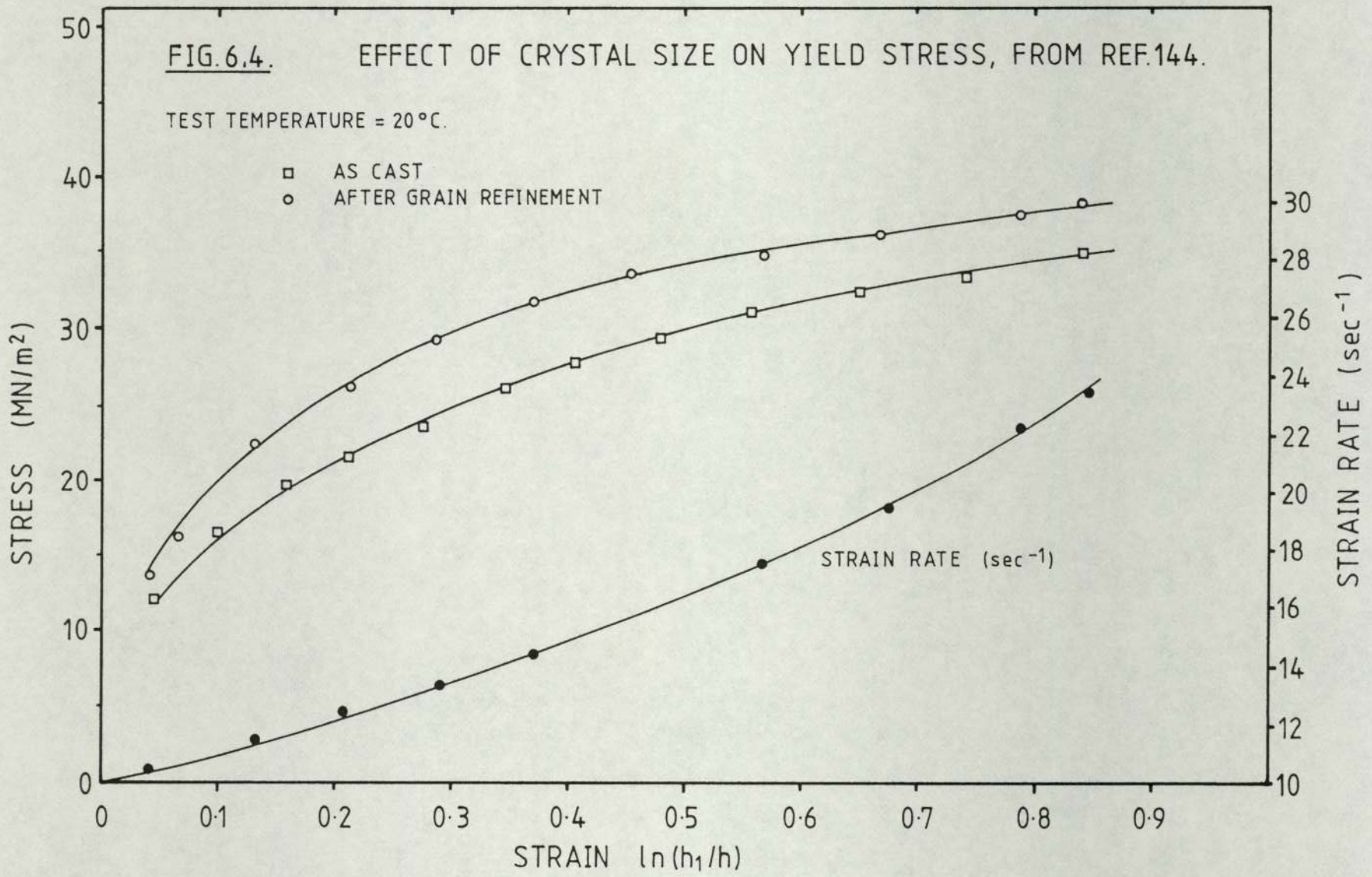
FIG.6.4. EFFECT OF CRYSTAL SIZE ON YIELD STRESS, FROM REF.144.
TEST TEMPERATURE = 20°C.
AS CAST
AFTER GRAIN REFINEMENT
STRAIN RATE (sec⁻¹)
STRESS (MN/m²)
STRAIN RATE (sec⁻¹)
STRAIN ln(h1/h)
0
10
20
30
40
50
0·1
0·2
0·3
0·4
0·5
0·6
0·7
0·8
0·9
10
12
14
16
18
20
22
24
26
28
30

where $\bar{\sigma}$ = representative stress.

$d\bar{\varepsilon}$ = representative strain increment.

J = mechanical equivalent of heat.

ρ = material density.

c = specific heat of material.

For lead, J = 4186.452 N.m/kg.deg.C.

ρ = 11348.76 kg/m^3.

c = 0.031.

The integral represents the area under the uniaxial yield stress curve between the limits of strain.

A realistic value of the mean yield stress may be taken from Figure 6.2, say 17 N/mm^2. Assuming a thickness strain of 0.6,

$$dT = 17\left\{\frac{MN}{m^2}\right\} \times 0.6 \times \frac{1}{0.031} \times \frac{1}{11348.76}\left\{\frac{m^3}{kg}\right\} \times \frac{1}{4186.452}\left\{\frac{kg.deg.C}{N.m}\right\}$$

dT = 6.93 deg.C. (12.47 deg.F.)

It is unlikely that this temperature rise would be achieved at slow strain rates where heat would be allowed to dissipate through the machine platens.

6.3. Testing of Steels.

No material testing was performed on the steel grades used in the experimental programme at BSC. Yield data for steel is widely available in the literature although data for continuously cast steels is still sparse. The reader is advise to consult, for example, Ingham (66) for yield data on the following steel grades at nominal temperatures of 1000, 1100 and 1200 deg.C and at strain rates of 3 and 12 s^{-1}.

321 S 31	Stainless.
316 S 11	Stainless.
709 M 40	Alloy Steel.
534 A 99	Alloy Steel.
722 M 24	Alloy Steel.

CHAPTER SEVEN

EXPERIMENTAL TEST PROGRAMME AND PROCEDURES

7.1. Introduction.

In order to study the effect of rolling on square section continuously cast stock, two general areas were investigated.

a. The effect of various rolling geometries and pass schedules on achieving a homogeneous, fully wrought structure throughout a billet cross section with particular attention to grain refinement.

b. The effect of various rolling geometries and pass schedules on the elimination of porosity, as a representative defect, in the central region of a billet cross section.

In the laboratory, rolling experiments on square cross section lead billets were carried out in order to simulate the hot rolling of steel.

7.2. Initial Experimental Tests.

7.2.1. Roll Preparation.

It was known from the experience of mill operators and from the published literature, for example Gorecki (11), that large reductions and large diameter rolls would be required when using lead billets to model the rolling of continuously cast billets, in terms of both billet size and reduction.

In order to determine the characteristics of rolling square stock on the Aston experimental mill, initial rolling trials were carried out using various sized cast lead billets. Table 7.1. outlines the tests made.

Using rolls of 114 mm diameter, the tests illustrated the difficulty in rolling billet sizes in excess of 20 mm square section on the available equipment, even with the moderate reductions taken.

Test	h1	r	Hm/L	L/D	Hm/D	α	Roll?
1	71.0	1.27	8.296	0.074	0.617	8.6	No
2	70.4	0.76	11.10	0.055	0.611	6.6	No
3	70.2	2.54	5.75	0.105	0.602	12.1	No
4	58.4	2.54	4.76	0.105	0.499	12.1	No
5	46.5	5.84	2.41	0.158	0.380	18.4	No
6	45.5	6.86	2.16	0.170	0.367	19.9	No
7	20.1	3.38	1.33	0.121	0.160	14.0	No
8	19.9	0.38	4.24	0.041	0.172	4.7	Yes
9	19.6	3.12	1.36	0.113	0.153	13.4	Yes
10	19.2	1.14	2.30	0.071	0.162	8.1	Yes

All square stock.

h1 = Billet initial height (mm). r = Reduction (mm).

Hm = (h1+h2)/2. α = Entry angle (deg).

L = Horizontal projection of the arc of contact (mm).

D = Roll diameter, constant for all tests at 114 mm.

Table 7.1. Initial rolling Trials.

This was primarily due to the low friction conditions between the rolls and the billet, the roll barrels being ground to a smooth finish of 0.008815 micron CLA (mean).

Obviously, to effect a realistic programme of testing, the ability to roll large stock sizes at large reductions is needed. Additionally, from these early results, geometric limiting conditions of $Hm/D < 0.16$ and $L/D < 0.10$ appear to be necessary for the steady state rolling of square section lead billet. In this context, steady state refers to the billet rolling at a constant rate throughout its length, no stop-start motion or stick-slip between the rolls and the billet.

A geometric examination of a typical billet mill at the British Steel Thryborough plant showed that for a billet initial height of 114 mm reduced by 22% (1.28:1) in cross sectional area with rolls of 660 mm diameter, then $Hm/D = 0.146$ and $L/D = 0.162$ with an entry angle of 18.9 deg.

A cursory comparison of the experimental test conditions with this data certainly illustrated the significance of the limiting geometry mentioned above. Considering the small entry angles of the experimental tests, it can be inferred that the magnitude of the frictional condition between the roll and the workpiece was not sufficient for steady state rolling to take place. In addition, the effect of the roll diameter is significant in relation to friction when rolling square section stock.

In conclusion, in order to effect a realistic experimental programme in terms of reduction and geometric similarity with industrial rolling practice, either the

magnitude of the frictional coefficient between the rolls and the workpiece and/or the diameter of the rolls would need to be increased.

It was not practicable to increase the roll diameter by a significant amount due to limitations imposed by the mill frame and so the frictional condition of the rolls was altered. A pair of 149 mm nominal diameter flat barreled rolls were shot blasted in order to roughen the barrel surface and so increase the friction coefficient. After shot blasting, the surface finish of the roll barrels was assessed by Talysurf measurement as being:

Top roll (as installed in mill)	0.0544 micron CLA.
Bottom roll (as installed in mill)	0.0495 micron CLA.

These figures contrast with those initially detailed in Section 5.1.2. Additional modification to the roll bearing blocks allowed roll gaps of up to 84 mm to be achieved when using these new rolls.

7.2.2. Billet Preparation.

The initial rolling trials mentioned earlier were made using as-cast pure lead billets of square cross section. Figure 7.1 shows a photomacrograph of a transverse section through a typical cast lead billet.

Three distinct regions of crystal macrostructure are

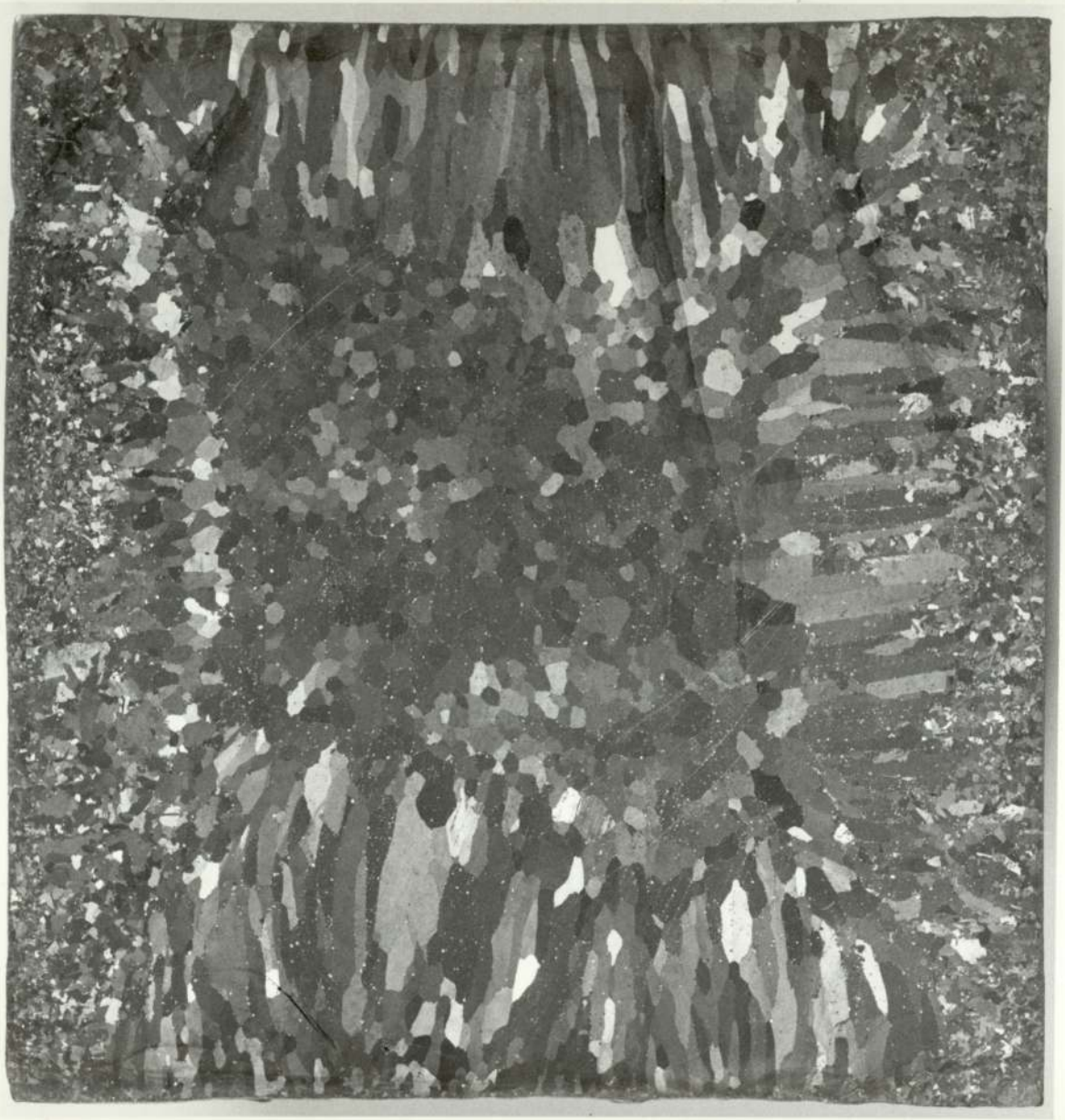

FIG. 7.1.

TRANSVERSE SECTION THROUGH CAST LEAD BILLET.

clearly visible. The outer layer of chill crystals, where the metal has cooled rapidly upon contact with the mould walls, the zone of columnar crystals with ordered orientation and the central zone of equi-axed crystals (see also Section 2.2.). Also visible are four interface 'planes of weakness' created by solidification impingement inwards extending from the billet corners to the equi-axed/columnar interface. During the initial rolling trials it was observed that at both ends of the billet, 'wedges' of deformation were visible in the deformed crystal structure, showing up in similar form to a slip line field type of pattern.

It was feared that these wedges would coincide with the planes of weakness during rolling leading to the possibility of the billet splitting or bursting along these lines. They are in fact, as their name suggests, planes of potential physical weakness where the solidifying dendritic crystals meet from orthogonal directions, pushing forward any impurities present into the area ahead of the solidifying front.

The three distinct zones of crystal size and shape formed during solidification of a billet makes it difficult to assess quantitatively the effect of working on the material structure. The questions are where to base measurements of crystal size and how to assess the reaction of the three zones to deformation. Clearly resolving these

questions is a major metallurgical project in itself.

Thus it was decided to pre-work and anneal all lead test billets in order to create a uniform grain structure throughout, ie. a totally equi-axed billet structure. The preparation of the billets is discussed in Section 7.3.3.

7.2.3. Specimen Preparation and Etching Technique.

In order to study the effect of rolling on the recrystallisation and consolidation of a billet, transverse sections (perpendicular to the direction of rolling) were taken from the test billet before and after each roll pass. A piece approximately 15 mm thick was cut from the trailing end of the billet prior to rolling and another section cut some 60 mm from the trailing end after rolling, an amount to account for the billet ends where unsteady deformation occurs (end effects). These pieces were then machined flat using a 127 mm diameter end mill enabling the whole specimen surface to be machined in one pass. Clean paraffin was used as a lubricant and coolant (applied copiously) and was found to give an excellent surface finish at a tool rotational speed of 500 rpm and feed rate of 0.05 mm/rev.

A number of tests were made to determine the optimum polishing-etching technique for lead. The most convenient method, taking into account the agressive acids involved in some of the suggested etching solutions, was found to be to

polish using an industrial brass polish followed by a final polish using ammonium molybdate solution. The specimen was then cleaned and fully immersed in a solution of glacial acetic acid, nitric acid and water, swabbing the prepared surface with cotton wool during the etch to remove dissolved particles. After etching for twenty to thirty minutes, the specimen was washed in water and dried. The actual preparation routine is outlined in Section 7.3.3. with subsequent modifications made to speed up the process.

Initial fears of this preparation technique were that time delays between the cutting of the specimen from the billet and the preparation would lead to static recrystallisation of the specimen at room temperature. In order to test for this, three transverse sections were cut from the same rolled lead billet, albeit at different locations along its longitudinal axis.

Specimen One: Machined, polished and etched immediately after rolling.

Specimen Two: Machined and left in laboratory for five days before polishing and etching.

Specimen Three: Placed in fridge for five days in order to lower its temperature well below that of room temperature ie. well below its recrystallisation temperature. It was polished and etched after this time delay.

The results of these tests showed there to be no significant difference between the measured grain sizes of the three test specimens and that no benefit was gained by either 'freezing' or immediate specimen preparation.

In fact the frozen billet, when polished and etched, showed traces of a fine grained structure present at the grain boundaries of the structure formed by subsequent recrystallisation after deformation. Although not measured, these grains were appreciably smaller than the local structure but still visible with the naked eye. The formation of these grains was presumably caused by the cold working effect of the polishing operation on the still cold lead specimen. In this case cold work refers to the situation where work is carried out at a temperature below the recrystallisation temperature of the material.

It was concluded that it would be perfectly acceptable to leave specimen preparation for a number of days after rolling although, as these tests were made in winter when the laboratory temperature was significantly colder than in summer, it was decided that it would be expedient to reduce the time delay between rolling and preparation in the warmer summer months.

7.3. Experimental Test Programme.

As mentioned in Section 7.1. the experimental test programme was split into two distinct parts:

7.3.1. Test Group I.

To obtain data on the effect of deformation by rolling on the crystal structure of a cast lead billet, to predict the reductions and rolling geometries required to ensure a homogeneous, fully wrought billet. These were split into tests involving one rolling pass and those involving two or more rolling passes with and without turning of the billet before subsequent passes.

Single Pass Tests:

Reductions in area of 10% to 55% (1.11 to 2.22:1) were made in one pass on four sizes of square cross section lead billet.

Multi Pass Tests:

Reductions in area totalling 20% to 55% (1.25:1 to 2.22: 1) were made in two or more passes of equal cross sectional area reduction on three sizes of square section lead billet. The results from these tests were used for comparison with those obtained by a single pass in order to determine the best rolling schedule for total billet recrystallisation. The effectiveness of turning a billet through 90 deg. before subsequent passes was assessed and

compared with rolling schedules where the billet was not turned. Degrees of recrystallisation achieved from reductions in area made in multi-passes were compared with those obtained from a single pass of equal total reduction in area. In billet rolling the shape of the product is important and so for all experimental tests the billet geometry, specifically the spread profile in the lateral direction, was measured after each roll pass.

7.3.2. Test Group II.

To obtain data on the effect of deformation by rolling on the consolidation of a representative defect present in the as cast billet. The reductions, rolling geometries and pass schedules required to close casting defects were assessed.

Lead billets of four sizes in square cross section were drilled with holes of various diameter along their longitudinal axes, in the direction of rolling from the rear end of the billet. The holes were used to simulate the presence of defects positioned centrally in the billet, for example porosity, and defects at radial distances from the billet centre, for example segregation.

Holes of diameter 6.35 mm positioned at the billet centre represented area fractions of 1.74%, 1.29%, 0.89% and 0.73% porosity in 43, 49.5, 60 and 66 mm square billets respectively.

Holes of diameter 4.76 mm positioned at the billet centre represented area fractions of 0.726%, 0.50%, and 0.408% porosity in 49.5, 60 and 66 mm square billets respectively.

Radial holes of diameter 3.175 mm represented area fractions of 0.323%, 0.222%, and 0.182% porosity/segregation in 49.5, 60 and 66 mm square billets respectively.

Small diameter holes positioned on the billet vertical axes were used to assess the depth of working. Similar sized holes were positioned on a radius from the billet centre. The radius was such that the area enclosed was equivalent to the central 10% of the billet cross section area, an area corresponding to the zone of major defects found in continuously cast steel billets (146). Although the area fraction of the modelled porosity in the lead billets was very much greater than that found in continuously cast steel billets, it was not practicable to drill holes of a smaller diameter in the lead even with special worm type drills. Additionally it was not practicable to drill to depths in excess of 150 mm with both the smaller and larger diameter drills due to uncontrollable drill wobble and subsequent 'wander' of the drill hole from the desired axis.

Reductions in area totalling 20% to 75% (1.25 to 4:1) were made in two or more passes, with and without turning, to study the deformation mechanics of the model defects.

For all the artificial defect tests, the hole areas, positions and axial orientation were measured before and after each pass in order to quantify the effect of the deformation. Additionally, the billet spread profiles were measured in order to quantify the material displacement in the billet outer regions with that measured in the regions adjacent to the holes.

7.3.3. Specimen Manufacture and Preparation.

Lead billets were cast in static, vertical metal moulds of three sizes, 50, 75 and 100 mm square as illustrated in Figure 7.2.

After casting the billets were removed from the mould and left to cool in air. When cool, the 100 mm square billets were machined down to 85 mm square using a large diameter end mill. All billets were then pre-worked by rolling. Reductions of 30% (1.43:1) were made in four passes with turning and the billet ends were cut off leaving a billet of approximately square section and 310 mm in length.

At this stage, the manufacture of the test specimens diverged along two different process routes.

a. Billets used in the single and multiple pass tests were annealed in a convection oven at approximately 250 deg.C. for eight hours for the 100 mm and 75 mm square billets

ITEM	DESCRIPTION	MATERIAL	No. OFF
1	BASE	MLD STEEL	1
2	MAIN SIDE PLATE	MLD STEEL	2
3	INNER PLATE	MLD STEEL	2
4	SCREW	MLD STEEL	1
5	CLAMP PLATE	MLD STEEL	4
6	12mm BOLT	MLD STEEL	4
7	12mm NUT	MLD STEEL	4
8	12mm WASHER	MLD STEEL	4

ALL DIMENSIONS IN mm

SCALE : FULL SIZE

NOTE:

DIMENSION A = 50, 75 OR 100mm.

DIMENSIONS B & C DEPEND ON A.

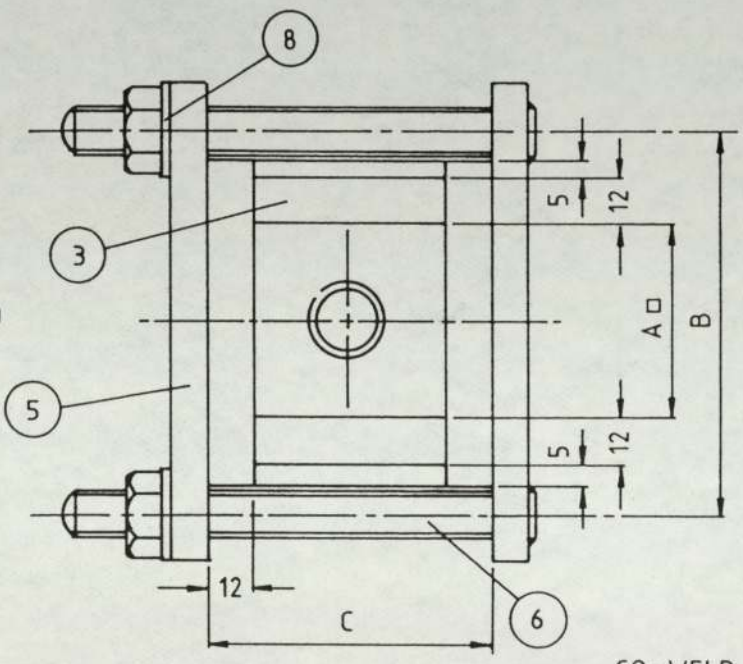

SECTION XX

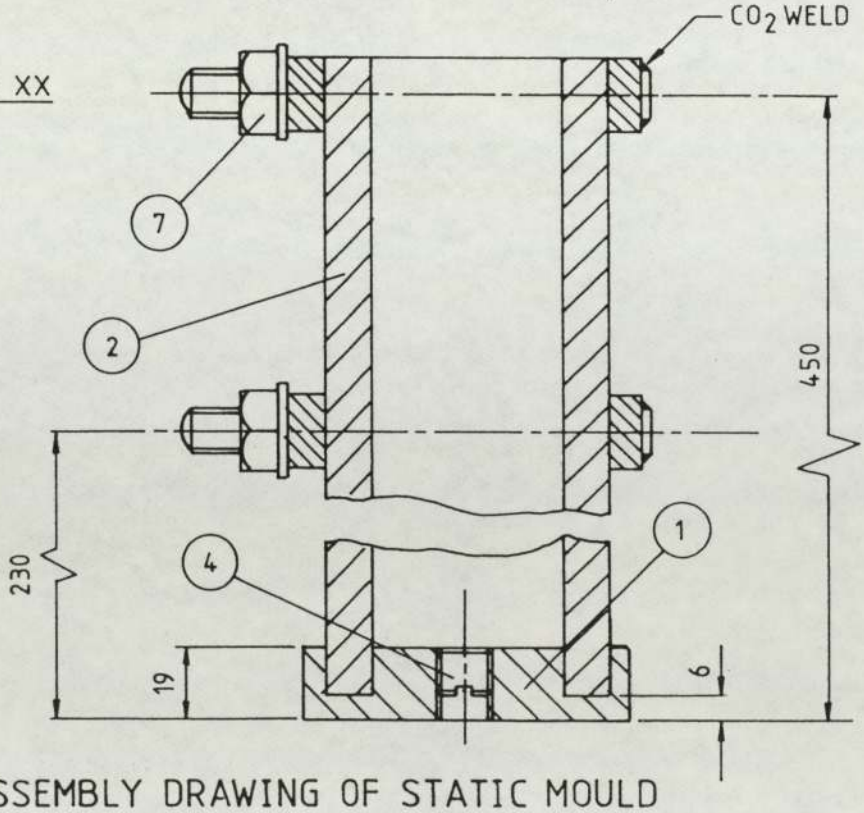

FIG.7.2.

ASSEMBLY DRAWING OF STATIC MOULD FOR CASTING LEAD SPECIMENS.

and six hours for the 50 mm square billet. The billets were allowed to cool in the oven overnight.

Figure 7.3. shows the three dimensional nature of the grain structure of a cast, worked and annealed lead billet. For some unknown reason a split developed in the billet surface/sub-surface during annealing. After cooling the two parts were gently eased apart to reveal the grain structure of the lead.

b. Billets used in the tests to determine the effect of rolling on artificial void or hole consolidation were mounted vertically in a jig and drilled longitudinally, to the various hole patterns illustrated in Figure 7.4. Guhring deep hole worm type fast helix drills of 6.35, 4.762 and 3.175 mm diameter were used, drilling to a depth of 125 to 150 mm, depending on the flute length of the drill. Paraffin was used as a lubricant and coolant, applied copiously during the drilling. Clogging-up of the drill helix with swarf occured readily when the drilled depth reached a value of approximately one half of the drill length. Hence, care had to be taken to feed the drill slowly and retract frequently to remove the swarf. After this drilling stage these billets were annealed at 250 deg.C. for six to eight hours depending on the billet cross section. Annealing was carried out post drilling since the heat generated during the drilling operation was considerable. Drilling after annealing would have caused

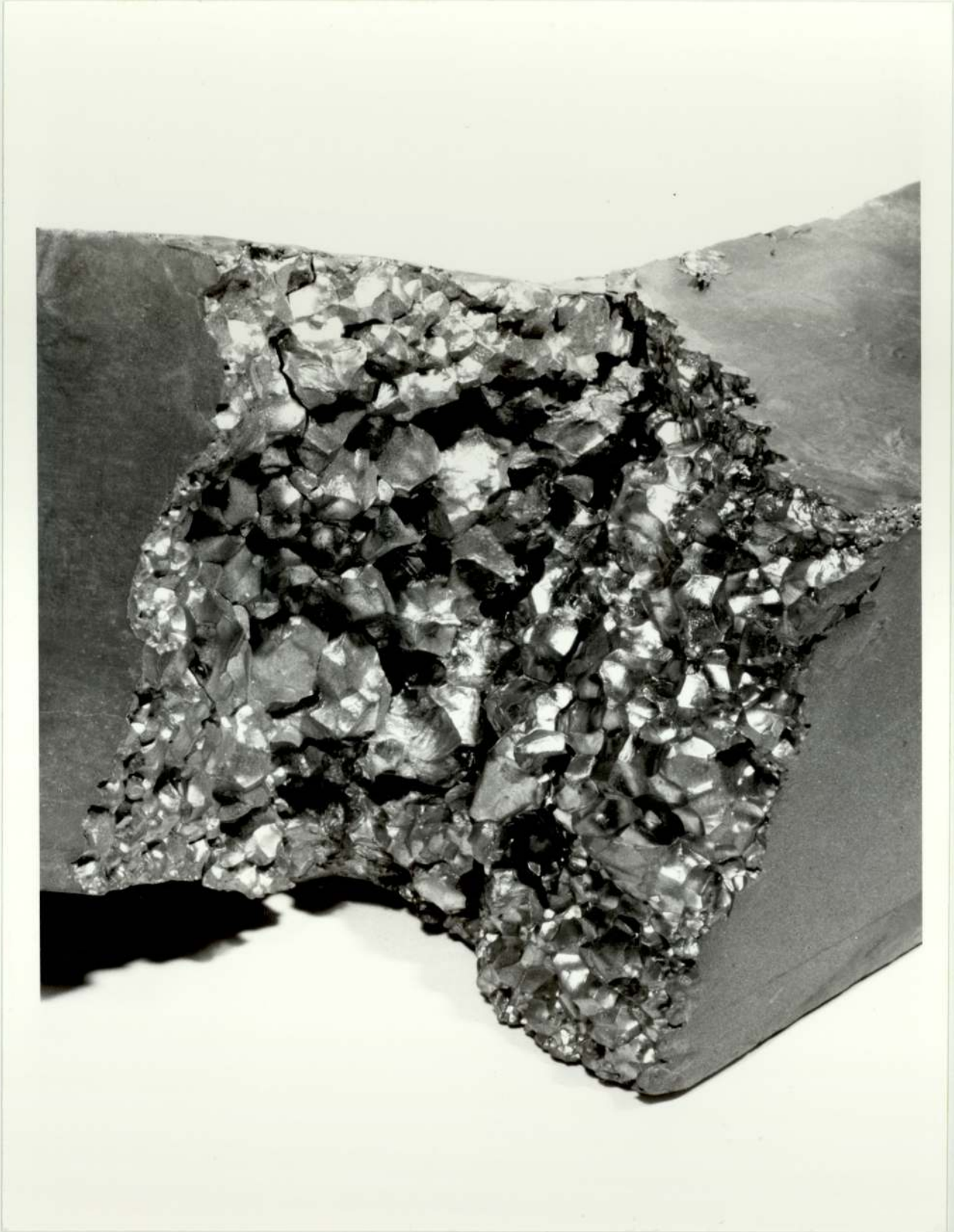

FIG. 7.3.

CAST LEAD BILLET SPLIT TO SHOW THE THREE DIMENSIONAL NATURE OF GRAIN STRUCTURE.

BILLET TYPE 1.

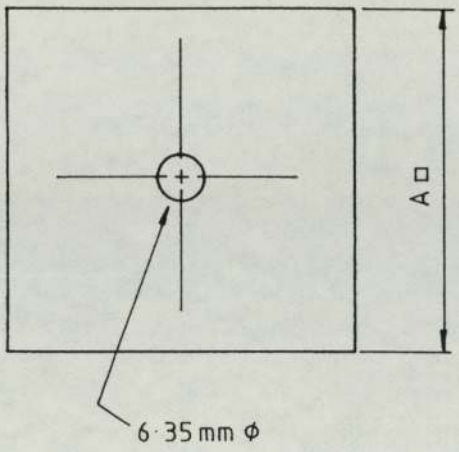

BILLET TYPE 2.

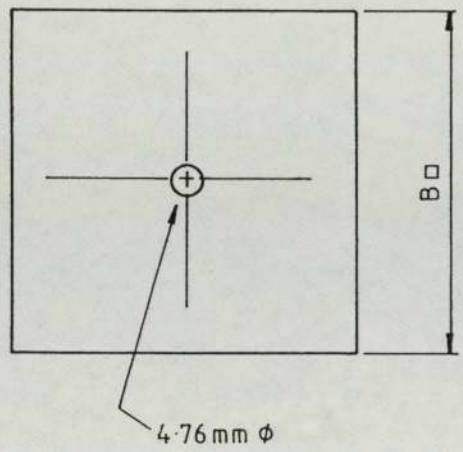

DIMENSION 'A' = 43, 49·5, 60 & 66mm.
DIMENSION 'B' = 49·5, 60. & 66mm.

BILLET TYPE 3.

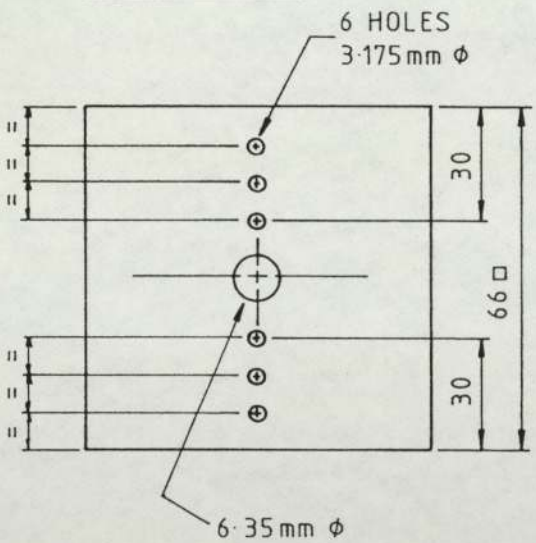

BILLET TYPE 4.

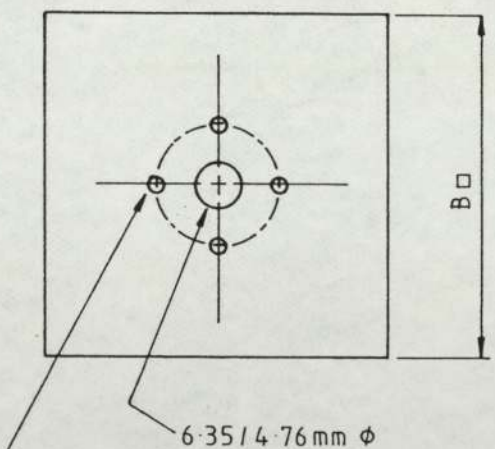

FIG. 7.4.

HOLE POSITIONING FOR VOID MODELLING ROLLING TRIALS WITH LEAD BILLETS.

localised recrystallization around the region of the hole.

Both billet types were machined to size using a 127 mm diameter end mill with paraffin lubrication. Opposite faces of the square billet were machined successively to ensure section uniformity and the billet ends were machined perpendicular to the longitudinal axis. Any swarf was removed from the drilled holes.

All billets were marked to identify a reference surface for metallurgical analysis and a specimen slice taken from the end of the billet designated the rear for preparation and etching to reveal the pre-rolled billet grain structure. The billet was then marked with reference points, using a scriber, for measurement of the billet width before and after each pass to assess the spread profile, Figure 7.5.

7.3.4. Test Procedure.

The lead billets were stored in the laboratory to ensure they were at the ambient temperature prior to rolling.

The power and the recording equipment were switched on 45 minutes prior to testing to ensure that the strain gauge bridges were stabilized. After this time period the bridge circuits were checked for balance using a spot galvonometer. The roll speed and the roll gap were set. The roll gap was checked between the roll barrels

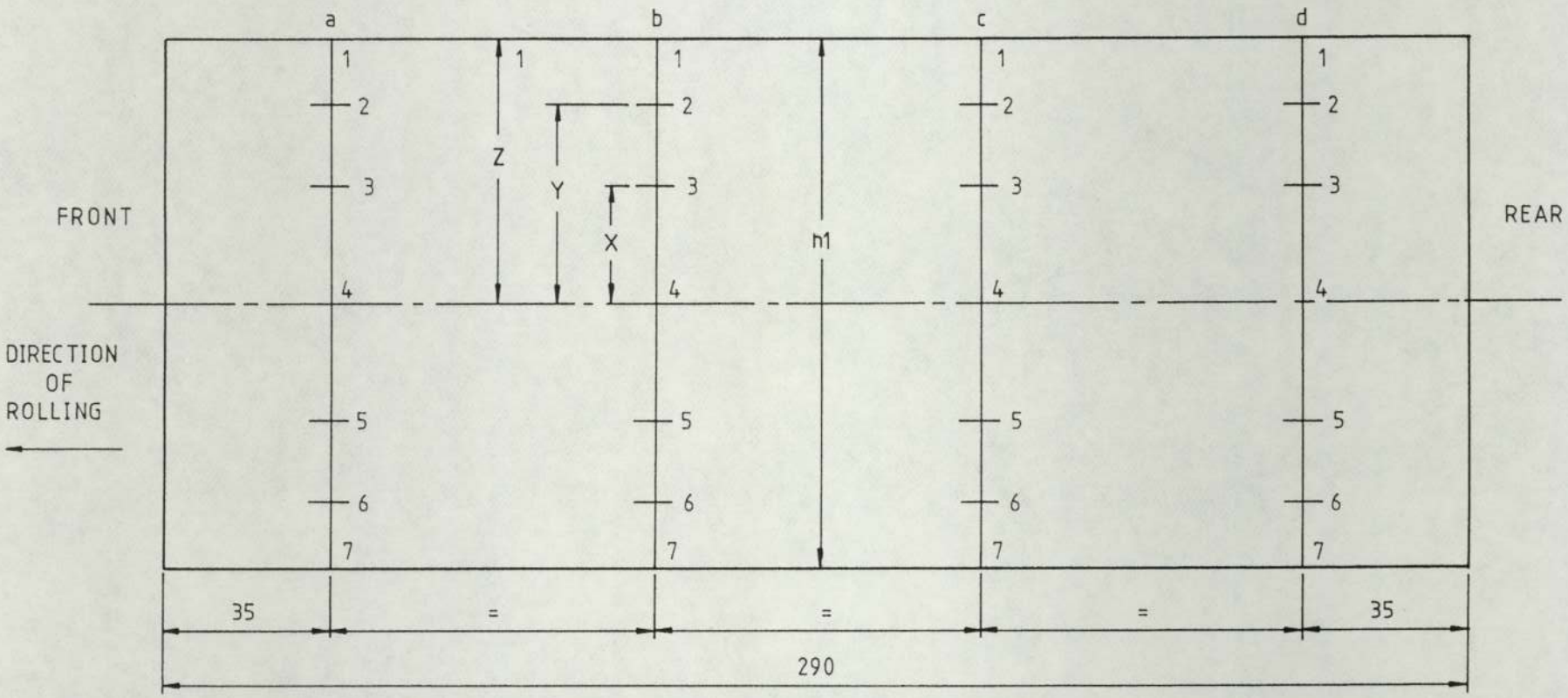

FIG. 7.5.

MEASURING SYSTEM FOR LEAD BILLET SPREAD.

FOR:	30 < h1 < 40 :	X = 10	Y = 15	Z = h1/2
	40 < h1 < 50 :	X = 12·5	Y = 20	Z = h1/2
	50 < h1 < 60 :	X = 17·5	Y = 25	Z = h1/2
	60 < h1 < 70 :	X = 17·5	Y = 30	Z = h1/2

ALL DIMENSIONS IN mm .

using slip gauges to ensure even roll gap across the width of the roll barrel. The roll speed was checked using a hand-held tachometer.

The billet height was measured at ten points along its length and the billet width was measured at the twenty points indicated in Figure 7.5. All values were noted.

Prior to rolling the billet surfaces and the roll barrels were cleaned and degreased using Inhibisol. The roll drive was then switched on and the calibration resistors switched in and out of the circuit to leave a permanent record of the scales used for the test, ie. the bridge current setting. The billet was then rolled, the roll drive and u.v. recorder stopped and the u.v. trace of loads and torques labelled and stored in a suitable light-proof container awaiting measurement.

After rolling the billet was measured for height and re-measured at the same twenty points on the width with a micrometer fitted with ball-end pieces. These were used since the usual flat micrometer anvils could not accurately measure the points on the deformed billet width due to the curvature, be it either convex or concave. After measurement a specimen slice was cut from the billet approximately 40 mm from the trailing end to avoid unsteady deformation effects in the region of the billet rear. The specimen was labelled and the reference surface marked.

At the completion of the test, possibly involving further passes, measurement and cutting of slices, the specimen(s) were machined flat on the faces perpendicular to the direction of rolling using a 127 mm diameter end mill. Clean paraffin was used as a lubricant and a coolant.

Further trials, subsequent to those outlined in Section 7.1.2.3. resulted in the elimination of the polishing operation in favour of using a heated etchant bath.

The specimens were immersed in a solution of,

3 parts Glacial Acetic Acid.
4 parts Nitric Acid.
16 parts Water.

heated to a temperature of 30 to 40 deg.C. and maintained at that temperature. The specimen surfaces were swabbed with cotton wool, while still immersed every five minutes or so to remove dislodged particles and deposited precipitate until the grain structure was clearly revealed. When satisfactory, the specimen was removed from the etchant and placed in a warm water bath for washing. The specimen was then shaken dry, the prepared surface sprayed with Isopropyl alcohol and dried under a hot air blower. If the surface was not satisfactory, then the specimen was replaced in the etchant for a few seconds and the drying procedure repeated.

During the course of this experimental work the specimens were prepared in batches of about a dozen. They

were taken to be photographed immediately after preparation since the prepared surface would oxidize after a day or so.

7.4. Works Test Programme and Procedures.

7.4.1. Introduction.

Two areas of testing were carried out during the works trials, similair to the experimental test programme outlined in Section 7.1. The two areas were:

a. The effect of various rolling geometries and pass schedules on the elimination of porosity, as a representative defect, in the central and adjacent regions of a conventionally cast, pre-rolled steel billet of 220 M 07 grade.

b. The effect of rolling on the microstructure of a limited number of continuously cast steel billets of an SAE 8620 grade to assess the effectiveness of using model materials to simulate the rolling of continuously cast steel.

7.4.2. Test Programme.

The purpose of these tests was to,

a. Establish the best method of assessing defect consolidation after various reductions in the presence

of a variety of hole/artificial void geometries.

b. Assess the modelling process as a realistic means of simulating the behaviour of continuously cast steel during rolling.

c. Compare the behaviour of the steel simulation tests with the lead simulation tests as outlined in Section 7.3. and 7.3.4.

7.4.3. Consolidation Tests.

Holes drilled along the billet longitudinal axis, positioned on the billet axis, were used primarily to simulate central defects. Holes positioned non-centrally were used solely to assess the depth of working, their position being arbitrary in terms of metallurgical defect simulation. Holes of 4.95 mm nominal diameter and approximately 80 mm depth were used.

A single hole of 4.95 mm diameter represented an area fraction of 0.764% porosity in a 50 mm square billet, a figure somewhat greater than that found in a typical continuously cast steel billet. Reductions in area totalling 10% to 40% were made in one, two or three passes with and without turning of the billet to study the deformation mechanics of the model defects. 40% was the limiting value of reduction, dependant on the mill geometry.

For all the tests, the hole area, position and axial

off-set were measured before and after each trial, it not being practicable to measure those values after each pass. The billet spread was measured after the trial and billet surface temperature noted post-furnace, pre-roll and post-roll prior to either water quenching or the next pass in the schedule.

7.4.3.1. Manufacture of Steel Test Billets.

Steel billets of grade 220 M 07, a carbon/carbon-manganese free cutting steel of the following chemical composition, nominally 50 mm square were cut into 320 mm lengths.

Chemical Composition:

0.15% C	0.90-1.30% Mn
0.07% P	0.20-0.30% S

Clamped so that the billet axis was vertical, the billet was drilled using a Guhring deep hole worm drill of 4.763 mm diameter resulting in 4.95 mm nominal diameter holes. The pattern of holes, single, four and five is shown in Figures 7.6. to 7.9. with the accompanying tables of dimensions. The holes were drilled to depths of approximatley 80 mm. The depth and diameter of the holes was a compromise to account for the material machinability and available equipment, it being difficult to drill succesfully to a sufficient depth (to avoid end deformation

BILLET No.	A	B	C	D
1	50·241	25·540	27·176	26·008
2	50·495	26·810	26·160	26·071
3	50·343	27·534	25·254	24·776
4	50·495	27·584	25·386	25·792
5	50·495	27·254	25·716	24·713
6	50·470	27·102	25·843	24·548
7	50·317	27·280	25·512	24·776
8	50·444	27·508	25·411	24·598
9	50·190	27·940	24·724	24·751
10	50·368	28·931	23·912	25·030
11	50·495	28·600	24·370	25·005

ALL DIMENSIONS IN mm

NOT TO SCALE

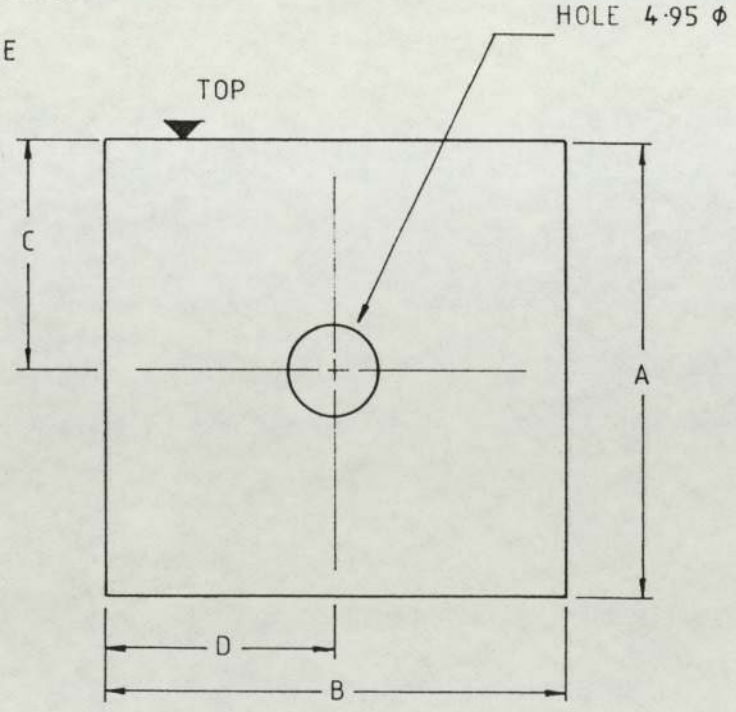

FIG. 7.6.

HOLE POSITION STEEL BILLET TYPE I.

BILLET No.	A	B	C	D	E	F	G	H
12	50·190	37·657	24·398	13·603	50·622	26·300	24·801	25·030
13	50·343	38·267	24·297	12·257	50·317	24·293	24·547	24·242
14	50·241	38·876	25·059	12·689	50·444	25·131	23·963	24·750
15	50·368	38·419	24·449	11·292	50·241	25·487	25·182	25·259
16	50·343	37·276	25·617	12·460	50·419	25·030	25·157	25·462
17	50·241	37·682	25·922	13·171	50·419	24·827	24·573	23·335

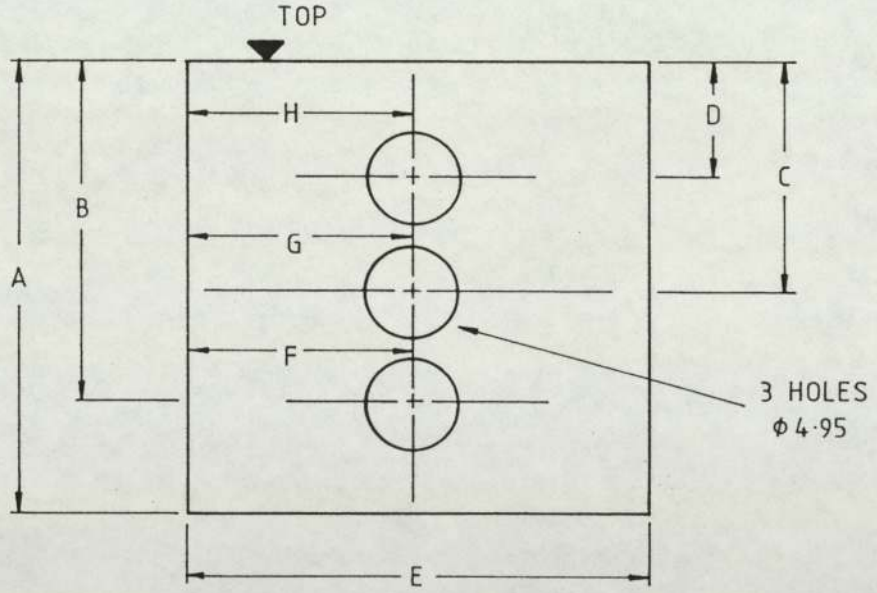

ALL DIMENSIONS IN mm

NOT TO SCALE

FIG. 7.7.

HOLE POSITION STEEL BILLET TYPE II.

BILLET No.	A	B	C	D	E	F	G	H	I	J	K	L
18	50·241	38·673	25·821	12·917	25·313	26·430	50·470	38·264	24·878	12·305	25·030	25·132
19	50·419	38·089	25·744	12·968	26·227	26·303	50·800	37·654	24·725	12·559	24·903	24·954
20	50·546	38·673	25·465	12·613	25·922	23·890	50·317	37·425	25·868	12·050	24·903	24·141
21	50·267	38·038	25·897	12·867	25·744	26·252	50·292	37·400	25·437	12·381	25·411	23·811

ALL DIMENSIONS IN mm

NOT TO SCALE

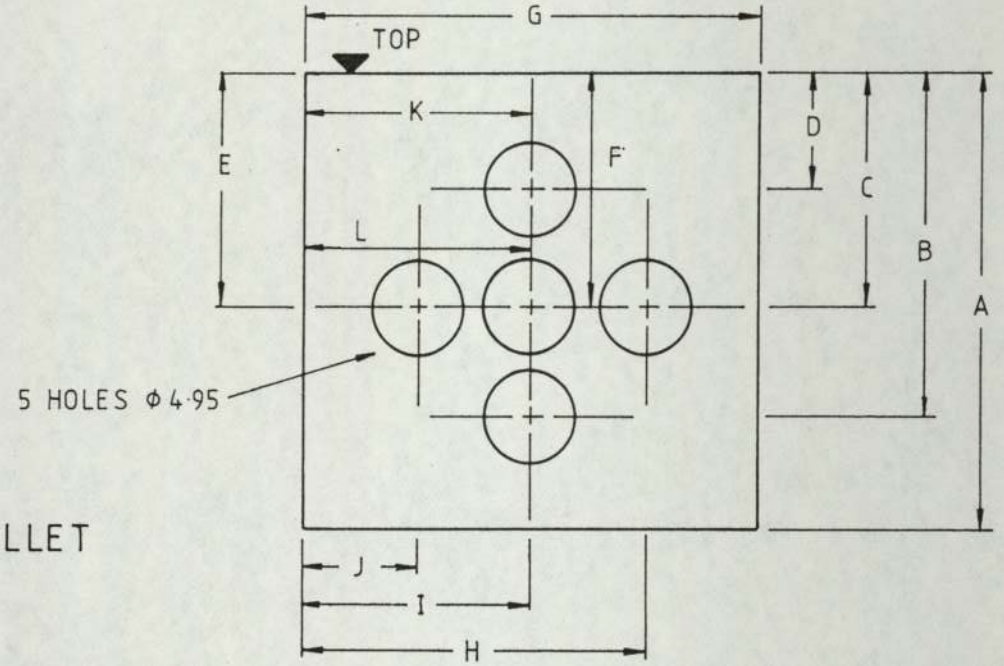

FIG. 7.8.

HOLE POSITION STEEL BILLET
TYPE III.

BILLET No.	A	B	C	D	E	F	G	H	I	J
22	48·311	35·777	10·530	36·031	12·257	48·514	37·273	10·603	37·984	12·381
23	48·514	35·752	13·146	36·362	13·146	48·412	35·545	12·279	35·495	11·771

ALL DIMENSIONS IN mm

NOT TO SCALE

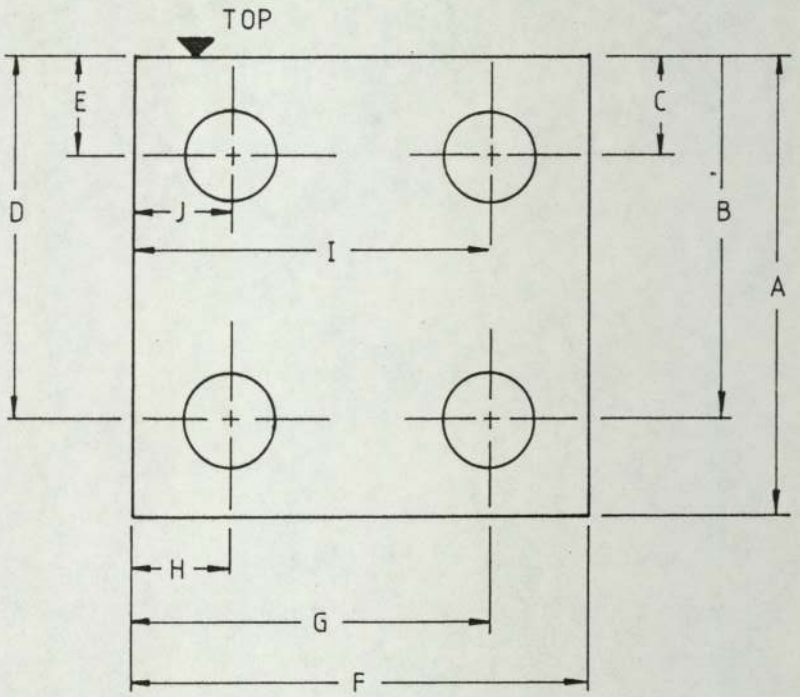

FIG. 7.9.

HOLE POSITION STEEL BILLET
TYPE IV.

effects) with small diameter drills. After drilling the billets were numbered, the hole positions measured and a reference surface marked on the billet.

7.4.3.2. Test Procedure.

Prior to testing the recording equipment was switched on to allow the strain gauge bridge circuits to stabilise. The circuits were then balanced and the u.v. recorder output set to a suitable datum point.

Before the billets were placed in the furnace, the holes were filled with a water based refractory paste to prevent oxidation of the hole surface in an attempt to more closely model a void deep in the continuously cast structure.

Having already specified the order of testing with respect to roll gaps and pass sequences, the billets were loaded into the furnace in the required order at five minute intervals. The furnace temperature was nominally 1320 deg.C. The steel billets were each soaked for fifty minutes to enable their temperature to equalize at approximately 1220 deg.C.

In order to retain a level of consistency in the testing, a time delay of fifteen seconds was nominated after removal of the billet from the furnace to allow for de-scaling, temperature measurement and transfer across the shop to the mill table. This time was rigidly adhered to for all

the tests.

After fifty minutes soak the billet was removed from the furnace and de-scaled by the mill operator. The u.v. recorder was switched on and the billet temperature measured using the hand held optical pyrometer described in Section 5.2.3. The mill operator then transferred the billet to the mill table. The roll gap for the first pass was pre-set, the analogue read out of roll gap was graduated in 0.8 mm (1/32 inch) divisions. When the fifteen second delay had expired the billet temperature was again measured and the billet then pushed into the roll gap. The billet temperature was measured after rolling.

If the particular test called for just one pass, then the billet was quenched immediately in a water bath to restrict static grain growth. After quenching the billet was left to cool in air. If further passes were required then the fifteen second rule applied again (between exit from the rolls and the start of the next pass) to allow the operator to transfer the billet to the mill table, re-set the roll gap and if necessary turn the billet through 90 deg. The temperature was measured as before and after the fifteen seconds the billet was rolled. If necessary the process was repeated according to the number of passes required to achieve the desired percentage reduction in area.

For tests where the billet was turned, the formula of Ekelund (147) was used to calculate the billet spread for

each pass and so determine the rolling schedule.

7.4.4. Continuously Cast Stock Tests.

In order to evaluate the effect of reduction on the consolidation of actual solidification defects, continuously cast steel billets of an SAE 8620 grade were rolled on the three-high mill. A comparison between these tests and the hole consolidation tests using lead and steel billets outlined in Sections 7.3.4. and 7.4.3. respectively should indicate the effectiveness or otherwise of modelling a continuously cast structure for the purposes of experimental deformation testing.

The size and geometry of the three-high mill dictated the reductions possible and hence the size of stock by its maximum roll gap, 63.5 mm with load cells installed. The production schedules of British Steel dictated that the minimum size of continuously cast stock available was 108 mm square. Hence, the minimum possible reduction in height using 108 mm square stock and a maximum roll gap of 63.5 mm would be 41%, approximately 37% in area (1.583:1).

The previous tests with 50 mm square steel stock (Section 7.4.3.) indicated a limiting reduction in height of the order of 40% for steady state rolling and acceptance of the stock into the roll gap. This equated to an entry angle of approximately 21 deg. Taking the entry angle as being

the primary limiting criteria for steady state rolling, the equivalent reduction in height for a 108 mm square billet would be of the order of 17%, ie. for the given mill geometry and stock height of 108 mm, the maximum reduction in height would be 17%.

Thus, to counteract these limits there were two options,

a. Use a mill having a larger roll gap and larger rolls to effectively decrease the entry angle.

b. Use smaller sized continuously cast stock.

Access to larger roll plant such as that available in a production mill was not possible and, as the minimum size of continuously cast stock produced by BSC was 108 mm square, it was decided to compromise by reducing the size of the 108 mm stock to suit the three-high mill.

To achieve a 17% reduction in height using the maximum roll gap of 63.5 mm would require an ingoing stock height of 76.5 mm. This would entail considerable machining, a removal of approximately 50% of the stock cross sectional area or, conversely, a 30% reduction in stock height. Referring to Figure 2.6, as an example, the consequences of such an operation would be to remove totally the outer layer of chill crystals and also a large proportion of the dendritic crystal structure, approaching the central equi-axed region.

The effect of removing part of the billet structure and deforming the remainder is not something, to the writers knowledge, that has been tried before. Certainly the effect will be to concentrate more work at the billet centre than would be the case with a 'full' billet. The effect on recrystallisation rates or the effect of the removal of the outer chill crystal layer is not known.

In an attempt to quantify this effect, albeit in a rather unsatisfactory manner, one billet was rolled as a square with the outer layers machined away in equal proportions on all four faces and another billet was rolled as a rectangle with only the roll contact faces machined. In this way the chill layer was retained on the billet side faces. Hopefully, a difference would be detected in the consolidation of the central regions for the two billets enabling a reasoned judgement to be made on the effectiveness of this method of testing.

To restrict the continuously cast rolling programme due to constraints of time and expense, the continuously cast billets were made up in the form of wedges 63.5 mm in height at the lead-in end and 76.5 mm in height at the trailing end of the billet. Hence, reductions in height in the range zero to 17% could be achieved along the billet length in one pass.

7.4.4.1. Manufacture of Continuously Cast Test Billets.

Continuously cast steel billets of an SAE 8620 grade having the following chemical composition were cut into two pieces each 610 mm in length. The design of the three test billets is shown in Figure 7.10.

Chemical composition:

0.18-0.23% C	0.7-0.9% Mn	0.20-0.35% Si
0.40-0.60% Cr	0.40-0.70% Ni	0.15-0.55% Mo
0.04% P (max)	0.04% S (max)	

7.4.4.2. Test Procedure.

Essentially the test procedure was identical to that outlined in Section 7.4.3.2. for the consolidation tests.

The test pieces were loaded into the furnace at intervals of fifteen minutes and soaked at the furnace nominal temperature of 1320 deg.C for approximately 75 minutes to reach a measured surface temperature of the order of 1270 deg.C. This would allow for temperature equalisation through the billet section. As before, a fifteen second delay was utilized to allow for de-scaling, temperature measurement and transfer to the mill table. The billet surface temperature was measured post-furnace, pre-roll and post roll. The billets were rolled in one pass only, the roll gap being set to its maximum value of 63.5 mm with the load cells installed giving a range of reductions

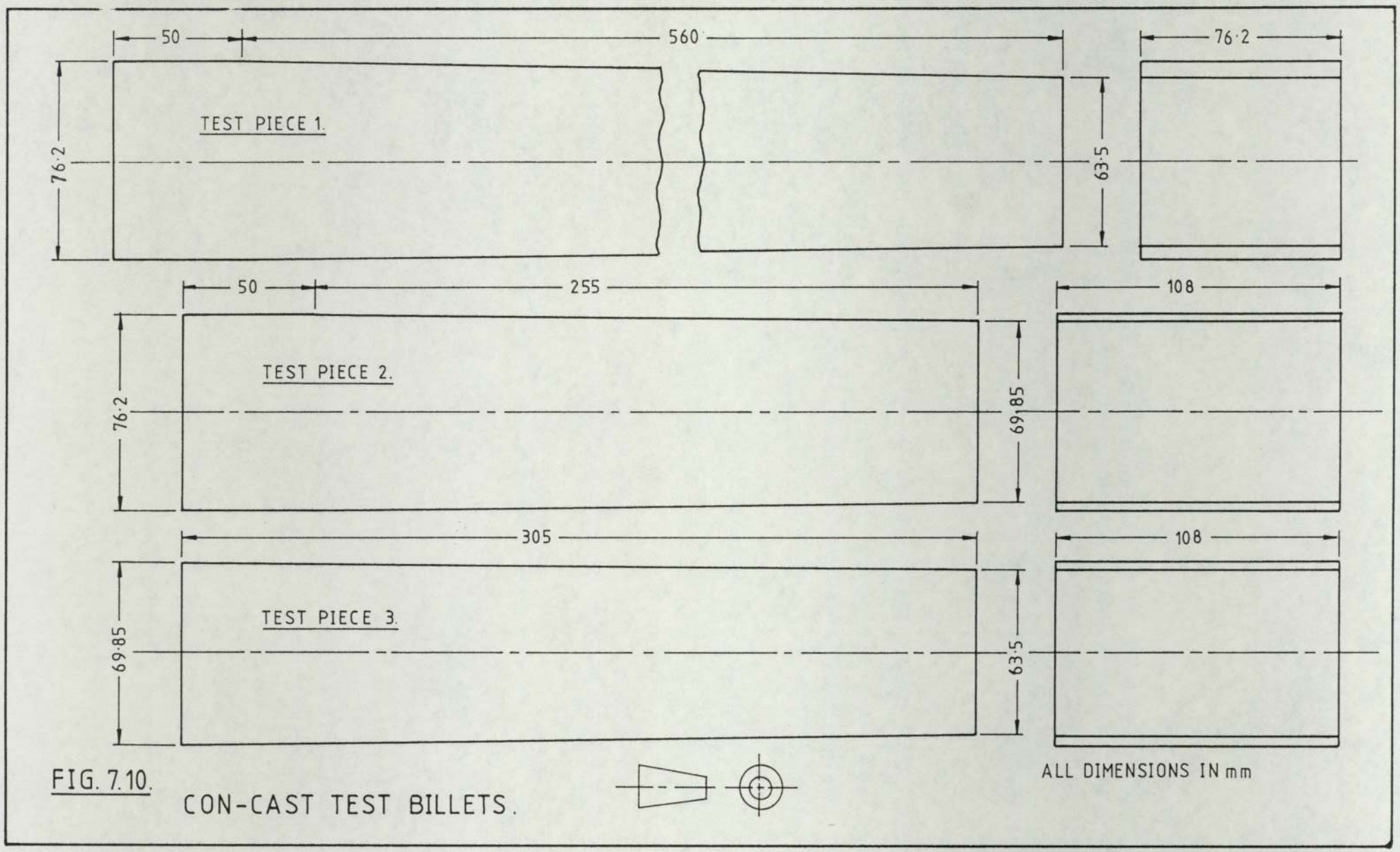

FIG. 7.10. CON-CAST TEST BILLETS.

in height of,

Zero to 17% for test billet 1.

Zero to 8.5% for test billet 2.

Zero to 8.5% for test billet 3.

After rolling the billets were immediately quenched in water and left to cool in air.

7.5. Data Collection Techniques.

7.5.1. Lead Billet Grain Size Estimation.

The preparation of test pieces taken perpendicular to the billet length (in the direction of rolling) is described in Section 7.3.4.

Photomacrographs were taken of the prepared surface depending on the following factors;

a. If the structure of the prepared surface was clearly definable by eye then a photomacrograph of the whole of the prepared surface was taken. The negative was then enlarged to fill a standard six inch square plate and the magnification factor determined by reference to the true dimensions of the specimen.

b. If the structure of the prepared surface was not definable by eye then a photomacrograph of the central portion of the surface was taken at magnifications of

40.5 or 81.

The linear intercept or Heyn procedure as described in ASTM E112-80 (147) was used to estimate the specimen grain size. A uniform two-dimensional reference grid was constructed on the photomacrograph and a count of the number of grain boundary intercepts along each line in the X and Y directions made. Since the magnification of the photomacrograph was known, the number of grain boundary intercepts per unit length could be calculated. The linear intercept is given by,

$$\bar{d} = \frac{L}{N} \quad \ldots\ldots\ldots\ldots\ldots\ldots\ldots\ldots \quad 7.1$$

where N = Number of grain boundary intercepts counted along a traverse of length L (mm).

Values for each linear traverse were calculated, the mean linear intercept being the average of these values.

The mean linear intercept, $\bar{d}$, is less than the average diameter of the grains comprising the macrostructure, $\bar{D}$, which in turn is less than the maximum grain diameter, Dm. By assuming reasonable shapes for real grains and obtaining a mean diameter of rotation (148),

$$\bar{D} \simeq 1.75\ \bar{d} \quad \ldots\ldots\ldots\ldots\ldots\ldots\ldots\ldots \quad 7.2$$

Also, assuming $\bar{D}$ to be the circumscribed sphere of rotation,

$$Dm \simeq 1.86\ \bar{d} \quad \ldots\ldots\ldots\ldots\ldots\ldots\ldots\ldots \quad 7.3$$

7.5.2. Confidence Limits for Grain Size Estimation.

Since the determination of grain size is not an exact measurement, no estimation can be complete without also determining the precision within which the determined size may, with normal confidence, be considered to represent the actual average grain size of the specimen. In this context normal confidence is taken to represent the expectation that the actual error will be within the stated uncertainty 95% of the time. The confidence limit (CL) is expressed in the same units of measurement as the average grain size. Relative confidence limit (RCL) is used when the CL is divided by the average measurement to yield a fractional or percentage uncertainty.

The method used is as follows,

a. Variance of the observed counts about the unknown true mean intercept number, $\bar{N}$,

$$Vo = \frac{\Sigma(Ni - \bar{N})^2}{(n - 1)} \quad \ldots\ldots\ldots\ldots\ldots\ldots \quad 7.4$$

where Ni = Number of grain boundary intercepts counted along traverse i.

n = Number of traverse counts made.

b. Apparent standard deviation of the counts,

$$So = \sqrt{Vo} \quad \ldots\ldots\ldots\ldots\ldots\ldots\ldots\ldots \quad 7.5$$

c. The coefficient of variation,

$$CV = \frac{So}{\bar{N}} \quad \ldots\ldots\ldots\ldots\ldots\ldots\ldots\ldots \quad 7.6$$

d. The percentage accuracy of the grain size determined from Equation 7.1. is read directly from Figure 9 (147). When multiplied by the mean linear intercept the 95% relative confidence limit is obtained. Alternatively, the grain size may be expressed as an ASTM number according to Table 7.2,

ASTM Number	Mean Linear Intercept $\bar{d}$ (mm)
00	0.451
0	0.319
1	0.226
2	0.160
3	0.113
4	0.080
5	0.056
6	0.040
7	0.028
8	0.020
9	0.014
10	0.010
11	0.007
12	0.005

Table 7.2. Relationship between ASTM grain size and mean linear intercept.

7.5.3. Lead Billet Void Measurement.

For all void tests, as detailed in Section 7.3.2. the following measurements were made,

a. Void axis position relative to the billet edges.
b. Void major and minor axis lengths.
c. Void axis rotation.
d. Void cross-sectional area.

All prepared transverse sections were projected onto the screen of a shadowgraph image projector at magnification of 20 or 50 depending on the void size. The void axis position, axial lengths and axis rotation were measured directly from the screen projection. The void shape was traced onto paper and the area enclosed by the hole circumference measured from the tracing using a planimeter having an absolute Vernier value of 0.01 sq.in (6.452 sq.mm).

The void y and z axial lengths were measured before and after rolling using the convention illustrated in Figure 7.11. Throughout the roll schedule the void axial measurements were always referred to the original void coordinate system (y,z).

The sign convention adopted for the measurement of linear and shear strains is as follows:

a. Linear strains:

Tensile strains = negative

Compressive strains = positive

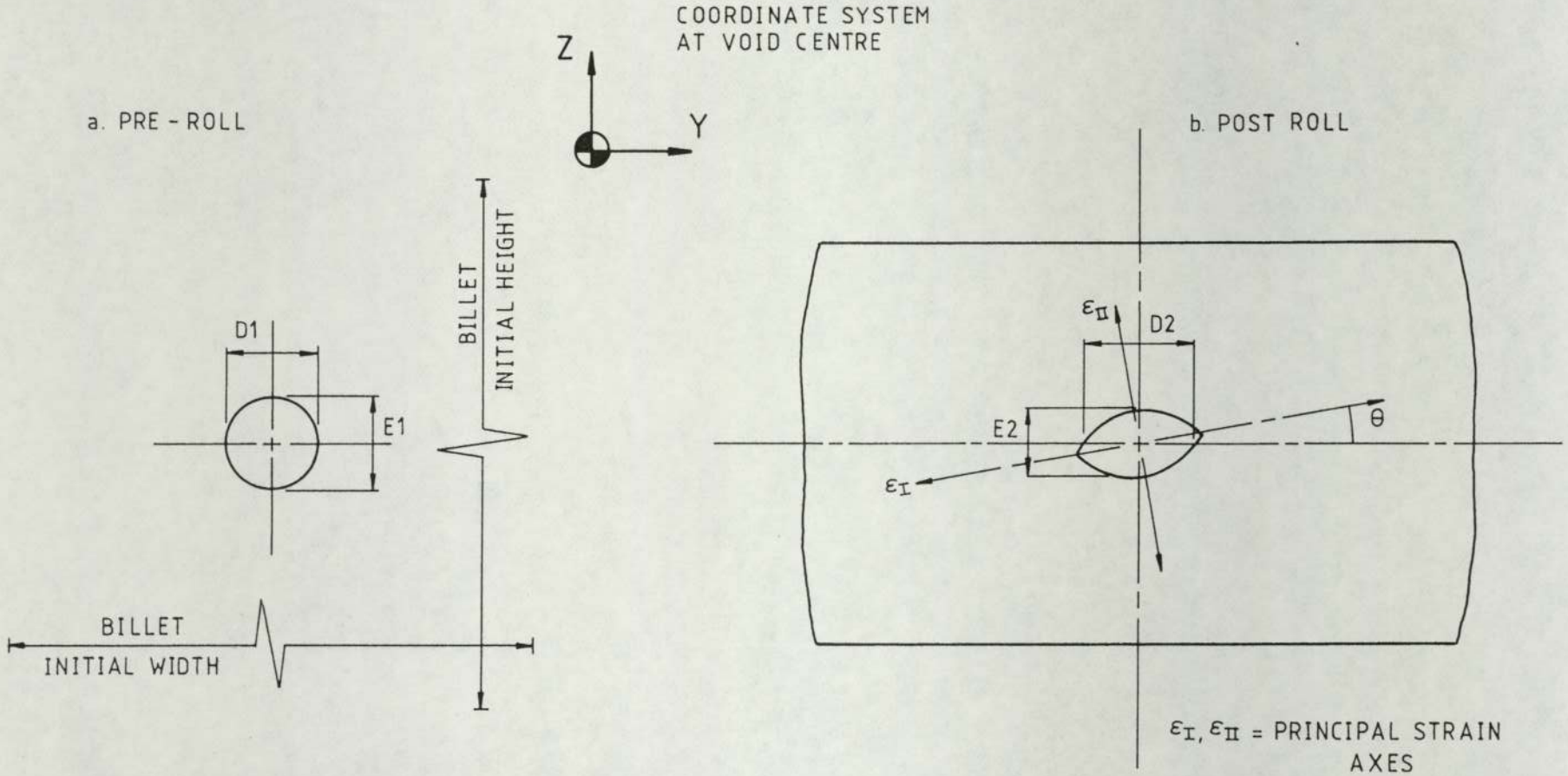

FIG. 7.11.

VOID MEASUREMENT CONVENTION.

b. Shear strains:

In the case where the major and minor axes of the deformed void do not align with the original (y,z) coordinate system,

Clockwise axial rotation = positive shear strain

Anticlockwise axial rotation = negative shear strain

In any case, $\gamma_{yz} = -\gamma_{zy}$

From Figure 7.11b, the linear strains along the y and z axes are given by (85,150),

$$\varepsilon_y = \ln \left\{ \frac{D1}{D2} \right\} \quad , \quad \varepsilon_z = \ln \left\{ \frac{E1}{E2} \right\} \quad \ldots\ldots\ldots\ldots \quad 7.7$$

and the shear strain, γ_{yz}, is simply the angle in radians, θ, between the original (y,z) axes and the major and minor axes of the deformed void.

The principal strains, ie. the maximum and minimum values of strain along the major and minor axes of the deformed void are given by,

$$\varepsilon_I = 0.5 \, (\varepsilon_y + \varepsilon_z) + 0.5 \sqrt{ (\varepsilon_y - \varepsilon_z)^2 + \gamma_{yz}^2 } \quad \ldots\ldots \quad 7.8$$

$$\varepsilon_{II} = 0.5 \, (\varepsilon_y + \varepsilon_z) - 0.5 \sqrt{ (\varepsilon_y - \varepsilon_z)^2 + \gamma_{yz}^2 } \quad \ldots\ldots \quad 7.9$$

and the maximum shear strain is given by,

$$\gamma_{max} = \pm \, 0.5 \sqrt{ (\varepsilon_y - \varepsilon_z)^2 + \gamma_{yz}^2 } \quad \ldots\ldots\ldots \quad 7.10$$

CHAPTER EIGHT

EXPERIMENTAL RESULTS

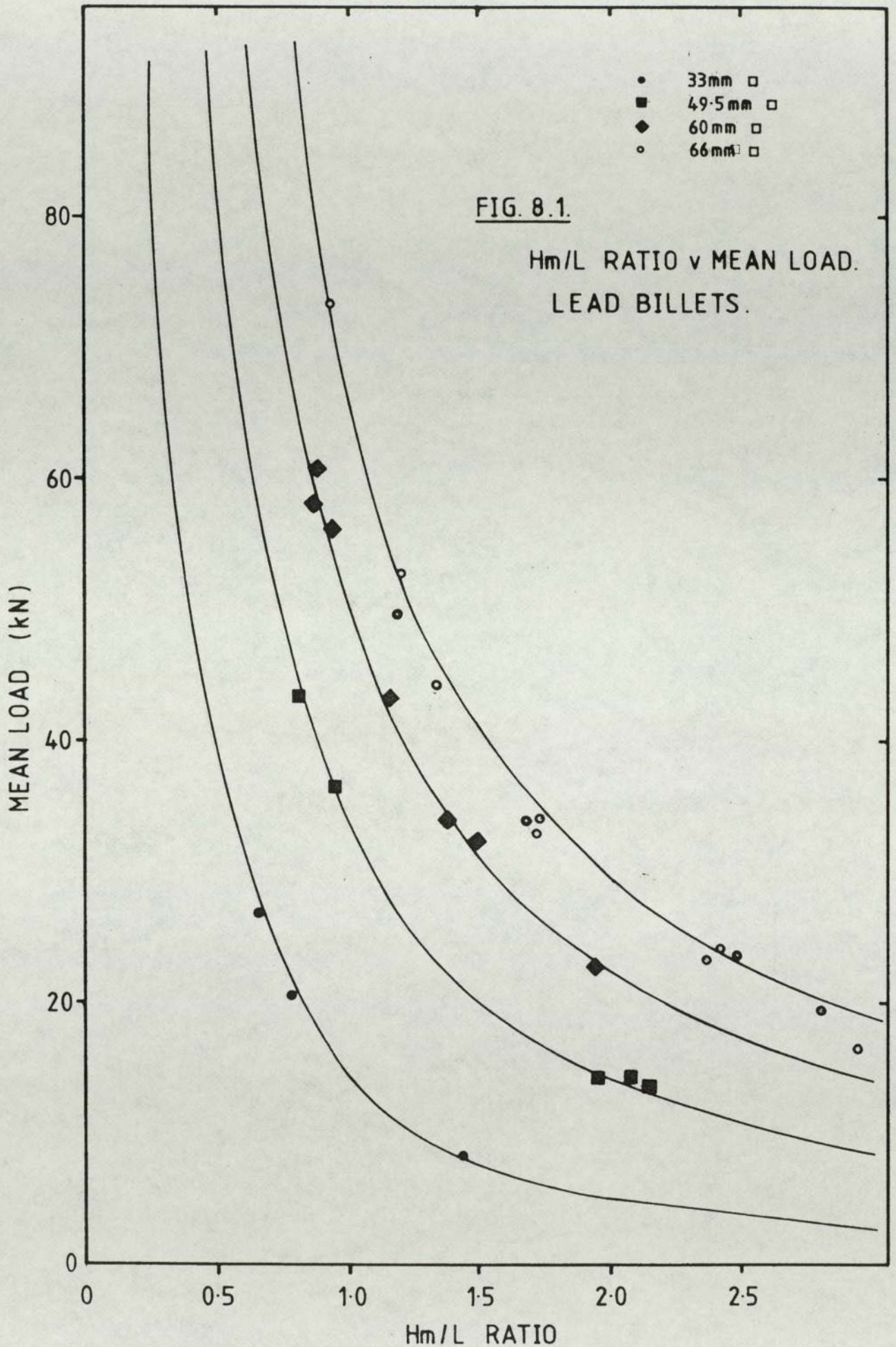
33mm
49·5mm
60mm
66mm
FIG. 8.1.
Hm/L RATIO v MEAN LOAD.
LEAD BILLETS.
MEAN LOAD (kN)
0
20
40
60
80
0
0·5
1·0
1·5
2·0
2·5
Hm/L RATIO

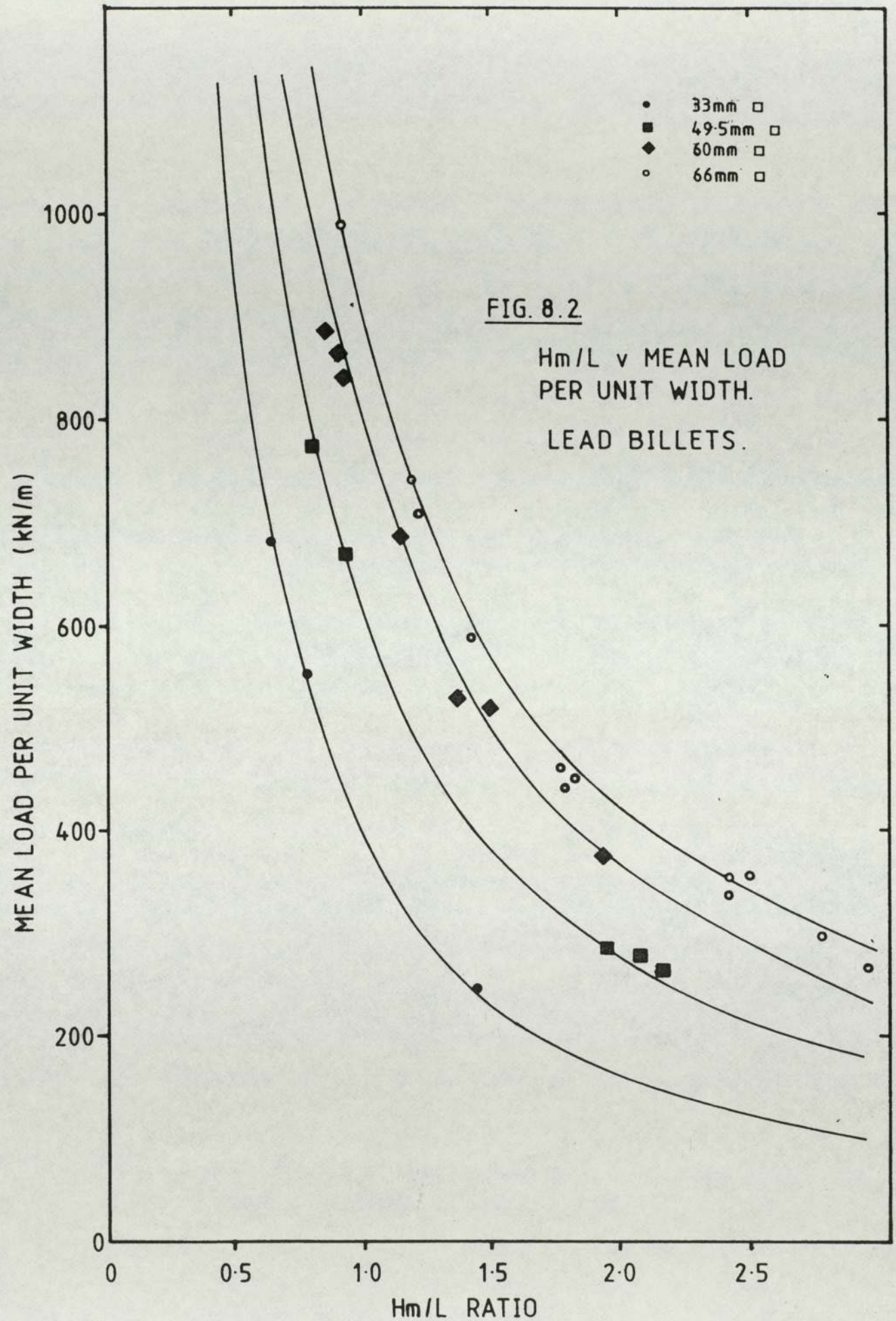

FIG. 8.2

Hm/L v MEAN LOAD PER UNIT WIDTH.

LEAD BILLETS.

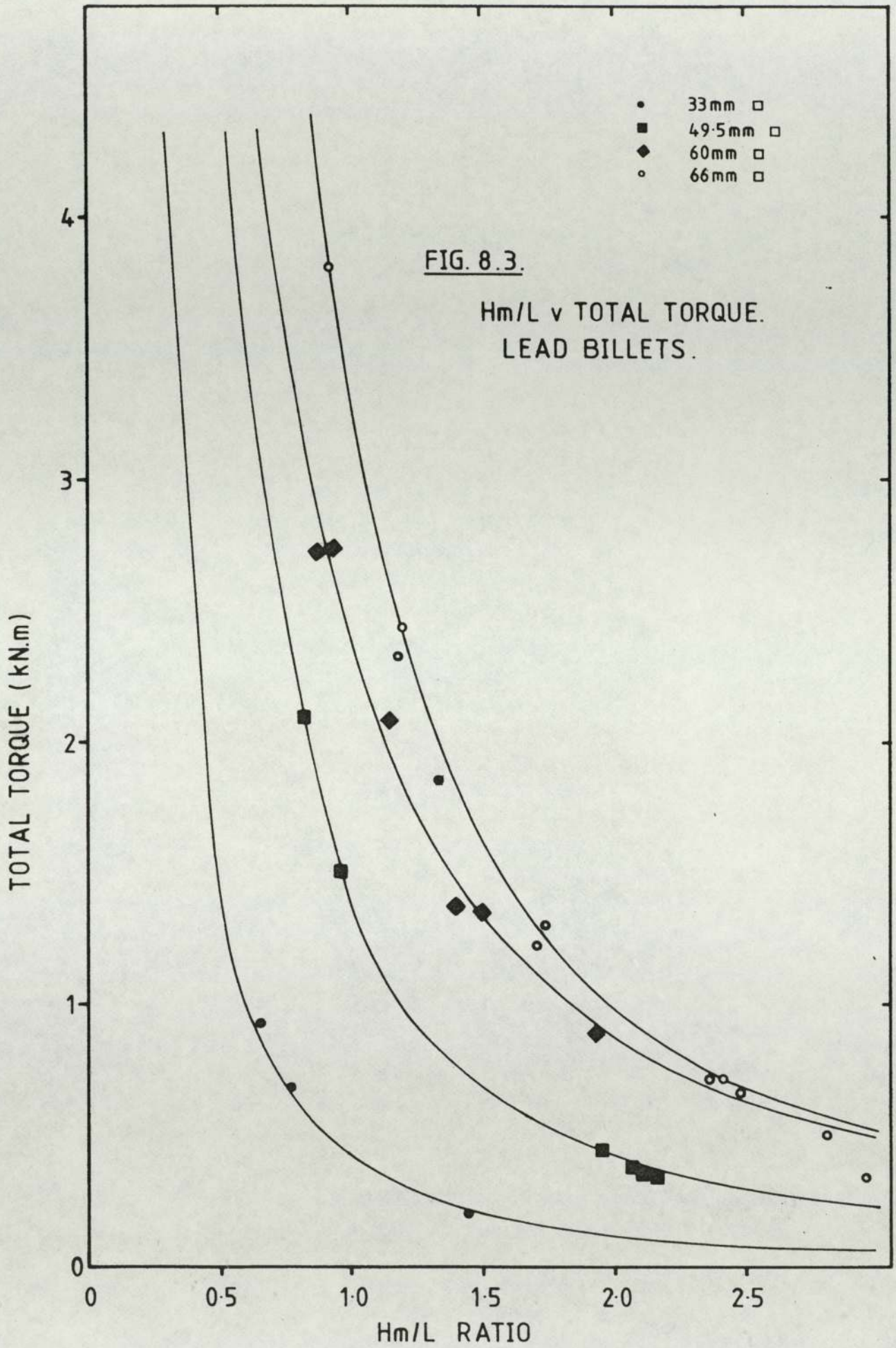
33mm
49·5mm
60mm
66mm
FIG. 8.3.
Hm/L v TOTAL TORQUE.
LEAD BILLETS.
TOTAL TORQUE (kN.m)
Hm/L RATIO
0
1
2
3
4
0
0·5
1·0
1·5
2·0
2·5

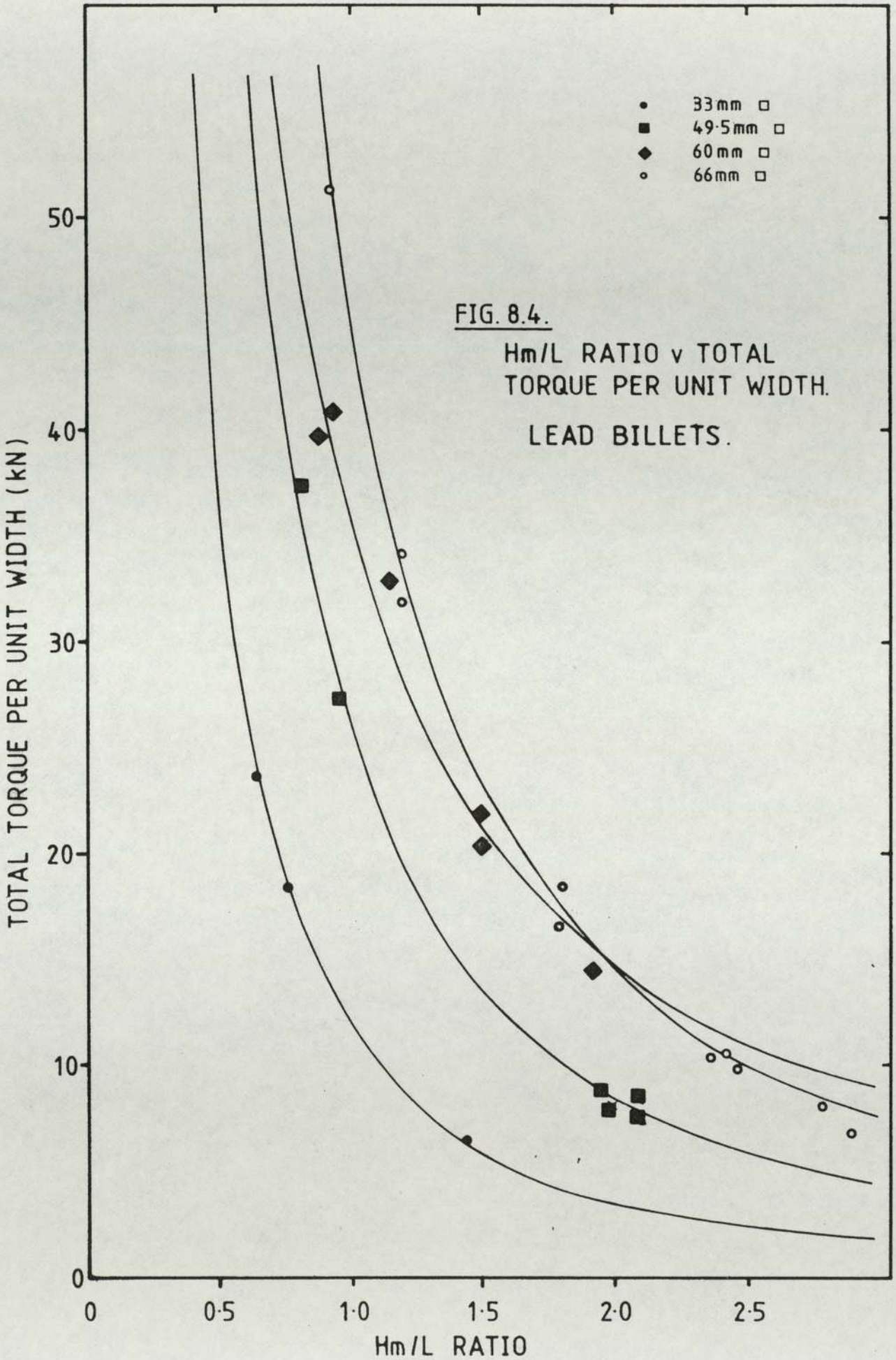
33mm □
49·5mm □
60mm □
66mm □
FIG. 8.4.
Hm/L RATIO v TOTAL TORQUE PER UNIT WIDTH.
LEAD BILLETS.
TOTAL TORQUE PER UNIT WIDTH (kN)
0
10
20
30
40
50
0
0·5
1·0
1·5
2·0
2·5
Hm/L RATIO

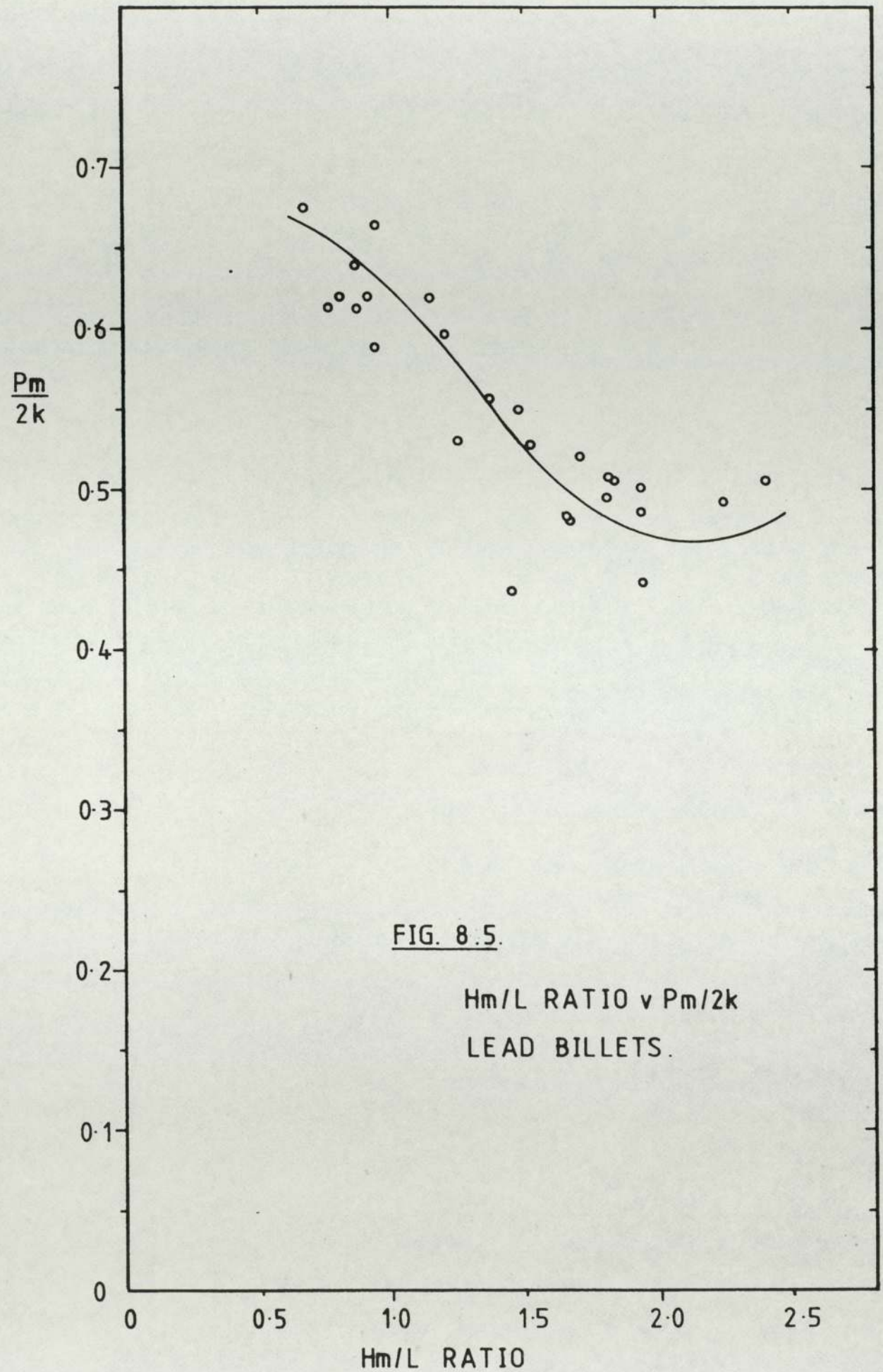

FIG. 8.5.

Hm/L RATIO v Pm/2k

LEAD BILLETS.

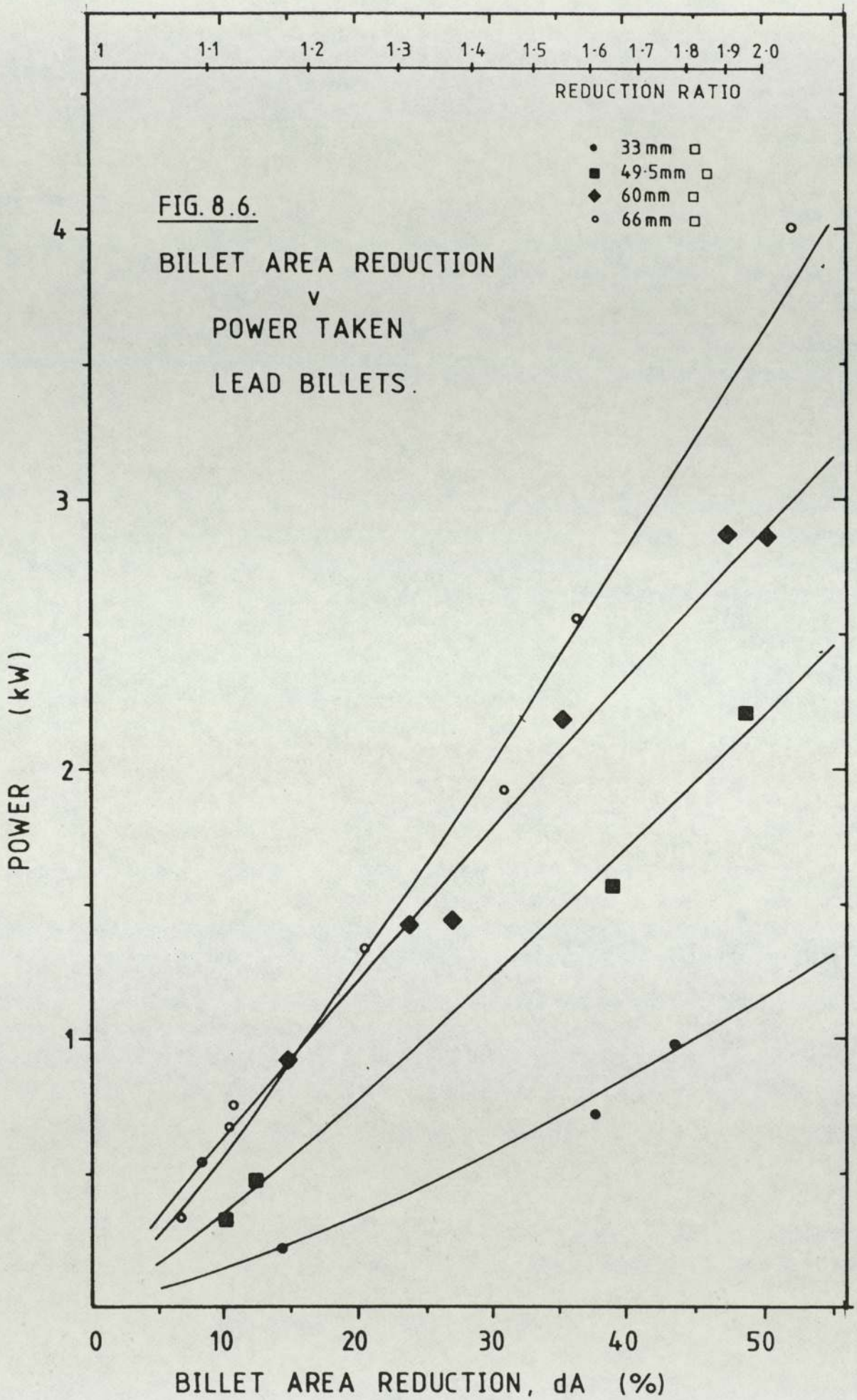
1
1·1
1·2
1·3
1·4
1·5
1·6
1·7
1·8
1·9
2·0
REDUCTION RATIO
33mm
49·5mm
60mm
66mm
FIG. 8.6.
BILLET AREA REDUCTION
v
POWER TAKEN
LEAD BILLETS.
POWER (kW)
4
3
2
1
0
10
20
30
40
50
BILLET AREA REDUCTION, dA (%)

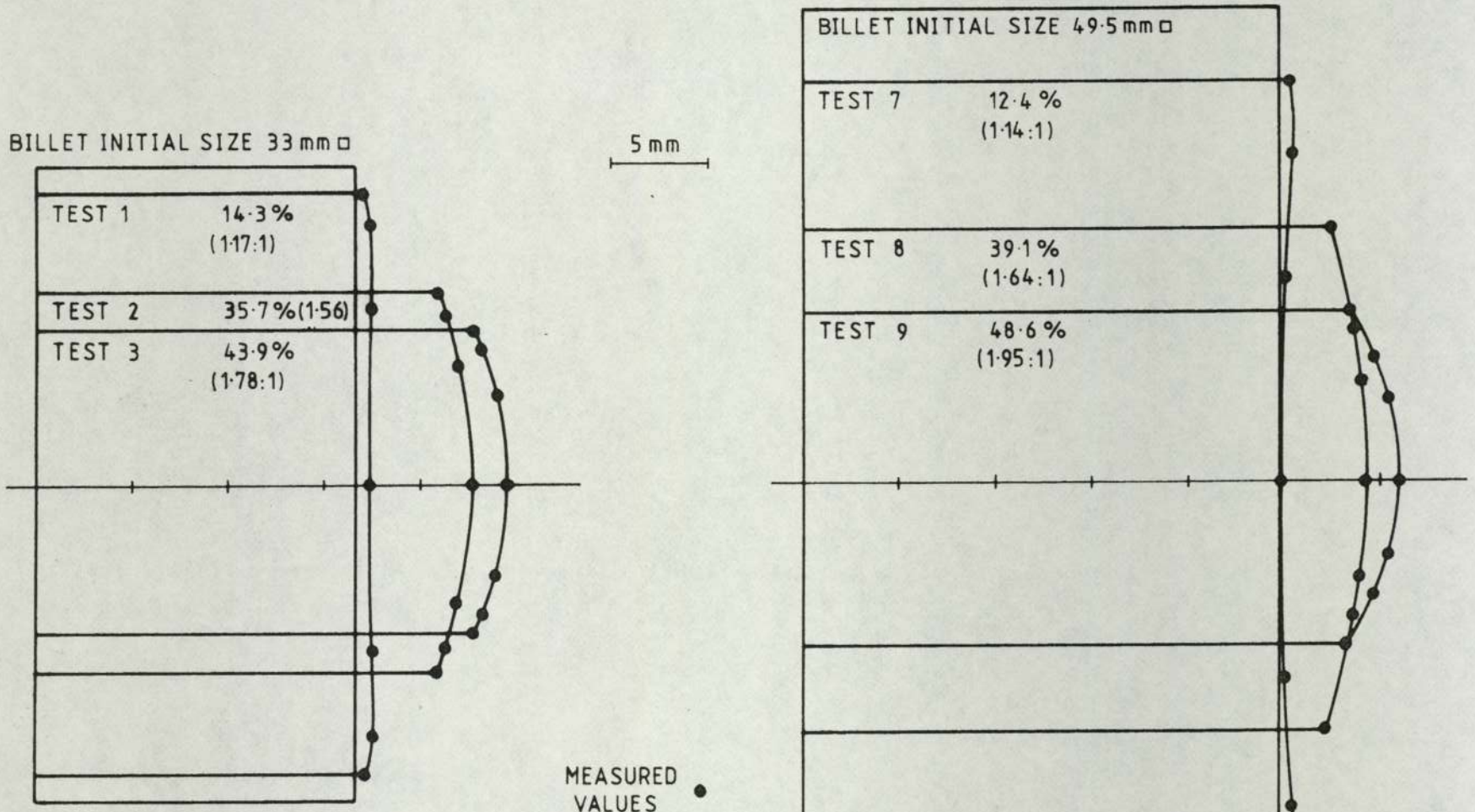

FIG. 8.7.
WIDTH POLYNOMIAL PLOTS FOR VARIOUS REDUCTIONS IN AREA.

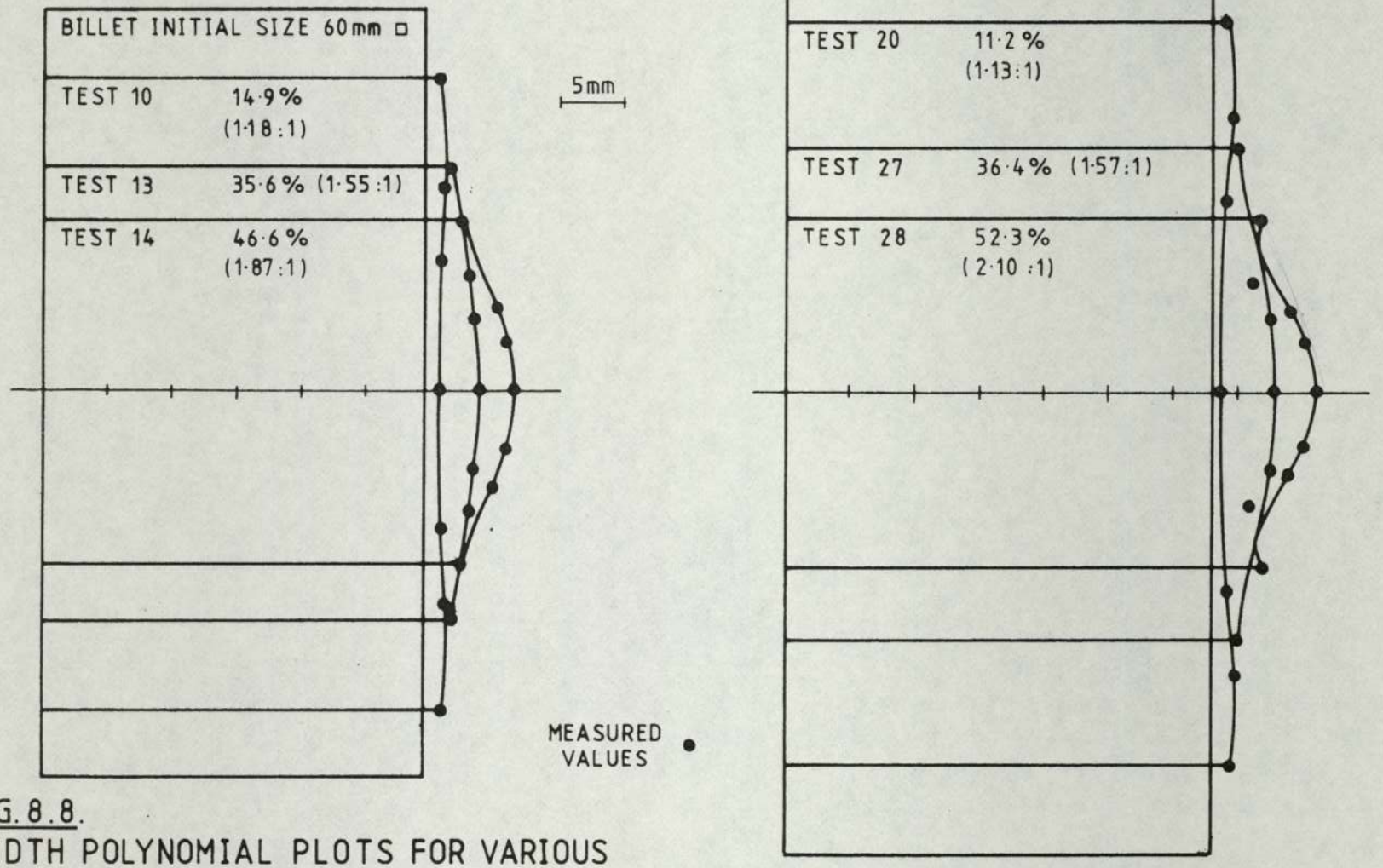

FIG. 8.8.
WIDTH POLYNOMIAL PLOTS FOR VARIOUS REDUCTIONS IN AREA.

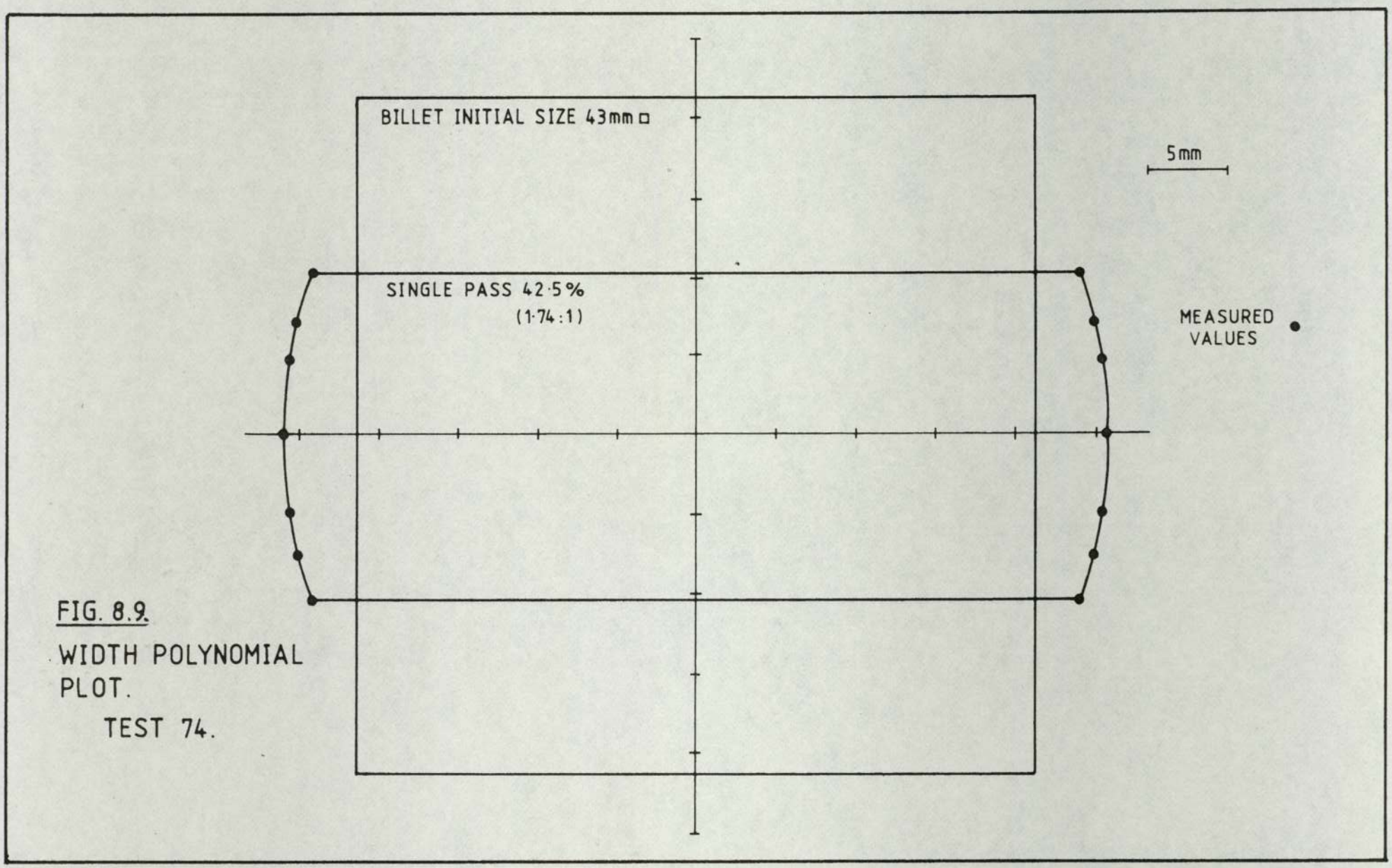

FIG. 8.9.

WIDTH POLYNOMIAL PLOT.

TEST 74.

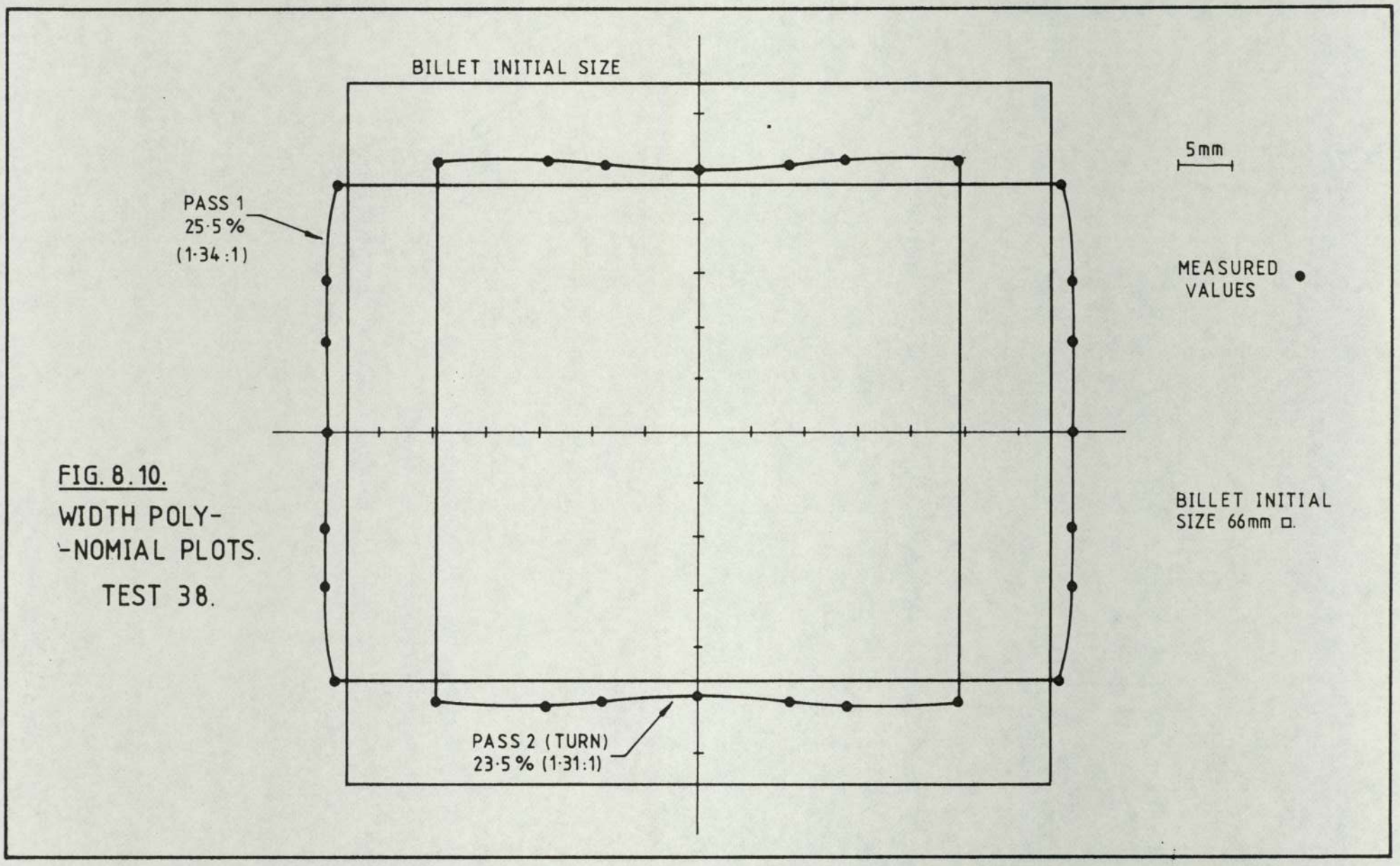

FIG. 8.10.
WIDTH POLY-
-NOMIAL PLOTS.
TEST 38.

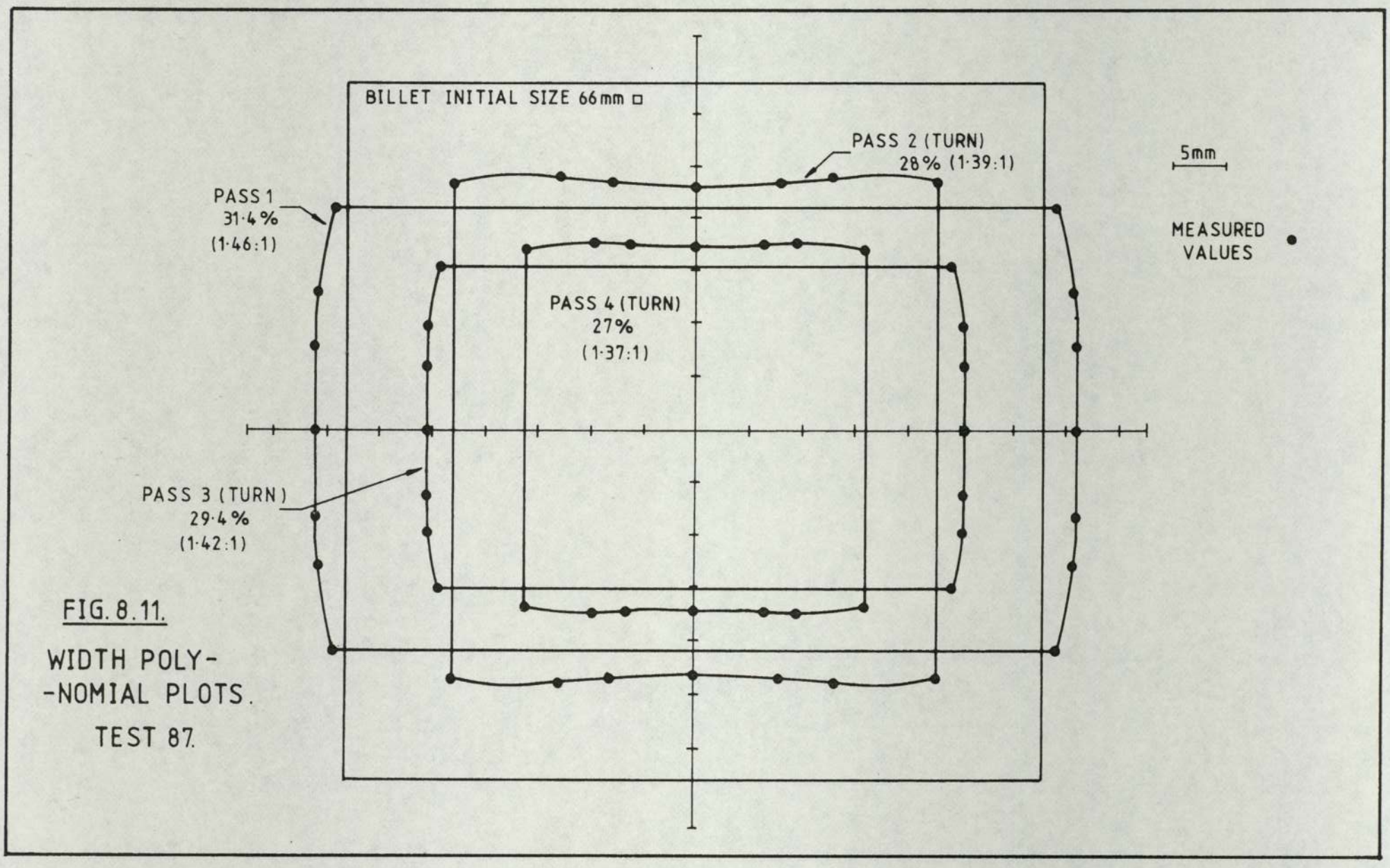

FIG. 8.11.

WIDTH POLY-
-NOMIAL PLOTS.

TEST 87.

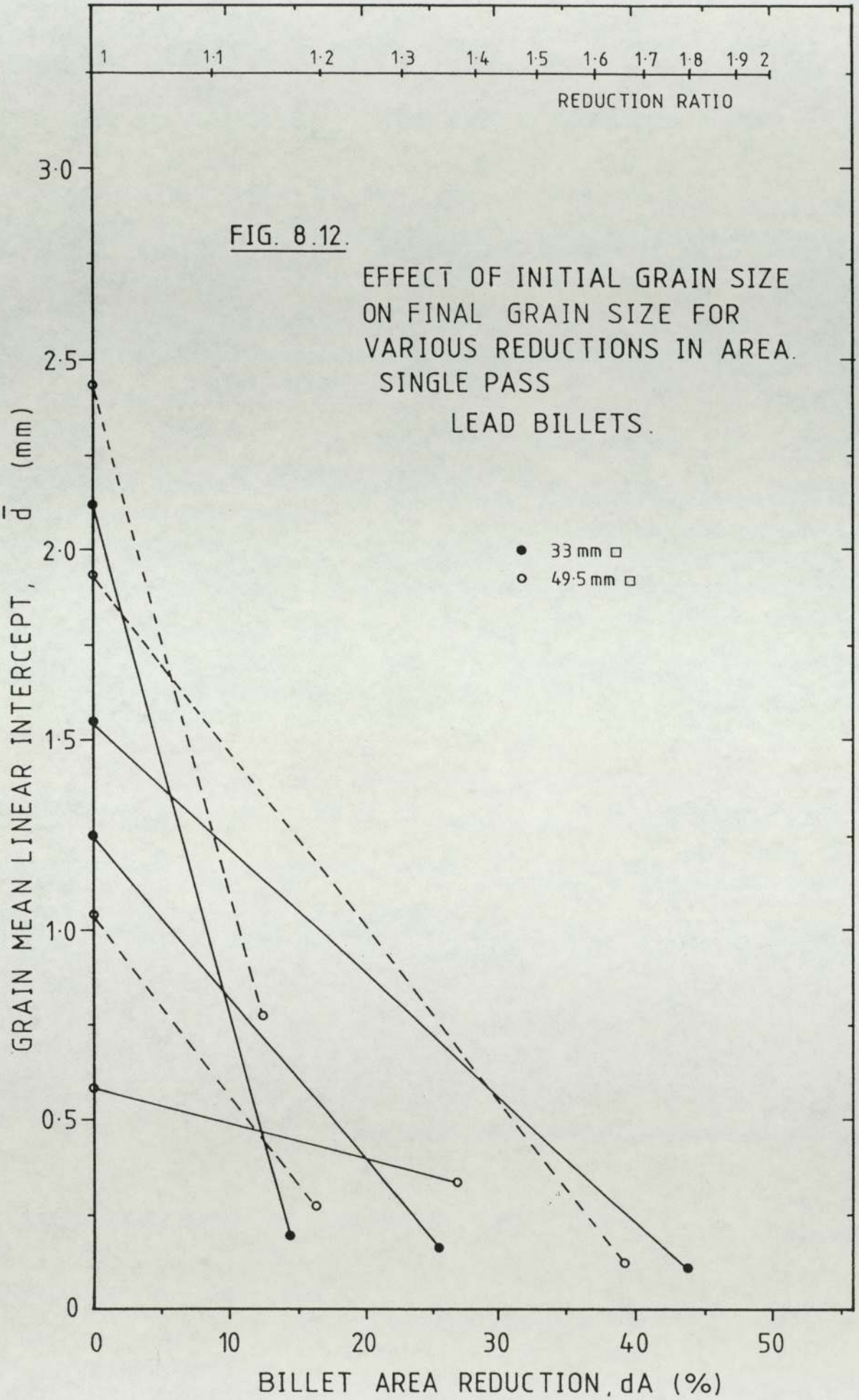

FIG. 8.12.

EFFECT OF INITIAL GRAIN SIZE ON FINAL GRAIN SIZE FOR VARIOUS REDUCTIONS IN AREA. SINGLE PASS LEAD BILLETS.

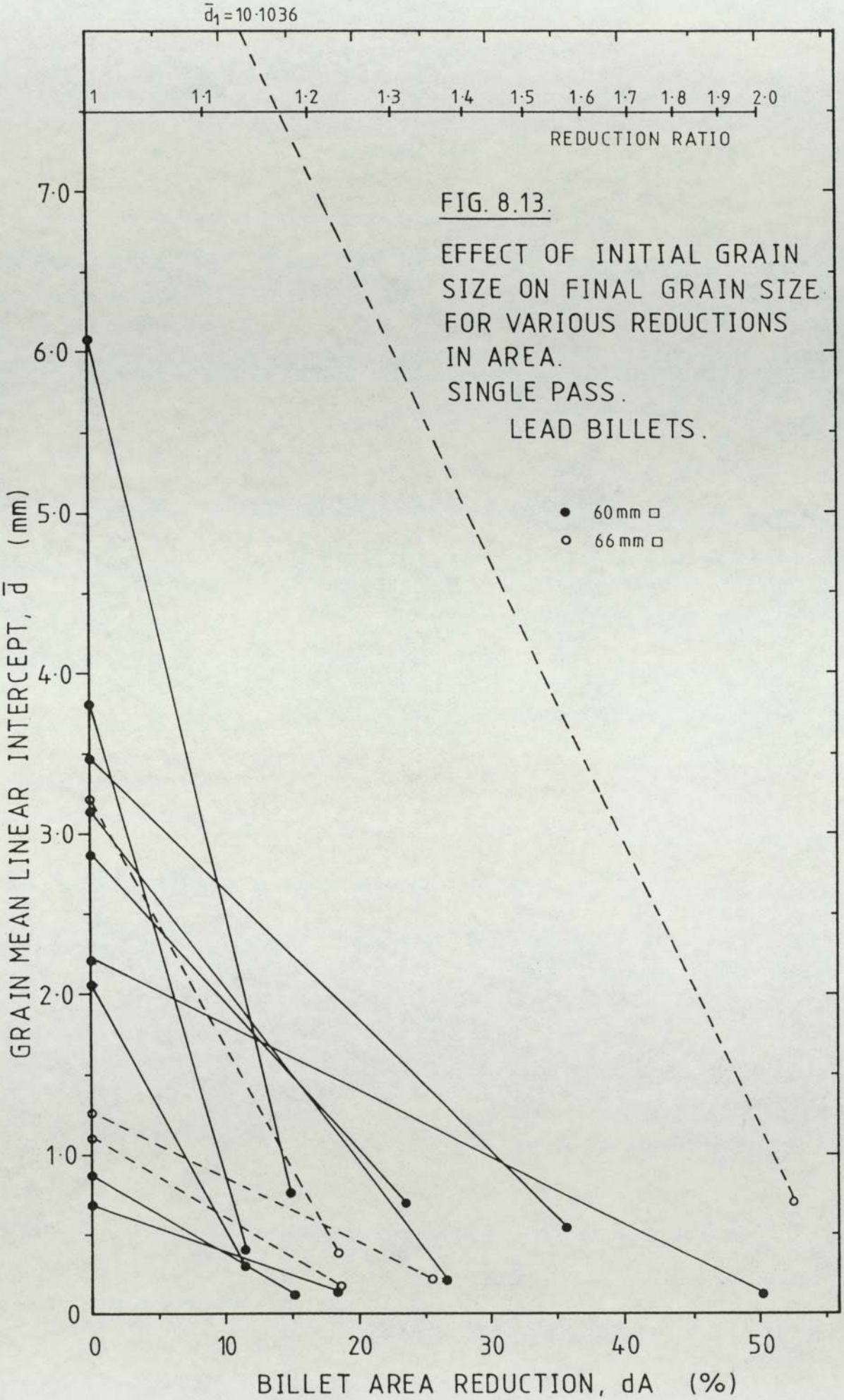

FIG. 8.13.

EFFECT OF INITIAL GRAIN SIZE ON FINAL GRAIN SIZE FOR VARIOUS REDUCTIONS IN AREA.
SINGLE PASS.
LEAD BILLETS.

A.

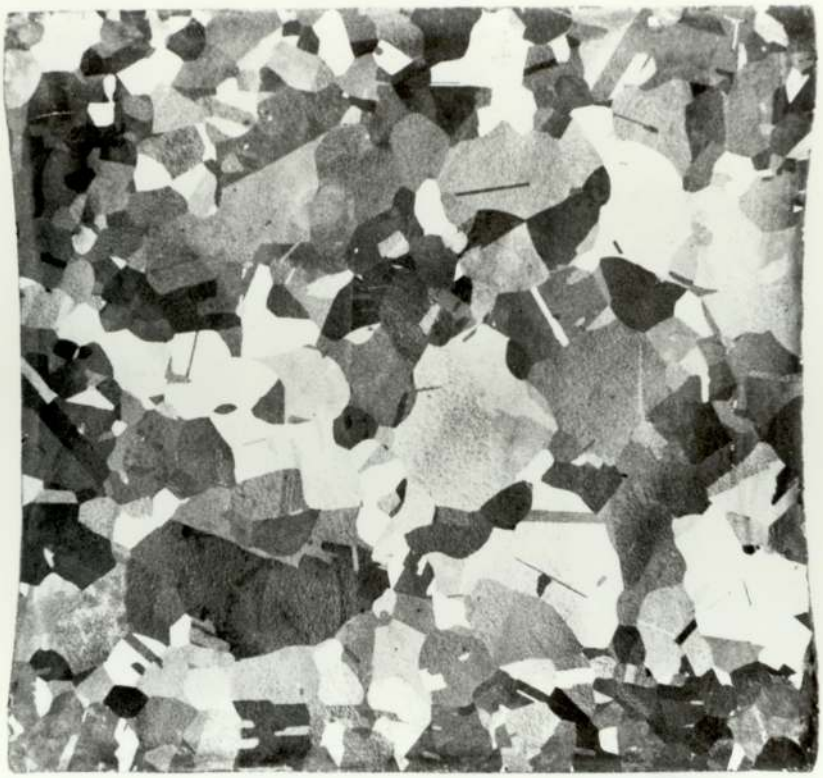

x 1·675

x 2·161

B.

FIG. 8.14.

RECRYSTALLIZATION DUE TO ROLLING.
SINGLE PASS. LEAD BILLET. TEST 52.

A. INITIAL STRUCTURE	$\bar{d} = 2{\cdot}8806 \pm 0{\cdot}1370$ mm.	60mm □.
B. ROLLED STRUCTURE	$\bar{d} = 0{\cdot}6702 \pm 0{\cdot}0294$ mm.	23·89% (1·314)

A.

x 1·307

B.

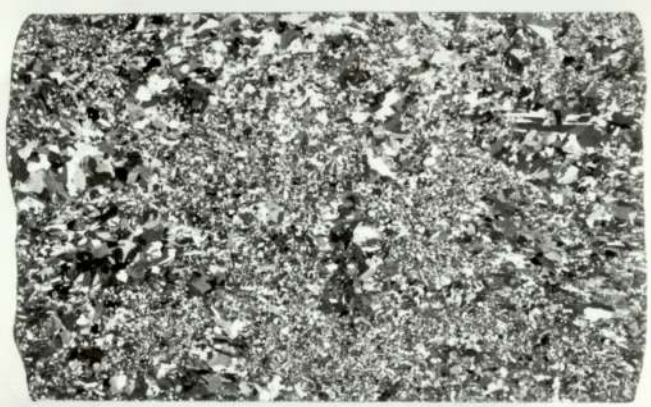

x 1·264

C.

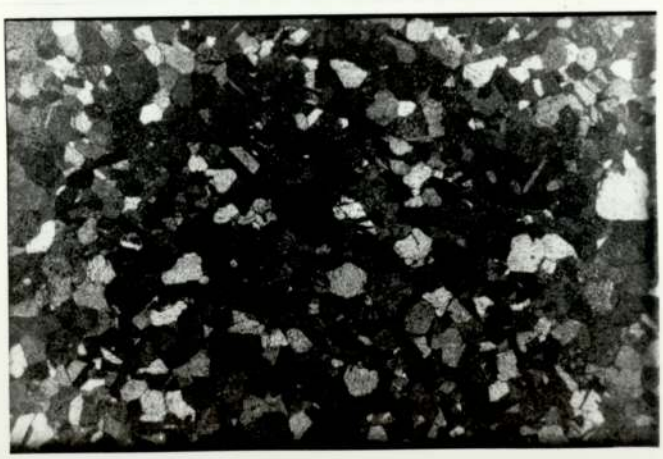

x 40·5

FIG. 8.15.

RECRYSTALLIZATION DUE TO ROLLING.
SINGLE PASS. LEAD BILLET. TEST 53.

A. INITIAL STRUCTURE. $\bar{d}$ = 3·1340 ± 0·06773mm. 60mm □.
B. ROLLED STRUCTURE. $\bar{d}$ = 0·2137 ± 0·0263mm. 26·9% dA (1·368)
C. ROLLED STRUCTURE CENTRAL AREA - HIGH MAG.

A.

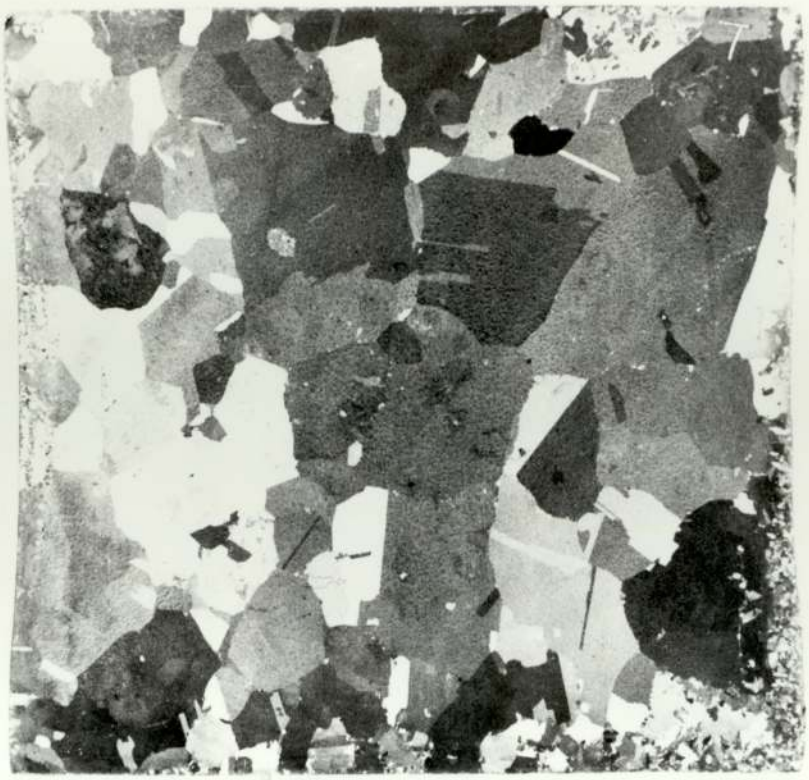

x 1·675

x 2·032

B.

FIG. 8.16.

RECRYSTALLIZATION DUE TO ROLLING.
SINGLE PASS. LEAD BILLET. TEST 54.

A. INITIAL STRUCTURE. $\bar{d}$ = 3·8163 ± 0·4439 mm. 60 mm □.
B. ROLLED STRUCTURE. $\bar{d}$ = 0·5570 ± 0·0317 mm. 35·6% dA (1·553)

A.

x 1·424

B.

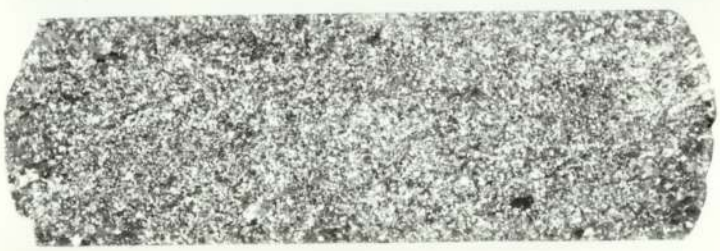

x 1·251

C.

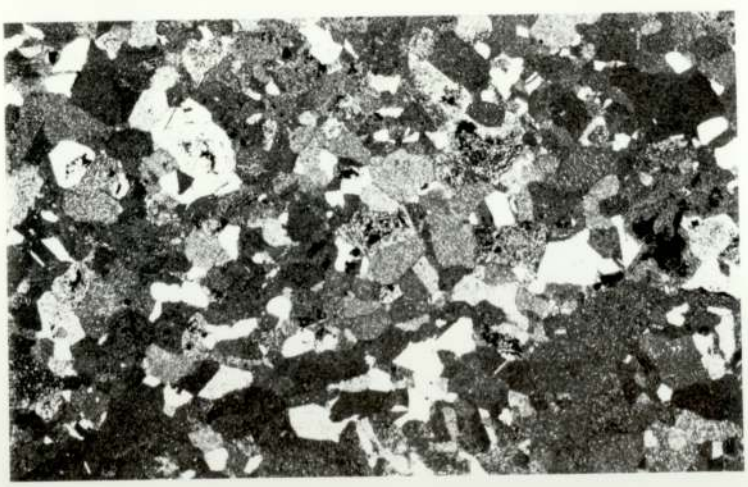

x 40·5

FIG. 8.17.

RECRYSTALLIZATION DUE TO ROLLING.
SINGLE PASS. LEAD BILLET. TEST 55.

A. INITIAL STRUCTURE. $\bar{d}$ = 2·2135 ± 0·1830 mm. 60mm □.
B. ROLLED STRUCTURE. $\bar{d}$ = 0·1259 ± 0·0104 mm. 50·18% dA (2·007)
C. ROLLED STRUCTURE. CENTRAL AREA - HIGH MAG.

A.

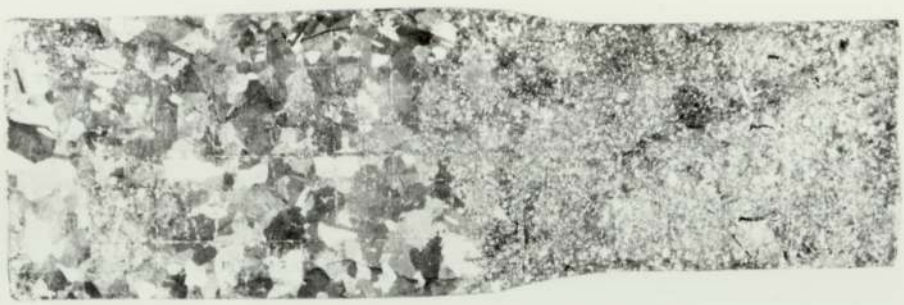

B.

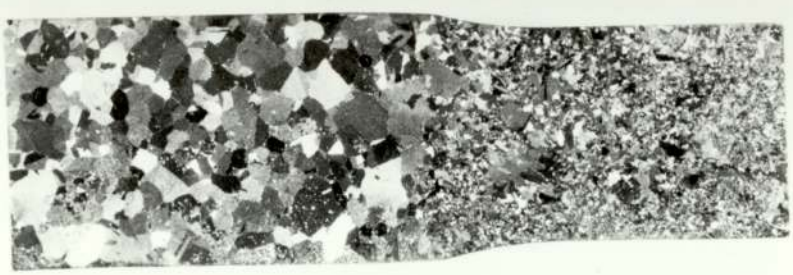

C.

x 0·775

FIG. 8.18.

DEFORMATION ZONE GEOMETRY.
SINGLE PASS. LEAD BILLET. TEST 43.

INITIAL STRUCTURE.	$\bar{d}$ = 2·4370 ± 0·2707 mm.	49·5 mm □.
ROLLED STRUCTURE.	$\bar{d}$ = 0·7774 ± 0·0610 mm.	12·36 % dA (1·141)

A. BILLET OUTER WIDTH SURFACE.
B. BILLET LONGITUDINAL CENTRE LINE.
C. BILLET-ROLL CONTACT SURFACE.

A.

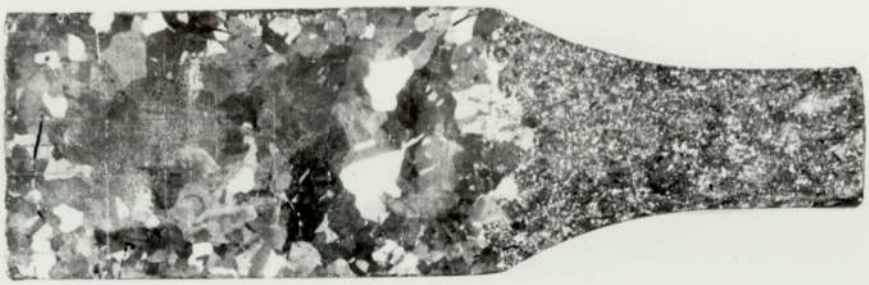

B.

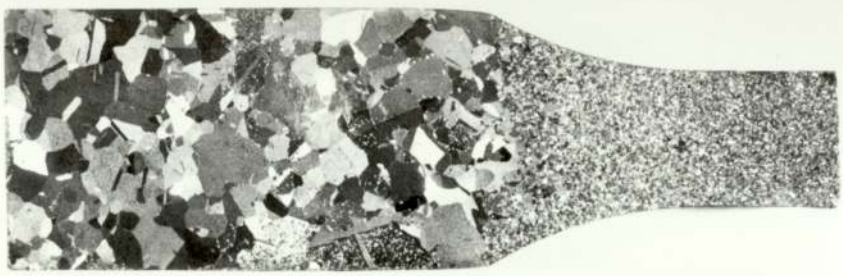

C.

x 0·700

FIG. 8.19.

DEFORMATION ZONE GEOMETRY.
SINGLE PASS. LEAD BILLET. TEST 46.

INITIAL STRUCTURE. $\bar{d} = 1{\cdot}9437 \pm 0{\cdot}1494$ mm. 49·5 mm □.
ROLLED STRUCTURE. $\bar{d} = 0{\cdot}1400 \pm 0{\cdot}0177$ mm. 39·07% dA (1·641)

A. BILLET OUTER WIDTH SURFACE.
B. BILLET LONGITUDINAL CENTRE LINE.
C. BILLET-ROLL CONTACT SURFACE.

A.

B.

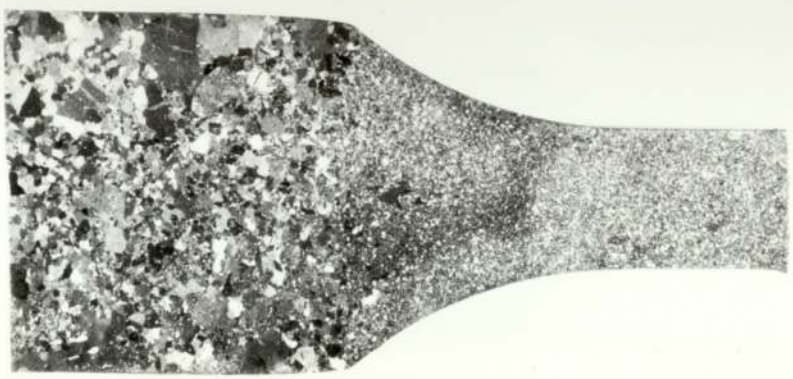

C.

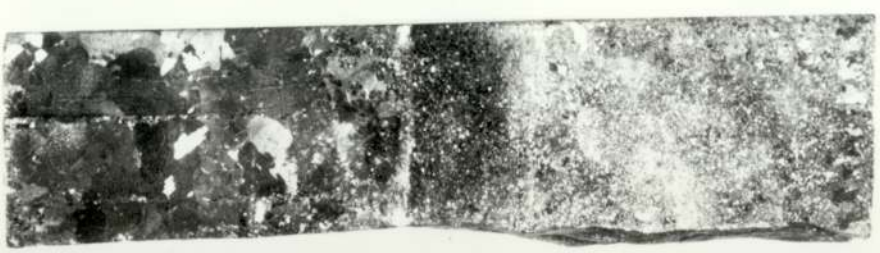

x 0·696

FIG. 8.20.

DEFORMATION ZONE GEOMETRY.
SINGLE PASS. LEAD BILLET. TEST 59.

INITIAL STRUCTURE. $\bar{d}$ = 10·1036 ± 1·5153mm. 66mm □.
ROLLED STRUCTURE. $\bar{d}$ = 0·6822 ± 0·0836mm. 52·25% dA (2·094)

A. BILLET OUTER WIDTH SURFACE.
B. BILLET LONGITUDINAL CENTRE LINE.
C. BILLET-ROLL CONTACT SURFACE.

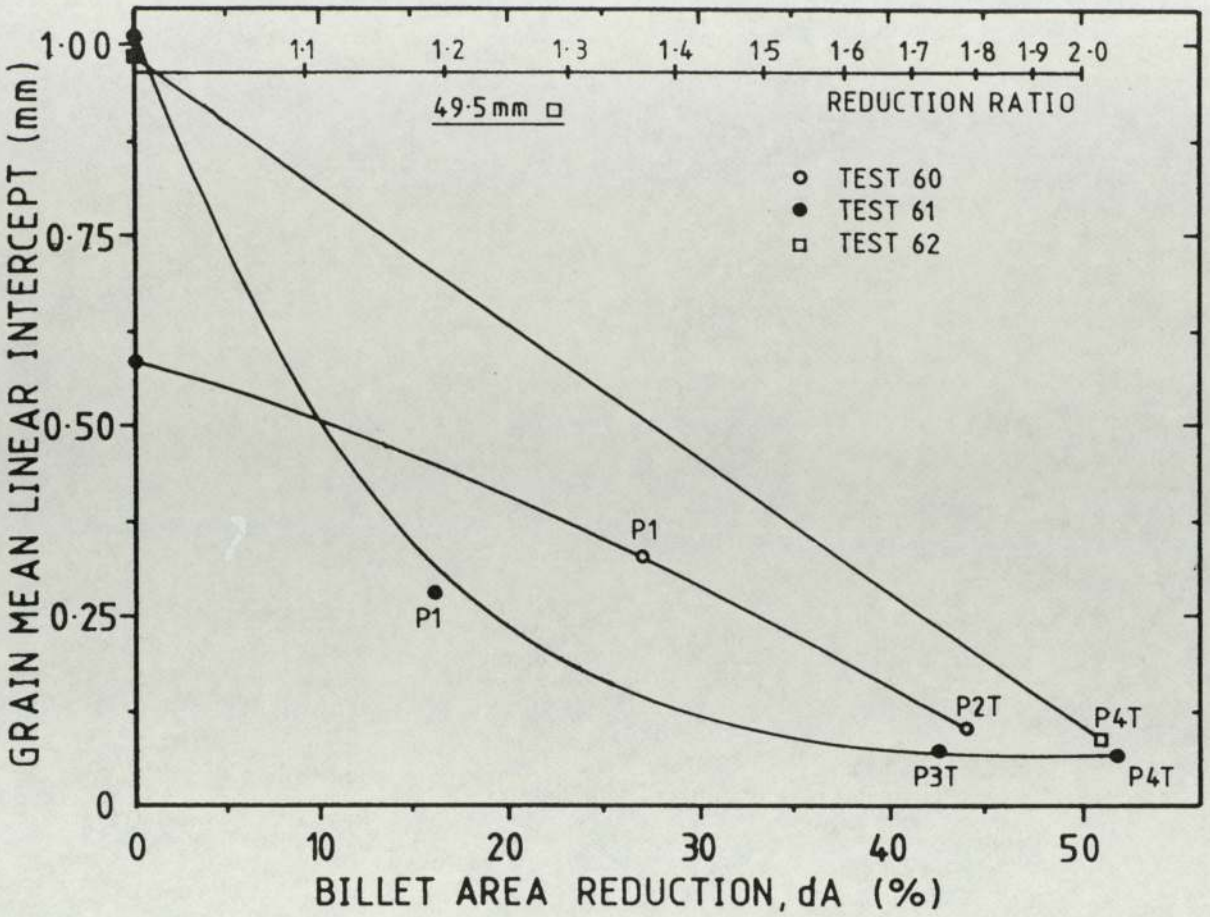

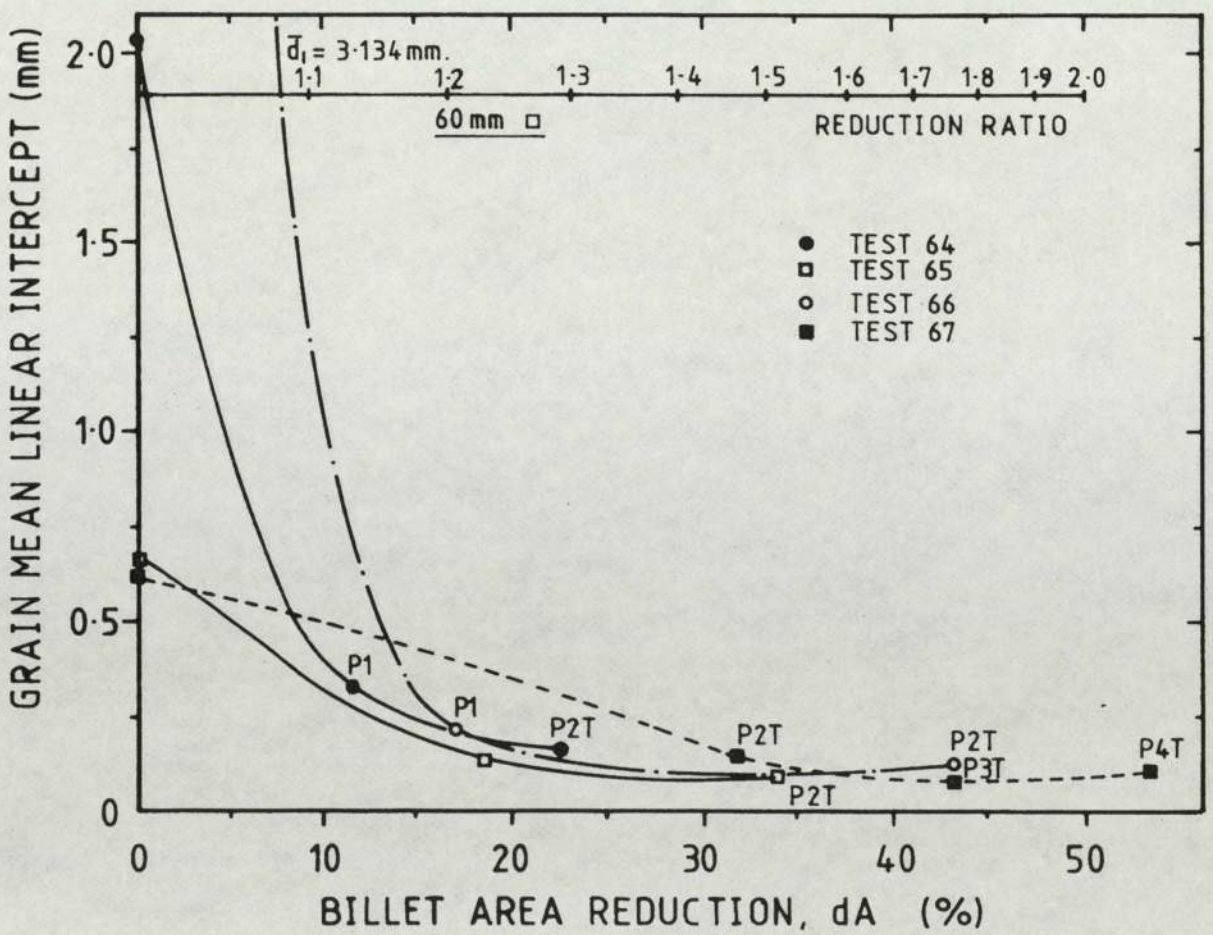

FIG. 8.21.

LEAD GRAIN REFINEMENT WITH REDUCTION.

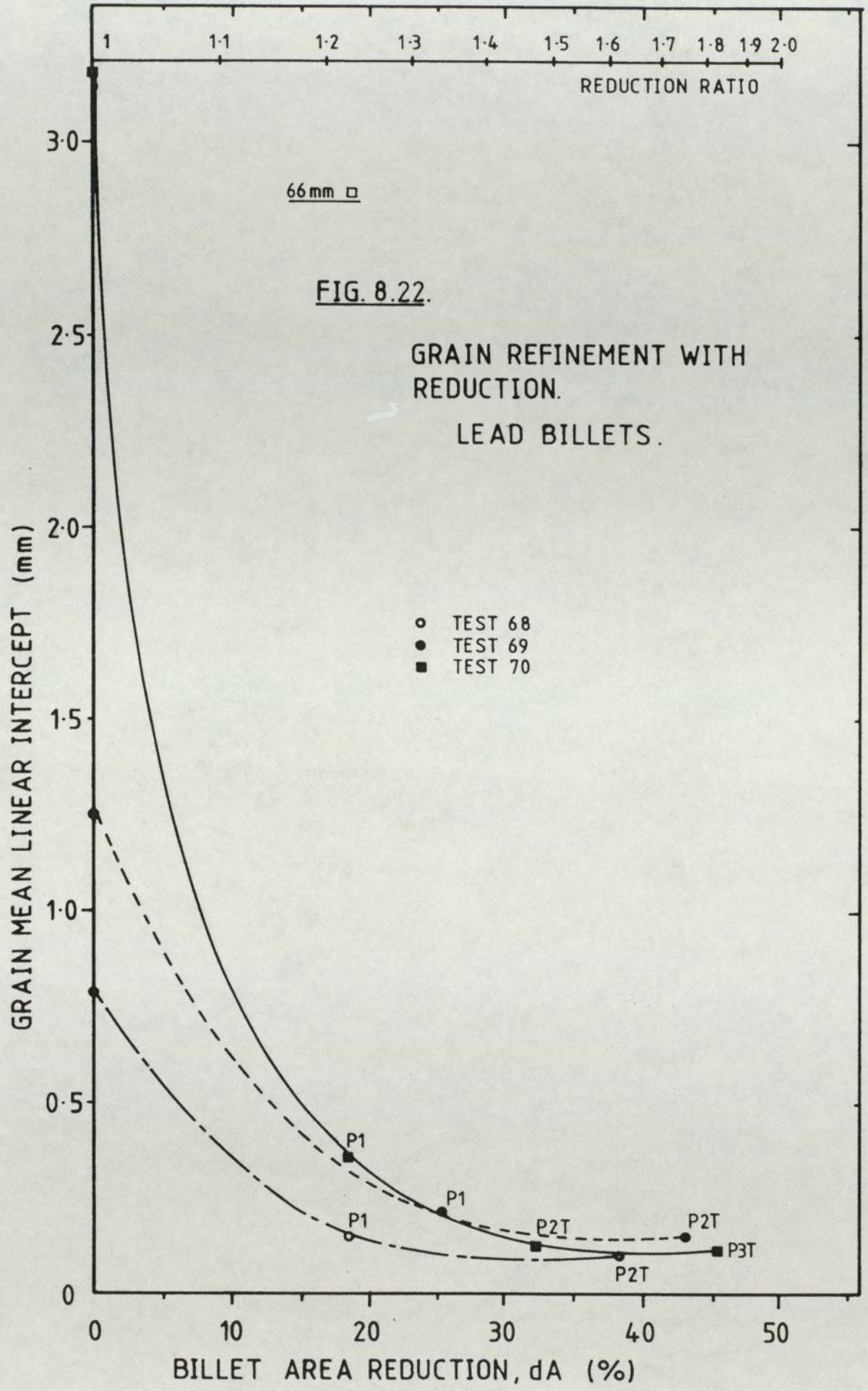
1
1·1
1·2
1·3
1·4
1·5
1·6
1·7
1·8
1·9
2·0
REDUCTION RATIO
66mm □
FIG. 8.22.
GRAIN REFINEMENT WITH REDUCTION.
LEAD BILLETS.
TEST 68
TEST 69
TEST 70
GRAIN MEAN LINEAR INTERCEPT (mm)
3·0
2·5
2·0
1·5
1·0
0·5
0
P1
P1
P1
P2T
P2T
P2T
P3T
0
10
20
30
40
50
BILLET AREA REDUCTION, dA (%)

A.

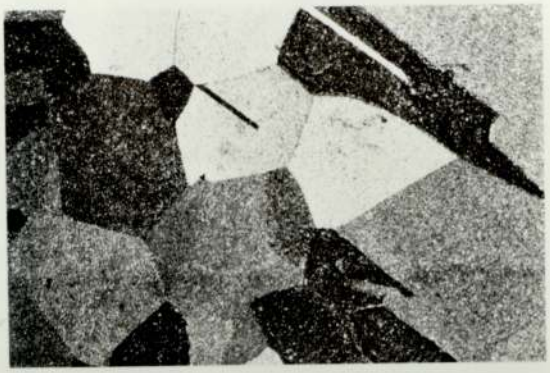

x 40·5

B.

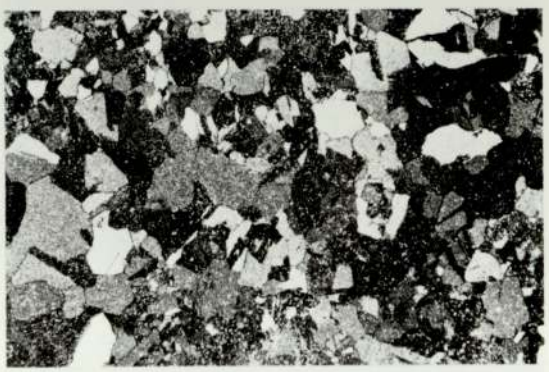

x 40·5

C.

x 40·5

D.

x 81

FIG. 8.23.

RECRYSTALLIZATION DUE TO ROLLING.
MULTI-PASS. LEAD BILLET. TEST 67.

A. INITIAL STRUCTURE.	$\bar{d}$ = 0·6387 ± 0·1236mm.	60mm □.
B. ROLLED STRUCTURE PASS 2T.	$\bar{d}$ = 0·1332 ± 0·0195mm.	31·98% dA (1·470)
C. ROLLED STRUCTURE PASS 3T.	$\bar{d}$ = 0·0953 ± 0·0050mm.	43·14% dA (1·759)
D. ROLLED STRUCTURE PASS 4T.	$\bar{d}$ = 0·1053 ± 0·0171 mm	53·59% dA (2·155)

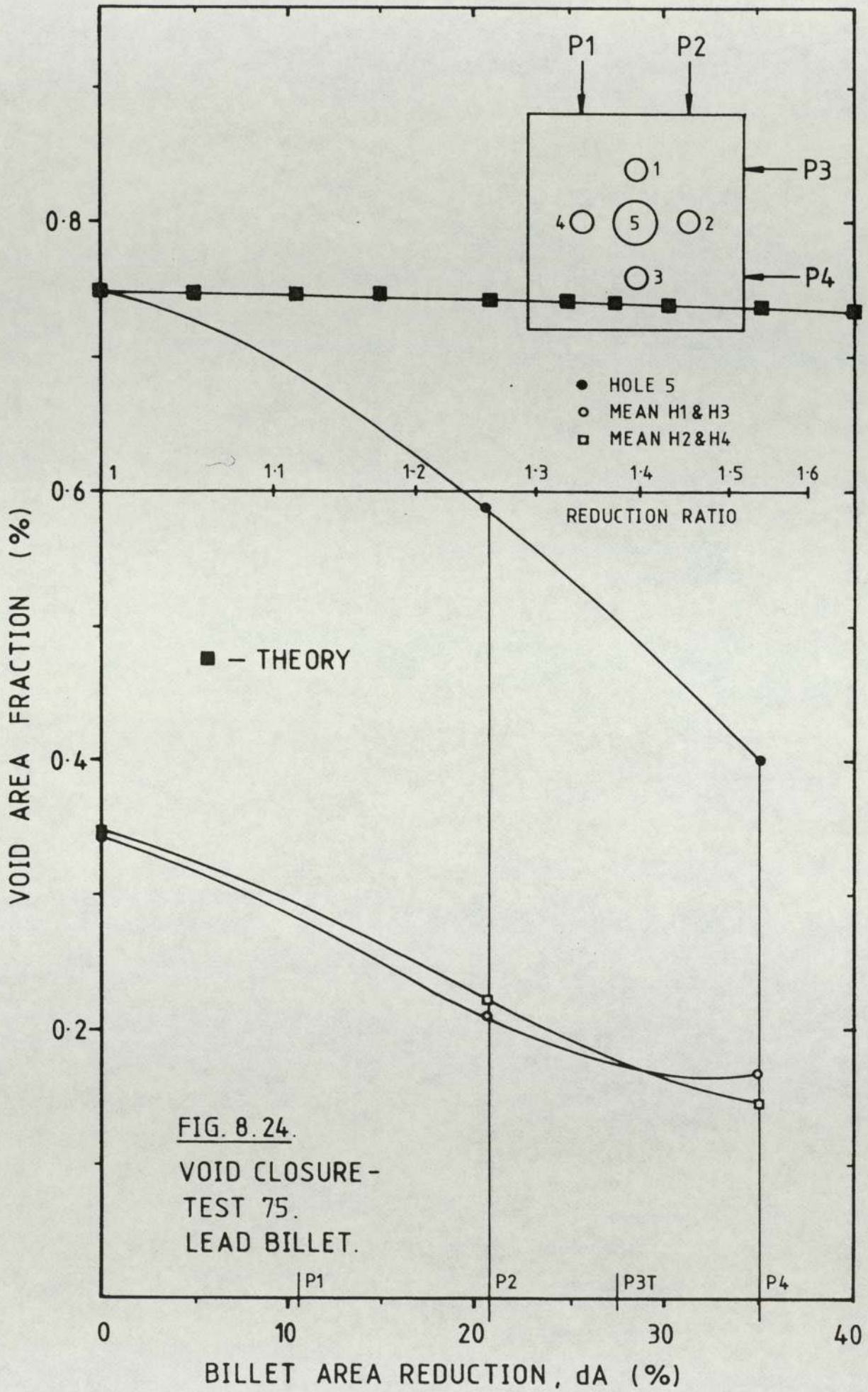

FIG. 8.24.
VOID CLOSURE - TEST 75. LEAD BILLET.

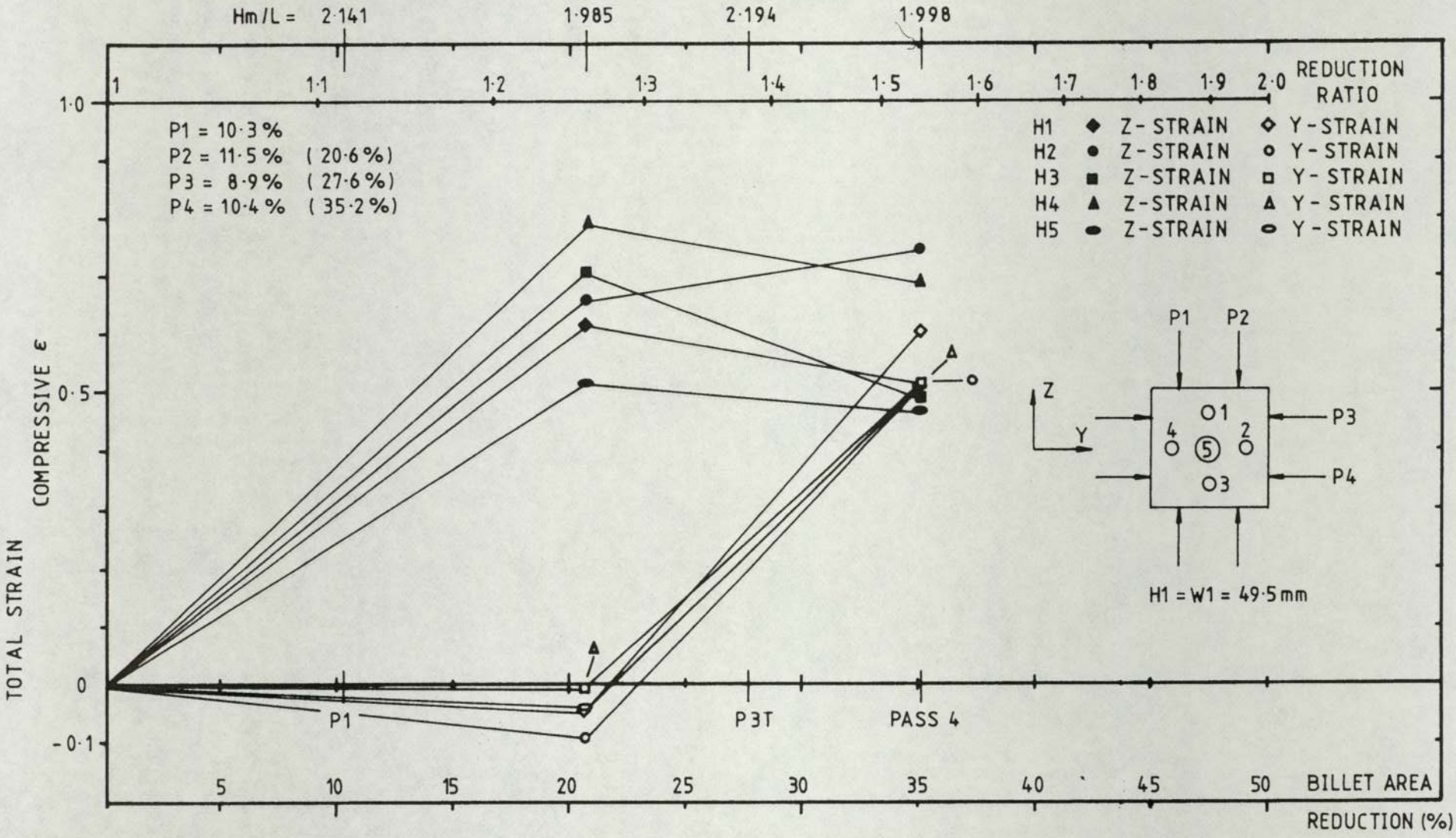

FIG. 8.25. EFFECT OF PASS SCHEDULE ON VOID AXIAL STRAINS. TEST 75.

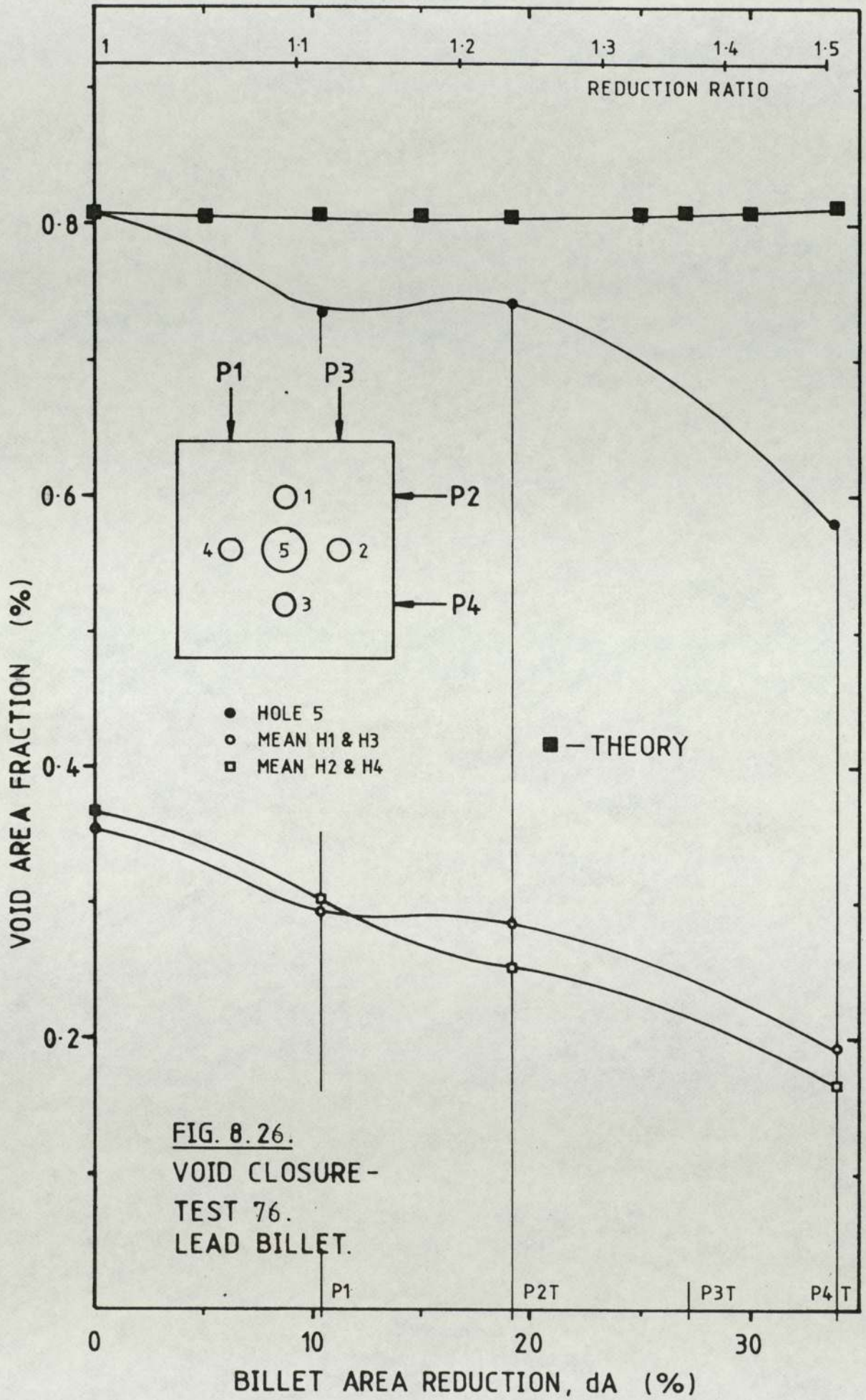

FIG. 8.26.
VOID CLOSURE - TEST 76.
LEAD BILLET.

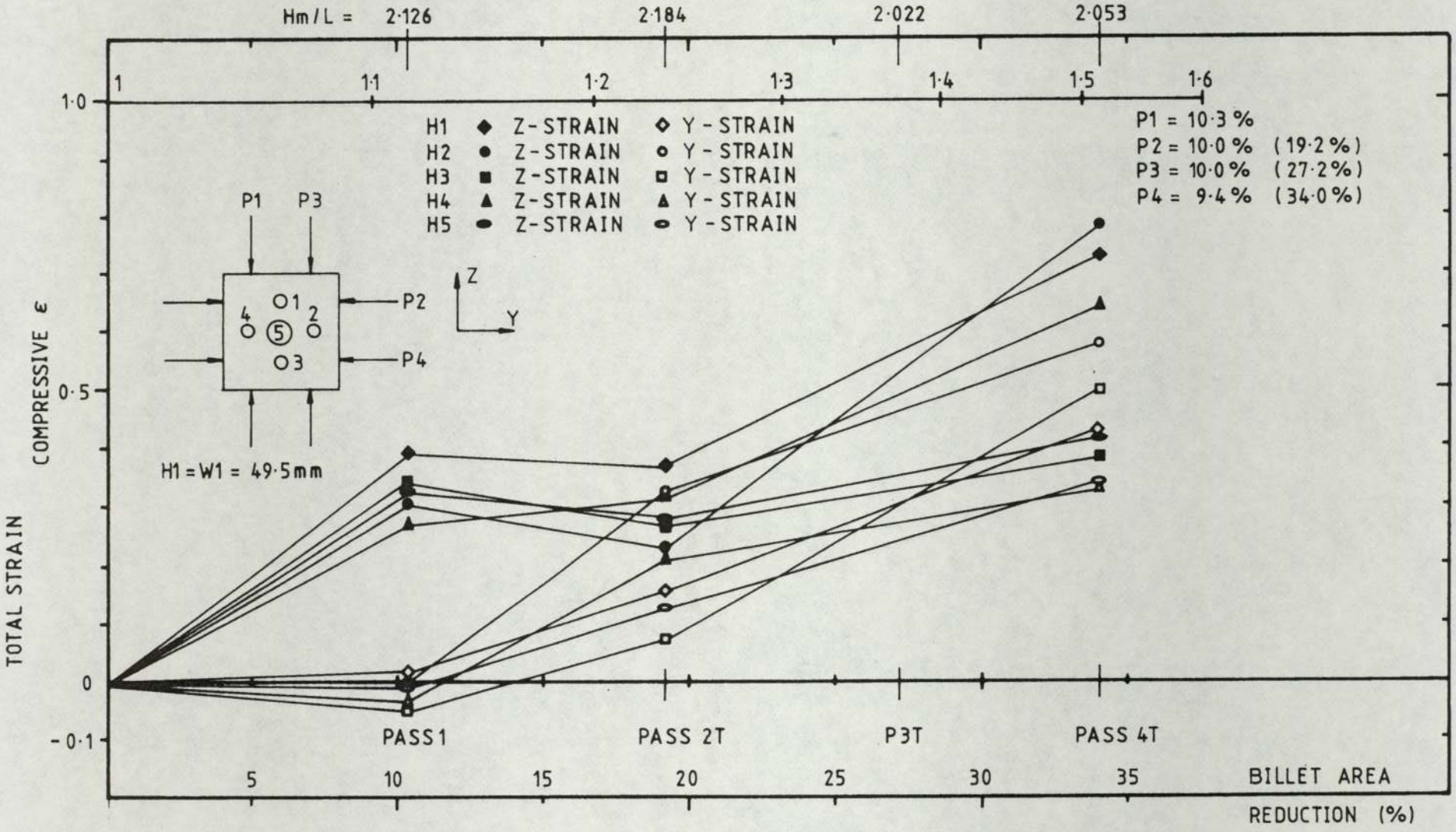

FIG. 8.27. EFFECT OF PASS SCHEDULE ON VOID AXIAL STRAINS. TEST 76.

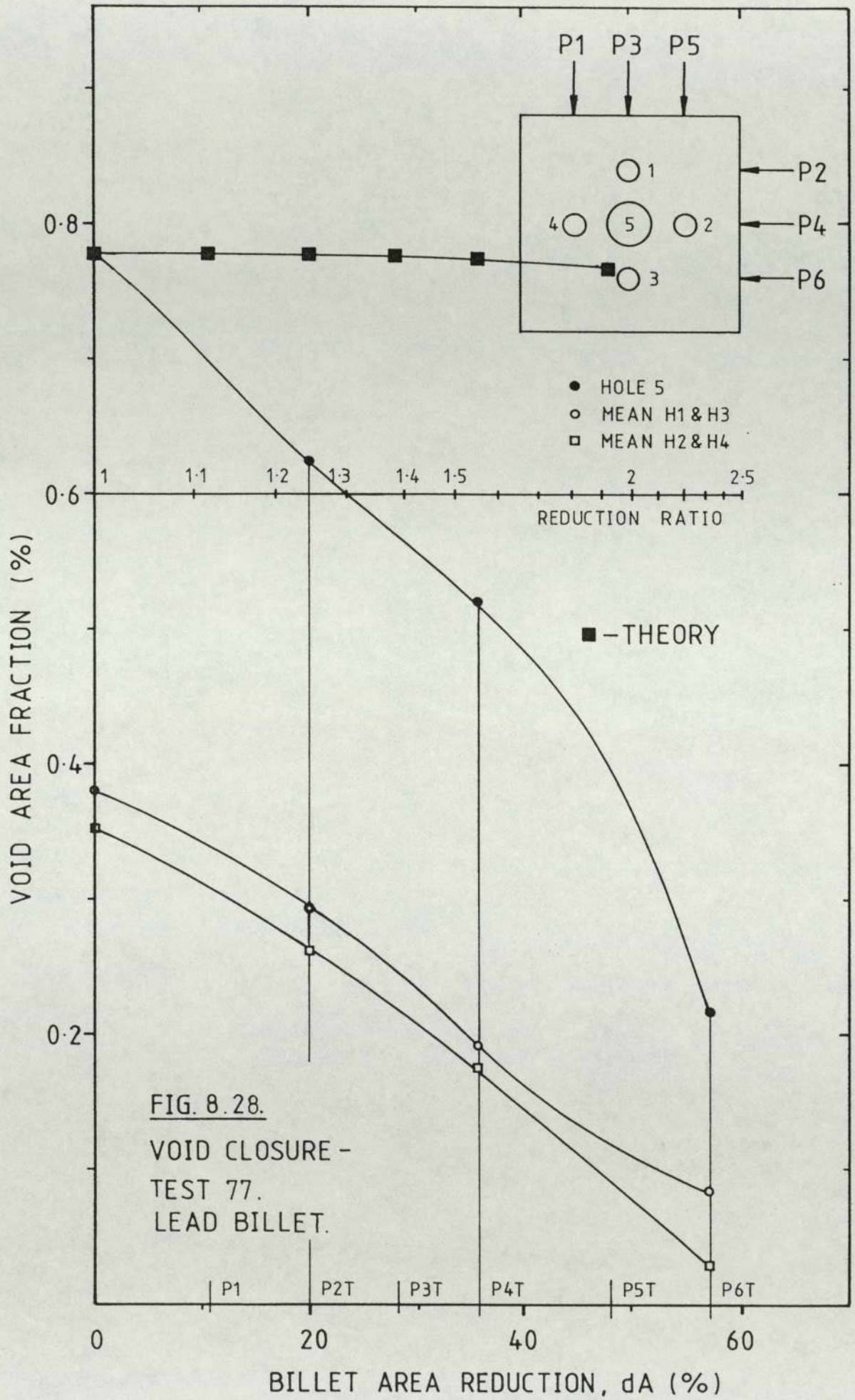

FIG. 8.28.

VOID CLOSURE - TEST 77. LEAD BILLET.

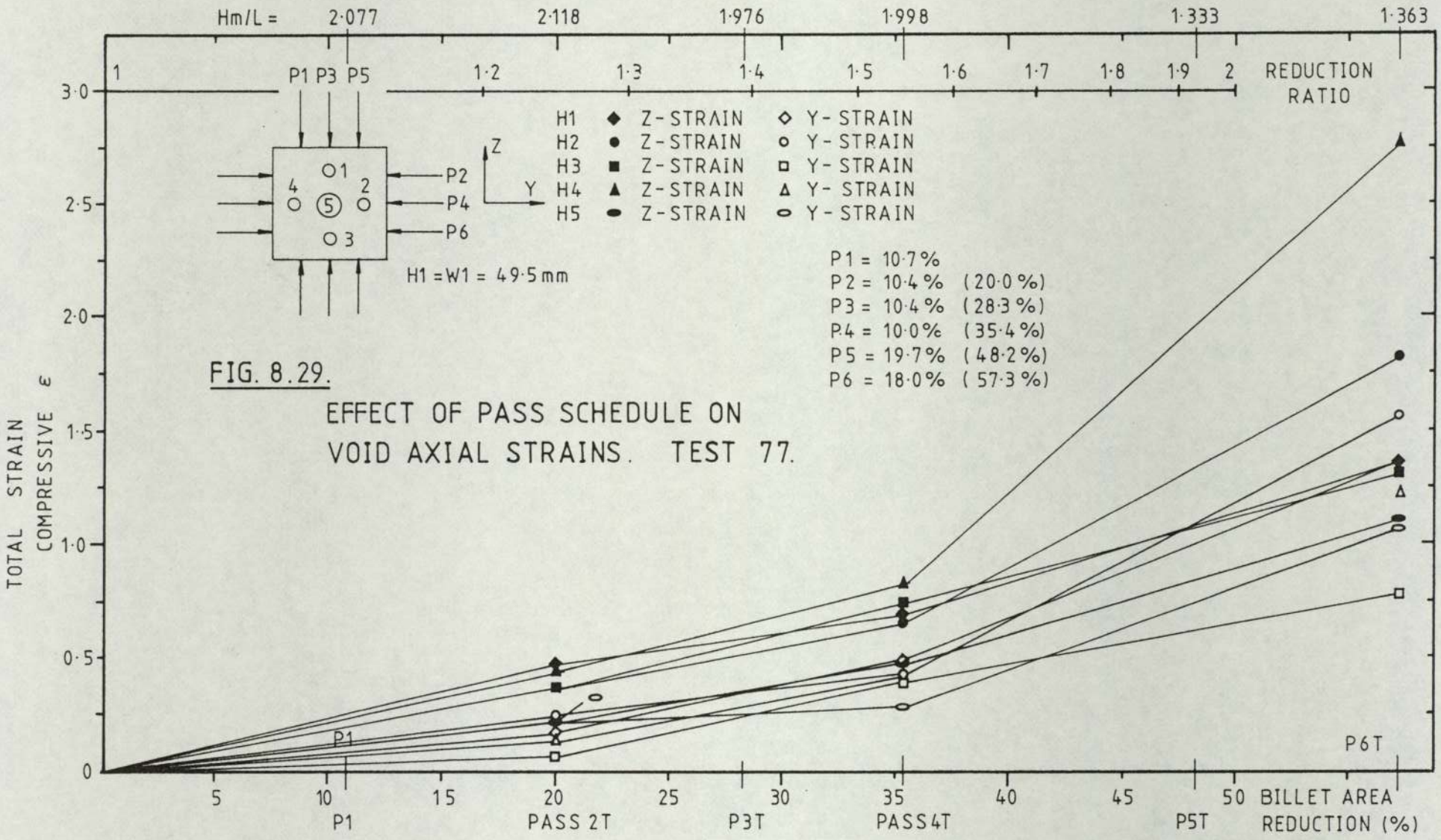

FIG. 8.29.

EFFECT OF PASS SCHEDULE ON VOID AXIAL STRAINS. TEST 77.

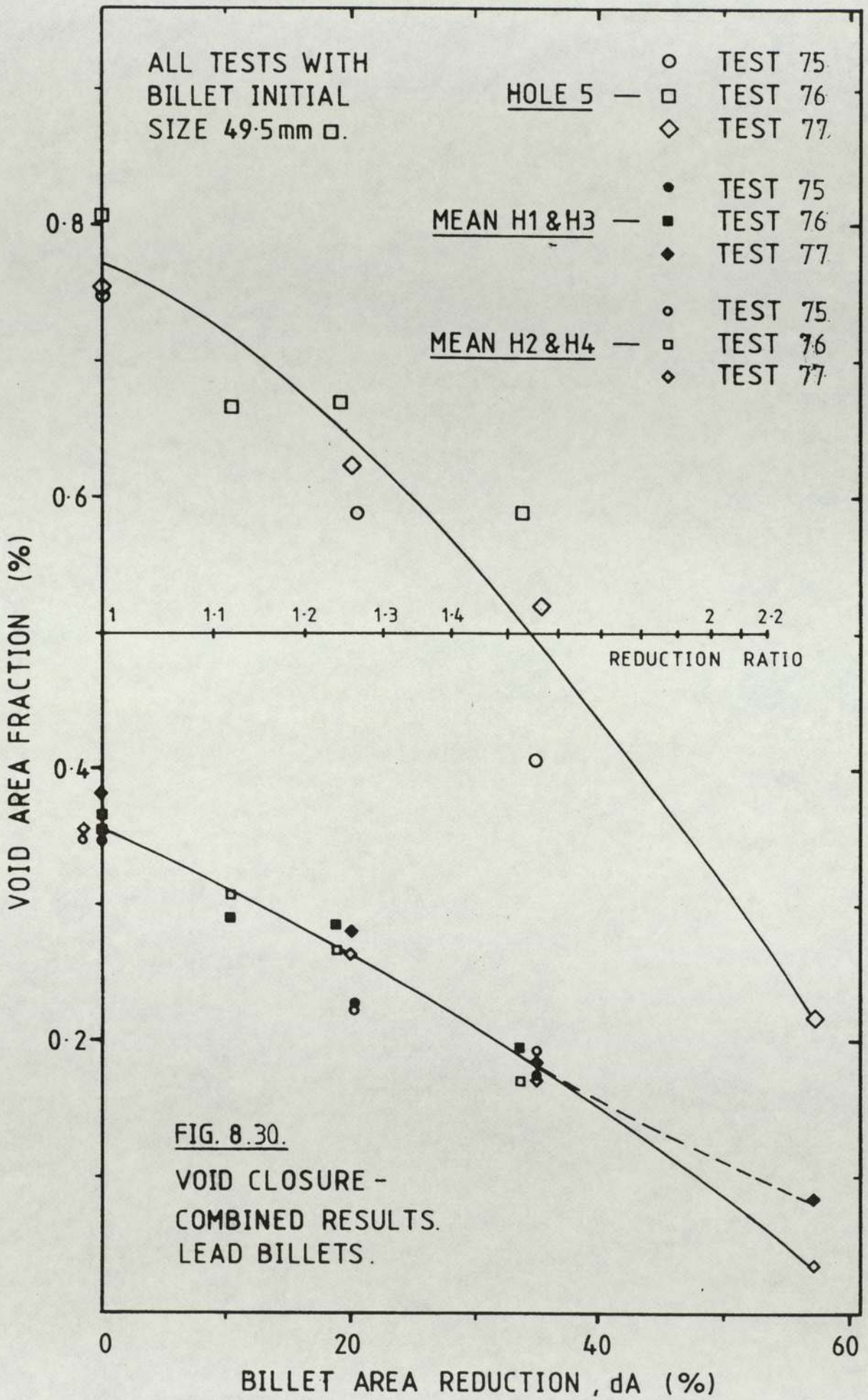

FIG. 8.30.

VOID CLOSURE - COMBINED RESULTS. LEAD BILLETS.

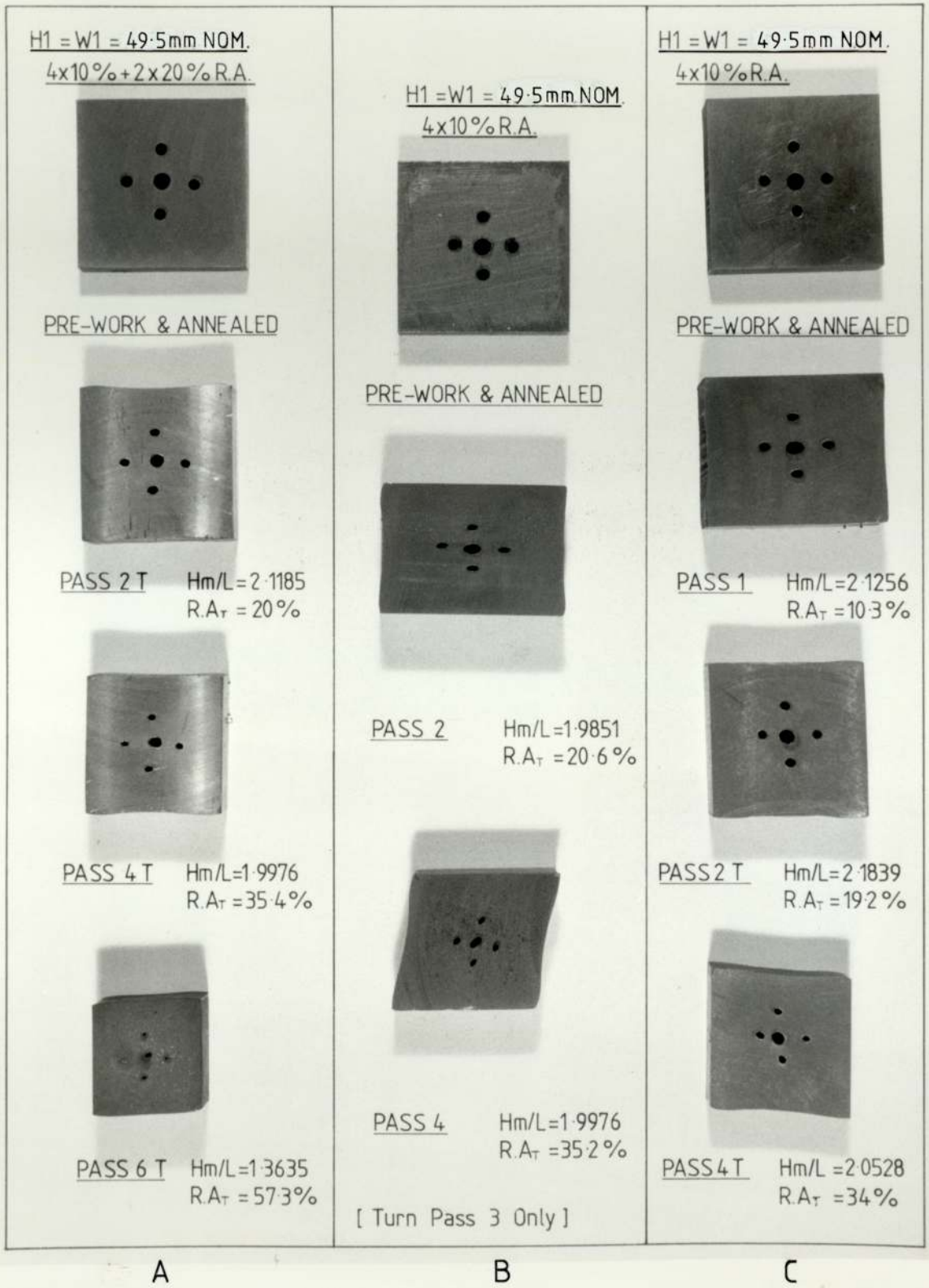

FIG. 8.31.

VOID CLOSURE. LEAD BILLETS.

A. TEST 77
B. TEST 75 x 0·560
C. TEST 76

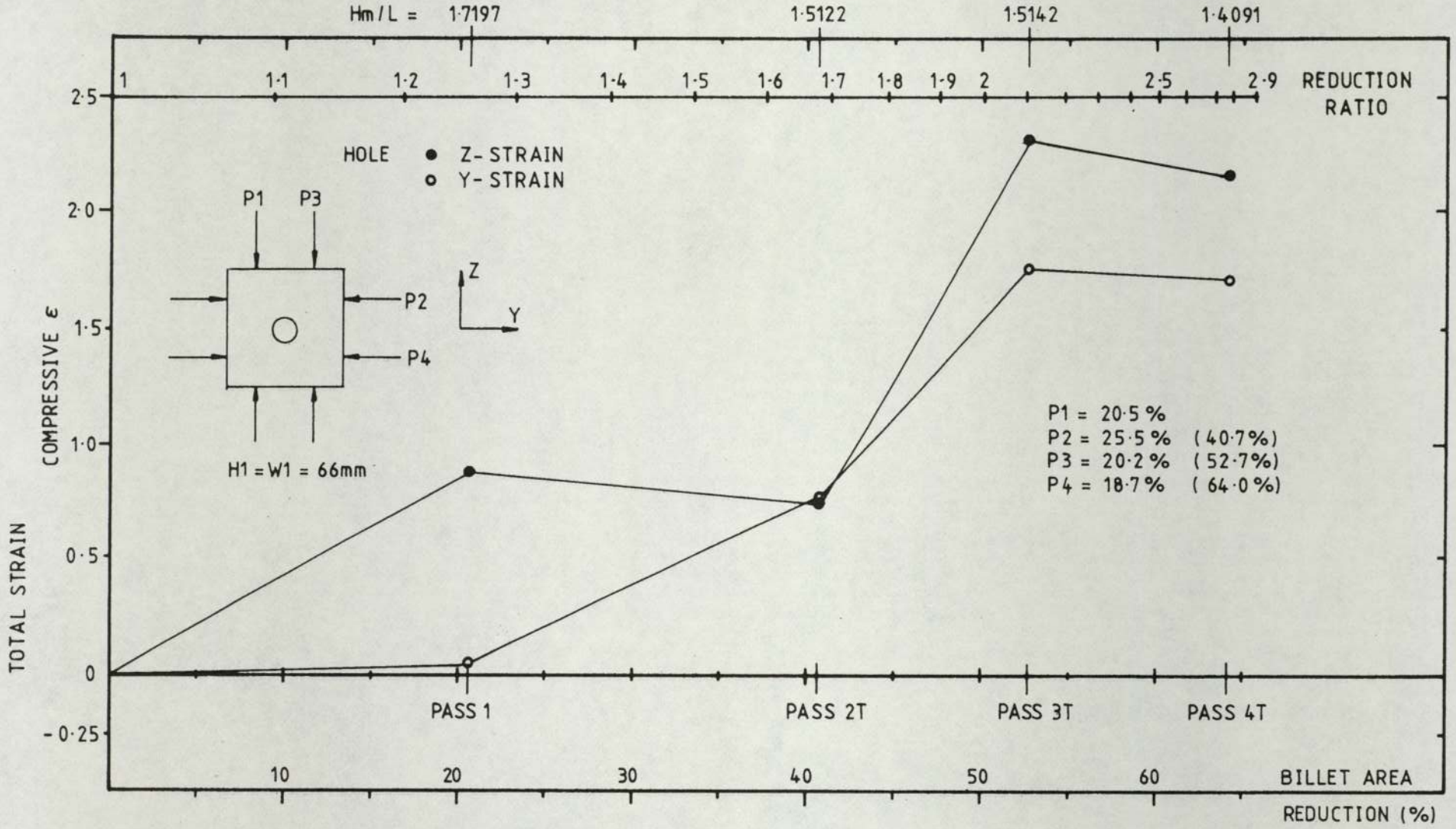

FIG. 8.32. EFFECT OF PASS SCHEDULE ON VOID AXIAL STRAINS. TEST 81.

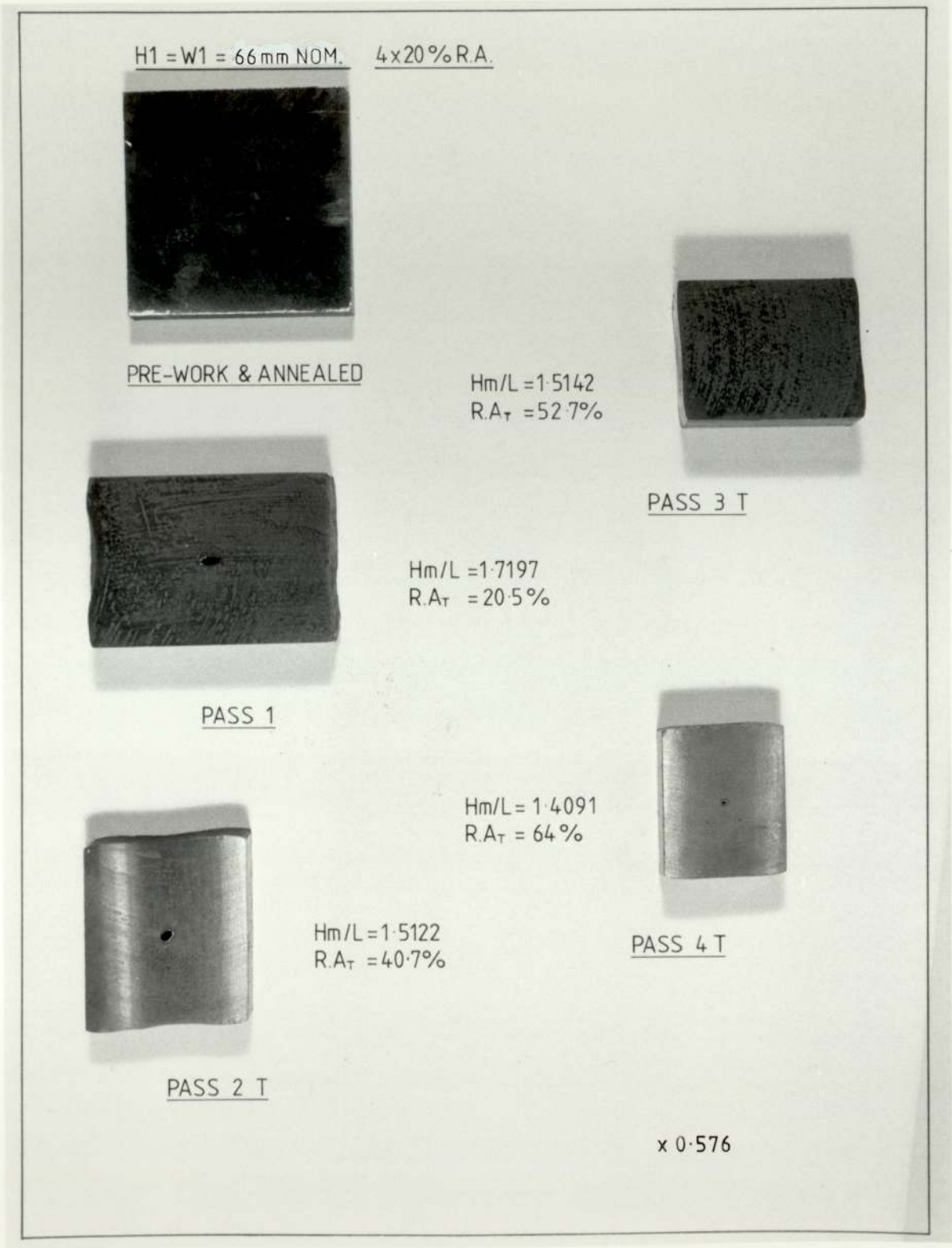

FIG. 8.33.

VOID CLOSURE LEAD BILLET.

TEST 81.

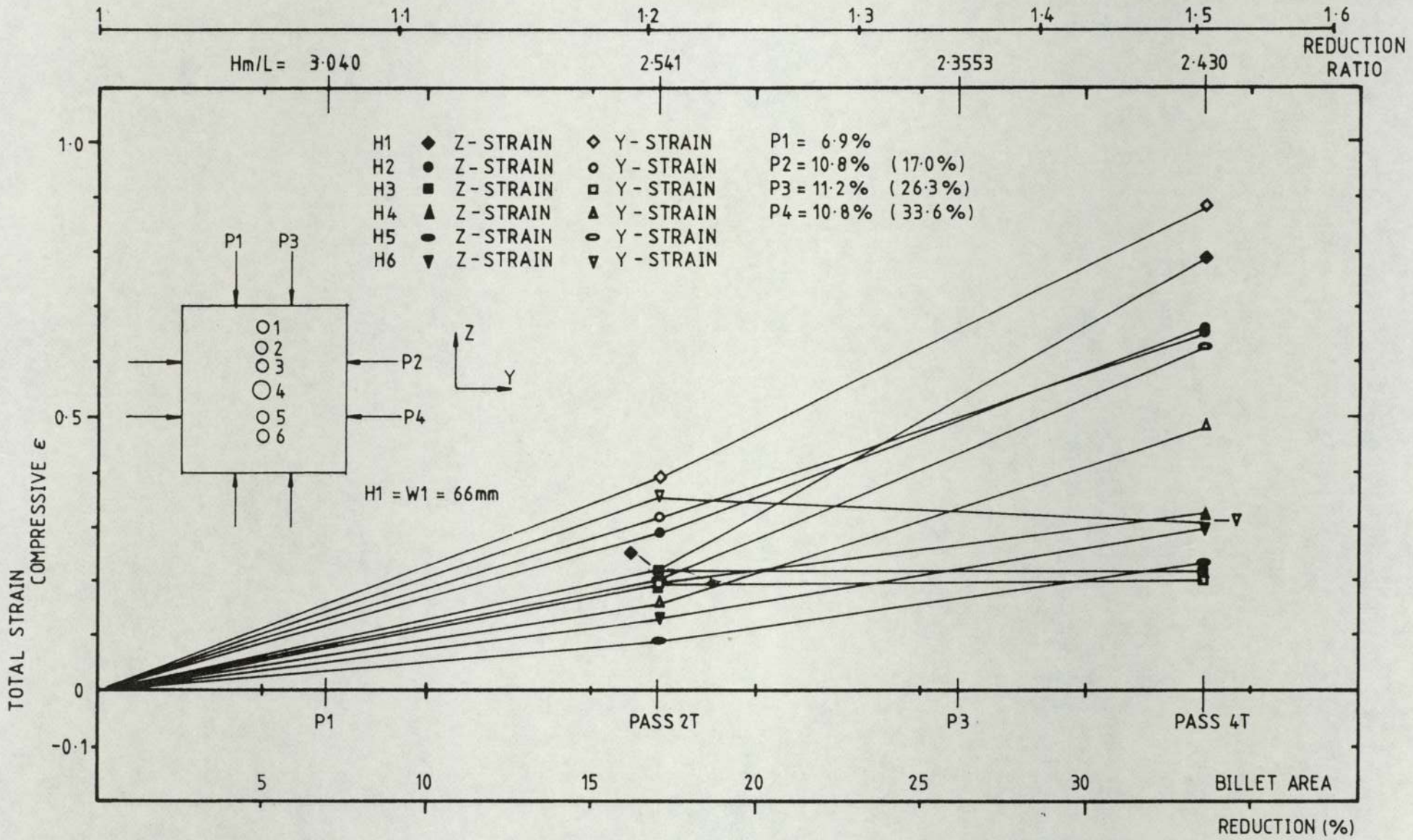

FIG. 8.34. EFFECT OF PASS SCHEDULE ON VOID AXIAL STRAINS. TEST 82.

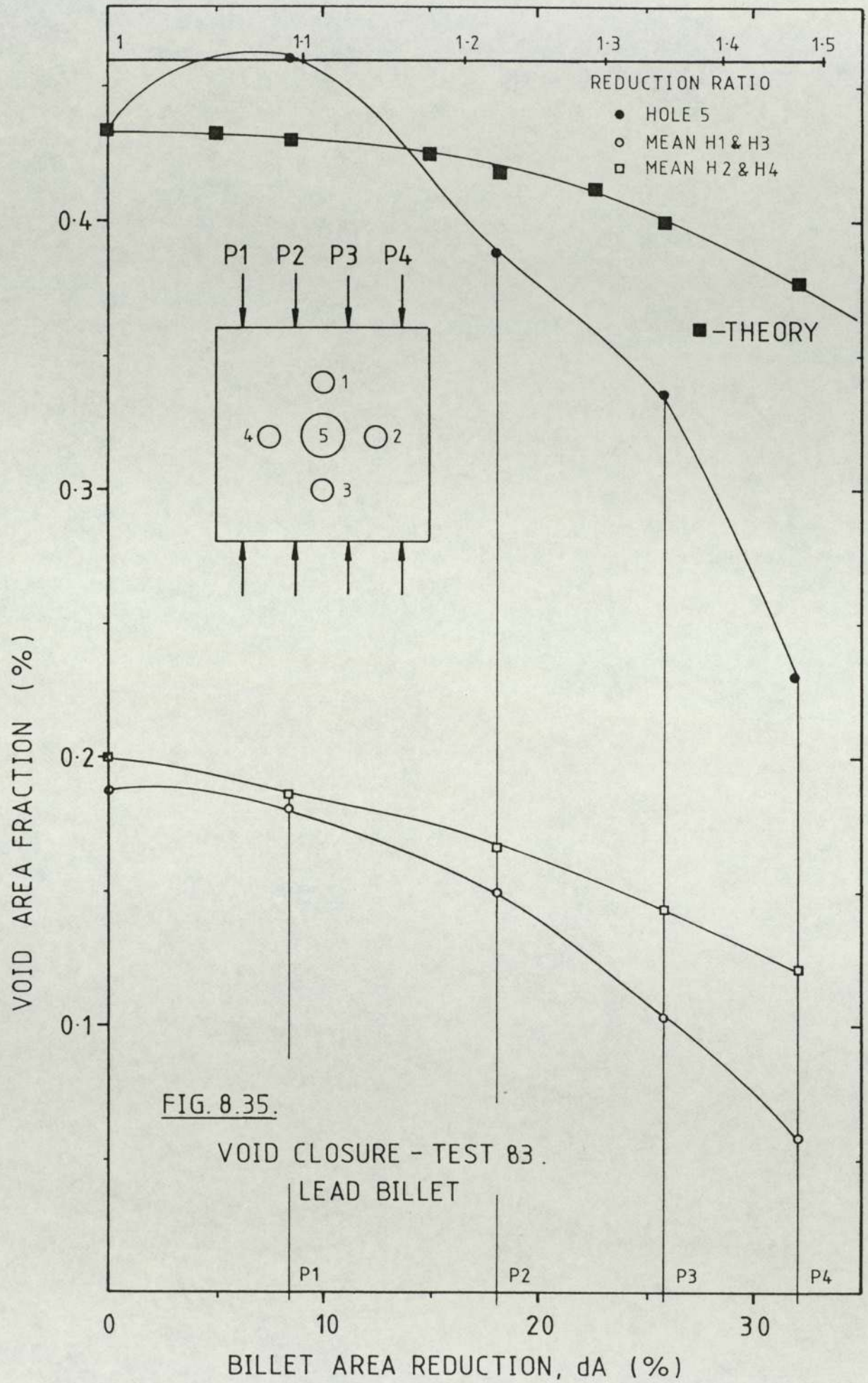

FIG. 8.35.

VOID CLOSURE - TEST 83.
LEAD BILLET

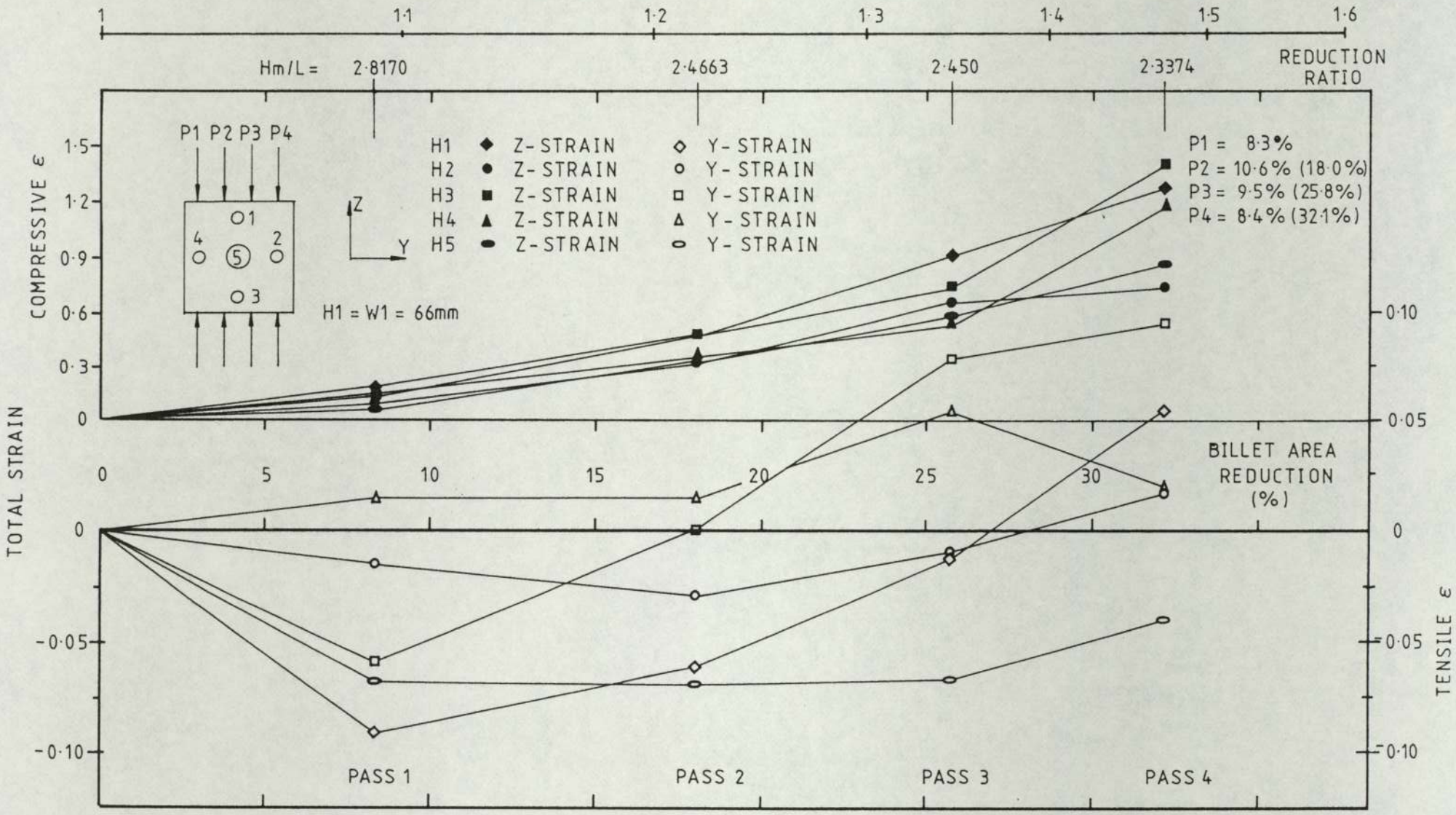

FIG. 8.36. EFFECT OF PASS SCHEDULE ON VOID AXIAL STRAINS. TEST 83.

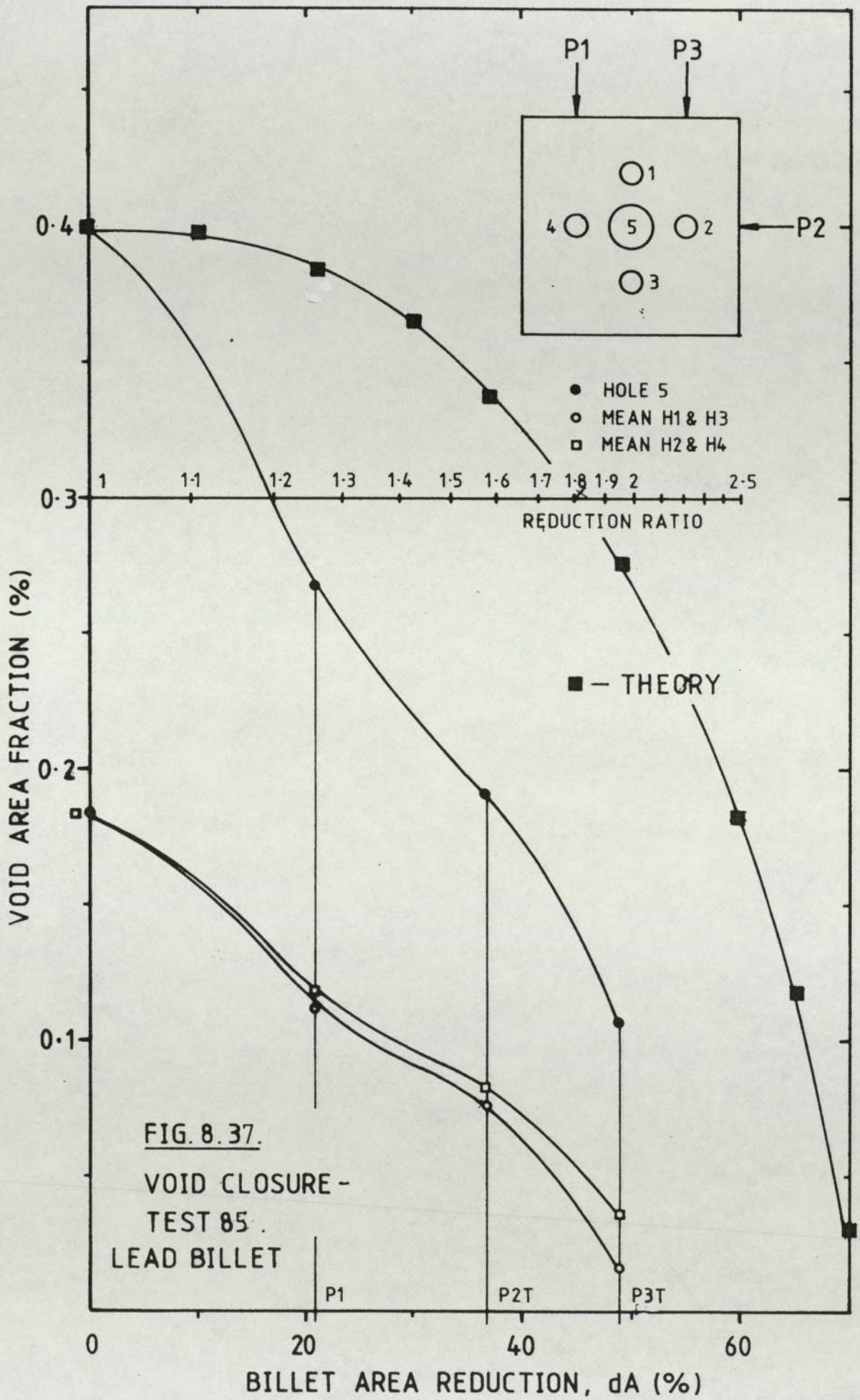

FIG. 8.37.

VOID CLOSURE - TEST 85. LEAD BILLET

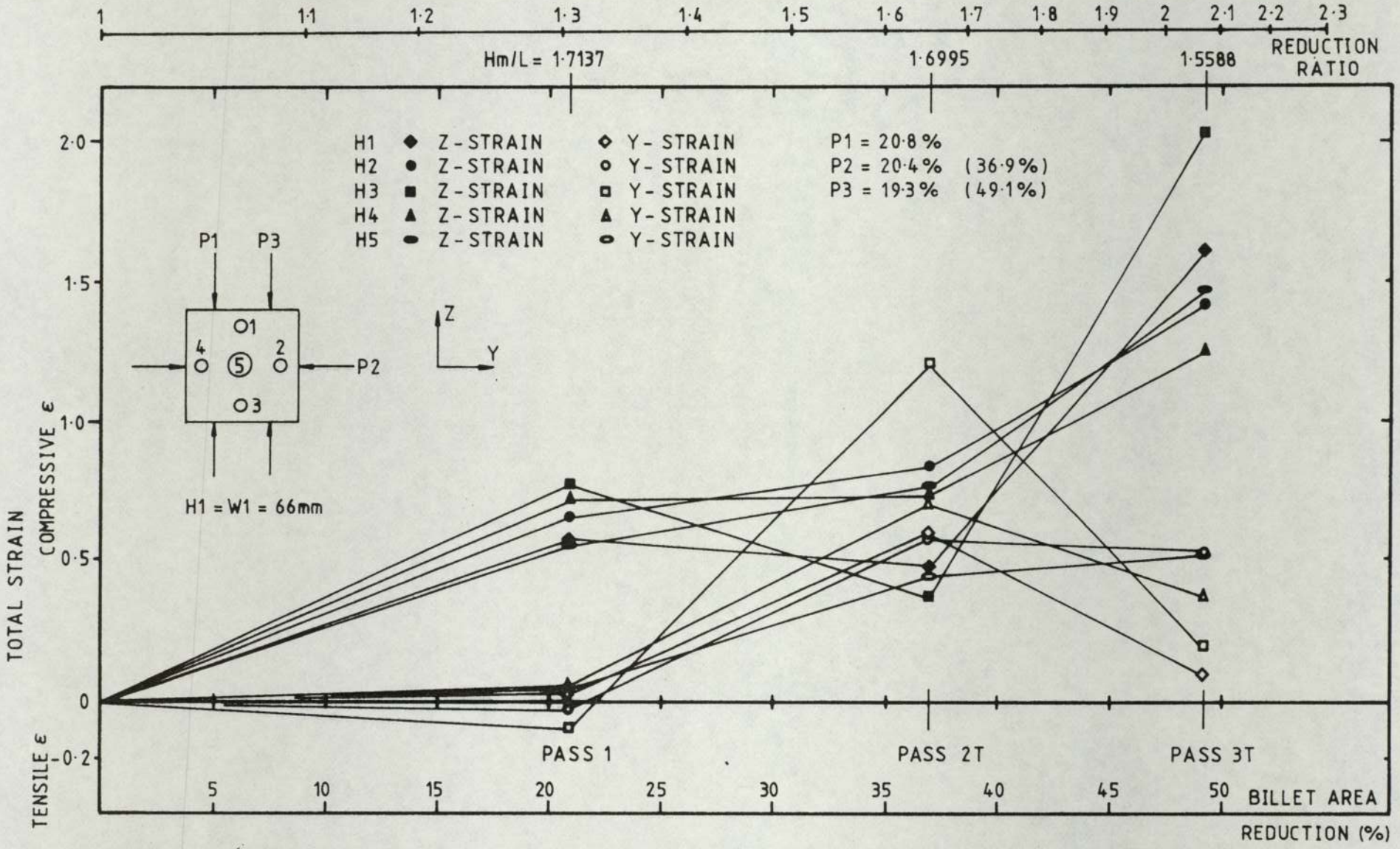

FIG. 8.38. EFFECT OF PASS SCHEDULE ON VOID AXIAL STRAINS. TEST 85.

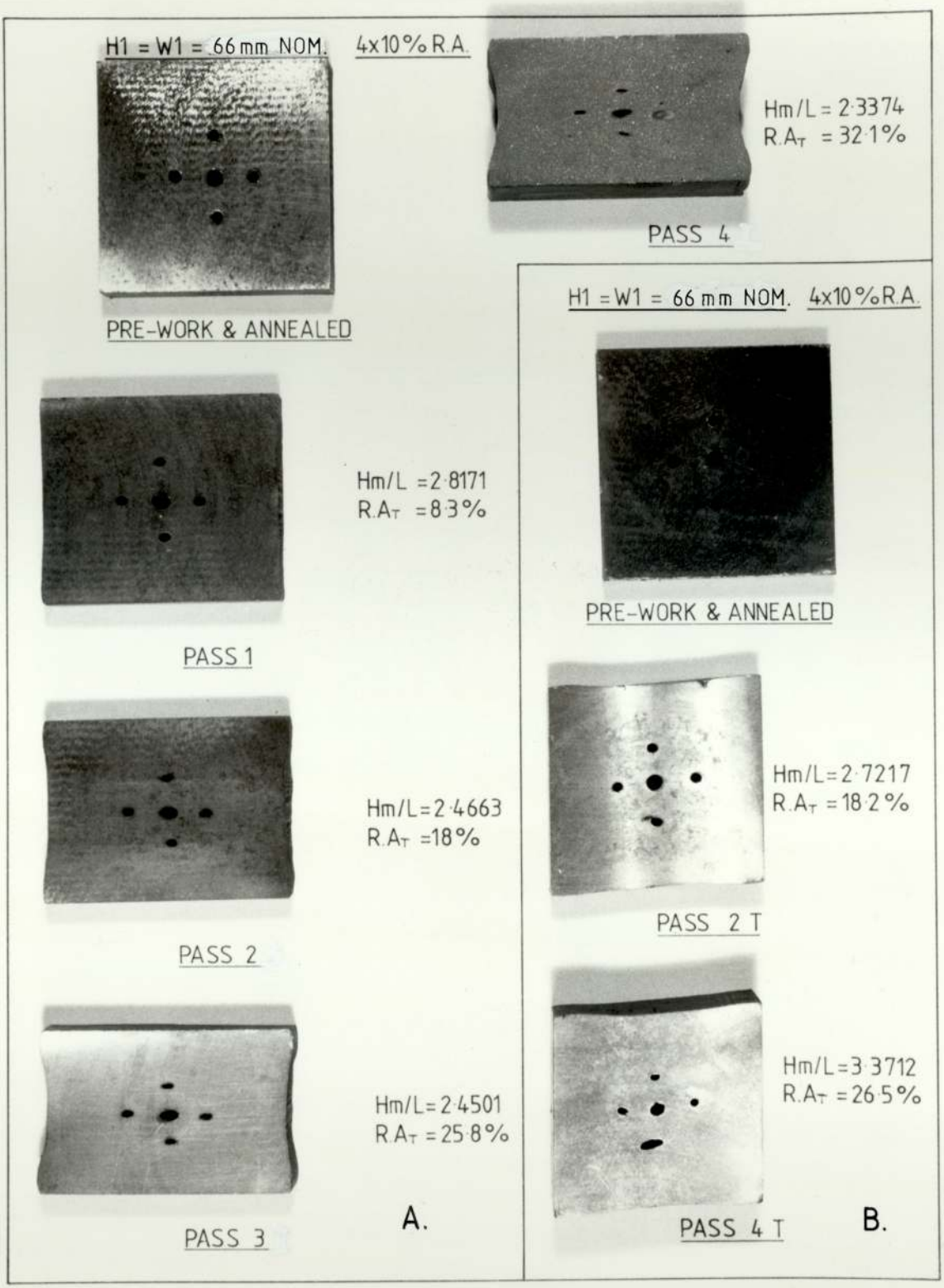

FIG. 8.39.

VOID CLOSURE. LEAD BILLETS.

A. TEST 83
B. TEST 86

x 0·576

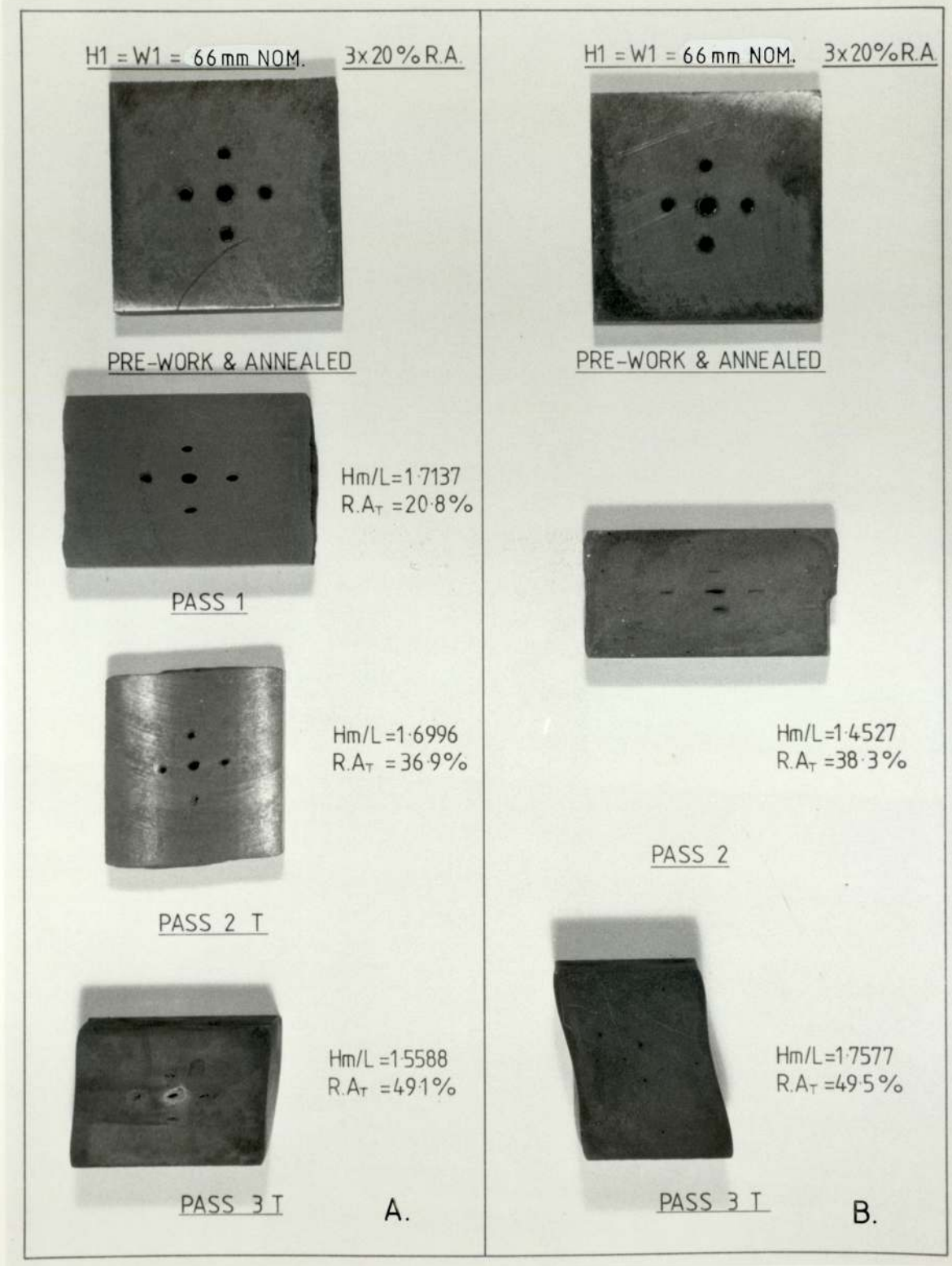

FIG. 8.40.

VOID CLOSURE. LEAD BILLETS.

A. TEST 85
B. TEST 84 x 0·576

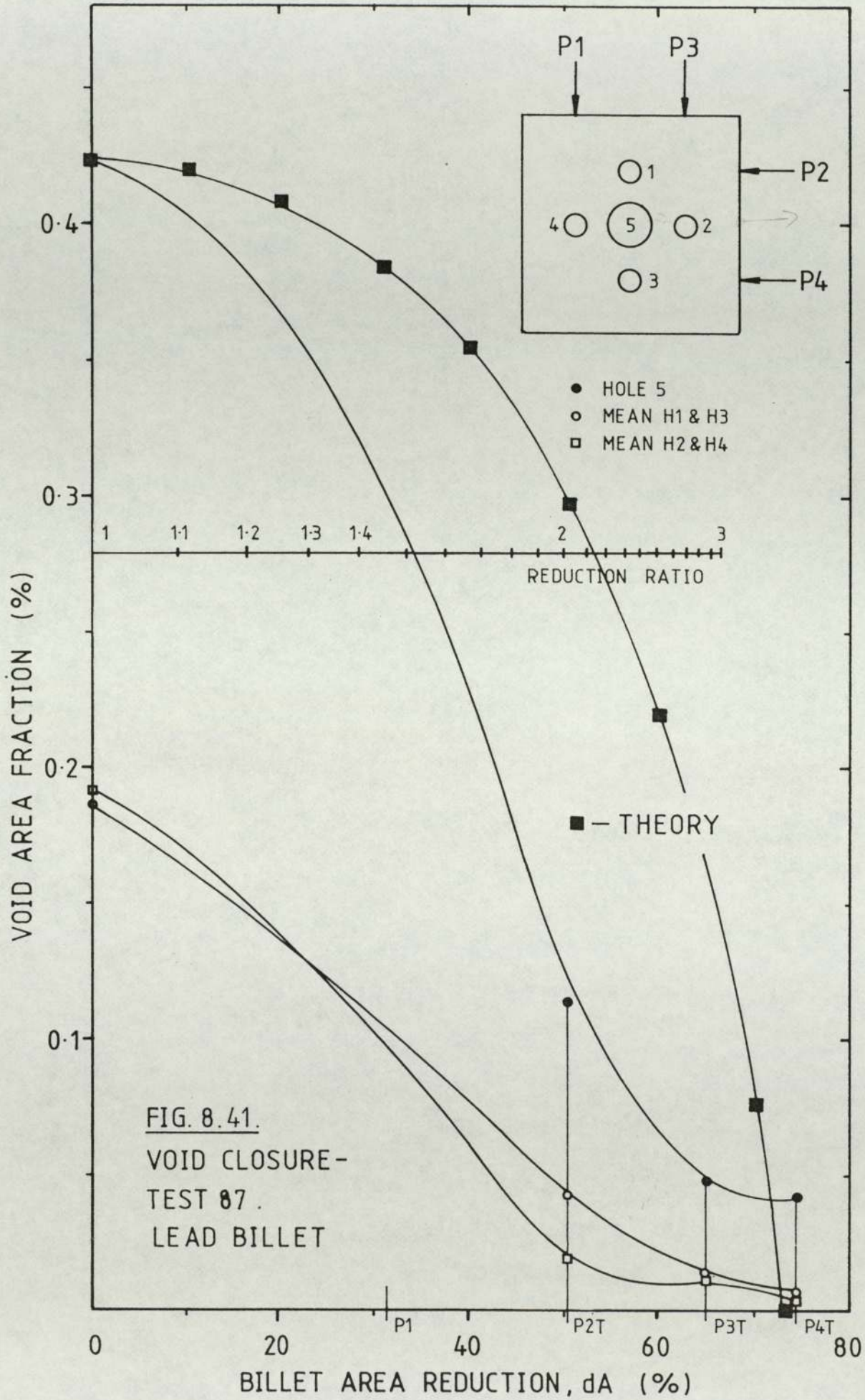

FIG. 8.41.
VOID CLOSURE-
TEST 87.
LEAD BILLET

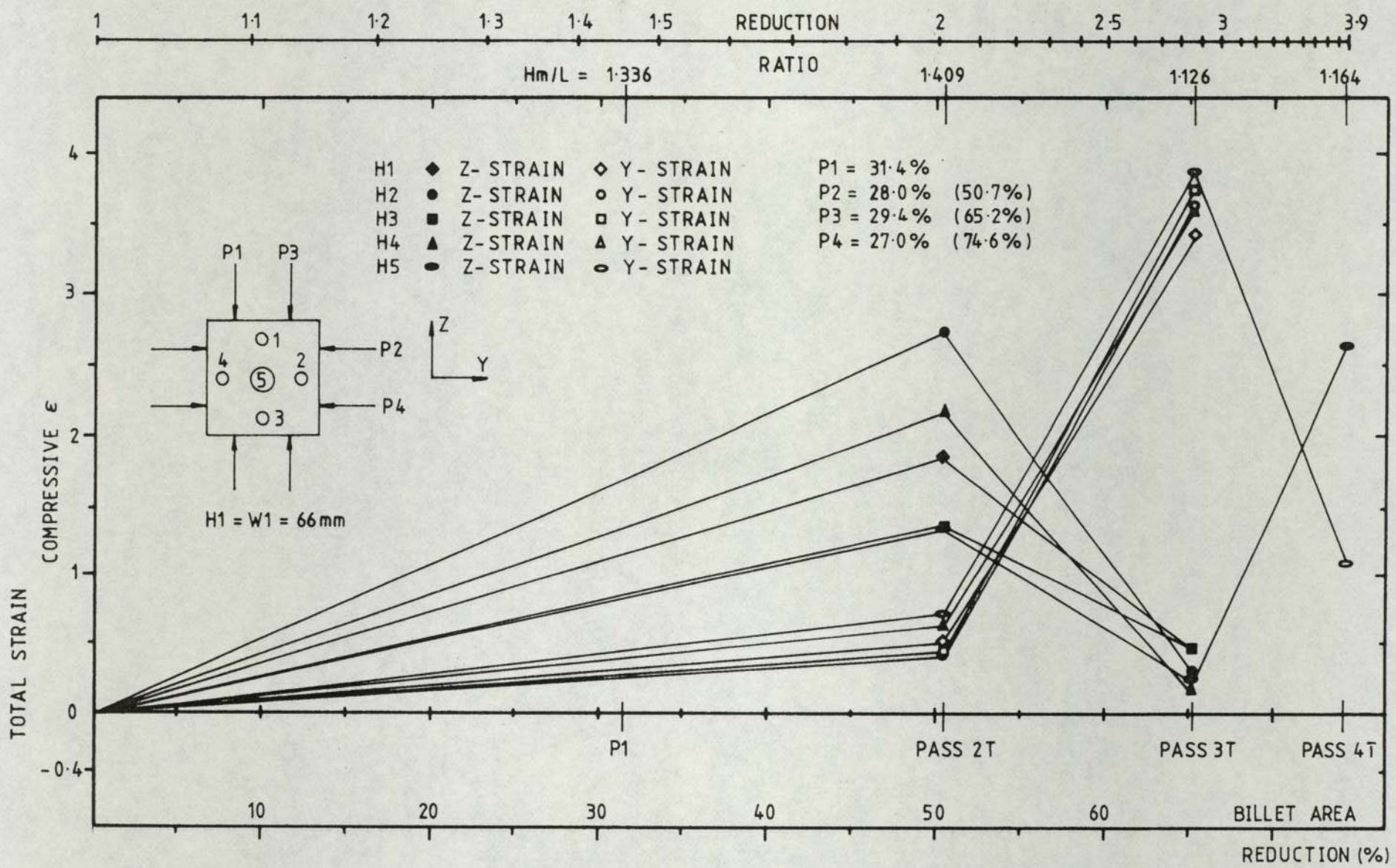

FIG. 8.42. EFFECT OF PASS SCHEDULE ON VOID AXIAL STRAINS. TEST 87.

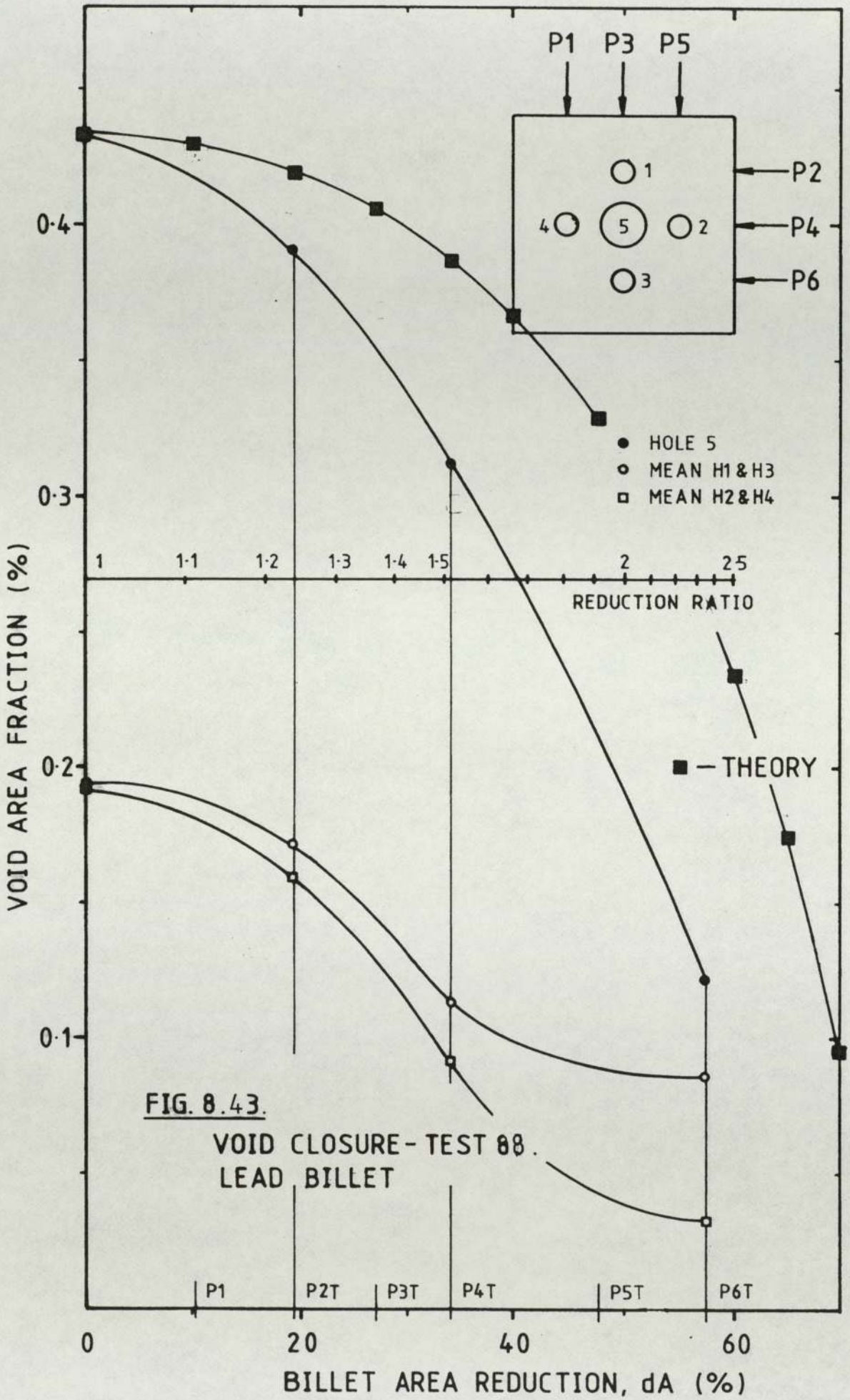

FIG. 8.43.

VOID CLOSURE - TEST 88.
LEAD BILLET

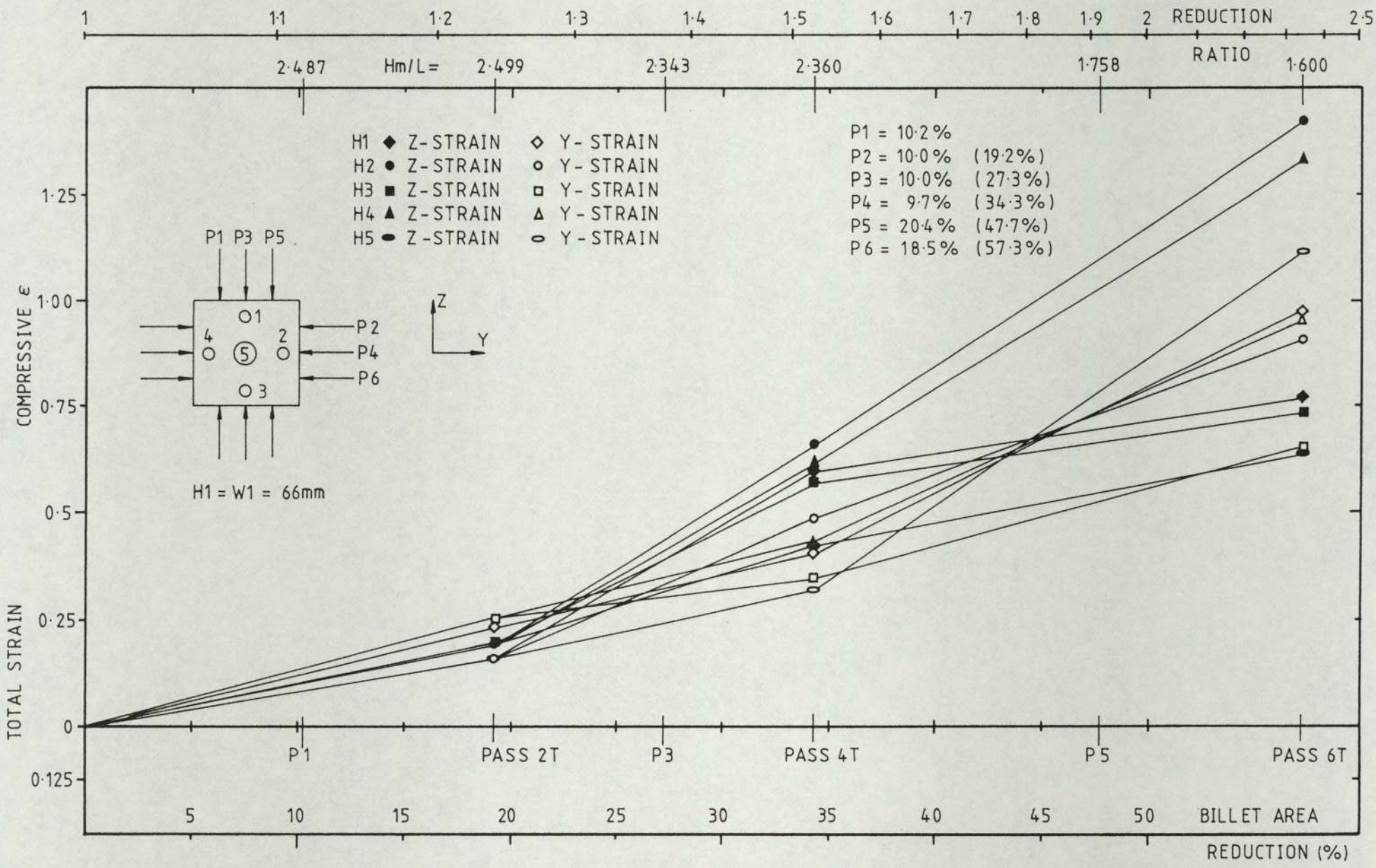

FIG. 8.44. EFFECT OF PASS SCHEDULE ON VOID AXIAL STRAINS. TEST 88.

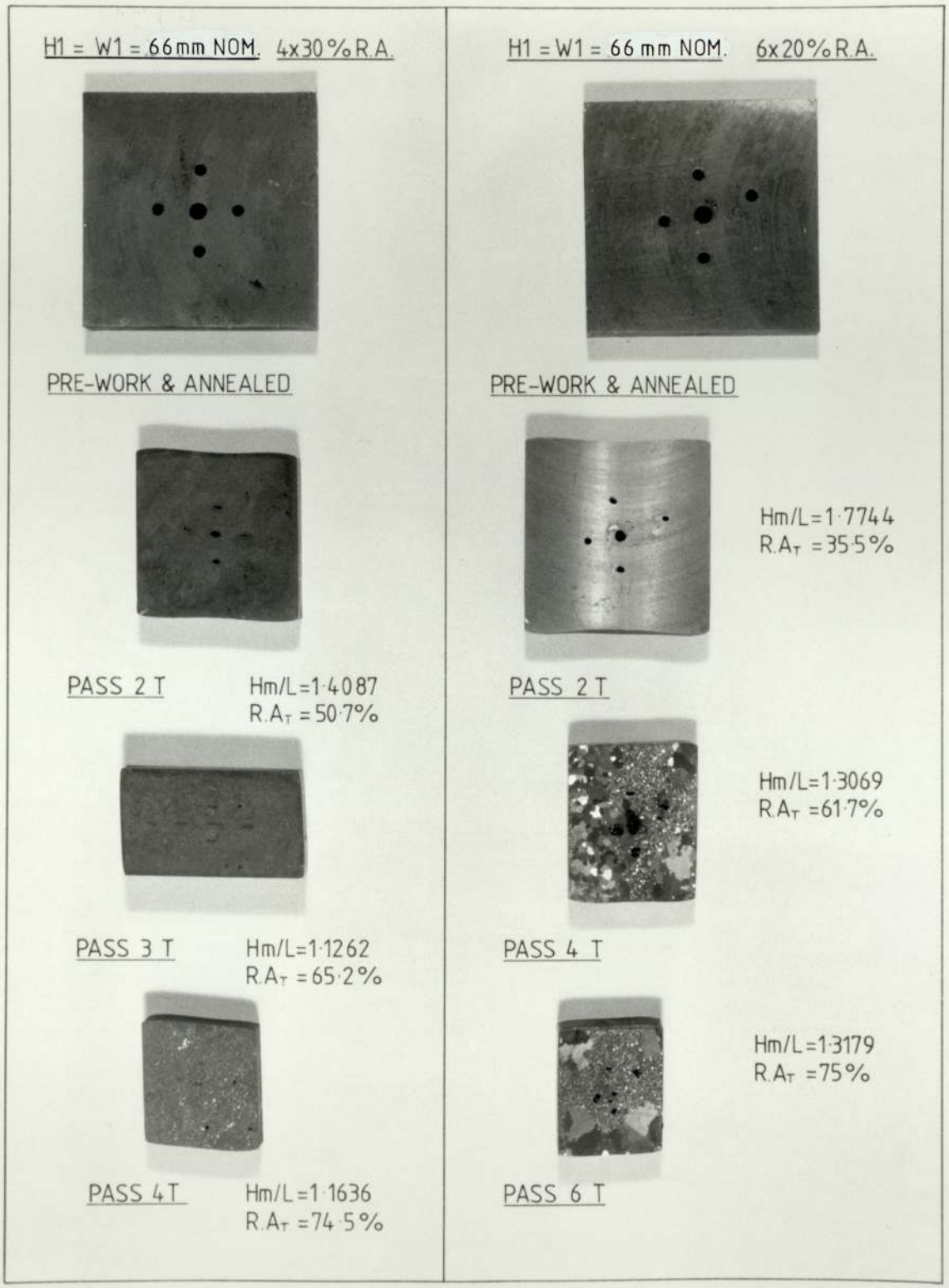

A. B.

FIG. 8.45.

VOID CLOSURE. LEAD BILLETS.

A. TEST 87
B. TEST 89

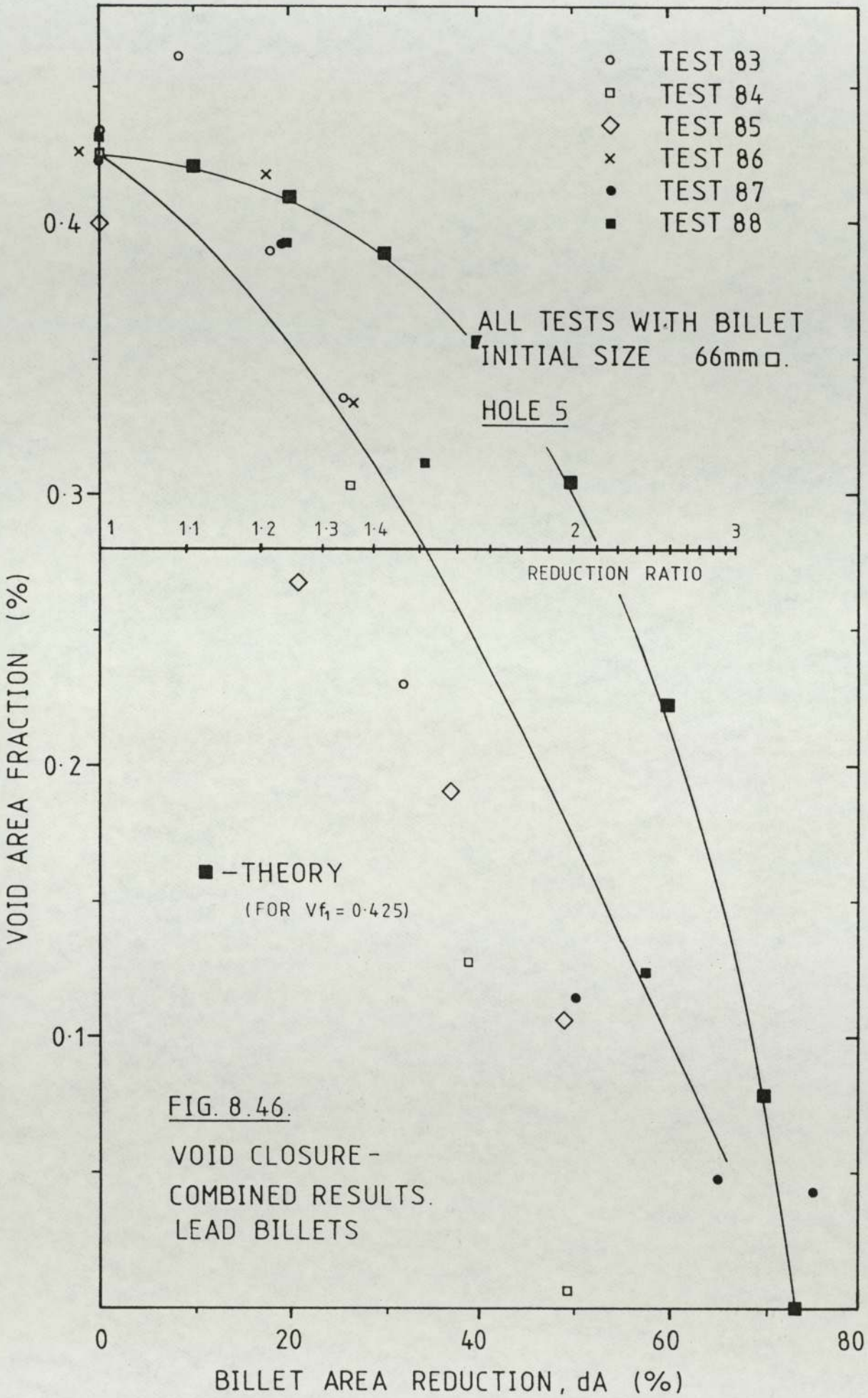

FIG. 8.46.

VOID CLOSURE - COMBINED RESULTS. LEAD BILLETS

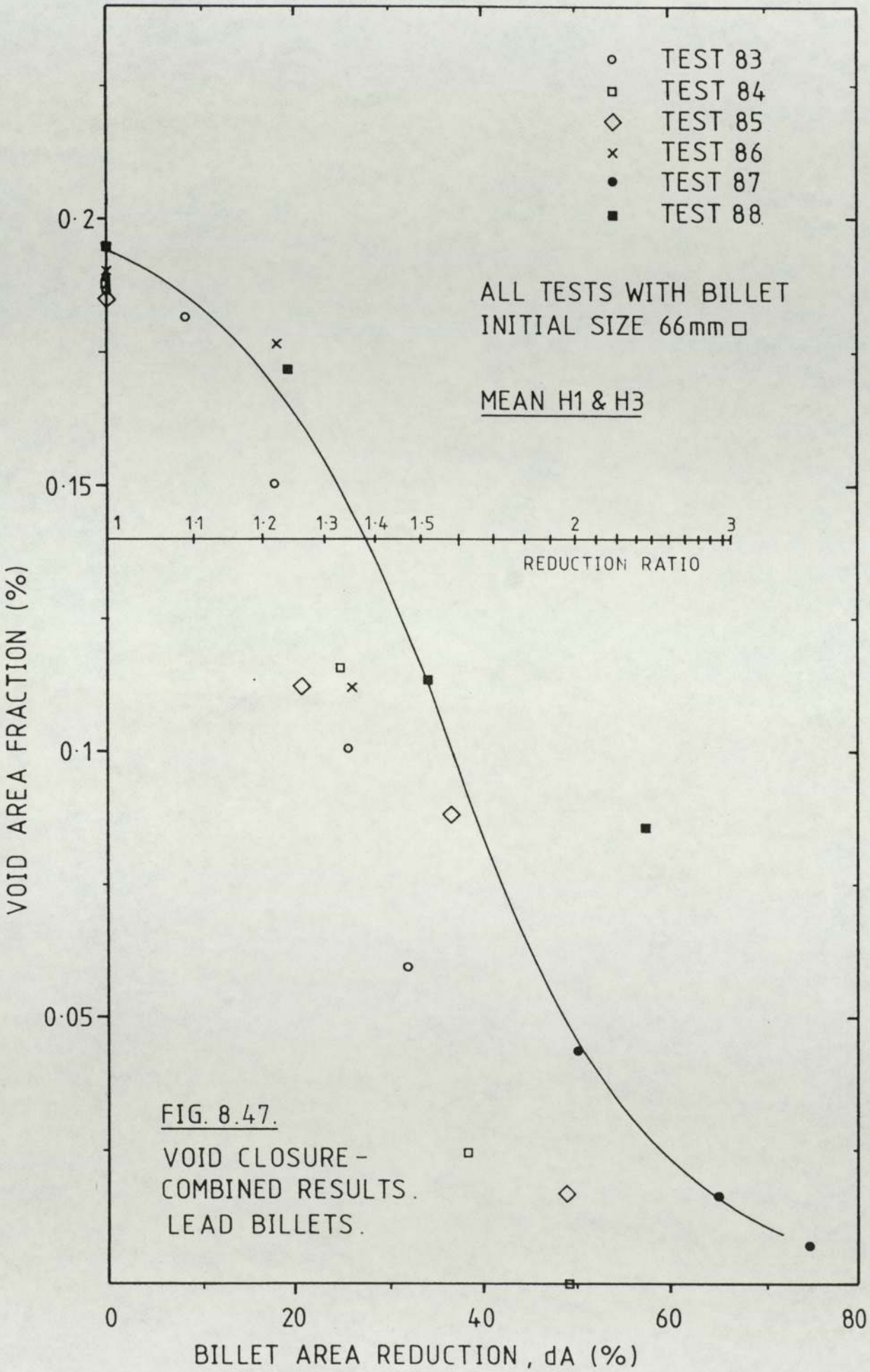

FIG. 8.47.

VOID CLOSURE - COMBINED RESULTS. LEAD BILLETS.

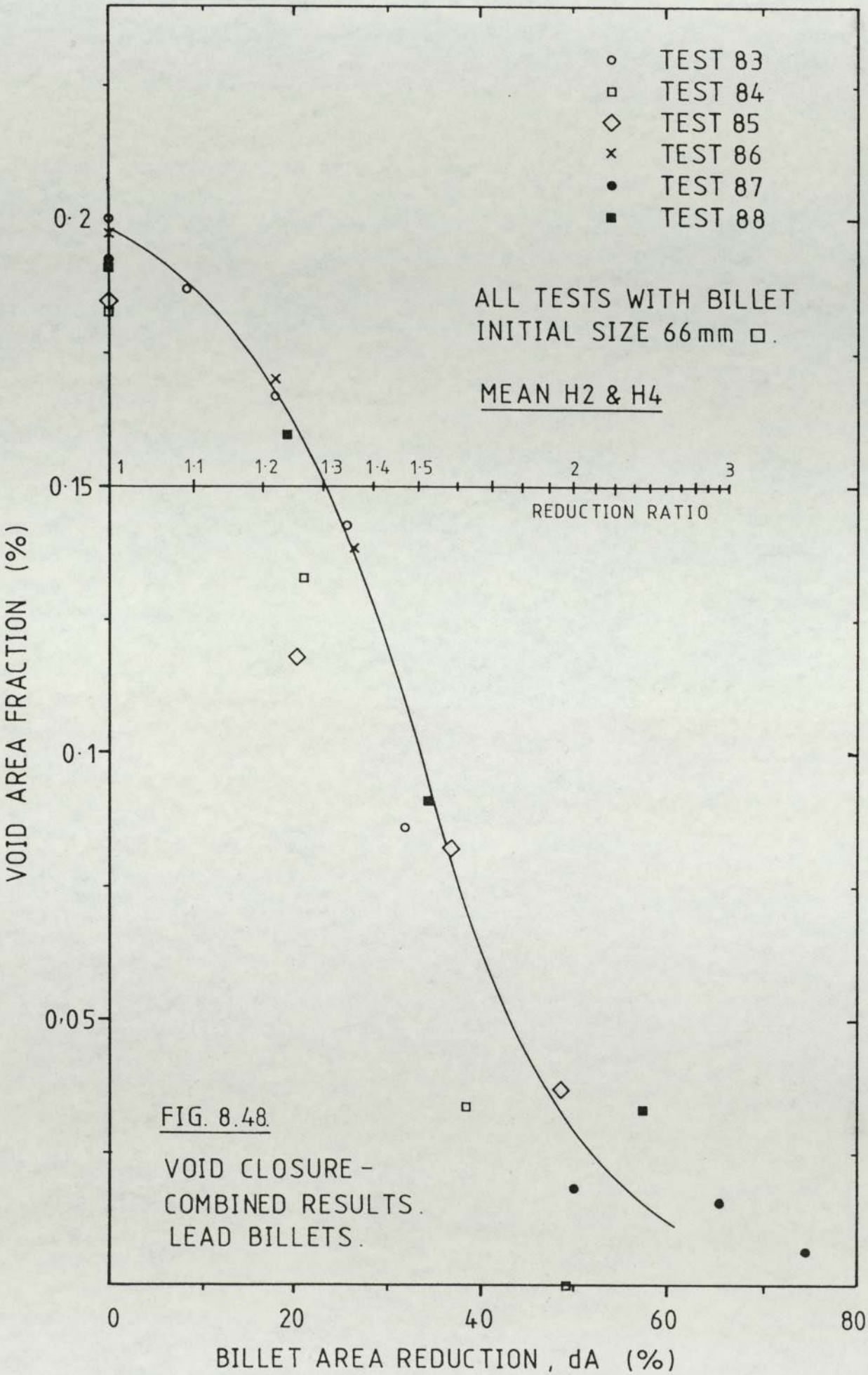

FIG. 8.48.

VOID CLOSURE - COMBINED RESULTS. LEAD BILLETS.

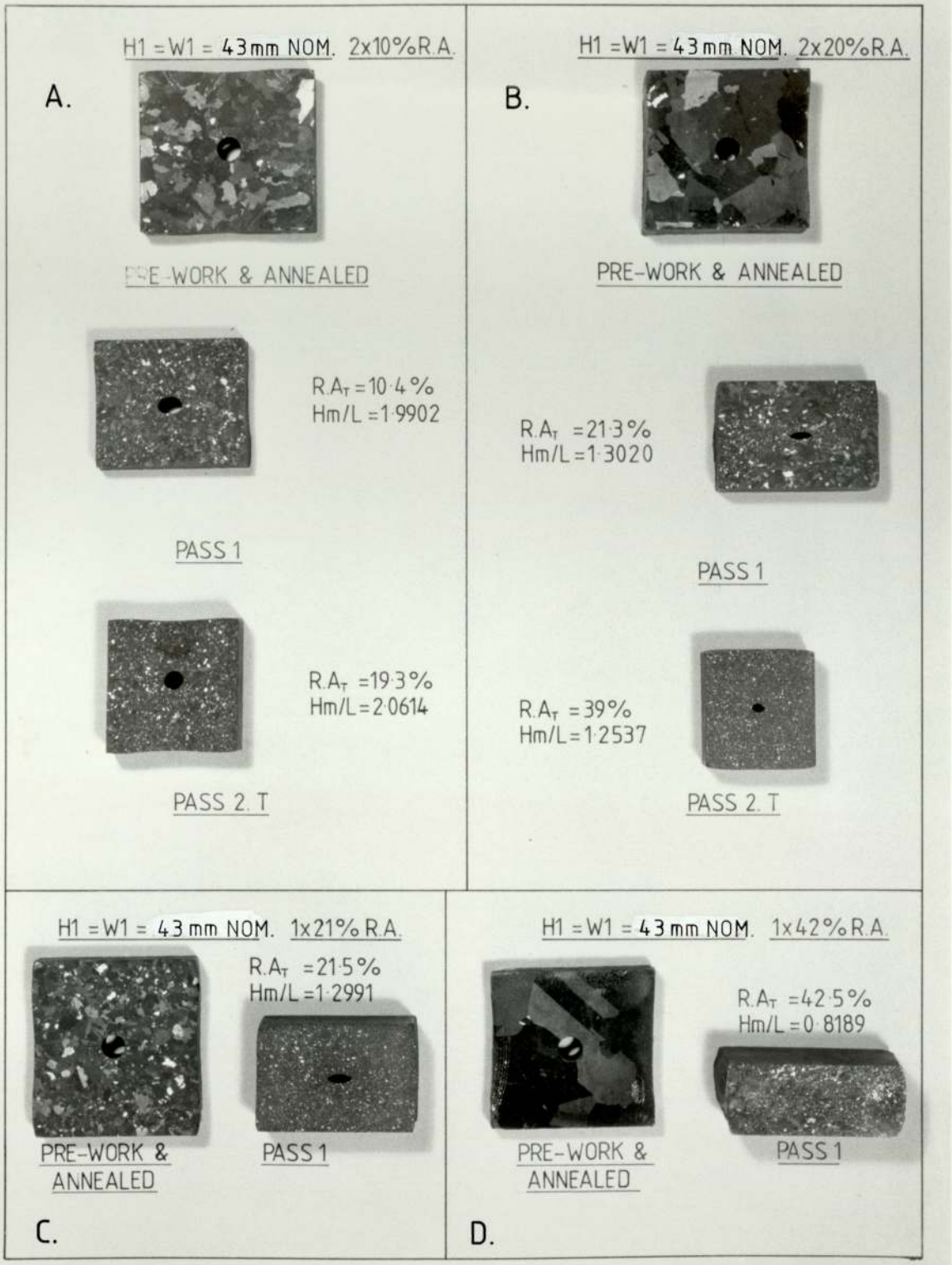

FIG. 8.49.

VOID CLOSURE. LEAD BILLETS.

A. TEST 71.
B. TEST 72
C. TEST 73
D. TEST 74

x 0·562

H1 = W1 = 60 mm NOM. 1x37% R.A.

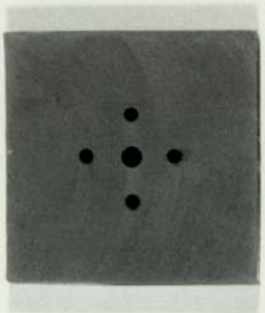

PRE-WORK & ANNEALED

Hm/L = 1·1386
$R.A_T$ = 36·7%

PASS 1

A.

H1 = W1 = 60 mm NOM. 2x20% R.A.

PRE-WORK & ANNEALED

Hm/L = 1·6715
$R.A_T$ = 40·3%

PASS 2 T

B.

FIG. 8.50.

VOID CLOSURE. LEAD BILLETS.

A. TEST 79
B. TEST 78

A.

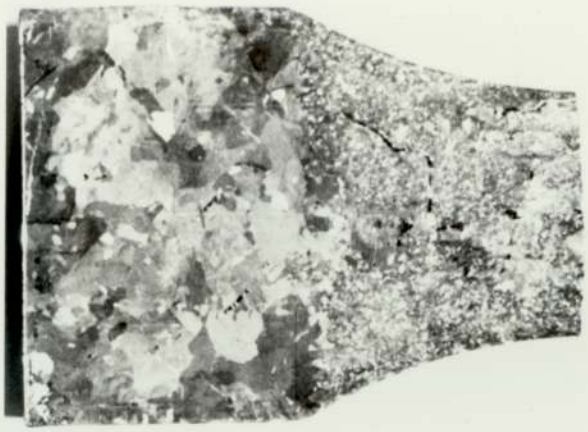

x 0·900

B.

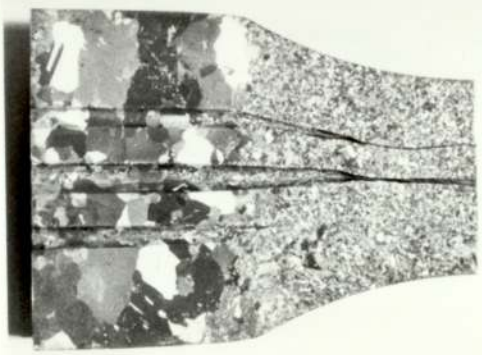

x 0·742

C.

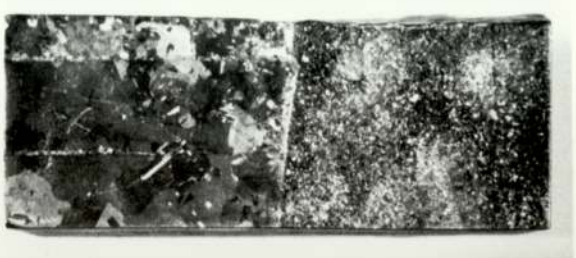

x 0·900

FIG. 8.51.

VOID CLOSURE DURING ROLLING.
SINGLE PASS. LEAD BILLET. TEST 79.

ROLL: 36·74% dA (1·581) 60mm □.

A. BILLET OUTER WIDTH SURFACE.
B. BILLET LONGITUDINAL CENTRE LINE.
C. BILLET-ROLL CONTACT SURFACE.

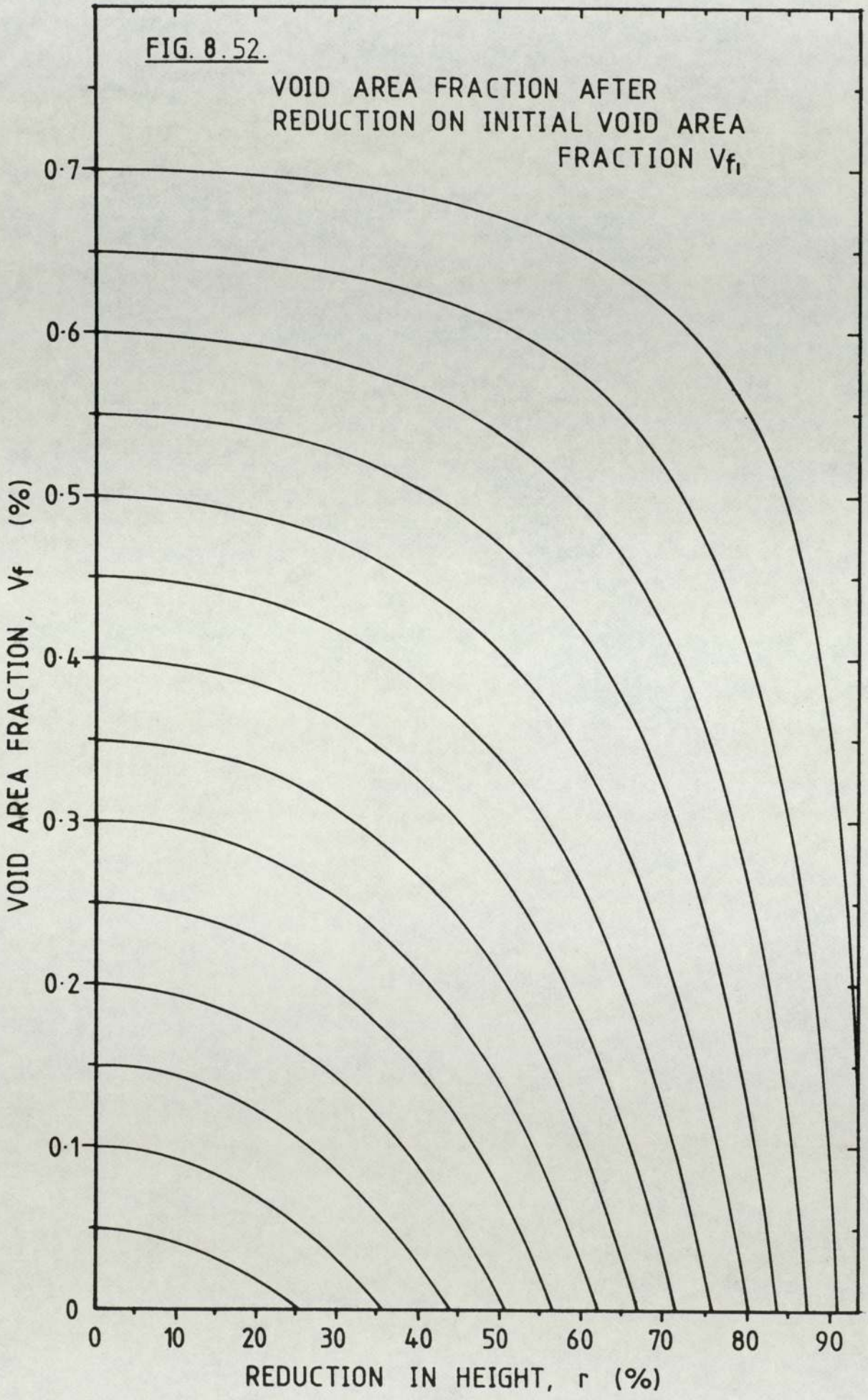
FIG. 8.52.
VOID AREA FRACTION AFTER REDUCTION ON INITIAL VOID AREA FRACTION V_{f_1}
0·7
0·6
0·5
0·4
0·3
0·2
0·1
0
VOID AREA FRACTION, V_f (%)
0
10
20
30
40
50
60
70
80
90
REDUCTION IN HEIGHT, r (%)

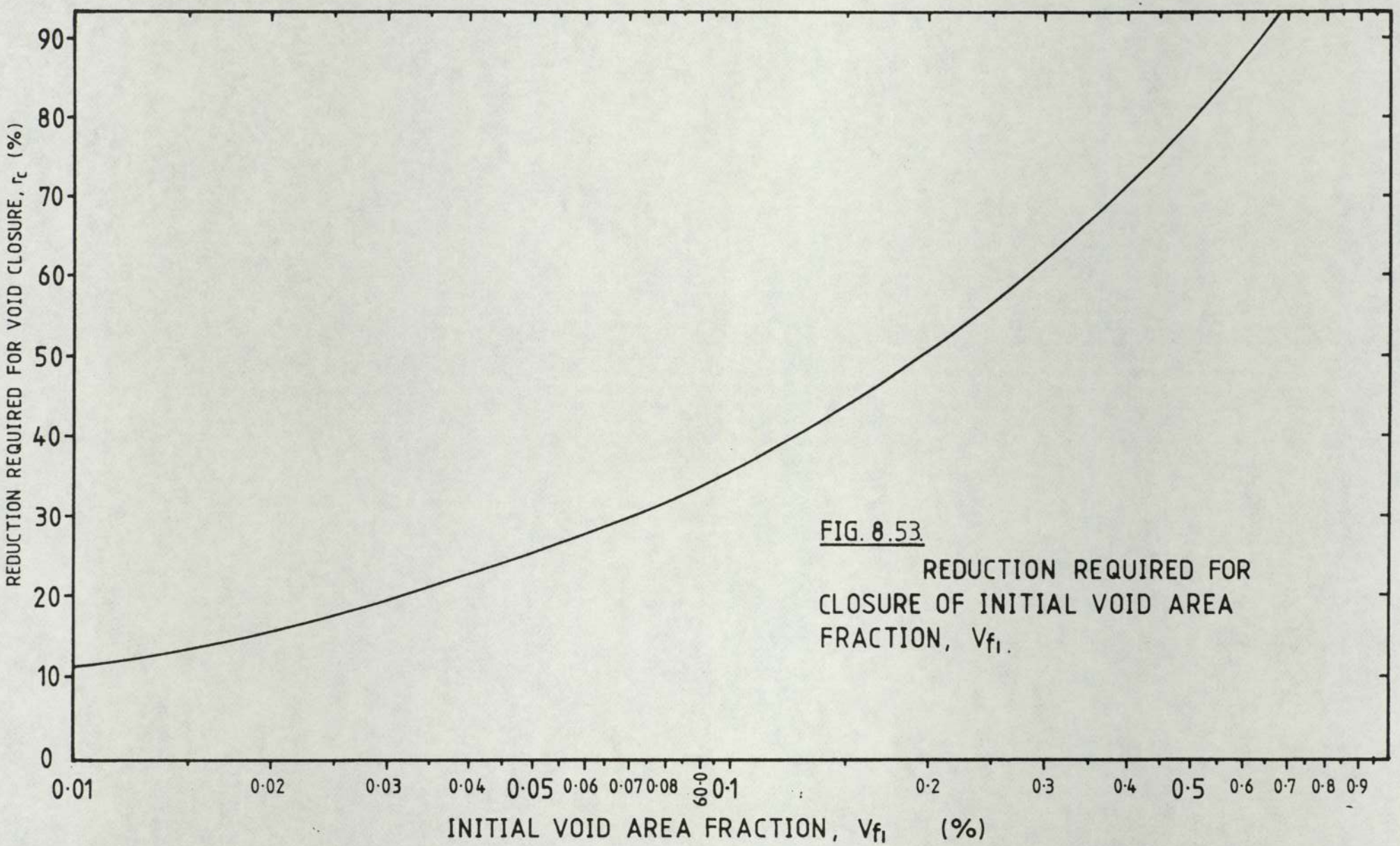

FIG. 8.53

REDUCTION REQUIRED FOR CLOSURE OF INITIAL VOID AREA FRACTION, V_{fi}.

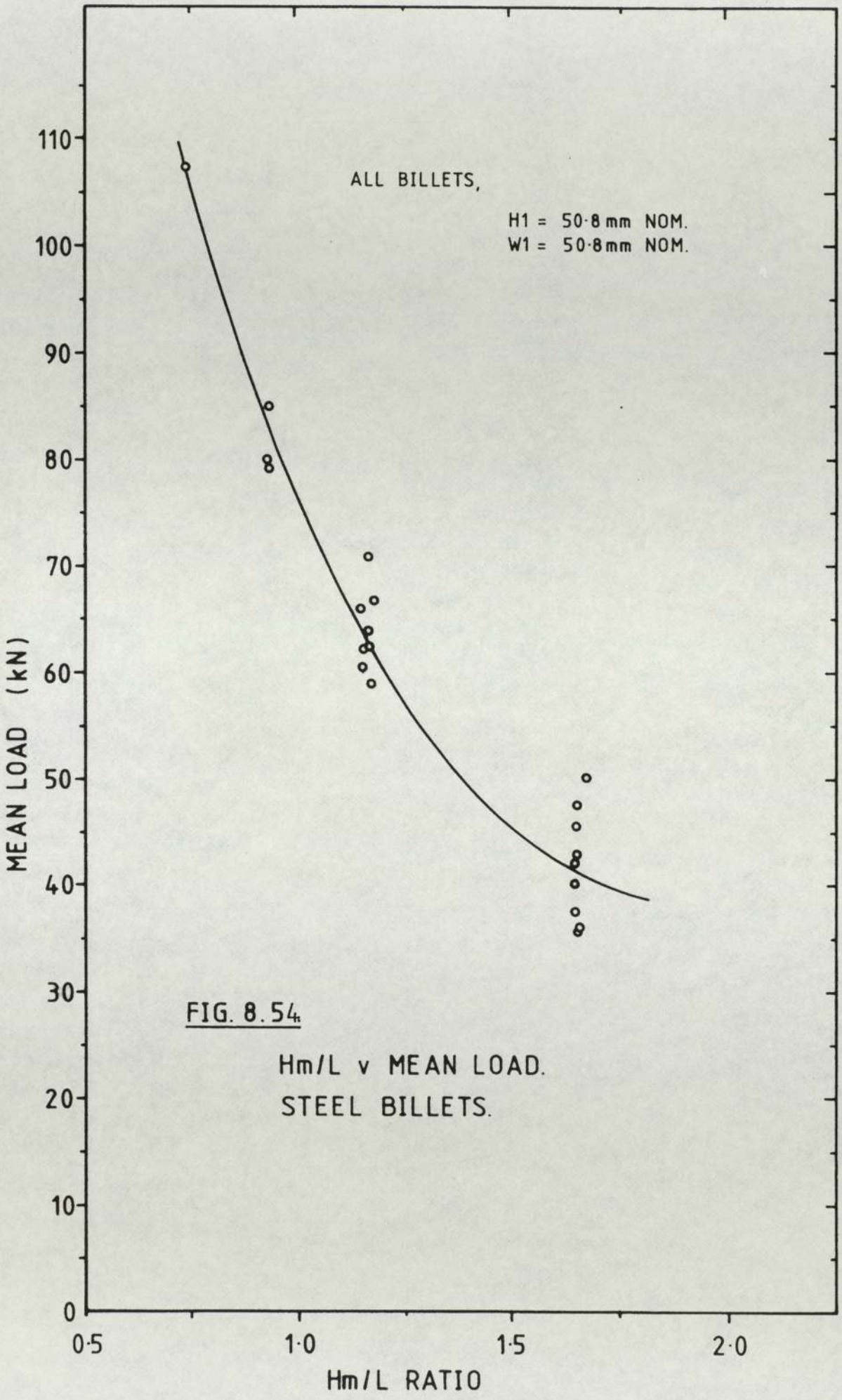

FIG. 8.54

Hm/L v MEAN LOAD.
STEEL BILLETS.

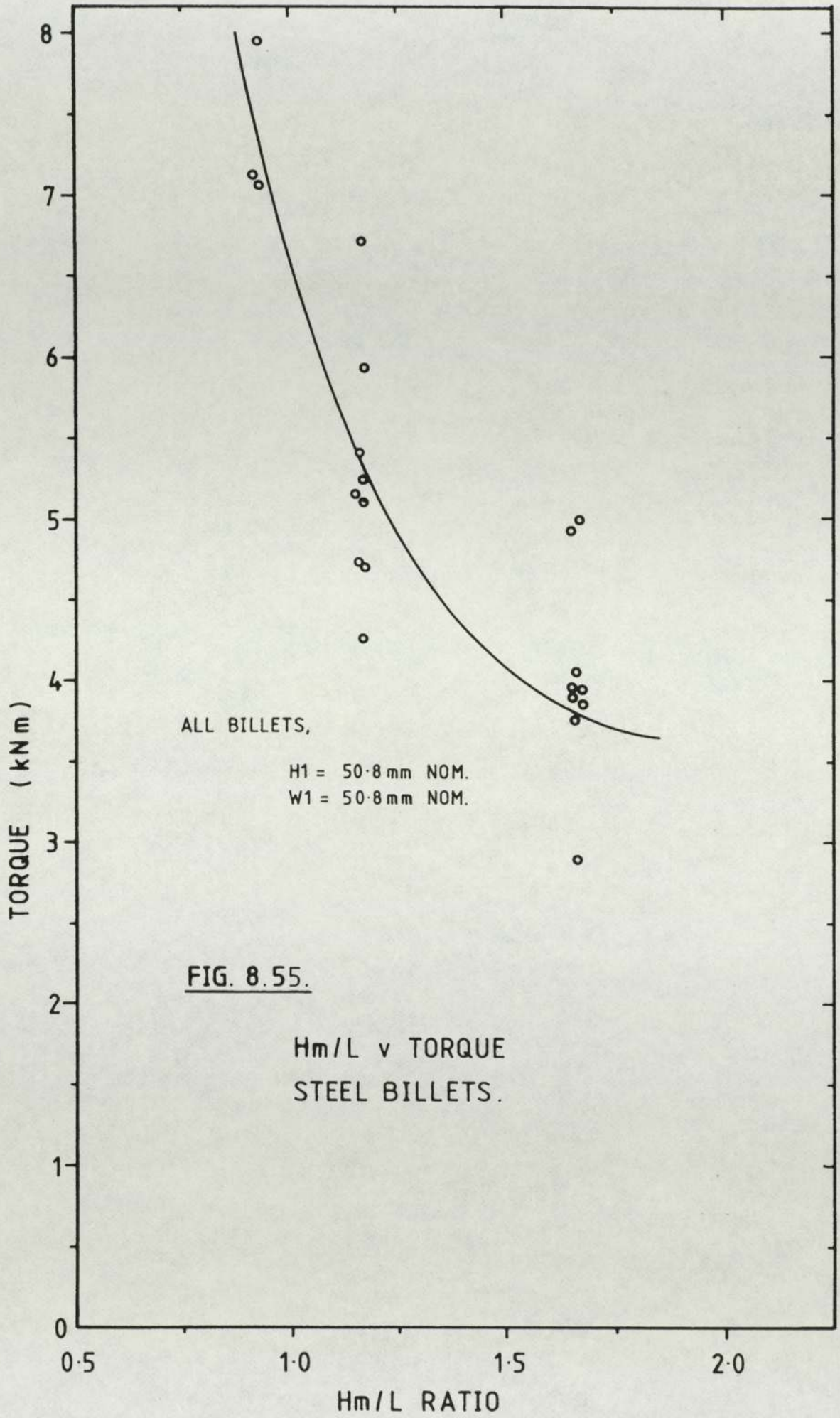

FIG. 8.55.

Hm/L v TORQUE
STEEL BILLETS.

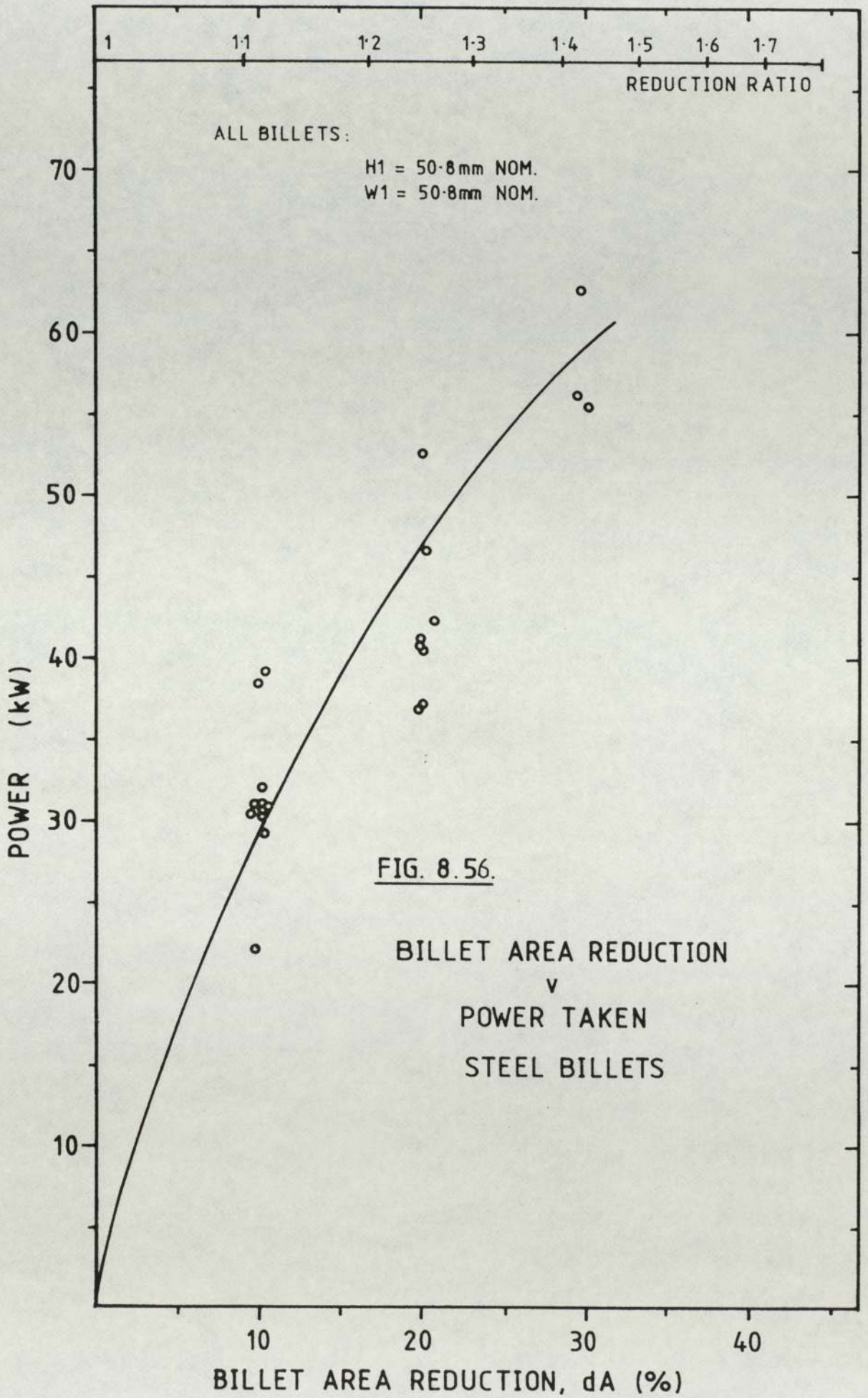

FIG. 8.56.

BILLET AREA REDUCTION
v
POWER TAKEN
STEEL BILLETS

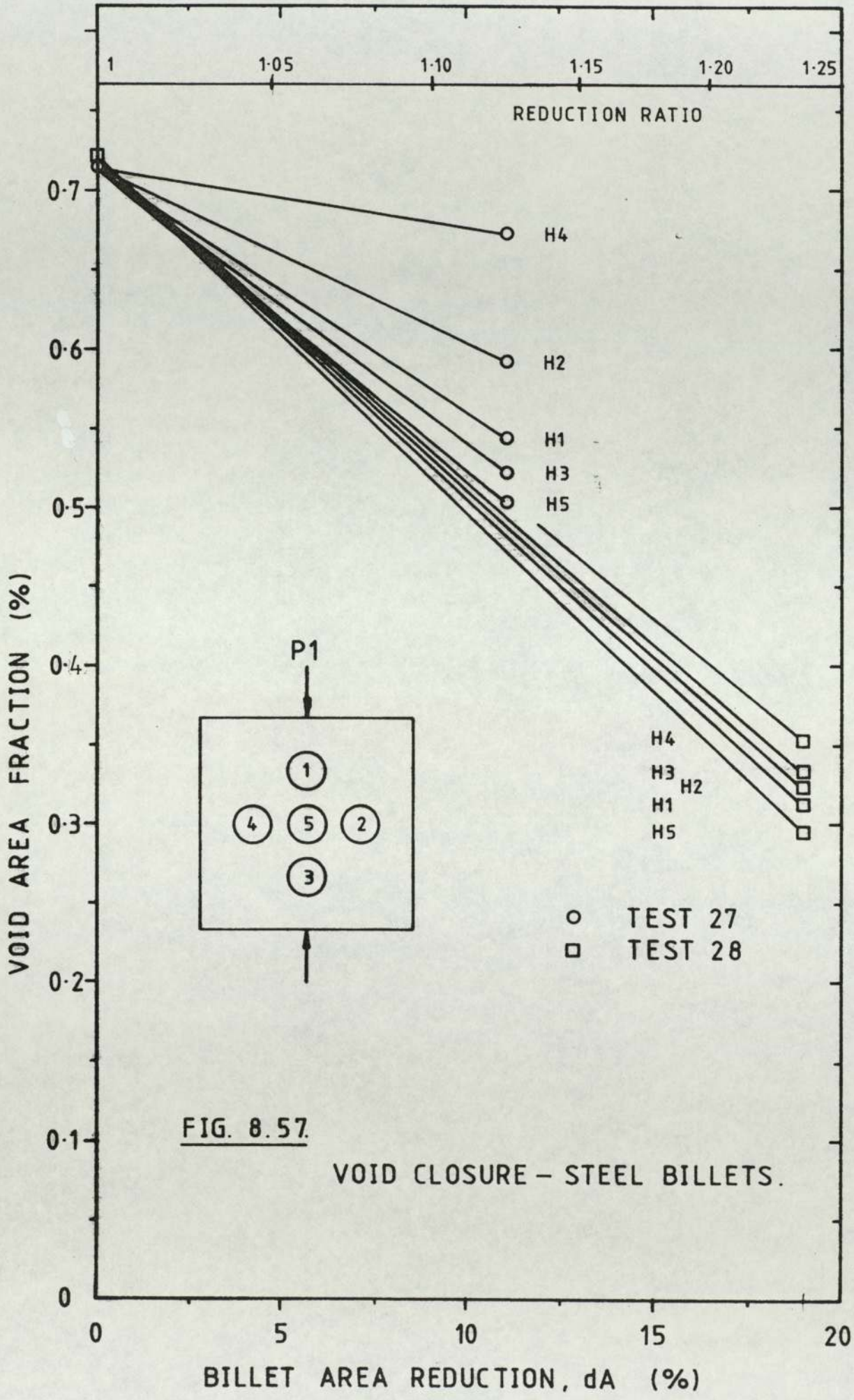

FIG. 8.57.

VOID CLOSURE – STEEL BILLETS.

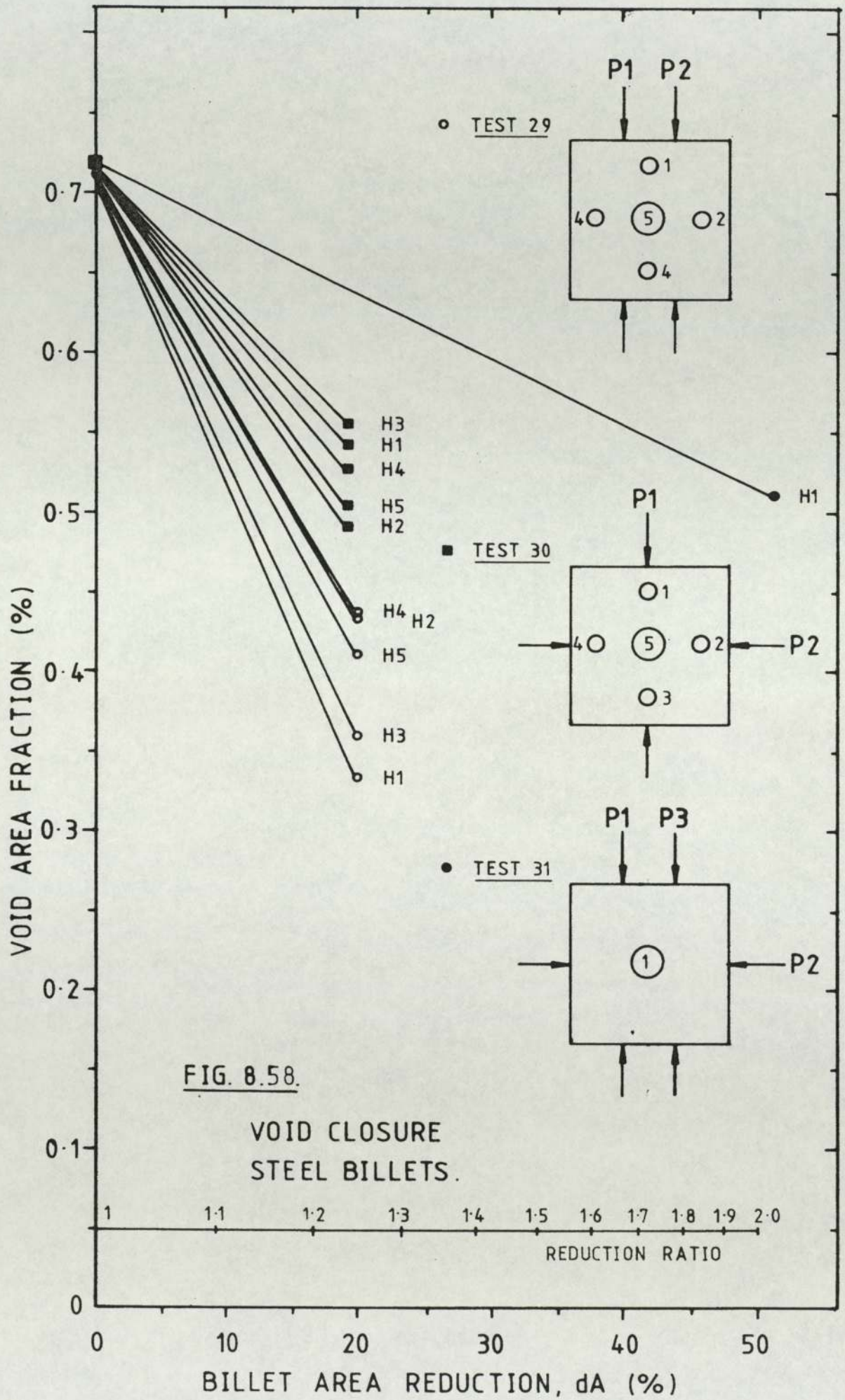

FIG. 8.58.

VOID CLOSURE
STEEL BILLETS.

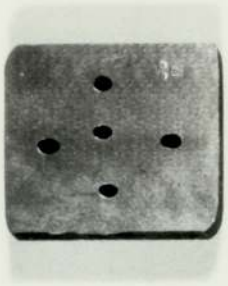

A. PASS 1 1x10%
Hm/L = 1·6711

B. PASS 2 2x10%
Hm/L = 1·6711
1·4777

C. PASS 2 2x10% T
Hm/L = 1·6711
1·6488

D. PASS 1 1x20%
Hm/L = 1·1701

E. PASS 3 3x20% T
Hm/L = 1·1701, 1·1724,
1·0803

FIG. 8.59.

VOID CLOSURE. STEEL BILLETS.

A. TEST 27
B. TEST 29
C. TEST 30 x 0·559
D. TEST 28
E. TEST 31

CHAPTER NINE

DISCUSSION OF RESULTS

9.1. The Mechanism of Rolling Square Section Lead Billets.

In order to assess the mechanism of rolling square section lead billets, total reductions in cross-sectional area in the range 7 to 54% (1.075 to 2.174:1 reduction ratio) were achieved in single and multi-passes to obtain data on rolling load, torque and spread of stock. Single pass tests were compared with multi-pass tests of equivalent total area reduction in terms of product shape and rolling efficiency.

Figures 8.1. to 8.4. illustrate the variation in mean load, mean load per unit width, total torque and total torque per unit width with reduction for single pass tests. The magnitude of the mean load and total torque, Figures 8.1. and 8.3. respectively, show an increase with the size of the stock and the Hm/L ratio. For a fixed stock size, a low value of Hm/L ratio (high reduction) will equate to a longer roll-material arc of contact than for a high value of Hm/L ratio (low reduction). Consequently, rolling with a low Hm/L ratio will result in a larger roll-material contact area over which the interface frictional stress acts. The rolling process at these geometries is thus friction sensitive. The rapid increase in the gradient of the curves in Figures 8.1. and 8.3. confirms that deformation at Hm/L ratios below approximately 1.50 is influenced by the interface friction.

Figures 8.2. and 8.4. illustrate the variation of the mean load per unit width and the total torque per unit width

with Hm/L ratio. The profile of the curves is seen to follow that exhibited in Figures 8.1. and 8.3. with the exception that the difference in mean load per unit width and total torque per unit width decreases as the stock size increases. This may be explained by the fact that for a given rolling geometry, as the stock size is increased the extent of the spread (increase in roll-material contact area) tends to stabilize. For Figures 8.2. and 8.4. the roll-material contact area was calculated as,

$$\text{area} = (w1 + 2/3(w2-w1)) \quad \ldots\ldots\ldots \quad 9.1$$

The spread and geometry of the deformation zone is described later in this section.

Hm/L ratio is plotted against the dimensionless ratio Pm/2k in Figure 8.5. where $k = Y/\sqrt{3}$ and Pm = mean roll pressure. A mean value of the yield stress in compression, for lead was taken to be 23.2 N/mm^2. Although the general form of the curve is difficult to define from such a small spread of Hm/L values, the curve drawn through the points illustrates a sensitivity to rolling geometry at $Hm/L < 2.00$. The general form of the curve shows a similarity with the P/2k - h/b curve for indentation between flat parallel dies (66).

In a previous study, Ingham (66) rolled wide lead slabs (h1 = 15 mm, w1 = 90 mm) in the range $1 \leq HmL \leq 8.74$. His results showed a sensitivity to friction when rolling at

a geometry of $Hm/L < 1.3$. When $Hm/L \leq 1$ his analysis predicted a rapid rise in roll load and certainly the results plotted here in Figure 8.1. confirm his prediction.

Figure 8.6. shows the variation in power with billet reduction in area. An increase of stock size results in an increase in power required for a given degree of reduction. This power is made up of a number of components and so the effect of friction is not easily assessed. For the purposes of this work the power taken is of secondary importance compared to the extent of deformation since the continuously cast steel billet size is close to the required finished product size.

A representative selection of results, Figures 8.7. to 8.11, was compiled from the measurements of width spread. These measurements were used to deduce the coefficients for approximating polynomials to describe the width spread. The polynomials are plotted in the figures. For all the single pass rolling trials a 5 mm square reference grid was scribed on to the roll-material contact surface in order to assess the material flow at this interface. Up to approximately 35% reduction in billet area (1.5385:1) these grids were still visible and showed there to be no relative movement between material and roll over the whole of the billet initial width in the transverse direction. The grid was not elongated in the transverse direction nor was it distorted due to shear at this

interface. However, as would be expected, the grid was elongated in the direction of rolling. Certainly the assumption of sticking friction in the transverse direction made in the theoretical analysis is shown to be valid. The use of roughened rolls will have contributed to the advantageous increase in friction at this interface.

The mechanism of spread can be explained, from Figures 8.7, 8.8 and 8.9, as being a flow of material from the inner material layers in the width direction with consequential fold-over onto the roll surface. At low reductions in area the spread is confined to those areas of the workpiece adjacent to the roll-material interface, that is "dog-bone" type spread. This is illustrated clearly in the spread profile formed at reductions in area of 14.3% (1.117:1) and 12.4% (1.14:1) in Figure 8.7. for tests 1 and 17 respectively. At these reductions the concentration of strain is restricted to the layers of material adjacent to the roll and the influence of interface friction will be low, allowing a limited amount of material to flow onto the roll surface.

Comparison of Figures 8.7. and 8.8. shows that as the stock size increases for reductions in the region of 13% (1.149:1) the amount of spread at the roll-material interface increases marginally. At reductions exceeding approximately 35% the spread at the billet centre exceeds that of the other layers. The strain concentration will thus be greater at

the material centre for these reductions. The well known barreling type spread (convex spread) occurs and, as the reduction is increased, the extent of fold-over of material onto the roll increases. As can be seen in Figures 8.7. and 8.8. for reductions exceeding 35%, the extent of surface spread for a small sized billet is greater in relation to w1 than for a larger billet size. In Figure 8.7. the transition from dog-bone spread to barreling is smooth and the polynomial fits the measured values with good agreement. However, with larger stock sizes, Figure 8.8, the relationship begins to break-down at reductions of approximately 45% whereby the polynomial shows three points of inflexion. The degree of the polynomial and hence the accuracy of the curve fit is governed by the number of data points used. A greater number of data points would increase the accuracy of the fit but may also result in an increase in inter-point oscillation. An alternative method allows the degree of the polynomial to be kept low and provides flexibility by using a sufficient number of polynomial segments joined in a smooth manner. Piecewise polynomial functions such as cubic splines may offer a more detailed fit to the experimental data over a superior range of rolling reduction.

The greater bulge profile reflects the greater magnitude of redundant work of deformation due to the increased shear of material in the vicinity of the bulge (internal work of

deformation) and also the greater the magnitude of frictional work at the roll-material interface, restricting the relative movement of the workpiece at this interface.

Additionally, when rolling lead, two further characteristics of the deformation zone were noted,

a. Zones of stick/slip:

Two distinct zones were visible on the rolled surface, one zone restricted to paths adjacent to the billet edges along the length of the rolled billet, the other occupying the remainder of the rolled billet surface. The formation of these zones is deduced to be a variation in asperity on the rolled surface caused by the sticking of the workpiece to the roll over the extent of the billet initial width and relative slip of material being flowed along the roll at the workpiece edges. The extent and definition of these zones became more pronounced as the reduction and the billet size was increased. Potapkin and Bobukh (62) have noted that the presence of tensile stresses can cause roughness on the surface of the rolled stock for materials of 'low plasticity'. Certainly, the sticking of material to the roll surface will generate tensile stresses at the roll-material interface preventing material flow across the roll surface leading to the spread mechanism described earlier.

b. Upstream deformation:

On the approach to the deformation zone, material at the centre of the billet rolled surface is drawn into the

deformation zone at a higher rate than material in the billet centre and at the billet corners. The resulting profile of the roll-material contact surface just prior to entering the deformation zone is one of a slightly concave form (negative crown). The extent of this upstream deformation is dependent on the billet size, the reduction and the interface friction. No attempt has been made to quantify this deformation in the present work although its presence is acknowledged. Tagawa (13) has shown deformation to occur preferentially near the surface of the workpiece at the entry to the deformation zone. He identified a compressive stress in layers below the roll-material interface, for a significant distance upstream of the deformation zone. In the theoretical analysis of Chapter Four, the redundant work done in causing this effect is infered to be negligible in comparison with the overall work of deformation by the assumption that the entry plane is vertical from the first roll-material contact point to the billet longitudinal centre line (Figure 4.1.).

Figures 8.10. and 8.11. illustrate the spread profiles of billets being progressively reduced in a number of passes. For both tests, approximately equal reductions were taken at each pass, 2 x 25% (2 x 1.335:1) and 4 x 30% (4 x 1.429:1) for tests 38 and 37 respectively.

When rolling through plain flat rolls, the aspect ratio of the workpiece (ratio of workpiece height to width) becomes

important in achieving stability during rolling and preventing billet twist in the roll gap. Consequently, for these tests, reductions in excess of 35 to 40% (1.538 to 1.667:1) were not practicable.

When rolled at reductions less than 35% the spread profile was of the dog-bone type. Turning of the billet for subsequent passes entailed rolling on the width of the previous pass. Consequently, most of the deformation was concentrated in the areas where the spread was greatest from the previous pass. Thus, although the required product shape/section is more easily controlled by rolling at these conservative reductions, the central regions may not receive sufficient deformation. The effect of reduction on the workpiece macrostructure is discussed in the next section.

The first part of the theoretical analysis in Section 4.2.3. enables one to calculate directly the strain field in the deforming billet using a simplified method utilising experimentally derived data on billet spread. Comparison between a theoretical calculation of roll torque and measured roll torque are given in Appendix J.

9.2. Effect of Pass Geometry on Grain Refinement.

Total reductions in cross sectional area in the range 10 to 55% (1.11 to 2.22:1) were achieved in single and multi-

passes in order to assess the effect of pass geometry on workpiece structural refinement. When rolling continuously cast stock, the cast size is close to the required product size. As explained in Section 2.2. the cast structure is likely to contain defects and so the requirement of the rolling process is to achieve a fully dense wrought structure consonant with dimensional accuracy in the finished product.

The preparation of test billets, detailed in Section 7.3.3, was difficult to control sufficiently to obtain a similar grain structure for each billet at the start of a test. Figures 8.12. and 8.13. illustrate the effect of initial mean grain size on the final grain size after reduction (see also Section 7.5.1. and Appendix C.1). The variability of the initial mean grain size is large, in the range 0.55 to 10.126 mm, and to a certain extent dependent on the billet initial size.

A number of factors will affect the recrystallization kinetics, for example, the amount of deformation received in the pre-working operation. At small strains, fewer nuclei will be created per unit volume and the incubation time for the formation of new grains is longer. A small number of nuclei will lead to large grains. If the strain is low enough to just reach the critical strain (the strain just necessary to initiate recrystallization), the result will be an extremely coarse grain size after transformation. A strain gradient throught the material thickness will lead to

different areas having different final grain sizes. The pre-work strain will affect the grain size for annealing. Recrystallization nuclei occur preferentially at grain boundaries so the extent of the latter will influence the kinetics of the process. Thus, recrystallization will occur more readily in a fine grained material due to the large grain boundary area per unit volume.

The purity of the metal is another factor in determining the propensity for recrystallization. The lead swarf from the preparation and also the lead billets used in the rolling tests was recycled, so there was the possibility of picking up impurities in the melt for the next cast. Work on lead (151) has shown that extremely small traces of impurities such as antimony, tellurium and tin, have a marked effect on grain growth during recrystallization. Impurity atoms tend to segregate to interfaces such as grain boundaries, preferential sites for the formation of recrystallization nuclei and interfere with the rearrangement of parent atoms into the strain-free lattice to form a nucleus.

The rolled mean grain size (mean linear intercept, $\bar{d}$) was measured a substantial period of time after rolling. The dynamic structural changes (dynamic recrystallization) during the roll pass leave the workpiece in an unstable state and provide the driving force for static recovery and static recrystallization to an extent depending

on the rolling reduction. Since lead may recrystallize at room temperature, static recrystallization and grain growth is possible. It should be noted here that increases in surface temperature of up to 19 deg.C were recorded when rolling lead at high reductions.

Since grain boundaries are the favoured sites for the nucleation of new grains, the grain size after recrystallization will depend on the initial grain size, the strain and on the Zener-Holloman parameter, Z. The latter two control the driving force for recrystallization.

The Zener-Holloman parameter is given by,

$$Z = \dot{\varepsilon} \exp\left\{\frac{Q}{R\,T}\right\} \quad \ldots\ldots\ldots\ldots\ldots 9.1$$

where Q = activation energy for the deformation process (J/mole).

R = the gas constant (8.31 J/mole.K).

T = temperature (K).

Fine grain sizes will be obtained after high strain at high Z (high temperature).

Figures 8.14. to 8.17. show examples of specimens before and after rolling in single passes. The variability in the initial grain size between different test billets is clearly evident. At low values of reduction, 10 to 15% (1.11 to 1.176:1), the billet structure is refined to a certain degree

throughout the section. The localized sites of recrystallization can be seen in some low reduction tests, the work being confined to material layers adjacent to the roll surface, including the corner regions. Low reductions result in the structure on the billet width faces being less worked than other areas leaving a grain structure extended in the width direction. When the spread profile of the billet is of the dog-bone type, these areas will not be sufficiently worked to realize effective recrystallization. However, at reductions exceeding 30 to 35% (1.428 to 1.538:1), where the spread profile changes to the barreling type, the structure will be worked throughout the section sufficently for total refinement; the effect of static recrystallization and grain growth is not known here. At reductions approaching 50% (2:1) the deformed grain size may be less than 10% of that of the initial grain size.

Reductions in area less than 25% (1.333:1) will achieve a recrystallized grain size as low as 20% of the initial grain size. The distribution of the 20% refinement through the section is a function of the initial grain size, the reduction taken and the initial billet size.

For grain refinement throughout the section, reductions in excess of 40% (1.667:1) in single passes are required. The spread of the billet will be fully convex (barelling) and the grain structure will have been refined throughout the section. However, at high reductions the desired square

section is not achieved. The shape of the resulting product may be a controlling factor over the amount of reduction.

Figures 8.18, 8.19 and 8.20. show sections of billets rolled in single passes. The diagrams show the outer width face of the billet (A), the grain structure on the billet longitudinal centre line (B) and the billet surface in contact with the roll (C). The extent of the recrystallized zone is visible in the three views and gives an indication of the deformed zone and the entry plane. The lower view (C) also gives an indication of the extent and form of the spread as the material passes through the deformation zone. The assumption made in the theoretical analysis given in Section 4.2.4. that a parabolic arc delineates the lateral flow through the deformation zone is therefore valid.

One can see from the view of the roll contact surface (C) that material at the centre of the surface has been deformed earlier than that at the edges due to the upstream deformation mentioned in Section 9.1; the recrystallization zone varies across the width of the billet.

The view on the material longitudinal centre line (B) shows recrystallization to occur immediately upon contact with the roll with the recrystallization front taking the form of an arc from the initial roll contact point to the billet longitudinal centre axis. In Figures 8.19. and 8.20. where the recrystallization front is clearly defined, it can

be infered that deformation occurs mainly at the surface on entry to the deformation zone, while on the exit side the deformation will be largely in the central region (13). Examination of billets rolled in this manner has shown that the majority of the centre spread occurs towards the rear of the deformation zone.

Figure 8.18. shows a distinct variability in the grain size on the billet longitudinal centre line through the thickness, however the shape of the recrystallization front is difficult to deduce. The front is more clearly defined in Figures 8.19. and 8.20. and shows that as the reduction is increased (Hm/L is reduced) the tendency is for the recrystallization front on the longitudinal centre line to move upstream of the deformation zone, so that in effect more work is concentrated in the central area early in the deformation zone.

Figures 8.21. and 8.22. illustrate the effect of grain refinement with reduction for multiple pass rolling tests (refer also to Appendix C.2.). Total reductions in the range 22.5% to 54% (1.290 to 2.174:1) were achieved for comparison of the structure with the single pass tests at equivalent total reductions.

As mentioned earlier, first pass reductions in area of less than 25% (1.333:1) will achieve a recrystallized grain size as low as 20% of the initial grain size. The gradients of the curves plotted in Figures 8.21. and 8.22. show that

the rate of recrystallization is greater for large grain sizes. When the grain size is reduced, further reduction leads to smaller decreases in size indicated by the reduction in the curve gradients. This may be explained by the fact that is better to deform the structure at high rates while the driving force for recrystallization is low ie. there is a low grain boundary area per unit volume. As recrystallization proceeds the grain boundary area per unit volume increases with subsequent increase in the required driving force. Figures 8.21. and 8.22. also show that at high reductions it is possible for there to be an increase in the grain size due to the processes of static recovery, static recrystallization and subsequent grain growth between passes and after the final pass. The extent of these changes will depend on the initial grain size, the strain and the temperature. Consequently, when rolling lead one can only specify a refined structural 'size' that incorporates these phenomena.

At low reductions in two or more passes with a turn at each pass, the depth of recrystallization will only significantly affect areas adjacent to the rolled surface. Due to the spread of the material (dog-bone type at low reductions), the subsequent pass will tend to work areas where spread was greatest in the previous pass. Consequently, recrystallization is more complete in the billet corner regions.

At low reductions in two or more passes on the same face, the depth of recrystallization will still only affect the layers adjacent to the rolled surface. Reduction in excess of 30% (1.4286:1) per pass is required to achieve a fully wrought structure in three or four passes with turning. The important practical inference is that with this schedule the billet shape is controlled and a product of square proportion results.

In comparing single and multi-pass rolling schedules of equal total area reductions, it is preferable from a production point of view to roll at reductions of 30% (1.4286:1) per pass in two or more passes with a turn to achieve a total reduction of approximately 60% (2.5:1), say, rather than one large pass of 60%. Product shape is far better controlled in the multi-pass schedule and it has been shown that passes of 30 to 35% (1.4286 to 1.5385:1) will result in a homogeneous, fully recrystallized structure throughout the section. The effect of the Hm/L ratio is also significant in achieving the desired wrought structure. Rolling with $Hm/L \leq 1.4$ will lead to full recrystallization in a billet section. This will depend on the roll diameter and the stock initial size.

Figure 8.23. shows an example of the recrystallization at the center of a lead billet transverse section when rolled in four passes to a total reduction in area of 53.59% (2.155:1). Two passes with a turn, totalling 31.98%

(1.470:1) resulted in a mean linear intercept of 20.85% that of the initial grain size. Two further passes result in a mean linear intercept of 16.21% that of the initial grain size.

9.3. Rolling of Square Section Lead Billets to Assess the Effect of Pass Geometry on Model Void Consolidation.

Holes were drilled in various formations along the longitudinal axes of lead billets in order to study consolidation of voids when rolling continuously cast stock. Billets were rolled in single and multi-passes at reductions in the range 6.9% to 36% per pass (1.074 to 1.5625:1), totalling up to 75% (4:1).

Figures 8.24. and 8.25. illustrate the reduction in void area fraction and the cumulative axial strain for a four pass sequence of 10% (1.111:1) reduction in area per pass with a turn after pass two only. During the first passes ε_y is tensile and ε_z compressive but when the billet is turned after pass two the strain is reversed on the y and z axes. During the pass sequence the void area fraction is always reduced but at these low reductions it is relatively easy to change the direction of the applied strain by turning too early in the schedule. After pass four, the cumulative strains were ε_y = 0.5002, ε_z = 0.4774 and the void area fraction for hole 5 = 0.4095% from an initial void area

fraction of 0.7509%, a 64.66% consolidation. The theory predicts void closure at r_c = 97.6%.

Figures 8.26. and 8.27. illustrate the rate of reduction in void area fraction and the cumulative axial strain for a four pass sequence of 10% (1.111:1) reduction in area per pass with a turn after each pass. During the first pass ε_y is tensile and ε_z compressive but when the billet is turned the strain is reversed on the axes. During pass two there is void enlargement but then void reduction during the remainder of the pass schedule, where the axial strain remains essentially compressive. After pass four, the cumulative strains were ε_y = 0.3384, ε_z = 0.4091 and the void area fraction for hole 5 = 0.5913% from an initial void area fraction of 0.8054%, a 51.56% consolidation. The theory predicts void closure at r_c = 101.3%.

Figures 8.28. and 8.29. illustrate the rate of reduction in void area fraction for a six pass sequence of 10% (1.111:1) reduction in area per pass for the first four passes followed by two further passes of 20% (1.25:1). Although pass one is not measured it is likely that the strain on the y axis will be tensile as for the two previous tests. After pass two both strains are compressive and all holes have been reduced by a significant extent. As the reduction is increased the magnitude of the cumulative strain on both axes increases. After pass four, the cumulative strains were, ε_y = 0.2683, ε_z = 0.4750 and the

void area fraction for hole 5 = 0.5206% from an initial void area fraction of 0.7790%, a 56.84% consolidation. The application of two further passes at 20% shows a rapid increase in the compressive strain on the void axes with corresponding decrease in void area fraction. After pass six, the cumulative strains were, ε_y = 1.0617, ε_z = 1.1165 and the void area fraction for hole 5 = 0.2089%, an 88.55% consolidation. The theory predicts void closure for r_c = 99.6%.

Figure 8.30. illustrates a combination of results taken from the three previous tests (75, 76 and 77). The curves drawn through the points approximate the reduction for an average void area fraction.

Figure 8.31. shows specimens taken from test 75 (B), test 76 (C) and test 77 (A). The size of the initial void area fraction can be seen for each test and is substantial in relation to the billet initial size. For test 75 the compression of the voids with axial extension in the transverse direction is visible, the void area is reduced and the deformation follows the theoretical Solution A (Figure 4.3.). Upon turning after pass two the billet has twisted in the roll gap during pass three. In test 76 the voids alternate between elliptical and circular section during the pass sequence, due to the alternate tensile/compressive strain on the void axes with the turning of the billet. After pass four, the section shows similar

twist to test 75, shear in the roll gap. Test 77 follows the same schedule as test 76 to pass 4 where it then undergoes two further passes of 20% resulting in beneficial void closure. For this size of billet, where the initial void area fraction is large in relation to the billet initial size, the theoretical prediction of reduction required for void closure (r_c) is a gross overestimation; values in excess of 90% are predicted by the analysis.

Figures 8.32. to 8.48. show the variation in void area fraction with reduction and the axial strain measured from the deformed voids for an initial billet size of 66 mm square.

Figures 8.32. and 8.33. illustrate the rate of reduction in void area fraction and the cumulative axial strain for a four pass sequence of 20% (1.25:1) reduction in area per pass with a turn after each pass. At this reduction the first pass strains are all compressive, however turning produces tensile ε_z . The mechanism of closure is ellipse-circle-ellipse with progressive void closure at all times in the sequence. However, at pass four the void is enlarged with both pass axial strains and tensile. The closure of the void can be seen in Figure 8.33, still visible after 64% (2.778:1) reduction. After pass four the cumulative strains were, ε_y = 1.7188, ε_z = 2.1740 and the void area fraction, Vf = 0.0405% from an initial void area fraction of 0.7316%, a 98.01% consolidation. The reduction required for

void closure is predicted as r_c = 96.5%.

Figure 8.34. shows the void axial strains for a test billet having a distribution of voids at various depths below the billet surface. Hole 1 is subject to the largest strain due to its proximity to the surface. There is some tensile strain when the billet is turned but the reduction of voids is effective as the cumulative strain increases. After pass four, the cumulative strains were, ε_y = 0.4829, ε_z = 0.3135 and the void area fraction for hole 4 = 0.4947% from an initial void area fraction of 0.7780%, a 57.76% consolidation. The cumulative strains for hole 1 were ε_y = 0.7926 and ε_z = 0.9824 with a void area fraction of 0.0302% from an initial void area fraction of 0.1627%, an 86.92% consolidation. The reduction required for void closure is predicted as r_c = 79.36% (for hole 4).

Figures 8.35. and 8.36. illustrate the rate of reduction in void area fraction and the cumulative axial strain for a four pass sequence of 10% (1.111:1) reduction in area per pass with no turn ie. reduction on the same faces throughout the pass sequence. In the early passes the strain along the y-axis of the voids is tensile gradually reducing in tensile nature as the reduction is increased. The compressive strain on the void z-axis increases throughout the pass sequence, it being similar in magnitude for all the voids. As the reduction increases the tensile strain in the radial voids reduces and tends to compressive at pass

four. The tensile strain on the y-axis for hole 5 is approximately constant throughout the pass schedule. After pass four, the cumulative strains were, $\varepsilon_y = -0.0399$, $\varepsilon_z = 0.8971$ and the void area fraction for hole 5 = 0.2312% from an initial void area fraction of 0.4344%, a 63.84% consolidation. The reduction required for void closure is predicted as $r_c = 74.37\%$. Figure 8.39 (A) shows specimens of test sections through the schedule. The voids are substantially reduced but are still prominent after pass four.

Figure 8.40 (B) shows test specimens for three passes at 20% (1.25:1) reduction in area to a total of 49.52% (1.981:1) with a turn after pass two only. After pass two the voids have been significantly reduced to the elliptical form predicted in Solution A of the theoretical analysis. After pass two, the void area fraction for hole 5 = 0.1277% and after pass three it is 0.0085% from an initial void area fraction of 0.4278%, consolidations of 81.58% and 99% respectively, the other holes effectively being closed. The difficulty in rolling on the billet long axis is shown by the twist of the billet during pass three, but this has the beneficial effect of imposing on the voids an additional shear strain effecting preferential closure over test 87 (Figures 8.41. and 8.42.). The reduction required for void closure is predicted as $r_c = 73.8\%$.

Figures 8.37. and 8.38. illustrate the rate of reduction

in void area fraction and the cumulative axial strain for a three pass sequence of 20% (1.25:1) reduction in area per pass with a turn after each pass to a total of 49.1% (1.965:1). The initial pass shows a minimal tensile axial strain, increasing to compressive as the schedule proceeds. There is always void closure although the rate of closure varies according to the axial strain field. The large variation in the axial strain for hole 3 points to a non-equal spacing of the billet in the roll gap. Figure 8.40 (A) shows billet sections during the pass schedule. A small shear strain has been applied to the billet in the roll gap due to twist but the voids are still visible after pass three. After pass three, the cumulative strains were, ε_y = 0.5004, ε_z = 1.4799 and the void area fraction for hole 5 = 0.1073% from an initial void area fraction of 0.4002%, an 86.36% consolidation. The reduction required for void closure is estimated as r_c = 71.38%.

Figure 8.39 (B) shows billet sections for a four pass schedule of 10% (1.111:1) reduction in area per pass with a turn each pass to a total of 26.51% (1.361:1). The void fraction is still substantial after pass four with a large increase in fraction of one of the radial voids. During the preparation of that specimen swarf may have collected in the void in the remainder of the billet. This may be the cause of poor closure of the void in further passes. After pass four, the cumulative strains were, ε_y = 0.1968, ε_z = 0.3500 and the void area fraction for hole 5 = 0.3355% from an

initial void area fraction of 0.4285%, a 42.45% consolidation. The reduction required for void closure is estimated as r_c = 73.86%.

Figures 8.41. and 8.42. illustrate the rate of reduction in void area fraction and the cumulative axial strain for a four pass sequence of 30% (1.429:1) reduction in area per pass with a turn after each pass to a total of 74.6% (3.937:1). There is a more rapid decrease in void fraction due to the increased reduction up to approximately 50% (2:1). Above this figure, after pass two, the axial strain field for all voids exhibits extreme fluctuation. Although pass one was not measured it is to be expected that ε_y is tensile. After pass four, the cumulative strains were, ε_y = 1.0848, ε_z = 2.6357 and the void area fraction for hole 5 = 0.0435% from an initial void area fraction of 0.4241%, a 97.39% consolidation. The reduction required for void closure is estimated as r_c = 73.50%. Figure 8.45 (A) shows billet sections for this pass schedule. Good closure of voids is seen to be achieved after pass four.

Figures 8.43. and 8.44. illustrate the rate of reduction in void area fraction and the cumulative axial strain for a four pass sequence of 10% (1.111:1) reduction in area per pass with a turn after each pass to a total of 34.3% (1.522:1), followed by a further two passes at 20% (1.25:1) with a turn after each pass to a total of 57.3% (2.342:1). The rate of closure accelerates after pass four

with the larger reductions with proportional increases in compressive axial strain. After pass four, the cumulative strains were, ε_y = 0.3153, ε_z = 0.4183 and the void area fraction for hole 5 = 0.3138% from an initial void area fraction of 0.4332%, a 52.41% consolidation. After pass six, the cumulative strains were, ε_y = 1.1192, ε_z = 0.6337 and the void area fraction for hole 5 = 0.1221%, an 87.97% consolidation. The reduction required for void closure is estimated as r_c = 74.27%.

Figure 8.45 (B) shows billet sections for a six pass sequence of 20% (1.25:1) area reduction per pass with a turn each pass to a total of 74.99% (3.998:1). A good billet section has been retained throughout the schedule although the closure is not as efficient as test 87 (Figures 8.41. and 8.42.). After pass six, the void area fraction for hole 5 = 0.1339% from an initial void area fraction of 0.4578%, a 92.69% consolidation. The reduction required for void closure is estimated as r_c = 76.35%.

Figures 8.46, 8.47. and 8.48. illustrate combined results for the selection of tests outlined above. The median curve is drawn for an initial mean void area fraction of 0.425% in Figure 8.46. for comparison with the theoretical curve.

Void closure for initial void area fractions less than 0.45% and at low reduction in area is underestimated by the

theory but rapidly approaches the results of experiment for reductions in excess of 40% (1.667:1). This indicates that upper bound Solution A is a valid solution for the material flow at these high reductions. However, for initial void fractions in excess of 0.45%, the theory gives a gross underestimation of void closure over all reductions. The assumption in the analysis of void closure, Section 4.3.3, that the material flow is independent of the direction of rolling (x-direction) is therefore questionable. Certainly, Figure 8.51. shows that the rate of void closure varies along the length of the roll gap. Essentially, Equation 4.40, based on upper bound Solution A, assumes that the deformation can be approximated by a homogeneous plane strain model. Thus, the reduction for void closure, expressed by Equation 4.40. (r_c = h1/H1), will be inaccurate since this relation neglects material flow in the direction of rolling.

The reduction required for void closure, Equation 4.49, is seen to be independent of the rolling geometry, dependent only on the reduction (r) and the initial void area fraction (Vf_i). The results have shown that voids in small billets will close at a faster rate than similar sized voids in larger billets, for equal reductions in area. Therefore, the rolling geometry (Hm/L ratio) and the frictional conditions between roll and material assume significance when determining void closure. The theoretical analysis is based on reduction of a void in one direction in

one pass so that a variation between theory and experiment will be expected when turning the billet during a roll schedule.

Figures 8.47. and 8.48. illustrate combined results for the radial voids taken as a mean of (H1+H3) and (H2+H4). No theoretical curve is drawn for comparison since the analysis is based on a single void situated at the billet centre. As the reduction increases the rate of void closure is seen to accelerate at reductions in excess of 20% (1.25:1) but slows down as the void fraction reaches a point where further closure requires a proportionately large increase in reduction.

Figure 8.49. shows four tests conducted on 43 mm square billets with a single void situated at the billet centre. The area fraction of the void is large and a theoretical analysis would produce meaningless results as for tests 75, 76 and 77. However, the effect of different pass schedules is quite evident in the figure.

Figure 8.49 (A) shows two passes of 10% (1.111:1) with a turn each pass to a total of 19.27% (1.239:1). After pass two, the void area fraction = 1.5194% from an initial void area fraction of 2.0337%, a 39.69% consolidation.

Figure 8.49 (B) shows two passes of 20% (1.25:1) with a turn each pass to a total of 38.97% (1.638:1). After pass two, the void area fraction = 0.6107% from an initial void

area fraction of 1.9569%, an 80.96% consolidation.

Figure 8.49 (C) shows one pass of 21.54% (1.274:1). After the pass the void area fraction = 0.8041% from an initial void area fraction of 1.9390%, a 67.46% consolidation.

Figure 8.49 (D) shows one pass of 42.50% (1.739:1). After the pass the hole is totally closed, having been totally compressed in the direction of the applied stress. However, a trace line is still visible at the centre showing void compression and extension in the transverse direction.

Figure 8.50. shows sections of two tests made on 60 mm square billets. Figure 8.50 (A) shows a single pass at 36.7% (1.580:1), all voids being closed. However, in the centre region, the void is still visible as a trace line. Figure 8.50 (B) shows the result of two passes at 20% (1.25:1) reduction in area per pass with a turn after each pass to a total of 40.34% (1.676:1). The voids are still visible in the matrix and after pass two, the area fraction for hole 5 = 0.4332% from an initial void area fraction of 0.5325%, an 18.6% consolidation.

Figure 8.51. shows a billet stopped in the roll gap at a reduction of 36.7% (1.581:1). Figure 8.51 (B) shows a section along the billet vertical centre line clearly showing the closure of the voids (H1, H3 and H5) as the billet moves

through the deformation zone. Of particular interest is the manner in which the radial holes flow through the deformation zone following a typical streamline. There is some void consolidation on entry to the deformation zone but the closure rate increases close to the exit from the deformation zone. The majority of the void closure occurs close to the exit from the roll gap. Tagawa (13) has shown the deformation to be larger in the central layers on the output side of the roll gap, explaining that the strain in the billet becomes uniform through the thickness on exit from the deformation zone.

In the experimental tests, void consolidation always occured in the pass even with one axial strain tensile. The magnitude of the compressive strain was always superior to the magnitude of the tensile strain and, in the range of reductions taken, both strains were never tensile at the same time. Repeated reduction on the same face showed the strain perpendicular to the direction of the applied stress to be always tensile although its magnitude reduced during the pass sequence.

Comparison of tests conducted with one centrally situated void and those conducted with both a central void and radial voids has shown there to be a considerable difference in strain on the axes of the central void. The strain on the central void is much greater, everything else being equal, for a single void than for a central void with

a distribution of radial voids. For example, with one void and repeated reduction on the same face, for a total reduction of 32.1% (1.472:1), the cumulative strains were $\varepsilon_y = -0.0399$ and $\varepsilon_z = 0.8971$. For a distribution of radial voids and one central void, the cumulative strains were $\varepsilon_y = 0.4829$ and $\varepsilon_z = 0.3135$ for a total reduction of 33.58% (1.5056:1).

From the model tests the mechanism of void closure can be explained as being primarily one of compression in the direction of the applied stress and spread in the direction perpendicular to the applied stress. For complete closure and adhesion there should be diffusion as the boundary faces of the void make contact. Movement of the contact points relative to one another will be beneficial in achieving optimal adhesion.

In the experimental tests, optimal reduction in void area fraction for large size billets has been achieved by using a schedule of reductions in the region of 30% (1.429:1) per pass to a total reduction of approximately 70% (3.333:1) in three or four passes with turning. The initial passes need to be as large as possible to achieve large compressive strains in the central region. Results show that a rapid decrease in void area fraction with corresponding increase in the compressive strain field in the region of the central void can be achieved in early passes with a rolling geometry of $Hm/L \leq 1.4$. Rolling with a geometry of $Hm/L \geq 2$,

approximately 10% (1.111:1) area reduction, will result in tensile or at best small compressive strains on the void axis perpendicular to the direction of applied stress.

The presence of shear strains increases the effectiveness of the reduction process and will promote flow of the approaching void contact points relative to one another. Alternatively, the application of one large reduction in the region of 40% (1.667:1) will certainly effect void closure, especially for small size billets. In this case the void will be compressed to closure leaving a trace line. Further reduction perpendicular to the direction of the original stress will open-up the void unless effective welding has been achieved. Since the void surface was open to atmosphere, the possibility of oxidation and subsequent poor welding cannot be ignored.

In general, for the reductions taken, it has been shown that the axial strain will be dependent on the direction of the applied stress. Even with a large reduction of approximately 30% (1.429:1) in one pass, it is not possible to close the void (dependent also on h1). For low reductions in area, less than 20% (1.25:1), the applied stress will produce a compressive strain in its direction and a tensile strain perpendicular to the direction of application. At repeated low reductions the direction of applied stress will affect the magnitude of the cumulative strain and its nature (tensile or compressive). High

reductions, greater than 30% (1.429:1) are preferable to achieve a rapid increase in compressive cumulative strain on the void axes.

The influence of reduction on the void area fraction described by equation 4.48. is presented in Figure 8.52. for various initial area fractions of voids. For example, after a reduction of 25% (1.333:1) all billets with an initial area fraction $\leq$ 0.05% will be free from voids but billets with an initial void area fraction of 0.2%, say, still have a void area fraction of 0.143%.

The analysis predicts a steady reduction in void area fraction from high initial void fractions coupled with a rapid reduction in the former at large reductions in height. The analysis has been shown to break down for values of initial void area fraction in excess of 0.6% since reductions greater than 90% are predicted to achieve void closure. Figure 8.53. illustrates the variation in reduction required for void closure, r_c , with void initial area fraction, Vf_I . The theory predicts a rapid rise in the reduction required in proportion to Vf_I .

A schedule in excess of 30% (1.5385:1) per pass, to a total of approximately 60% (2.5:1), has been shown to result in a homogeneous, fully recrystallized structure throughout the billet section. At the reductions required to achieve full consolidation, in excess of 65% (2.857:1), the

achievement of a fully refined section will be made.

The results compare favourably with those of other workers in this field (13,15,16,18,22,23,29) who, amongst others, have quoted reductions in the range 20% to 90% (1.25 to 10:1) for the attenuation of a fully wrought billet product (see Section 2.4.1.).

9.4. Works Trials.

As part of this present work and also the initial experimental work for the British Steel project 'Extending the Product Size Range for Continuously Cast Sections', trials were carried out on 50 mm square section billets to evaluate the effect of a range of reductions on consolidation of solidification defects. The following is a resumé of the early trials.

9.4.1. Effect of Pass Geometry on Model Void Consolidation in Steel Billets.

Figures 8.54, 8.55. and 8.56. respectvely illustrate the effect of reduction (Hm/L ratio) on the mean load, torque and power taken when rolling square section steel billets. The profiles of the curves are similar to those obtained when rolling square section lead billets, Figures 8.1, 8.2. and 8.6. The rolling load and torque curves exhibit a similar dependance on friction for reduction geometries where

Hm/L < 1.5. Certainly it is probable that sticking friction occured during the rolling of the steel, especially so since the roll surface was rough.

Figures 8.57, 8.58. and 8.59. illustrate the effect of pass geometry on void consolidation for a number of billets. Billets were rolled at a nominal temperature of 1250 deg.C. prior to the first pass.

Figure 8.57. shows the reduction in void area fraction after single pass reductions of 11% (1.12:1) and 19% (1.25:1), Hm/L = 1.6711 and 1.1701 respectively. For test 27 (one pass at 11% reduction in area) the deformation of the voids is similar to that obtained in the lead trials. Holes two and four exhibit a tensile strain on the y-axis perpendicular to the direction of the applied stress, the strain on the z-axis being compressive. For hole 5, the cumulative strains were, ε_y = 0.0480, ε_z = 0.3954 and the void area fraction = 0.5036% from an initial void area fraction of 0.7214%, a 37.63% consolidation. For test 28 (one pass at 19% reduction in area) the voids are deformed to elongated ellipses with holes two and four again exhibiting tensile strain on the y-axis. The strain on the z-axis for all holes is compressive. For hole 5, the cumulative strains were, ε_y = 0.1154, ε_z = 0.8562 and the void area fraction = 0.2954% from an initial void area fraction of 0.7236%, a 61.76% consolidation. Compared with test 27, the increased reduction has resulted in a decrease in the tensile

strain component on the y-axis with corresponding increase in the compressive strain component on the z-axis for all voids.

Figure 8.58. shows the reduction in void area fraction for twin pass total reductions of 19% (1.25:1) with a turn each pass, 19.83% (1.25:1) on the same face and a three pass total reduction of 51.2% (2.05:1) with a turn each pass. For test 29 (two repeated passes of equal reduction on the same face totalling 19.83% area reduction) the voids are deformed to a similar shape as for test 28. However, the consolidation is not as efficient and the magnitude of the y and z-strains are less. For hole 5, the cumulative strains were, $\varepsilon_y = 0.0265$, $\varepsilon_z = 0.7196$ and the void area fraction = 0.4137% from an initial void area fraction of 0.7142%, a 53.56% consolidation. For test 30 (two repeated passes of equal reduction on alternate faces totalling 19%) the voids are reduced in area to a circular form due to the alternate direction of applied stress but the consolidation is not as efficient as for one single equal reduction (test 28). The magnitude of the cumulative strains are also reduced. For hole 5, the cumulative strains were, $\varepsilon_y = 0.2259$, $\varepsilon_z = 0.3213$ and the void area fraction = 0.5039% from an initial void area fraction of 0.7192%, a 43.25% consolidation. For test 31 (three equal passes with turn totalling 51.2%), the single central void is reduced to circular form. The magnitude of the cumulative strains in this case is similar to taking two repeated passes on the same face to 19% (1.23:1). The cumulative strains

were, ε_y = 0.0265, ε_z = 0.7411 and the void area fraction = 0.5125% from an initial void area fraction of 0.7229%, a 57.65% consolidation.

It was not possible to measure void sizes or axial strains after each pass as with the lead trials. The consolidation of voids in the steel billets is greater than that obtained in the lead trials with similar reduction due to the lower values of Hm/L achieved in the steel mill. Reductions in the range $1.08 \leq Hm/L \leq 1.6711$ were achieved during steel rolling due to the large roll diameter. However, the percentage reduction was low due to the geometry and capacity of the mill.

In general, for a single central void, consolidation (closure of the void) was achieved with a thickness reduction of approximately 35% (1.67:1) in one pass. In terms of billet metallurgy, the refinement of the structure was apparent in the rolled billet. Although not directly related to consolidation, full recovery of mechanical properties equal to those of a fully wrought billet may be related to refinement of the structure on achievement of full consolidation.

9.4.2. Effect of Pass Geometry on Solidification Defects in Continuously Cast Billet.

To simulate the effect of a range of degrees of

deformation between 0 and 17% in thickness, continuously cast wedge sections were rolled in the BSC experimental mill. The reduction achieved was dependent solely on the geometry and the capacity of the mill.

Pre-roll examination of the continuously cast billets indicated the diversity of the axial porosity and the difficulty in establishing a method to characterize it. Casting defects were distributed in a random pattern near the billet centre line, surrounded by a matrix of microporosity extending radially as far as the billet quarter thickness. Ultrasonic examination established the location of large defects before and after rolling but was not suitable for assessing the degree of consolidation over the range of reductions achieved.

Referring to a communication from BSC (152), metallographic examination of the wedge sections indicated a ferrite and unresolved pearlite structure in the as-cast condition. After rolling, the front of the wedge section showed a martensite/bainite structure with increasing proportions of Widmanstätten ferrite nucleated at the prior austenite boundaries. The rear of the wedge, having undergone approximately 17% reduction in thickness, possessed a much finer grain size at the edge of the section, resulting in a higher volume fraction of proeutectoid ferrite. Although there was much less evidence of porosity at the rear of the wedge there was relatively little

refinement of the grain size at the section centre, and hence decrease in hardenability due to the slower relative cooling rate and coarser structure.

The results from the steel trials indicate that full recovery of mechanical properties, to a level normally achieved in wrought billets, may not only be dependent on closure of the central cavities ie. consolidation, but also on the subsequent refinement of the microstructure. The complexity of the porous matrix in a continuously cast steel billet necessitates the use of a simulation model to assess the effect of working on defect consolidation. The use of holes drilled along the billet longitudinal centre line to model solidification defects and holes drilled radially to model porosity gives an acceptable means of characterizing consolidation during the rolling operation.

CHAPTER TEN

CONCLUSIONS
AND
SUGGESTIONS FOR FUTURE WORK

10.1. Conclusions.

1. The rolling load has been shown to increase sharply when $Hm/L < 1.5$.
2. Use of grids scribed onto the rolled surface, has shown that sticking friction occurs over the width of the rolled stock.
3. The use of experimentally derived spread data to develop approximating polynomials describing the geometry of the deformation zone has been shown to be a valid technique. Third order polynomials have been developed which give good agreement with experimentally derived data, by generalizing the deformation zone and surface shape into three categories according to the rolling geometry (Hm/L ratio), namely,

$$0.6538 \leq Hm/L \leq 0.9257$$

$$0.9257 \leq Hm/L \leq 1.4419$$

$$1.4419 \leq Hm/L \leq 2.4142$$

4. The extent of the deformation zone was, in most cases, clearly defined by recrystallization.
5. The extent of deformation through the rolled section varies with the reduction ratio and consequently the geometry (Hm/L). Single passes in excess of 40% (1.667:1) will result in deformation through the section at $Hm/L \leq 1.4$. However, that extent of reduction does not produce the desired square product shape since a section with convex edges results.
6. Rolling in a multi-pass schedule to a total reduction

equal to that of a single pass gives a product of the desired section, but will not achieve equivalent deformation through the section unless the reduction per pass is greater than 30% (1.429:1). This is due to the accumulation of deformation at the billet surface with inadequate penetration to the centre.

7. For efficient through deformation and retention of product shape, a multi-pass schedule of 30% (1.429:1) per pass to a total reduction in the order of 60% (2.5:1) is recommended. Low reductions in the early passes are not recommended; high reductions in the early passes have been shown to give a substantial increase in the rate of recrystallization.

8. Void reduction occured in each pass since the magnitude of the axial compressive strain was always greater than the axial tensile strain, if any were present. Although the strain perpendicular to the direction of the applied stress can be tensile at the billet centre in the first pass (up to -0.07 measured in these trials), further passes result in a reduction of this tensile strain.

9. The specific location of voids in the billet section has a direct effect on the strain field at the billet centre. For example, the presence of radial voids around a central one will reduce the intensity of the cumulative compressive strain at the centre by as much as 35%.

10. Single passes greater than 40% (1.667:1) will effect

closure of the void when the Hm/L ratio $\simeq$ 1.2. The void will be compressed to closure leaving a trace line. Unless effective welding has taken place during the deformation the void may re-open if rolled in further passes perpendicular to the previous pass.

11. In order to achieve large cumulative compressive strains on voids, the early passes need to be large.

12. Optimal reduction and closure of central and radial voids was achieved using a schedule of reductions in the region of 30% (1.429:1) per pass to a total of 70% (3.333:1) in three or four passes with a turn each pass. This equates to a Hm/L ratio per pass of $\simeq$ 1.2.

13. Rolling on alternate faces increases the likelihood that shear strains will be generated in the billet central regions due to slight misalignment in the roll gap caused by the billet shape from the previous pass. Shear strains increase the likelihood of void closure and welding by promoting lateral displacement of approaching void surfaces relative to one another. Thus the mechanism of void closure is primarily one of compression in the direction of the applied stress and spread in the perpendicular direction.

14. At the reduction required to achieve full void consolidation, in excess of 65% (2.857:1), a fully refined section will be achieved. For these reductions, cumulative strains in excess of ε_y = 1.10 and ε_z = 2.70 will be required around the centrally located void. For

product integrity, the consolidation of voids is most important. At the reduction required to achieve this, total billet recrystallization is assured.

15. A theoretical analysis of the rolling process based on a simplified variational principle has been made. Using experimental data for billet spread the calculations are simplified since the surface shape of the deforming region is defined. Although not complete, the solution is made clear in principle. Standard mathematical techniques are applicable.

16. An analysis of void closure using a simplified upper bound approach has been made for a single, centrally situated circular void. For initial void area fractions less than 0.45% the theory predicts the resulting void area fraction and reduction required for void closure, giving good agreement with experimental data. However, the analysis was made on the assumption of single pass rolling and so void reduction in multi-pass schedules with turn will need additional analysis for accuracy. The chosen upper bound solution agrees with the mechanism of void closure assessed by experiment.

17. The theoretical analysis (Section 4.2.) can be used to predict the magnitude and state of strain at the centre of a homogeneous material (no defects) when rolling. If greater than the strain required to close a void then consolidation will take place. Alternatively, consolidation probability could be assessed by evaluating

the sequential increment of strain at the void after a pass to the overall billet thickness strain. For example, if the hole strain exceeds the overall strain by a factor 'm', where m is a number dependent on the tolerated final defect size, then consolidation will take place,

ie. for each pass, where n = pass number,

D = void diameter,

H = billet height

$$\ln\left\{\frac{D_n}{D_{n+1}}\right\} \geq m \ln\left\{\frac{H_n}{H_{n+1}}\right\} \quad \ldots\ldots\ldots \quad 10.1$$

18. When rolling steel billets in the works trials, a thickness reduction of 35% in one pass, approximately 40% (1.67:1) reduction in area, achieved total void closure when rolling at $Hm/L \simeq 1.2$. The mechanism of void closure is in agreement with that observed in the laboratory when rolling lead. However, the extent of void closure is greater with equal reduction due to the lower values of Hm/L achieved in the steel mill. Insufficient data was accumulated to fully test for compliance between lead and steel trials at higher reductions.

19. Examination of continuously cast steel stock has revealed the diversity of axial porosity and the difficulty in characterization with a view to estimating the

requirements for consolidation by rolling.

20. The low reduction achieved when rolling the continuously cast wedges indicated that porosity could be eliminated with little refinement of the surrounding structure. Full recovery of the mechanical properties to a level achieved in wrought billets is dependent on cavity consolidation, welding and subsequent refinement of the microstructure. The complexity of the porous matrix in a continuously cast billet necessitates the use of a model to simulate the effect of working on consolidation. The use of holes drilled into the billet gives an acceptable means of assessing consolidation and measuring the resulting strain field necessary for product integrity.

10.2. Suggestions For Future Work.

For convenience of theoretical analysis the experimental work was concerned with the rolling of square section stock. In industrial practice, the fully open pass with flat rolls is rarely used in the breakdown of ingot to billet or square billet to round, for example. Fully or partially enclosed passes are the norm. Further work using enclosed pass rolling will be informative in a number of respects. The increased lateral restraint and frictional forces on the side faces of the workpiece in an enclosed pass will significantly affect the rolling load and

torque. Rolling in an enclosed pass will have a beneficial effect on the consolidation of defects. The increased lateral restraint will cause the stress state at the billet centre to be more compressive. Rolling of other sections, for example rounds, would give a better understanding of the effect of closed passes on defect consolidation. Consequently, friction will be an important parameter in the rolling operation. A better understanding of the mechanics of friction during rolling for all geometric conditions and pass types (open or closed) would enable theoretical development and lead to improved prediction by calculation.

The effect of shear in the centre region of a deforming section is beneficial in terms of defect consolidation. The effect of section rolling, ie. square to round or square to diamond (12), on the microstructure and central consolidation would seem to merit further investigation since the deformation mechanism would result in major material shear in achieving a different product section from the input section.

When rolling square section in an open pass, the use of rolls with differing friction characteristics, different roll speeds or unequal setting of the billet in the roll gap would result in a difference in material flow above and below the billet longitudinal centre line in the direction of rolling. This could lead to an increase in relative movement between void contact points and hence better

welding.

Although not assessed here, the effect of a temperature gradient through the stock when rolling, ie. a hot interior with either a free or force cooled exterior, could give valuable information on the state of stress at the stock centre (15,16,28). Use of a relatively cool exterior would have the effect of an artificial increase in roll diameter since the stock outer layers would be 'stiffer' than the internal layers. Rolling with low Hm/L ratios has been shown to give improved central consolidation. In fact, Tagawa (13) has shown that a difference in temperature of 280 deg.C. will give a 5 to 10% increase in the compressive stress at the stock centre.

The model defect (void) work should be continued by using more realistically proportioned defects as found in continuously cast billets. The minimum void area fraction used in these tests was approximately 0.4%, significantly larger than that found in a continuously cast steel billet, but restricted due to the workability of the lead. The use of other materials for modelling may be considered.

Materials such as aluminium or copper machine more easily than lead so that smaller drills could be used to manufacture smaller model defects. Apart from drilling, thought could be given to alternative methods of introducing model defects into a billet in a controlled manner; spark errosion (in steel) or by direct casting.

The behaviour of lead at room temperature has shown it to be an excellent material for simulation of hot steel. Control of grain size by working and annealing proved to be difficult. An alternative would be to use alloying elements such as tellurium which can restrict the grain size by anchoring the grain boundaries. Very close control of the alloying element would be necessary for consistency since the material yield stress can be drastically altered.

The theoretical analysis allows definition of the deformation zone. Other workers have shown the stress to be important when considering central consolidation (11,13). Consequently, it should be a simple matter to extend the analysis using, for example, a slab analysis to determine the rolling load and subsequently predict the stress field.

APPENDIX A

TABULATED RESULTS OF COMPRESSION TESTS

A.1. Uniaxial Compression Tests on Pure Lead at 20 Deg.C.

A.1.1. 300 mm/min. $\dot{\varepsilon}_o$ = 0.201 per sec.

Red'n (%)	Strain ln(h1/h)	Load (kN)	Stress (N/mm^2)
1.25	0.0126	1.525	2.978
2.50	0.0253	3.100	5.977
5.00	0.0513	5.050	9.487
10.00	0.1054	8.400	14.949
15.00	0.1625	10.800	18.154
20.00	0.2231	13.300	21.040
30.00	0.3567	17.500	24.225
40.00	0.5108	23.550	27.943
50.00	0.6931	28.500	28.178

A.1.2. 228 mm/min. $\dot{\varepsilon}_o$ = 0.150 per sec.

Red'n (%)	Strain ln(h1/h)	Load (kN)	Stress (N/mm^2)
1.25	0.0126	1.625	3.173
2.50	0.1253	3.500	6.748
5.00	0.0513	5.500	10.332
10.00	0.1054	8.875	15.794
15.00	0.1625	11.250	18.910
20.00	0.2231	13.750	21.752
30.00	0.3567	18.500	25.609
40.00	0.5108	24.000	28.476
50.00	0.6931	29.500	29.166

A.1.3. 200mm/min. $\dot{\varepsilon}_o$ = 0.139 per sec.

Red'n (%)	Strain ln(h1/h)	Load (kN)	Stress (N/mm^2)
1.25	0.0126	1.500	2.929
2.50	0.0253	3.125	6.025
5.00	0.0513	5.250	9.863
10.00	0.1054	8.500	15.127
15.00	0.1625	11.000	18.490
20.00	0.2231	13.500	21.356
30.00	0.3567	18.250	25.263
40.00	0.5108	23.500	27.883
50.00	0.6931	29.100	28.771

A.1.4. 153 mm/min. $\dot{\varepsilon}_o$ = 0.1003 per sec.

Red'n (%)	Strain ln(h1/h)	Load (kN)	Stress (N/mm^2)
1.25	0.0126	1.325	2.598
2.50	0.0253	3.375	6.534
5.00	0.0513	5.625	10.609
10.00	0.1054	8.375	14.965
15.00	0.1625	10.875	18.352
20.00	0.2231	13.250	21.044
30.00	0.3567	17.750	24.668
40.00	0.5108	22.500	26.801
50.00	0.6931	28.000	27.798

A.1.5. 217 mm/min. $\dot{\varepsilon}_o$ = 0.0832 per sec.

Red'n (%)	Strain ln(h1/h)	Load (kN)	Stress (N/mm^2)
1.25	0.0126	0.875	1.709
2.50	0.0253	2.250	4.338
5.00	0.0513	5.250	9.863
10.00	0.1053	8.125	14.459
15.00	0.1625	10.750	18.070
20.00	0.2231	13.000	20.565
30.00	0.3567	17.625	24.398
40.00	0.5108	22.250	26.400
50.00	0.6932	27.625	27.313

A.1.6. 100mm/min. $\dot{\varepsilon}_o$ = 0.066 per sec.

Red'n (%)	Strain ln(h1/h)	Load (kN)	Stress (N/mm^2)
1.25	0.0126	1.000	1.953
2.50	0.0253	2.900	5.591
5.00	0.0513	4.650	8.735
10.00	0.1053	7.200	12.813
15.00	0.1625	9.300	15.633
20.00	0.2231	11.650	18.430
30.00	0.3567	16.200	22.425
40.00	0.5108	21.500	25.510
50.00	0.6932	27.050	26.744

A.1.7. 50 mm/min. $\dot{\varepsilon}_o$ = 0.033 per sec.

Red'n (%)	Strain ln(h1/h)	Load (kN)	Stress (N/mm^2)
1.25	0.0126	1.100	2.148
2.50	0.0253	2.500	4.820
5.00	0.0513	4.850	9.111
10.00	0.1054	7.950	14.148
15.00	0.1625	10.200	17.146
20.00	0.2231	12.350	19.537
30.00	0.3567	16.750	23.187
40.00	0.5108	20.750	24.620
50.00	0.6931	25.250	24.964

A.1.8. 13 mm/min. $\dot{\varepsilon}_o$ = 0.00854 per sec.

Red'n (%)	Strain ln(h1/h)	Load (kN)	Stress (N/mm^2)
1.25	0.0126	0.625	1.249
2.50	0.0253	1.375	2.713
5.00	0.0513	3.625	6.970
10.00	0.1054	7.250	13.205
15.00	0.1625	9.750	16.772
20.00	0.2231	11.875	19.228
30.00	0.3567	15.625	22.134
40.00	0.5108	19.750	23.981
50.00	0.6931	22.500	22.768

A.1.9. 1.5 mm/min. $\dot{\varepsilon}_o$ = 0.000984 per sec.

Red'n (%)	Strain ln(h1/h)	Load (kN)	Stress (N/mm^2)
1.25	0.0126	0.500	0.983
2.50	0.0253	1.000	1.942
5.00	0.0513	2.750	5.203
10.00	0.1054	6.125	10.977
15.00	0.1625	8.250	13.965
20.00	0.2231	9.875	15.732
30.00	0.3567	11.375	15.857
40.00	0.5108	13.500	16.130
50.00	0.6931	15.375	15.310

APPENDIX B

SINGLE AND MULTI-PASS ROLLING TRIALS - LEAD BILLETS

LOAD AND TORQUE DATA

B.1. Single Pass Rolling of Square Section Lead Billets.

For all rolling trials,

Roll Diameter = 149 mm Roll Speed = 10 rpm.

B.1.1. h1 = 33 mm. w1 = 33 mm.

Test No.	Test Temp. (deg.C)	Red'n (mm)	Billet Area Red'n (%)	Mean Load (kN)	Total Torque (Nm)
1	16	5.9284	14.33	8.370	211.784
2	16	15.2070	25.66	20.600	691.030
3	13	18.7935	43.86	27.000	934.290

B.1.2. h1 = 49.5 mm. w1 = 49.5 mm.

Test No.	Test Temp. (deg.C)	Red'n (mm)	Billet Area Red'n (%)	Mean Load (kN)	Total Torque (Nm)
4	17	6.4262	10.29	13.906	355.130
5	16	6.4516	10.31	13.631	342.864
6	16	6.6294	10.72	14.514	368.566
7	16	7.5819	12.36	14.350	222.208
8	16	23.5052	39.07	36.667	1504.020
9	18	28.3464	48.60	43.742	2103.050

B.1.3. h1 = 60 mm. w1 = 60 mm.

Test No.	Test Temp. (deg.C)	Red'n (mm)	Billet Area Red'n (%)	Mean Load (kN)	Total Torque (Nm)
10	20	10.8737	14.93	23.017	892.436
11	20	18.8910	23.90	32.283	1359.950
12	16	18.7706	26.98	34.129	1361.930
13	20	24.7523	35.46	43.642	2088.470
14	20	33.2638	47.74	56.396	2743.570
15	16	35.0346	50.27	58.688	2707.290
16	16	35.3060	50.18	60.980	2733.510

B.1.4. h1 = 66 mm. w1 = 66 mm.

Test No.	Test Temp. (deg.C)	Red'n (mm)	Billet Area Red'n (%)	Mean Load (kN)	Total Torque (Nm)
17	18	5.7912	6.93	16.691	312.436
18	17	6.7818	8.34	19.487	500.122
19	15	8.5344	10.24	23.371	643.201
20	16	9.1288	11.19	24.013	718.566
21	17	9.2964	11.14	23.370	691.953
22	16	16.0274	20.55	33.937	1285.260
23	17	16.1797	20.62	33.213	1192.080
24	17	16.2306	20.81	33.215	1204.810
25	16	24.1554	31.44	43.528	1849.380
26	16	28.0670	35.73	49.297	2137.710
27	19	28.2448	36.48	52.909	2438.260
28	18	39.5478	52.25	73.634	3822.990

B.2. Multi-Pass Rolling of Square Section Lead Billets.

For all rolling trials,

Roll Diameter = 149 mm Roll Speed = 10 rpm.

B.2.1. h1 = 49.5 mm. w1 = 49.5 mm.

Test No.		Test Temp. (deg.C)	Red'n (mm)	Total Billet Area Red'n (%)	Mean Load (kN)	Total Torque (Nm)
29	P1	18	15.5956	26.856	25.209	909.489
	P2T	18	16.8910	44.028	19.729	761.936
30	P1	16	10.0076	16.476	18.035	569.723
	P2T	16	10.8204	29.986	18.234	616.451
	P3T	16	8.9916	43.516	15.643	482.019
	P4T	16	9.1948	50.880	12.654	497.561
31	P1	18	9.9560	16.139	18.035	544.289
	P2T	18	11.4046	31.066	18.234	627.502
	P3T	18	8.8976	42.746	15.444	455.148
	P4T	18	9.0094	51.921	12.355	350.322

B.2.2. h1 = 60 mm. w1 = 60 mm.

Test No.		Test Temp. (deg.C)	Red'n (mm)	Total Billet Area Red'n (%)	Mean Load (kN)	Total Torque (Nm)
32	P1	13	8.3363	11.483	20.028	579.021
	P2T	15	10.1016	22.509	20.625	591.193
33	P1	16	13.3680	18.492	27.301	953.744
	P2T	16	15.2197	33.781	23.615	916.854
34	P1	14	18.9636	26.900	35.372	1516.330
	P2T	14	17.7470	43.152	23.017	914.220
35	P1	16	10.9220	15.016	23.515	716.939
	P2T	16	12.0752	27.872	23.714	843.276
	P3T	16	10.2362	39.336	20.327	613.752
36	P1	18	12.3241	17.268	25.309	866.443
	P2T	18	13.4874	31.978	24.013	907.735
	P3T	18	9.9999	43.137	18.832	615.820
	P4T	18	12.1412	53.593	18.234	602.701

B.2.3. h1 = 66 mm. w1 = 66 mm.

Test No.	Test Temp. (deg.C)	Red'n (mm)	Total Billet Area Red'n (%)	Mean Load (kN)	Total Torque (Nm)
37 P1	14	15.1892	18.734	30.789	1283.890
P2T	14	16.4592	38.098	27.301	1092.840
38 P1	15	19.5834	25.528	37.265	1521.940
P2T	15	20.8534	43.018	30.789	1302.910
39 P1	16	14.5034	18.412	30.390	1179.910
P2T	16	14.9860	32.366	29.095	1159.670
P3T	16	12.3952	45.020	24.113	804.661

APPENDIX C

GRAIN SIZE MEASUREMENTS - LEAD BILLETS

C.1. Billet Grain Size Measurement (ASTM).

Single Pass Tests.

C.1.1. h1 = 33 mm. w1 = 33 mm.

Test No.	Area Red'n (%)	No. Intercepts Counted	Standard Deviation	Coefficient of Variation	Mean Linear Intercept (mm)	Change (%)
40		264	6.38748	0.38712	2.1321 ±0.4613	
P1	14.33	247	4.38990	0.31991	0.1923 ±0.0251	90.98
41		455	4.79957	0.18987	1.2479 ±0.0817	
P1	25.66	273	3.39982	0.22416	0.1681 ±0.0094	86.53
42		443	7.63997	0.31043	1.5606 ±0.1217	
P1	43.86	398	4.83722	0.21877	0.1140 ±0.0115	92.69

C.1.2. h1 = 49.5 mm. w1 = 49.5 mm.

Test No.	Area Red'n (%)	No. Intercepts Counted	Standard Deviation	Coefficient of Variation	Mean Linear Intercept (mm)	Change (%)
43		399	5.30537	0.23934	2.4327 ±0.2707	
P1	12.36	818	8.80656	0.19379	0.7774 ±0.0610	68.05
44		172	3.10004	0.30640	1.0527 ±0.1095	
P1	16.14	165	2.17607	0.23739	0.2818 ±0.0167	73.23

cont'd/...

Test No.	Area Red'n (%)	No. Intercepts Counted	Standard Deviation	Coefficient of Variation	Mean Linear Intercept (mm)	Change (%)
45		81	1.46528	0.32562	0.5930 ±0.0909	
P1	26.86	148	2.60216	0.31648	0.3365 ±0.0267	43.26
46		240	3.25475	0.18986	1.9437 ±0.1494	
P1	39.07	332	5.72119	0.31019	0.1400 ±0.0177	92.80

C.1.3. h1 = 60 mm. w1 = 60 mm.

Test No.	Area Red'n (%)	No. Intercepts Counted	Standard Deviation	Coefficient of Variation	Mean Linear Intercept (mm)	Change (%)
47		317	4.98396	0.28300	3.8197 ±0.2715	
P1	11.19	127	3.03842	0.43064	0.4054 ±0.0439	89.39
48		419	8.68115	0.33150	2.0500 ±0.3778	
P1	11.48	149	2.78241	0.33613	0.3241 ±0.0444	84.19
49		181	3.70170	0.36813	6.1031 ±0.7586	
P1	14.93	1186	7.68368	0.14253	0.7524 ±0.0268	87.67
50		82	2.61718	0.57450	0.7996 ±0.1158	
P1	15.02	391	4.01182	0.18469	0.1146 ±0.0097	85.66
51		82	1.97699	0.43397	0.6787 ±0.1207	
P1	18.49	240	3.54024	0.23602	0.1589 ±0.0128	76.58

cont'd/...

Test No.	Area Red'n (%)	No. Intercepts Counted	Standard Deviation	Coefficient of Variation	Mean Linear Intercept (mm)	Change (%)
52		365	3.84716	0.18972	2.8806 ±0.1370	
P1	23.89	1094	10.64150	0.17509	0.6702 ±0.0294	76.74
53		250	6.90436	0.38664	3.1340 ±0.6773	
P1	26.90	184	3.03315	0.26375	0.2137 ±0.0263	93.18
54		279	5.32750	0.34371	3.8163 ±0.4439	
P1	35.60	723	8.48171	0.16424	0.5570 ±0.0317	85.40
55		522	7.00419	0.24152	2.2135 ±0.1830	
P1	50.18	361	3.62137	0.18057	0.1259 ±0.0104	94.31

C.1.4. h1 = 66 mm. w1 = 66 mm.

Test No.	Area Red'n (%)	No. Intercepts Counted	Standard Deviation	Coefficient of Variation	Mean Linear Intercept (mm)	Change (%)
56		101	2.76828	0.49336	3.1932 ±0.6472	
P1	18.41	140	2.88108	0.37043	0.3577 ±0.0948	88.80
57		605	4.20948	0.09741	1.0756 ±0.0681	
P1	18.73	308	3.10386	0.18139	0.1474 ±0.0181	86.29
58		40	0.80845	0.36380	1.2529 ±0.2156	
P1	25.53	207	2.20293	0.19156	0.2179 ±0.0169	82.61
59		128	3.17876	0.44701	10.1036 ±1.5153	
P1	52.25	902	24.40560	0.48703	0.6822 ±0.0836	93.25

C.2. Billet Grain Size Measurement (ASTM).

Multi-Pass Tests.

C.2.1. h1 = 49.5 mm. w1 = 49.5 mm.

Test No.	Total Area Red'n (%)	No. Intercepts Counted	Standard Deviation	Coefficient of Variation	Mean Linear Intercept (mm)	Total Change (%)
60		81	1.46528	0.32562	0.5930 ±0.0909	
P1	26.86	148	2.60216	0.31648	0.3365 ±0.0500	43.27
P2T	44.03	414	3.95563	0.17198	0.1086 ±0.0085	81.69
61		172	3.10004	0.30640	1.0527 ±0.1788	
P1	16.14	165	2.17607	0.23739	0.2818 ±0.0310	73.23
P2T		NOT MEASURED				
P3T	42.75	285	3.48526	0.22012	0.0796 ±0.0081	92.44
P4T	51.92	327	3.09173	0.17019	0.0684 ±0.0053	93.50
62		56	1.45071	0.46630	0.9968 ±0.2222	
P4T	50.88	514	5.20432	0.18225	0.0875 ±0.0073	91.22

C.2.2. h1 = 60 mm. w1 = 60 mm.

Test No.	Total Area Red'n (%)	No. Intercepts Counted	Standard Deviation	Coefficient of Variation	Mean Linear Intercept (mm)	Total Change (%)
63		82	2.61718	0.57450	0.7996 ±0.2215	
P1	15.02	391	4.01182	0.18469	0.1147 ±0.0097	85.66

cont'd/...

Test No.	Total Area Red'n (%)	No. Intercepts Counted	Standard Deviation	Coefficient of Variation	Mean Linear Intercept (mm)	Total Change (%)
64		419	8.68115	0.33150	2.0500 ±0.3778	
P1	11.48	149	2.78241	0.33613	0.3241 ±0.0513	84.19
P2T	22.51	264	3.75734	0.25618	0.1728 ±0.0206	91.57
65		82	1.97699	0.43397	0.6787 ±0.1403	
P1	18.49	240	3.54024	0.23602	0.1589 ±0.0206	76.58
P2T	33.79	417	4.26565	0.16367	0.0899 ±0.0079	86.76
66		250	6.90436	0.38664	3.1340 ±0.6773	
P1	26.90	184	3.03315	0.26375	0.2137 ±0.0311	93.18
P2T	43.15	330	3.13847	0.15217	0.1132 ±0.0093	96.39
67		79	1.78684	0.40713	0.6387 ±0.1236	
P2T	31.98	348	6.04882	0.31287	0.1332 ±0.0195	79.15
P3T	43.14	469	3.07690	0.11809	0.0953 ±0.0050	85.08
P4T	53.59	254	4.95733	0.35131	0.1035 ±0.0171	83.79

C.2.3. h1 = 66 mm. w1 = 66 mm.

Test No.	Total Area Red'n (%)	No. Intercepts Counted	Standard Deviation	Coefficient of Variation	Mean Linear Intercept (mm)	Total Change (%)
68		82	2.61718	0.57450	0.7996 ±0.2215	
P1	18.73	308	3.10386	0.18139	0.1474 ±0.0122	81.56
P2T	38.10	431	6.04368	0.25240	0.1060 ±0.0124	86.74

cont'd/...

Test No.	Total Area Red'n (%)	No. Intercepts Counted	Standard Deviation	Coefficient of Variation	Mean Linear Intercept (mm)	Total Change (%)
69		40	0.80845	0.36380	1.2528 ±0.2156	
P1	25.53	207	2.20293	0.19156	0.2179 ±0.0192	82.61
P2T	43.02	293	3.78550	0.23256	0.1604 ±0.0173	87.20
70		101	2.76828	0.49336	3.1932 ±0.7548	
P1	18.41	140	2.88108	0.37043	0.3577 ±0.0627	88.80
P2T	32.37	354	4.52444	0.23006	0.1289 ±0.0137	95.96
P3T	45.02	377	6.23530	0.29771	0.1262 ±0.0176	96.05

APPENDIX D

HOLE CONSOLIDATION TRIALS - LEAD BILLETS

HOLE AREA FRACTION MEASUREMENTS

D.1. Hole Consolidation Tests, Lead Billets.

D.1.1. h1 = 42.5 mm. w1 = 42.5 mm.

Test No.	Total Area Red'n (%)	Hole No.	Hole Area (mm^2)	Hole Area Fraction (%)	Total Consolidation (%)
71		1	37.1290	2.0337	
P1	10.42	1	27.3548	1.6727	26.33
P2T	19.27	1	22.3934	1.5194	39.69
72		1	35.6535	1.9569	
P1	21.28	1	8.7580	0.6106	75.44
P2T	38.97	1	6.7903	0.6107	80.96
73		1	35.4675	1.9390	
P1	21.54	1	11.5400	0.8041	67.46
74		1	37.3709	2.0445	
P1	42.50	1	0	0	100.00

D.1.2. h1 = 49.5 mm. w1 = 49.5 mm.

Test No.	Total Area Red'n (%)	Hole No.	Hole Area (mm^2)	Hole Area Fraction (%)	Total Consolidation (%)
75		1	8.4406	0.3441	
		2	8.4247	0.3434	
		3	8.5161	0.3472	
		4	8.6290	0.3518	
		5	18.4193	0.7509	
P1	10.29		NOT MEASURED		
P2	20.55	1	4.2279	0.2169	49.91
		2	3.8047	0.1952	54.48
		3	4.2340	0.2173	50.28
		4	4.8017	0.2464	44.35
		5	11.4976	0.5900	37.58
P3T	27.63		NOT MEASURED		

cont'd/...

Test No.	Total Area Red'n (%)	Hole No.	Hole Area (mm^2)	Hole Area Fraction (%)	Total Consolidation (%)
P4	35.19	1	2.9144	0.1833	65.47
		2	2.4292	0.1528	71.17
		3	2.4729	0.1555	70.96
		4	2.2985	0.1446	73.36
		5	6.5092	0.4095	64.66
76		1	9.0053	0.3705	
		2	9.4140	0.3873	
		3	8.3658	0.3442	
		4	8.4303	0.3468	
		5	11.5752	0.8054	
P1	10.31	1	6.5574	0.3008	27.18
		2	6.4757	0.2970	31.21
		3	6.2761	0.2879	24.98
		4	7.0039	0.3213	16.92
		5	14.5978	0.6696	23.43
P2T	19.22	1	5.9329	0.3022	34.12
		2	4.9574	0.2525	47.34
		3	5.3376	0.2719	36.20
		4	5.0477	0.2571	40.12
		5	13.2112	0.6729	32.51
P3T	27.20		NOT	MEASURED	
P4T	34.03	1	3.3746	0.2105	62.53
		2	3.1785	0.1982	66.24
		3	2.8998	0.1808	65.34
		4	2.2400	0.1397	73.43
		5	9.4813	0.5913	51.56
77		1	9.1666	0.3826	
		2	8.8871	0.3710	
		3	9.1021	0.3799	
		4	8.1398	0.3398	
		5	18.6613	0.7790	
P1	10.72		NOT	MEASURED	
P2T	20.00	1	4.7955	0.2502	47.68
		2	5.1664	0.2696	41.87
		3	6.2125	0.3242	31.75
		4	4.9135	0.2564	39.64
		5	11.9260	0.6223	36.09
P3T	28.30		NOT	MEASURED	

cont'd/...

Test No.	Total Area Red'n (%)	Hole No.	Hole Area (mm^2)	Hole Area Fraction (%)	Total Consolidation (%)
P4T	35.43	1	2.9359	0.1898	67.97
		2	2.6004	0.1681	70.74
		3	2.8542	0.1845	68.64
		4	2.9454	0.1904	63.82
		5	8.0542	0.5206	56.84
P5T	48.20		NOT	MEASURED	
P6T	57.30	1	1.1286	0.1104	87.69
		2	0.4645	0.0454	94.77
		3	0.6150	0.0602	93.24
		4	0.3217	0.0315	96.05
		5	2.1359	0.2089	88.55

D.1.3. h1 = 60 mm. w1 = 60 mm.

Test No.	Total Area Red'n (%)	Hole No.	Hole Area (mm^2)	Hole Area Fraction (%)	Total Consolidation (%)
78		1	8.3333	0.2337	
		2	9.8064	0.2750	
		3	8.4140	0.2360	
		4	8.1666	0.2291	
		5	18.9838	0.5325	
P1	26.97		NOT	MEASURED	
P2T	40.34	1	3.1312	0.1472	62.43
		2	NOT	MEASURED - HOLE	SPOILT
		3	2.3406	0.1100	72.18
		4	2.1918	0.1030	73.16
		5	9.2146	0.4332	51.46
79		1	8.4462	0.2376	
		2	NOT	MEASURED - HOLE	SPOILT
		3	9.2795	0.2610	
		4	8.9785	0.2525	
		5	19.1451	0.5385	
P1	36.74	1	0.3449	0.0153	95.92
		2	NOT	MEASURED - HOLE	SPOILT
		3	0.1721	0.0077	98.15
		4	0.0387	0.0017	99.57
		5	0.6959	0.0309	96.37

D.1.4. h1 = 66 mm. w1 = 66 mm.

Test No.	Total Area Red'n (%)	Hole No.	Hole Area (mm^2)	Hole Area Fraction (%)	Total Consolidation (%)
80		1	32.9754	0.7561	
P1	35.73	1	0	0	100.00
81		1	31.9246	0.7316	
P1	20.45	1	12.0550	0.3473	62.24
P2T	40.72	1	6.6837	0.2584	79.06
P3T	52.67	1	0.3819	0.0185	98.80
P4T	64.00	1	0.6357	0.0405	98.01
82		1	7.0271	0.1627	
		2	8.0806	0.1870	
		3	7.7145	0.1786	
		4	33.6128	0.7780	
		5	7.6129	0.1762	
		6	7.6561	0.1772	
		7	NOT	MEASURED - HOLE	SPOILT
P1	6.93		NOT	MEASURED	
P2T	17.00	1	4.0591	0.1132	42.24
		2	4.2793	0.1193	47.04
		3	4.9892	0.1391	35.33
		4	22.8600	0.6375	31.99
		5	5.6021	0.1562	26.41
		6	4.5000	0.1255	41.22
		7	NOT	MEASURED - HOLE	SPOILT
P3T	26.26		NOT	MEASURED	
P4T	33.58	1	0.9194	0.0320	86.92
		2	2.3763	0.0828	70.59
		3	5.2150	0.1817	32.40
		4	14.1970	0.4947	57.76
		5	3.1400	0.1094	58.76
		6	NOT	MEASURED - HOLE	SPOILT
		7	NOT	MEASURED - HOLE	SPOILT

Test No.	Total Area Red'n (%)	Hole No.	Hole Area (mm^2)	Hole Area Fraction (%)	Total Consolidation (%)
83		1	8.0108	0.1841	
		2	8.5053	0.1954	
		3	8.3602	0.1921	
		4	8.9408	0.2054	
		5	18.9032	0.4344	
P1	8.34	1	7.8064	0.1957	2.55
		2	7.5290	0.1887	11.48
		3	6.7419	0.1690	19.36
		4	7.4032	0.1856	17.20
		5	18.3924	0.4611	2.70
P2	18.04	1	5.5107	0.1545	31.21
		2	5.8226	0.1633	31.54
		3	5.2471	0.1471	37.24
		4	6.0806	0.1705	31.99
		5	13.8763	0.3891	26.59
P3	25.83	1	3.4140	0.1058	57.38
		2	4.6019	0.1426	45.89
		3	3.1559	0.0978	62.25
		4	4.6505	0.1441	47.99
		5	10.9032	0.3378	42.32
P4	32.07	1	1.6430	0.0556	79.49
		2	2.5374	0.0858	70.17
		3	1.9037	0.0644	77.23
		4	NOT	MEASURED - HOLE	SPOILT
		5	6.8361	0.2312	63.84
84		1	8.3172	0.1914	
		2	7.8548	0.1807	
		3	8.1613	0.1878	
		4	8.2148	0.1890	
		5	18.5914	0.4278	
P1	25.62	1	3.8782	0.1124	53.37
		2	4.5752	0.1326	41.76
		3	3.8713	0.1122	52.57
		4	4.5545	0.1320	44.56
		5	10.4546	0.3030	43.77
P2	38.33	1	0.9118	0.0340	89.04
		2	0.8628	0.0322	89.02
		3	0.4043	0.0151	95.05
		4	0.9910	0.0370	87.94
		5	3.4237	0.1277	81.58

cont'd/...

Test No.	Total Area Red'n (%)	Hole No.	Hole Area (mm^2)	Hole Area Fraction (%)	Total Consolidation (%)
P3T	49.52	1	0	0	100.00
		2	0	0	100.00
		3	0	0	100.00
		4	0	0	100.00
		5	0.1858	0.0085	99.00
85		1	7.8871	0.1812	
		2	7.7903	0.1790	
		3	8.2043	0.1885	
		4	8.3494	0.1918	
		5	17.4193	0.4002	
P1	20.80	1	3.7892	0.1099	51.96
		2	3.7032	0.1074	52.46
		3	4.0146	0.1165	51.07
		4	4.4705	0.1297	46.46
		5	9.2430	0.2681	46.94
P2T	36.94	1	1.5957	0.0581	79.77
		2	2.2959	0.0836	70.53
		3	2.7441	0.0999	66.55
		4	2.2477	0.0819	73.08
		5	5.2602	0.1916	69.80
P3T	49.13	1	0.2701	0.0122	96.58
		2	0.6804	0.0307	91.27
		3	0.5084	0.0230	93.80
		4	0.9772	0.0441	88.30
		5	2.3759	0.1073	86.36
86		1	8.1613	0.1877	
		2	8.4624	0.1946	
		3	8.4084	0.1934	
		4	8.7150	0.2004	
		5	18.6343	0.4285	
P1	11.14		NOT	MEASURED	
P2T	18.24	1	5.5537	0.1562	31.95
		2	5.8922	0.1657	30.37
		3	7.0699	0.1989	15.92
		4	6.2849	0.1768	27.88
		5	14.9140	0.4195	19.96
P3T	23.11		NOT	MEASURED	

cont'd/...

Test No.	Total Area Red'n (%)	Hole No.	Hole Area (mm^2)	Hole Area Fraction (%)	Total Consolidation (%)
P4T	26.51	1	NOT	MEASURED - HOLE	SPOILT
		2	4.6460	0.1454	45.10
		3	3.6052	0.1128	57.12
		4	4.2348	0.1325	51.41
		5	10.7234	0.3355	42.45
87		1	8.1290	0.1854	
		2	8.3494	0.1904	
		3	8.3118	0.1896	
		4	8.4729	0.1932	
		5	18.5967	0.4241	
P1	31.44		NOT	MEASURED	
P2T	50.65	1	1.1613	0.0537	85.71
		2	0.4284	0.0198	94.87
		3	0.7535	0.0348	90.93
		4	0.3948	0.0182	95.34
		5	2.4895	0.1151	86.61
P3T	65.18	1	0.2710	0.0177	96.67
		2	0.2529	0.0166	96.97
		3	0.2297	0.0150	97.24
		4	0.2417	0.0158	97.15
		5	0.7587	0.0497	95.92
P4T	74.55	1	0	0	100.00
		2	0	0	100.00
		3	0	0	100.00
		4	0	0	100.00
		5	0.4860	0.0435	97.39
88		1	8.4193	0.1930	
		2	8.2580	0.1893	
		3	8.6129	0.1975	
		4	8.5053	0.1950	
		5	18.8924	0.4332	
P1	10.24		NOT	MEASURED	
P2T	19.21	1	6.4353	0.1826	23.56
		2	5.7368	0.1628	30.53
		3	5.7187	0.1623	33.60
		4	5.5535	0.1576	34.71
		5	13.7806	0.3911	27.06
P3T	27.27		NOT	MEASURED	

cont'd/...

Test No.	Total Area Red'n (%)	Hole No.	Hole Area (mm^2)	Hole Area Fraction (%)	Total Consolidation (%)
P4T	34.30	1	3.6869	0.1287	56.21
		2	2.8318	0.0988	65.71
		3	2.8826	0.1006	66.53
		4	2.4258	0.0847	71.48
		5	8.9918	0.3138	52.41
P5T	47.70		NOT	MEASURED	
P6T	57.30	1	2.0611	0.1108	75.52
		2	0.7441	0.0400	90.99
		3	1.1535	0.0620	86.61
		4	0.5196	0.0279	93.89
		5	2.2727	0.1221	87.97
89		1	8.7903	0.2024	
		2	9.0109	0.2075	
		3	9.0053	0.2074	
		4	NOT	MEASURED - HOLE SPOILT	
		5	19.8817	0.4578	
P1	20.55		NOT	MEASURED	
P2T	35.49	1	3.0021	0.1072	65.85
		2	2.8224	0.1007	68.68
		3	2.6976	0.0963	70.04
		4			
		5	7.4787	0.2669	62.38
P3T	48.31		NOT	MEASURED	
P4T	61.66	1	2.3166	0.1391	73.65
		2	1.8537	0.1113	79.43
		3	1.0099	0.0607	88.79
		4			
		5	4.1196	0.2474	79.28
P5T	68.98		NOT	MEASURED	
P6T	74.99	1	1.6077	0.1480	81.71
		2	1.6671	0.1535	81.50
		3	0.7312	0.0673	91.88
		4			
		5	1.4538	0.1339	92.69

APPENDIX E

HOLE CONSOLIDATION TESTS - LEAD BILLETS

HOLE AXIAL STRAIN MEASUREMENTS

E.1. Hole Consolidation Tests, Lead Billets.

Hole Axial Strain Measurements.

E.1.1. h1 = 42.5 mm. w1 = 42.5 mm.

Pass/ Hole No.	Z-axis total strain	Y-axis total strain	Axial rot'n (deg)	Shear strain γ_{yz}	Principal strain ε_I	Principal strain ε_{II}	Max. shear strain
71:							
P1: H1	0.3277	0.0036	0	0	0.3277	0.0036	0.1621
P2T: H1	0.2683	0.2267	0	0	0.2683	0.2267	0.0208
72:							
P1: H1	1.2603	0.0422	0	0	1.2603	0.0422	0.6091
P2T: H1	0.9275	0.5396	8.0	0.1396	0.9397	0.5274	0.2091
73:							
P1: H1	1.0692	0.0223	0	0	1.0692	0.0223	0.5235
74:	TOTAL HOLE CLOSURE RECORDED						

E.1.2. h1 = 49.5 mm. w1 = 49.5 mm.

Pass/ Hole No.	Z-axis total strain	Y-axis total strain	Axial rot'n (deg)	Shear strain γ_{yz}	Principal strain ε_I	Principal strain ε_{II}	Max. shear strain
75:							
P1:	NOT MEASURED						

cont'd/...

Pass/ Hole No.	Z-axis total strain	Y-axis total strain	Axial rot'n (deg)	Shear strain γ_{yz}	Principal strain ε_I	Principal strain ε_{II}	Max. shear strain
P2:							
H1	0.6199	-0.0114	5.0	0.0873	0.6229	-0.0144	0.3187
H2	0.6580	-0.0921	4.0	0.0698	0.6596	-0.0937	0.3767
H3	0.7009	0.0150	0	0	0.7009	0.0150	0.3430
H4	0.7952	-0.0046	8.0	0.1396	0.8012	-0.0106	0.3912
H5	0.5143	-0.0404	0	0	0.5143	-0.0404	0.2774
P3T:			NOT MEASURED				
P4:							
H1	0.5221	0.6023	39.0	0.6807	0.9049	0.2195	0.3427
H2	0.7454	0.5012	36.0	0.6287	0.9605	0.2861	0.3372
H3	0.4883	0.5054	43.5	0.7592	0.8765	0.1172	0.3797
H4	0.6838	0.5191	40.0	0.6981	0.9601	0.2428	0.3586
H5	0.4774	0.5002	44.0	0.7679	0.8729	0.1047	0.3841
76:							
P1:							
H1	0.3909	0.0148	0	0	0.3909	0.0148	0.1885
H2	0.3075	0	0	0	0.3075	0	0.1537
H3	0.3471	-0.0513	0	0	0.3471	-0.0513	0.1992
H4	0.2776	-0.0438	0	0	0.2776	-0.0438	0.1607
H5	0.3296	0.0102	0	0	0.3296	0.0102	0.1597
P2T:							
H1	0.3732	0.1560	14.5	0.2531	0.4314	0.0978	0.1668
H2	0.2305	0.3167	0	0	0.3167	0.2305	0.0431
H3	0.2654	0.0701	0	0	0.2654	0.0701	0.0977
H4	0.3197	0.2146	20.0	0.3491	0.4494	0.0849	0.1823
H5	0.2768	0.1288	22.5	0.3927	0.4126	-0.0070	0.2098
P3T:			NOT MEASURED				
P4T:							
H1	0.7352	0.4040	12.0	0.2094	0.7655	0.3737	0.1959
H2	0.7829	0.5870	6.0	0.1047	0.7960	0.5739	0.1111
H3	0.3830	0.4919	31.0	0.5411	0.7134	0.1615	0.2760
H4	0.6400	0.3293	19.0	0.3316	0.7119	0.2574	0.2272
H5	0.4091	0.3384	38.5	0.6720	0.7116	0.0359	0.3379
77:							
P1:			NOT MEASURED				

cont'd/...

Pass/ Hole No.	Z-axis total strain	Y-axis total strain	Axial rot'n (deg)	Shear strain γ_{yz}	Principal strain ε_I	Principal strain ε_{II}	Max. shear strain
P2T:							
H1	0.4651	0.1555	4.0	0.0698	0.4690	0.1516	0.1587
H2	0.3483	0.2305	0	0	0.3483	0.2305	0.0590
H3	0.3536	0.0584	13.0	0.2269	0.3922	0.0198	0.1862
H4	0.4426	0.1292	0	0	0.4426	0.1292	0.1567
H5	0.2053	0.2007	0	0	0.2053	0.2007	0.0023
P3T:			NOT MEASURED				
P4T:							
H1	0.6777	0.4878	8.0	0.0349	0.6793	0.4862	0.0965
H2	0.6636	0.4358	3.0	0.0524	0.6666	0.4328	0.1169
H3	0.7406	0.3791	6.0	0.1047	0.7480	0.3717	0.1882
H4	0.8223	0.4077	5.0	0.0873	0.8268	0.4032	0.2118
H5	0.4750	0.2683	8.0	0.1396	0.4964	0.2469	0.1247
P5T:			NOT MEASURED				
P6T:							
H1	1.3563	1.3715	30.0	0.5236	1.6258	1.1020	0.2619
H2	1.8162	1.5565	23.0	0.4014	1.9254	1.4473	0.2390
H3	1.3064	0.7649	14.0	0.2443	1.3327	0.7386	0.2970
H4	2.7827	1.2060	7.0	0.1222	2.7851	1.2036	0.7907
H5	1.1165	1.0617	36.0	0.6283	1.4044	0.7738	0.3153

E.1.3. h1 = 60 mm. w1 = 60 mm.

Pass/ Hole No.	Z-axis total strain	Y-axis total strain	Axial rot'n (deg)	Shear strain γ_{yz}	Principal strain ε_I	Principal strain ε_{II}	Max. shear strain
78:							
P1:			NOT MEASURED				
P2T:							
H1	0.8285	0.2243	28.0	0.4887	0.9150	0.1378	0.3896
H2	0.7744	0.3878	34.0	0.5934	0.9352	0.2270	0.3541
H3	0.6979	0.1994	26.0	0.4538	0.7857	0.1116	0.3371
H4		NOT	MEASURED - HOLE		SPOILT		
H5	0.4409	0.2014	33.0	0.5760	0.6331	0.0092	0.3119
79:			TOTAL HOLE CLOSURE RECORDED				

E.1.4. h1 = 66 mm. w1 = 66 mm.

Pass/ Hole No.	Z-axis total strain	Y-axis total strain	Axial rot'n (deg)	Shear strain γ_{yz}	Principal strain ε_I	Principal strain ε_{II}	Max. shear strain
80:		TOTAL HOLE CLOSURE RECORDED					
81:							
P1:							
H1	0.8778	0.0448	0	0	0.8778	0.0448	0.4165
P2T:							
H1	0.7236	0.7353	43.0	0.7505	1.1047	0.3542	0.3753
P3T:							
H1	2.3208	1.7652	33.0	0.5760	2.4431	1.6429	0.4001
P4T:							
H1	2.1740	1.7188	26.0	0.4538	2.2678	1.6250	0.3214
82:							
P1:			NOT MEASURED				
P2T:							
H1	0.2075	0.3914	10.0	0.1745	0.4262	0.1727	0.1268
H2	0.2877	0.3260	8.0	0.1396	0.3792	0.2345	0.0724
H3	0.2027	0.1994	6.0	0.1047	0.2534	0.1487	0.0524
H4	0.1913	0.1532	6.0	0.1047	0.2280	0.1165	0.0557
H5	0.0873	0.2057	9.0	0.1571	0.2449	0.0481	0.0984
H6	0.1373	0.3619	12.0	0.2094	0.4031	0.0961	0.1535
H7		NOT	MEASURED - HOLE		SPOILT		
P3T:			NOT MEASURED				
P4T:							
H1	0.7926	0.9824	22.0	0.3840	1.1017	0.6733	0.2142
H2	0.6539	0.6500	22.0	0.3840	0.8440	0.4599	0.1920
H3	0.2167	0.2141	34.0	0.5934	0.5121	-0.0813	0.2967
H4	0.3135	0.4829	10.0	0.1745	0.5198	0.2766	0.1216
H5	0.2397	0.6325	0	0	0.6325	0.2397	0.1964
H6		NOT	MEASURED - HOLE		SPOILT		
H7		NOT	MEASURED - HOLE		SPOILT		

Pass/ Hole No.	Z-axis total strain	Y-axis total strain	Axial rot'n (deg)	Shear strain γ_{yz}	Principal strain ε_I	Principal strain ε_{II}	Max. shear strain
83:							
P1:							
H1	0.1839	-0.0896	0	0	0.1839	-0.0896	0.1368
H2	0.1490	-0.0148	0	0	0.1490	-0.0148	0.0819
H3	0.1413	-0.0588	0	0	0.1413	-0.0588	0.1000
H4	0.1121	0.0148	0	0	0.1121	0.0148	0.0487
H5	0.0632	-0.0683	0	0	0.0632	-0.0683	0.0657
P2:							
H1	0.4716	-0.0606	0	0	0.4716	-0.0606	0.2661
H2	0.3242	-0.0294	0	0	0.3242	-0.0294	0.1768
H3	0.4778	0	0	0	0.4778	0	0.2389
H4	0.3610	0.0148	0	0	0.3610	0.0148	0.1731
H5	0.3655	-0.0683	0	0	0.3655	-0.0683	0.2169
P3:							
H1	0.9067	-0.0118	4.5	0.0785	0.9084	-0.0135	0.4609
H2	0.6422	-0.0119	4.5	0.0785	0.6445	-0.0142	0.3294
H3	0.7314	0.0794	2.0	0.0349	0.7319	0.0789	0.3265
H4	0.5400	0.0522	7.5	0.1309	0.5486	0.0436	0.2525
H5	0.5901	-0.0653	4.5	0.0785	0.5924	-0.0676	0.3300
P4:							
H1	1.2798	0.0542	10.0	0.1745	1.2860	0.0480	0.6190
H2	0.7372	0.0166	3.0	0.0524	0.7382	0.0156	0.3613
H3	1.3941	0.0953	0	0	1.3941	0.0953	0.6494
H4	1.1879	0.0166	3.0	0.0524	1.1885	0.0160	0.5862
H5	0.8971	-0.0399	7.0	0.1222	0.9011	-0.0439	0.4725
84:							
P1:			NOT	MEASURED			
P2:							
H1	3.4965	0.2311	0	0	3.4965	0.2311	1.6327
H2	3.4500	-0.2877	0	0	3.4500	-0.2877	1.8688
H3	3.0910	-0.1133	0	0	3.0910	-0.1133	1.6022
H4	2.7958	-0.1415	0	0	2.7958	-0.1415	1.4686
H5	1.6507	-0.0460	0	0	1.6507	-0.0460	0.8484
P3T:							
H1			HOLE	CLOSED			
H5			HOLE	CLOSED			
H3			HOLE	CLOSED			
H4			HOLE	CLOSED			
H2	1.1987	3.0445	40.0	0.6981	3.1083	1.1349	0.9867

Pass/ Hole No.	Z-axis total strain	Y-axis total strain	Axial rot'n (deg)	Shear strain γ_{yz}	Principal strain ε_I	Principal strain ε_{II}	Max. shear strain
85:							
P1:							
H1	0.5680	0.0308	0	0	0.5680	0.0308	0.2686
H2	0.6480	-0.0299	0	0	0.6480	-0.0299	0.3389
H3	0.7868	-0.0933	0	0	0.7868	-0.0933	0.4401
H4	0.7252	0.0466	10.0	0.1745	0.7362	0.0356	0.3503
H5	0.5730	0.0541	0	0	0.5730	0.0541	0.2595
P2T:							
H1	0.4657	0.5967	24.0	0.4189	0.7507	0.3117	0.2195
H2	0.8336	0.5584	29.0	0.5061	0.9840	0.4080	0.2880
H3	0.3814	1.2015	0	0	1.2015	0.3814	0.4101
H4	0.7239	0.7087	21.0	0.3665	0.8997	0.5329	0.1834
H5	0.7573	0.4280	13.5	0.2356	0.7951	0.3902	0.2025
P3T:							
H1	1.6094	0.0953	0	0	1.6094	0.0953	0.7570
H2	1.4169	0.5200	10.0	0.1745	1.4253	0.5116	0.4569
H3	2.0396	0.1899	0	0	2.0396	0.1899	0.9249
H4	1.2400	0.3475	20.0	0.3491	1.2729	0.3146	0.4792
H5	1.4799	0.5004	14.0	0.2443	1.4949	0.4854	0.5048
86:							
P1:			NOT MEASURED				
P2T:							
H1	0.2596	-0.0431	5.0	0.0873	0.2658	-0.0493	0.1575
H2	0.2588	0.1826	10.0	0.1745	0.3159	0.1255	0.0952
H3	0.2961	0.1327	9.0	0.1571	0.3277	0.1011	0.1133
H4	0.2162	0.0473	0	0	0.2162	0.0473	0.0844
H5	0.1489	0.0843	16.0	0.2793	0.2599	-0.0267	0.1433
P3T:			NOT MEASURED				
P4T:							
H1	0.1167	-0.6632	13.0	0.2269	0.1329	-0.6794	0.4061
H2	0.4945	0.1211	10.0	0.1745	0.5139	0.1017	0.2061
H3	0.7048	0.2454	8.0	0.1396	0.7152	0.2350	0.2401
H4	0.4925	0.3032	0	0	0.4925	0.3032	0.0947
H5	0.3500	0.1968	30.0	0.5236	0.5462	0.0006	0.2728
87:							
P1:			NOT MEASURED				

cont'd/...

Pass/ Hole No.	Z-axis total strain	Y-axis total strain	Axial rot'n (deg)	Shear strain γ_{yz}	Principal strain ε_I	Principal strain ε_{II}	Max. shear strain
P2T:							
H1	1.8540	0.4900	4.5	0.0785	1.8551	0.4889	0.6831
H2	2.7498	0.4755	4.5	0.0785	2.7505	0.4748	1.1378
H3	1.3564	0.4700	0	0	1.3564	0.4700	0.4432
H4	2.1914	0.6151	20.0	0.3491	2.2105	0.5960	0.8072
H5	1.3479	0.6919	11.0	0.1920	1.3617	0.6781	0.3418
P3T:							
H1	0.4511	3.4324	7.0	0.1222	3.4337	0.4498	1.4919
H2	0.2824	3.6050	4.0	0.0698	3.6054	0.2820	1.6617
H3	0.4520	3.7534	0	0	3.7534	0.4520	1.6507
H4	0.1979	3.6243	4.0	0.0698	3.6247	0.1975	1.7136
H5	0.2469	3.8918	0	0	3.8918	0.2469	1.8224
P4T:							
H1			HOLE CLOSED				
H2			HOLE CLOSED				
H3			HOLE CLOSED				
H4			HOLE CLOSED				
H5	2.6357	1.0848	14.5	0.2531	2.6460	1.0745	0.7857
88:							
P1:			NOT MEASURED				
P2T:							
H1	0.1747	0.2308	0	0	0.2308	0.1747	0.0281
H2	0.1823	0.1671	0	0	0.1823	0.1671	0.0076
H3	0.1974	0.2384	0	0	0.2384	0.1974	0.0205
H4	0.1823	0.2384	0	0	0.2384	0.1823	0.0281
H5	0.1542	0.1782	0	0	0.1782	0.1542	0.0199
P3T:			NOT MEASURED				
P4T:							
H1	0.5902	0.4047	26.0	0.4538	0.7426	0.2523	0.2451
H2	0.6615	0.4870	27.0	0.4712	0.8255	0.3230	0.2512
H3	0.5804	0.3502	13.0	0.2269	0.6269	0.3037	0.1616
H4	0.6235	0.4141	12.0	0.2094	0.6669	0.3707	0.1481
H5	0.4183	0.3153	30.0	0.5236	0.6336	0.1000	0.2668
P5T:			NOT MEASURED				
P6T:							
H1	0.7702	0.9752	34.0	0.5934	1.1866	0.5588	0.3139
H2	1.4259	0.9108	35.0	0.6109	1.5679	0.7688	0.3995
H3	0.7290	0.6435	41.0	0.7156	1.0466	0.3259	0.3603
H4	1.3275	0.9510	31.0	0.5411	1.4688	0.8097	0.3296
H5	0.6337	1.1192	30.0	0.5236	1.2335	0.5194	0.3570

Pass/ Hole No.	Z-axis total strain	Y-axis total strain	Axial rot'n (deg)	Shear strain γ_{yz}	Principal strain ε_I	Principal strain ε_{II}	Max. shear strain
89:							
P1:			NOT MEASURED				
P2T:							
H1	0.7315	0.4728	29.0	0.5061	0.8863	0.3180	0.2482
H2		NOT	MEASURED	- HOLE	SPOILT		
H3	0.6385	0.4658	12.0	0.2094	0.6879	0.4164	0.1357
H4	0.6297	0.5093	30.0	0.5236	0.8381	0.3009	0.2686
H5	0.4670	0.4720	8.0	0.1396	0.5393	0.3997	0.0698

APPENDIX F

SINGLE AND MULTI-PASS ROLLING TRIALS- STEEL BILLETS

LOAD AND TORQUE DATA

F.1. Single Pass Rolling Trials With Steel Billets.

h1 = 50.8 mm. w1 = 50.8 mm.

Roll Diameter = 300.04 mm.

Roll Speed = 75 rpm.

Material .... 220 M 07.

Test No.	No. Holes	Pre-Roll Temp. (deg.C)	Roll Temp. (deg.C)	Post-Roll Temp. (deg.C)	Red'n (mm)	Mean Load (kN)	Torque (kNm)
1	1	1230	1227	1181	5.531	47.079	3.781
2	3	1231	1196	1148	5.480	50.000	4.999
3	5	1227	1200	1151	5.531	37.538	4.948
4	1	1238	1202	1152	10.395	63.880	4.740
5	3	1262	1220	1160	10.268	62.870	5.130
6	5	1260	1216	1163	10.166	67.025	5.960
7	1	1287	1231	1149	14.497	80.365	7.080
8	1	1256	1221	1084	20.155	107.820	-----

Test Numbers 1,2,3 = 10% Area Reduction.

Test Numbers 4,5,6 = 20% Area Reduction.

Test Number 7 = 30% Area Reduction.

Test Number 8 = 40% Area Reduction.

F.2. Multi-Pass Rolling Trials With Steel Billets.

h1 = 50.8 mm. w1 = 50.8 mm.

Roll Diameter = 300.04 mm.

Roll Speed = 75 rpm.

Material .... 220 M 07.

Test No.	No. Holes	Pre-Roll Temp. (deg.C)	Roll Temp. (deg.C)	Post-Roll Temp. (deg.C)	Area Red'n (%)	Mean Load (kN)	Torque (kNm)
9 P1	1	1251	1231		10.0	41.338	3.883
P2				1773	10.0	45.180	4.512
10 P1	3	1263	1227		10.0	36.150	3.930
P2				1176	10.0	46.430	3.580
11 P1	5	1265	1216		10.0	45.830	2.870
P2				1147	10.0	49.245	3.580
12 P1	1	1262	1231		10.0	42.350	3.944
P2T				1181	10.0	38.190	4.086
13 P1	4	1256	1231		10.0	35.505	3.930
P2T				1170	10.0	36.610	4.240
14 P1	3	1260	1228		10.0	40.085	4.030
P2T				1197	10.0	35.550	3.980
15 P1	5	1262	1207		10.0	40.410	3.930
P2T				1186	10.0	37.490	3.270
16 P1	1	1255	1224		20.0	58.835	5.250
P2				1181	20.0	81.705	6.520
17 P1	3	1242	1209		20.0	70.875	5.400
P2				1182	20.0	92.630	7.030
18 P1	1	1208	1194		20.0	66.150	4.690
P2T				1141	20.0	------	-----
19 P1	4	1262	1218		20.0	60.010	5.150
P2T				1140	20.0	54.120	3.980
20 P1	3	1297	1231		20.0	61.845	4.290
P2T				1178	20.0	52.495	4.540

Test No.		No. Holes	Pre-Roll Temp. (deg.C)	Roll Temp. (deg.C)	Post-Roll Temp. (deg.C)	Red'n (mm)	Mean Load (kN)	Torque (kNm)
21	P1	1	1287	1231		20.0	62.040	6.720
	P2T					20.0	49.485	5.350
	P3T				1162	20.0	54.435	4.980
22	P1	1	1273	1229		30.0	79.815	7.130
	P2				1175	30.0	100.315	7.840
23	P1	1	1230	1202		30.0	85.600	7.990
	P2T				1151	30.0	69.900	4.540

F.3. Rolling of SAE 8620 Con-Cast Wedge Pieces.

Roll Diameter = 300.04 mm.

Roll Speed = 75 rpm.

Material .... SAE 8620 Con-Cast.

Test No.	Pre-Roll Temp. (deg.C)	Roll Temp. (deg.C)	Post-Roll Temp. (deg.C)	Max Red'n (mm)	Mean Load (kN)	Torque (kNm)
24 (W1)	1262	1252	1199	12.70	134.208	7.840
25 (W2)	1225	1205	1169	6.35	92.915	4.390
26 (W3)	1332	1240	1182	6.35	109.900	6.570

NB. Values of load and torque recorded at maximum reduction.

W1 = Test Piece 1.

W2 = Test Piece 2.

W3 = Test Piece 3.

(Refer to Figure 7.10)

APPENDIX G

HOLE CONSOLIDATION TRIALS - STEEL BILLETS

HOLE AREA FRACTION MEASUREMENTS

G.1. Hole Consolidation Tests, Steel Billets.

h1 = 50.8 mm. w1 = 50.8 mm.

Test No.	Total Area Red'n (%)	Hole No.	Hole Area (mm^2)	Hole Area Fraction (%)	Total Consolidation (%)
27		1	18.2922	0.7214	
		2	18.2922	0.7214	
		3	18.2922	0.7214	
		4	18.2922	0.7214	
		5	18.2922	0.7214	
P1	11.00	1	12.3658	0.5459	32.40
		2	13.3924	0.5912	26.77
		3	11.8277	0.5221	35.34
		4	15.2690	0.6740	16.53
		5	11.4086	0.5036	37.63
28		1	18.2922	0.7236	
		2	18.2922	0.7236	
		3	18.2922	0.7236	
		4	18.2922	0.7236	
		5	18.2922	0.7236	
P1	19.00	1	7.4262	0.3136	59.40
		2	7.7153	0.3258	57.82
		3	7.8640	0.3321	57.01
		4	8.3621	0.3531	54.29
		5	6.9946	0.2954	61.76
29		1	18.2922	0.7214	
		2	18.2922	0.7214	
		3	18.2922	0.7214	
		4	18.2922	0.7214	
		5	18.2922	0.7214	
P2	19.83	1	6.8710	0.3346	62.44
		2	8.9516	0.4360	51.06
		3	7.4355	0.3621	59.35
		4	8.9623	0.4365	51.00
		5	8.4948	0.4137	53.56

Test No.	Total Area Red'n (%)	Hole No.	Hole Area (mm^2)	Hole Area Fraction (%)	Total Consolidation (%)
30		1	18.2922	0.7192	
		2	18.2922	0.7192	
		3	18.2922	0.7192	
		4	18.2922	0.7192	
		5	18.2922	0.7912	
P2T	19.00	1	11.2258	0.5449	38.63
		2	10.1451	0.4925	44.54
		3	11.5215	0.5593	37.01
		4	10.9516	0.5316	40.13
		5	10.3817	0.5039	43.25
31		1	18.2922	0.7229	
P3T		1	7.7473	0.5125	57.65

APPENDIX H

HOLE CONSOLIDATION TESTS - STEEL BILLETS

HOLE AXIAL STRAIN MEASUREMENTS

H.1. Hole Consolidation Tests, Steel Billets.

Hole Axial Strain Measurements.

h1 = 50.8 mm. w1 = 50.8 mm.

Pass/ Hole No.	Z-axis total strain	Y-axis total strain	Axial rot'n (deg)	Shear strain γ_{yz}	Principal strain ε_I	Principal strain ε_{II}	Max. shear strain
27:							
P1:							
H1	0.2931	0.0480	0	0	0.2931	0.0480	0.1225
H2	0.3071	-0.0152	0	0	0.3071	-0.0152	0.1611
H3	0.4266	0.0699	0	0	0.4266	0.0699	0.1783
H4	0.2657	-0.0746	0	0	0.2657	-0.0746	0.1701
H5	0.3954	0.0480	0	0	0.3954	0.0480	0.1737
28:							
P1:							
H1	0.7631	0.0924	0	0	0.7631	0.0924	0.3353
H2	0.8494	-0.0021	4.0	0.0698	0.8508	-0.0035	0.4272
H3	0.7052	0.1292	4.0	0.0698	0.7073	0.1271	0.2901
H4	0.8086	-0.0552	0	0	0.8086	-0.0552	0.4319
H5	0.8562	0.1154	0	0	0.8562	0.1154	0.3704
29:							
P1:			NOT MEASURED				
P2:							
H1	0.8283	0.1173	3.5	0.0611	0.8296	0.1160	0.3568
H2	0.7792	-0.0623	4.0	0.0698	0.7806	-0.0637	0.4222
H3	0.7631	0.0924	0	0	0.7631	0.0924	0.3353
H4	0.7631	-0.0746	0	0	0.7631	-0.0746	0.4188
H5	0.7196	0.0265	0	0	0.7196	0.0265	0.3466
30:							
P1:			NOT MEASURED				
P2T:							
H1	0.2973	0.2130	0	0	0.2793	0.2130	0.0332
H2	0.3725	0.1940	0	0	0.3725	0.1940	0.0893
H3	0.2390	0.2003	0	0	0.2390	0.2003	0.0193
H4	0.2141	0.1815	0	0	0.3141	0.1815	0.0663
H5	0.3213	0.2259	0	0	0.3213	0.2259	0.0477

Pass/ Hole No.	Z-axis total strain	Y-axis total strain	Axial rot'n (deg)	Shear strain γ_{yz}	Principal strain ε_I	Principal strain ε_{II}	Max. shear strain
31:							
P1:				NOT MEASURED			
P2T:				NOT MEASURED			
P3T:	0.7411	0.0265	0	0	0.7411	0.0265	0.3573

APPENDIX J

THEORETICAL ANALYSIS AND ALTERNATIVE VOID MODELS

J.1. Theoretical analysis and calculation.

Following on from the theoretical analysis of the rolling problem in Section 4.2, calculations of rolling torque per unit width of billet were made for comparison with the experimental values given in Figure 8.4.

In the calculation of the elements of work that form the general integral equation, equation 4.14 (the plastic work of deformation, $\dot{E}p$, the frictional work done at the roll-workpiece interface, $\dot{E}f$, and the work done in shear at the entry and exit planes, $\dot{E}d$), the mean or effective stress, $\bar{\sigma}$, is an important factor for consideration.

An assumption made in the analysis is that the workpiece is a workhardening material, as defined by equation 4.7. Consequently, when a workhardening material is considered, the effective stress should be a function of the equivalent strain, $\bar{\varepsilon}$.

From the results of simple compression tests (Section 6.2.3.), a curve of the following form was fitted to the stress-strain data so obtained (Appendix A),

$$\bar{\sigma} = K \bar{\varepsilon}^{m}$$

where $K = 36.7320$

$m = 0.4654$

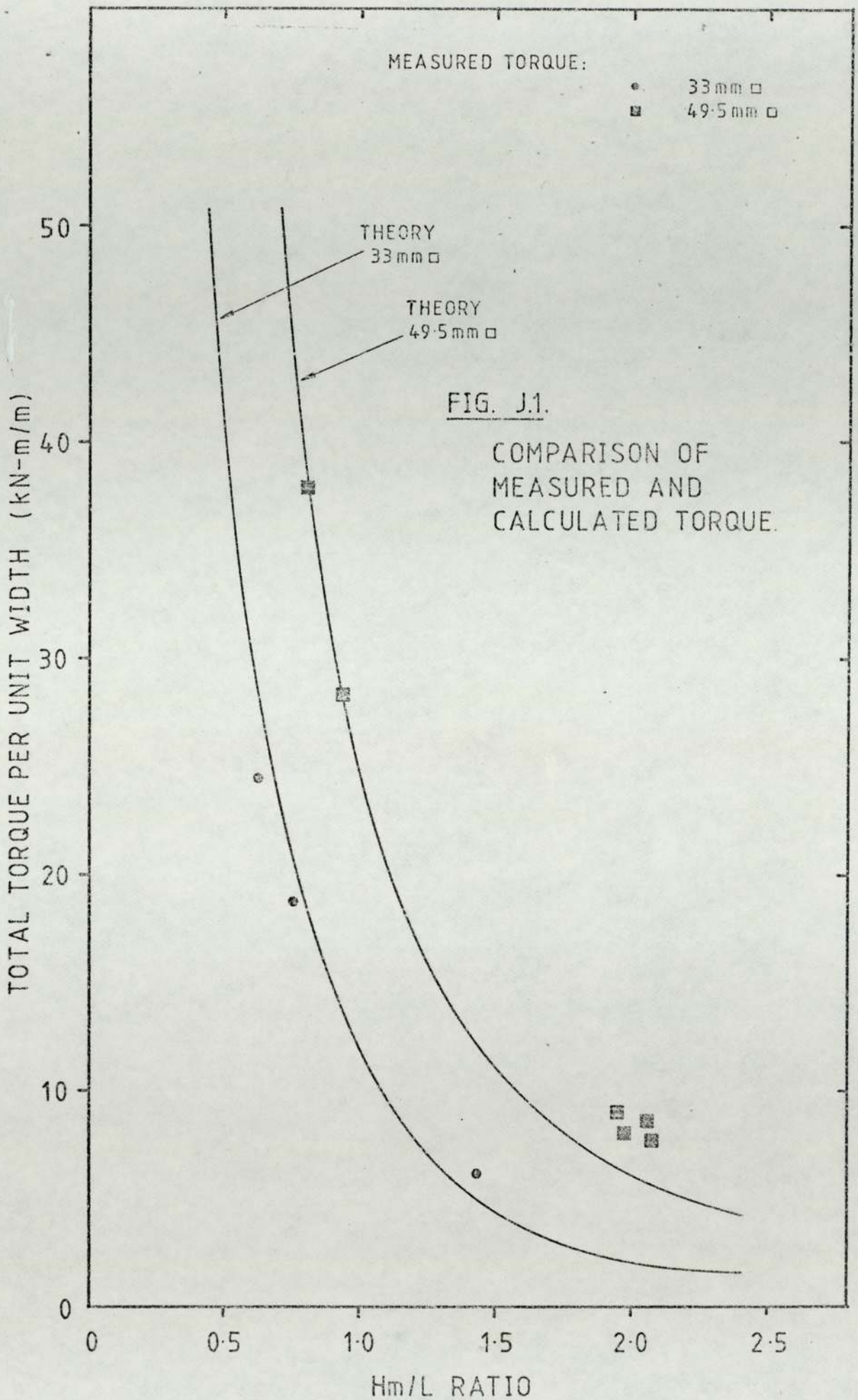

FIG. J.1.

COMPARISON OF MEASURED AND CALCULATED TORQUE.

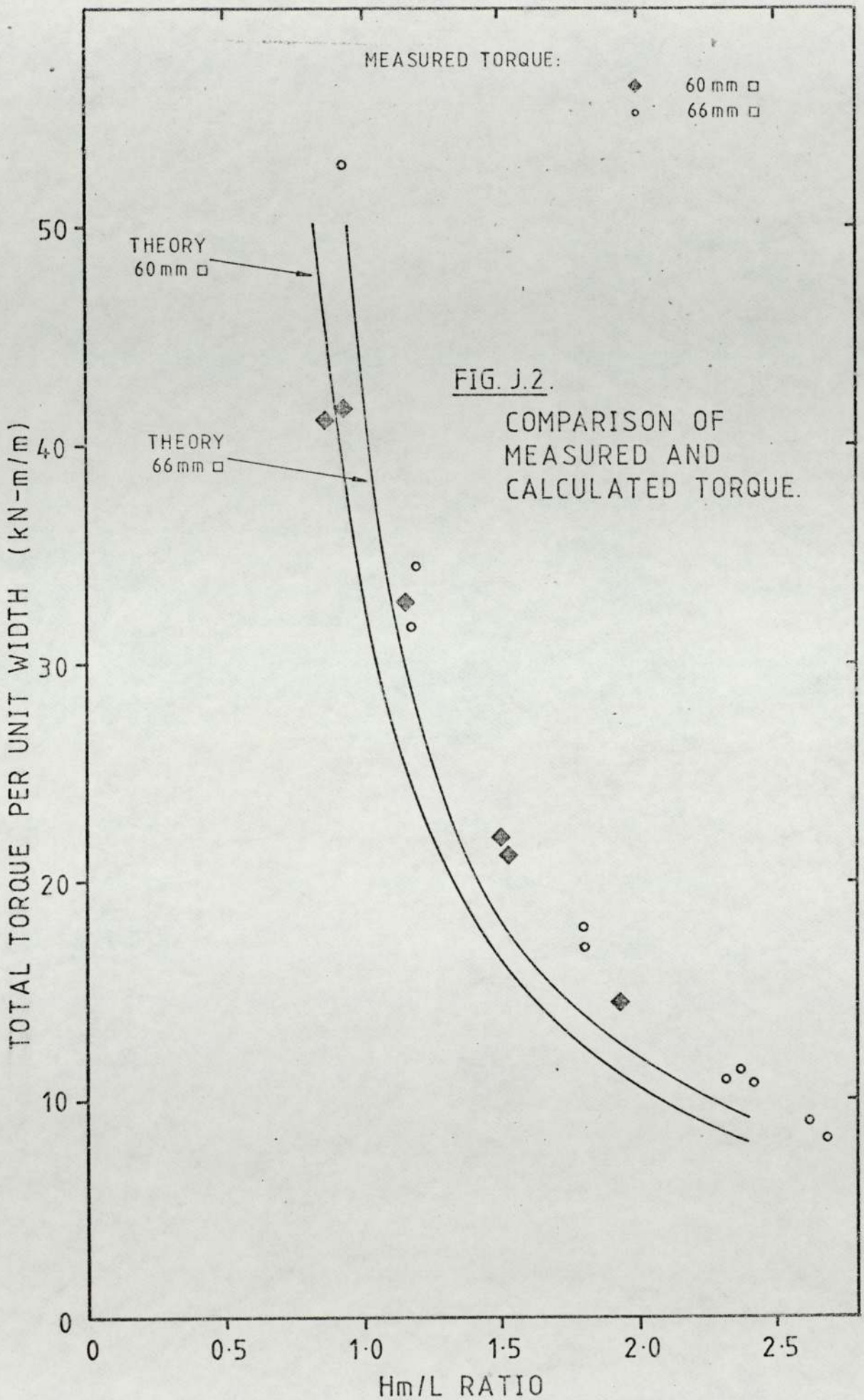

FIG. J.2.

COMPARISON OF MEASURED AND CALCULATED TORQUE.

In Figures J.1. and J.2, theoretical roll torque is compared with measured values for lead billets of 33, 49.5, 60 and 66 mm square cross section at various reductions (Hm/L ratio). The agreement between theory and experiment is good throughout the Hm/L range considered for all billet cross sections. However, for large reductions (low Hm/L ratios) the torque is overestimated by approximately 3% while for small reductions (high Hm/L ratios) the torque is underestimated by approximately 25%.

Reasons for the variations:

a. Slip between the roll and the workpiece was observed to occur during the rolling operation at high reductions (low Hm/L ratio). Consequently the plastic work done on the material will be reduced due to the slippage. Hence the torque measured will be less. The theory does not account for any relative slip during steady state rolling.

b. Ingham (66), who performed rolling trials on the same experimental mill at Aston, calculated that a frictional loss in the roll bearings would account for 2.4% of the total torque when rolling lead with 50 mm nominal diameter smooth rolls. Consequently, larger losses can be expected with larger rolls - larger journal bearings.

c. At high reductions, the amount of workpiece material spreading by migration onto the roll surface will increase resulting in a corresponding increase in the required roll

torque. Consideration of the measured spread values and the use of an empirical polynomial to describe the spread has shown there to be good agreement between the two (see Figures 8.7. to 8.11.), especially at high reductions. However, at low reductions where the spread takes the 'dog-bone' form, the width polynomial underestimates the actual spread due to the simplification imposed by use of the approximating coefficients, a1, a3 and a4. Since the spread is underestimated, the theoretical torque is underestimated also.

d. The polynomial used to describe the spread through the length of the deformation zone (equation 4.17.) is of a simplified form assuming a parabolic shape to the width increase as the material passes through the roll gap. This type of shape agrees well with that observed in practice, however the polynomial implies that the cross section taken perpendicular to the direction of rolling in the y-z plane is constant in form throughout the length of the deformation zone. In practice the spread profile can gradually change from say 'dog-bone' to 'bulge' as the material passes through the deformation zone. The failure of the polynomial to differentiate between different spread progression due to the constant coefficients will result in differences between calculated and measured torque. Other workers, notably On and Kobayashi (93), who have calculated roll torque using a similar analysis, used a minimization procedure to determine the shape of the rolled product from

steady state velocity fields. Coefficients were calculated for a third order polynomial to describe the instantaneous width. Agreement between calculated and measured torque was shown to be excellent.

The simplification of this analysis by using experimentally derived width data is judged to be the major cause of the over-underestimations in rolling torque. Certainly the basic width data is applicable, with confidence, for the material and sections rolled in this work. If a similar analysis on steel, for example, is required, then further experimental work will be necessary to compare the spread profiles with those determined in this work. Then can this analysis method be fully proven.

J.2. Alternative Void Models.

J.2.1. Introduction.

In addition to the two hole closure models presented in Chapter Four, an additional five models are considered here in terms of an upper bound on the required forming load.

In the models, the applied vertical load is assumed to advance with a constant velocity, taken as unity, thereby performing work at a fixed rate. If it is assumed there are no other losses this will be exactly balanced by the rate of performing work by shear on all the velocity discontinuities.

If the length of a velocity discontinuity is S, the

shearing force acting over it will be, for unit width in plane strain, $F = 1\ k\ S$, since the shear yield stress, k, is the same everywhere. If the magnitude of the velocity discontinuity is U, the rate of performing work by the force F will be, $F\ U = k\ U\ S$, and the rate of performing work internally is then,

$$\left[\frac{dW}{dt}\right]_{int} = \sum k\ U\ S$$

The rate of performing work externally by an applied pressure P acting on area 1.a at unity velocity is simply P a. Hence equating the rates of internal and external work,

$$P\ a = k \sum U\ S$$

or,

$$\frac{P}{2k} = \frac{1}{2a} \sum U\ S$$

The most likely velocity field will be the one requiring the least load.

In the upper bound velocity fields on the following pages, there is assumed to be a rigid or dead metal zone attached to the tool surface that moves vertically with the tool with uniform unity velocity. The models are analysed at the start of the deformation, ie. the first pass, the derived equations being applicable after some increment of deformation.

J.2.2. Upper Bound Models.

J.2.2.1. Model A.

According to Model A, Figure J.3, the material in zone 1 moves downwards with uniform unity velocity into the hole area as the dead metal in zone 2 moves horizontally with velocity u . The hole height reduces and the hole width elongates. Material flow is due to the line of velocity discontinuity, CF, the inclination of which is constant for a particular pass.

$$\left\{\frac{dW}{dt}\right\}_{int} = k\sum U\,S = k\,(u_1\ AF + u_{12}\ CF)$$

From the model geometry and the hodograph,

$$\left\{\frac{dW}{dt}\right\}_{int} = k\left\{2(H-h) - y + \frac{W^2}{(H-h-y)}\right\}$$

$$\left\{\frac{dW}{dt}\right\}_{ext} = P\ AB = P\ W$$

Hence,

$$\frac{P}{2\ k} = \frac{1}{2\ W}\left\{2(H-h) - y + \frac{W^2}{(H-h-y)}\right\} \quad .... \quad (A.1)$$

J.2.2.2. Model B.

According to Model B, Figure J.4, the material in zone 1 moves downwards with uniform unity velocity into the hole area as the dead metal in zone 2 moves horizontally with

FIG. J.3. MODEL A.

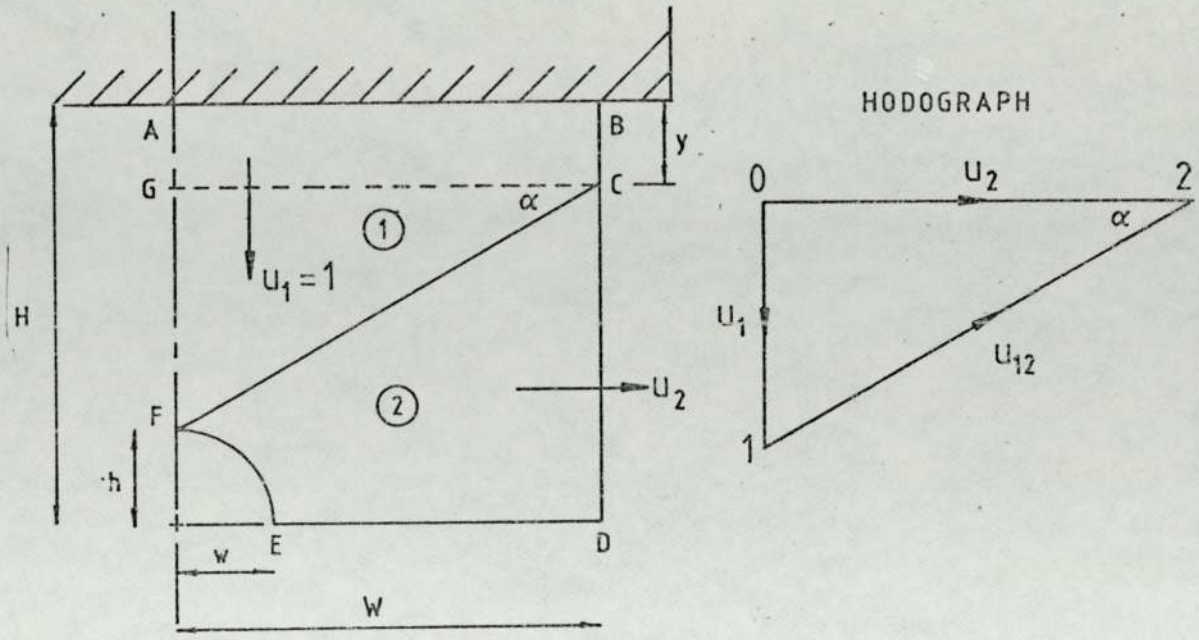

FIG. J.4. MODEL B.

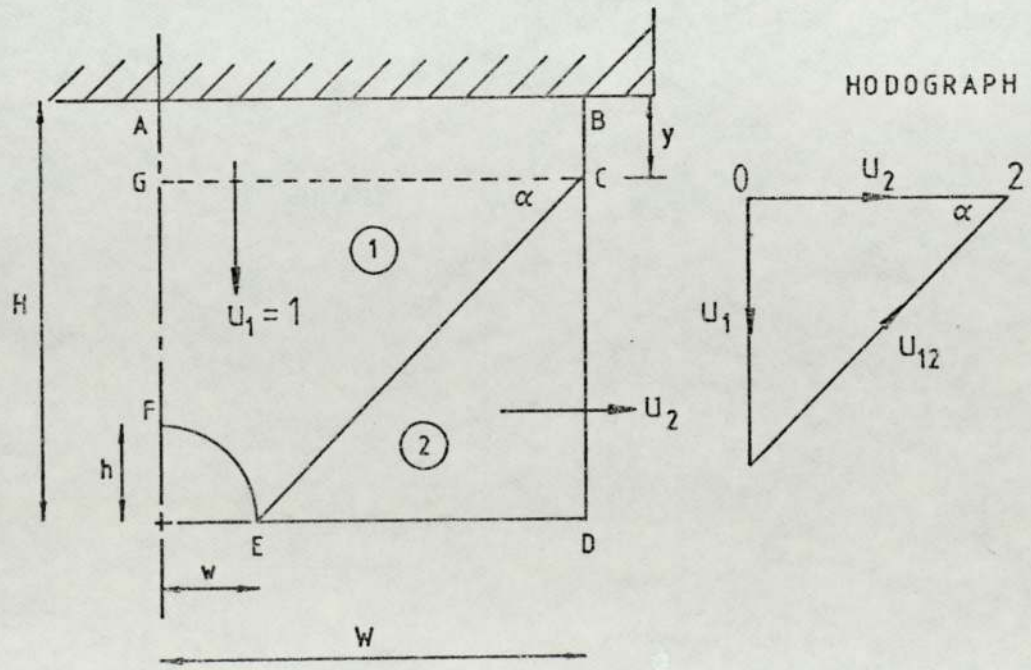

velocity u_2 . However, the hole side does not move in the width direction, there is only height reduction.

$$\left\{\frac{dW}{dt}\right\}_{int} = k\sum U\,S = k\,(u_1\ AF + u_{12}\ CE)$$

From the model geometry and the hodograph,

$$\left\{\frac{dW}{dt}\right\}_{int} = k\left\{2H - y + \frac{(W-w)^2}{(H-y)}\right\}$$

$$\left\{\frac{dW}{dt}\right\}_{ext} = P\ AB = P\ W$$

Hence,

$$\frac{P}{2\ k} = \frac{1}{2\ W}\left\{2H - y + \frac{(W-w)^2}{(H-y)}\right\} \quad \ldots\ldots\ldots \quad (A.2)$$

J.2.2.3. Model C.

According to Model C, Figure J.5, material in zone 1 moves vertically downwards with uniform unity velocity into the hole area reducing it in height. The material then experiences a tangential discontinuity CF and the absolute velocity in zone 2 is assumed parallel to chord EF. Material leaves the plastic region to enter the dead metal zone 3 across discontinuity CE. The exit velocity is horizontal.

$$\left\{\frac{dW}{dt}\right\}_{int} = k\sum U\,S = k\,(u_1\ AF + u_{12}\ CF + u_2\ EF + u_{23}\ CE) \ \ldots\ldots$$

$$\ldots\ldots \quad (A.3)$$

From the model geometry and the hodograph,

$$u_1 = 1 \qquad u_{12} = u_1 \frac{w\sqrt{W^2 + (H-h-y)^2}}{h\,w + w(H-h-y)}$$

$$u_2 = u_1 \frac{W\sqrt{h^2 + w^2}}{h\,W + w(H-h-y)} \qquad u_{23} = u_1 \frac{W\,h\sqrt{(W-w)^2 + (H-y)^2}}{h\,W + w(H-h-y)(H-y)}$$

$$u_3 = u_1 \frac{W}{(H-y)}$$ as expected, a ratio of the width/height.

Substitution of the above velocity components into equation (A.3) yields the equation for the internal work,

$$\left\{\frac{dW}{dt}\right\}_{int} = \frac{k}{A}\left\{(H-h)A + B + C + D\right\}$$

where, $A = h\,W + w(H-h-y)$

$B = w(W^2 + (H-h-y)^2)$

$C = W\,(h^2 + w^2)$

$D = W\,h\,((W-w)^2 + (H-y)^2)$

Equating this to the externally applied work, P W,

$$\frac{P}{2\,k} = \frac{1}{2\,W\,A}\,((H-h)A + B + C + D) \quad \ldots\ldots\ \ldots\ldots \quad (A.4)$$

J.2.2.4. Model D.

The assumption of material flow parallel to chord EF made in Model C is continued, indeed, this would apply to a diagonally shaped hole of side $\sqrt{h^2 + w^2}$, Figure J.6.

$$\left\{\frac{dW}{dt}\right\}_{int} = k\sum U\,S = k\,(u_1\,AF + u_{12}\,CF + u_2\,EF + u_{23}\,CE) \ \ldots$$

$$\ldots\ (A.5)$$

From the model geometry and the hodograph,

$$u_1 = 1 \qquad u_{12} = u_1\,\frac{w}{h} \qquad u_2 = u_1\,\frac{\sqrt{h^2+w^2}}{h}$$

$$u_{23} = u_1\,\frac{\sqrt{(W-w)^2+h^2}}{h} \qquad u_3 = u_1\,\frac{W}{h}$$

$$\left\{\frac{dW}{dt}\right\}_{int} = \frac{k}{h}\,(\,h(H+h) + w(W+w) + (W-w)^2\,)$$

Equating this to the externally applied work, P W,

$$\frac{P}{2\,k} = \frac{1}{2Wh}\,(h(H+h) + w(W+w) + (W-w)^2\,) \ \ldots\ (A.6)$$

J.2.2.5. Model E.

According to Model E, Figure J.7, material in zonw 1 moves vertically downwards with uniform unity velocity. The material then experiences tangential discontinuities CH and HG. In zone 2, the flow is assumed parallel to chord FG. In zone 3 the flow after discontinuity FH is horizontal and the flow in zone 4 is derived from the hodograph. The exit velocity in zone 5 is then horizontal. From the model geometry and the hodograph, Figure J.7,

$$u_1 = 1 \qquad u_{12} = u_1\,\frac{w}{h} \qquad u_2 = u_1\,\frac{\sqrt{h^2+w^2}}{h} \qquad u_{23} = u_1\,\frac{\sqrt{h^2+w^2}}{h}$$

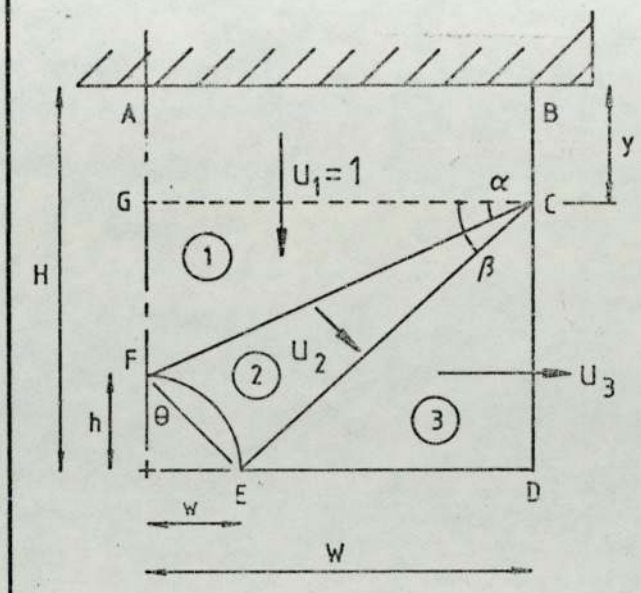

FIG. J.5. MODEL C.

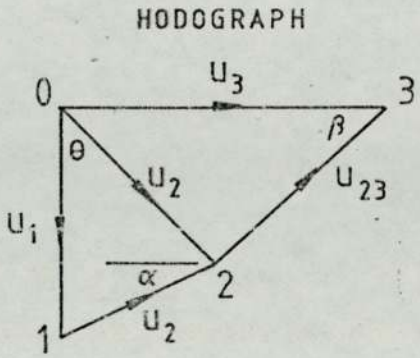

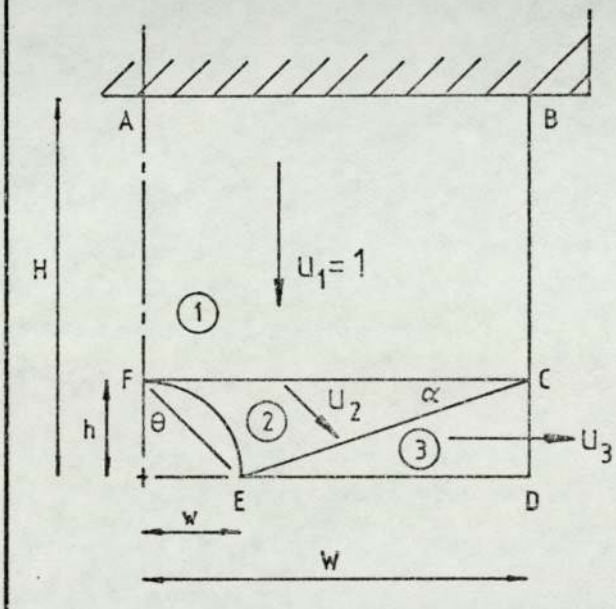

FIG. J.6. MODEL D.

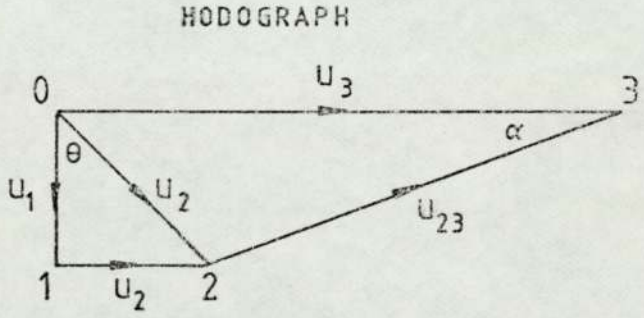

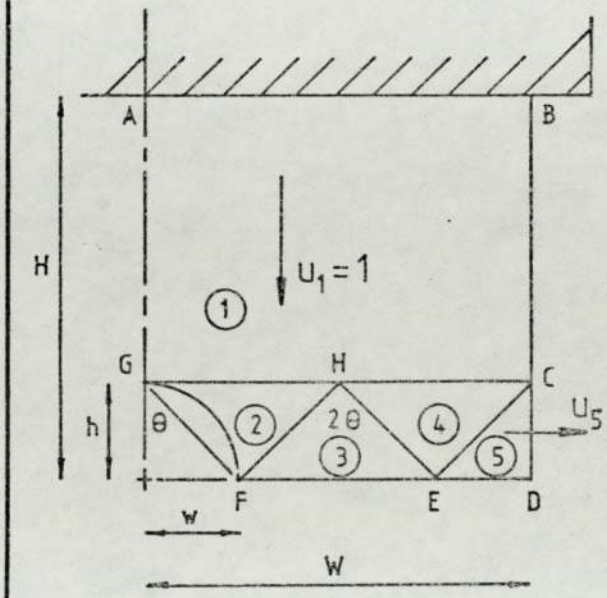

FIG. J.7. MODEL E.

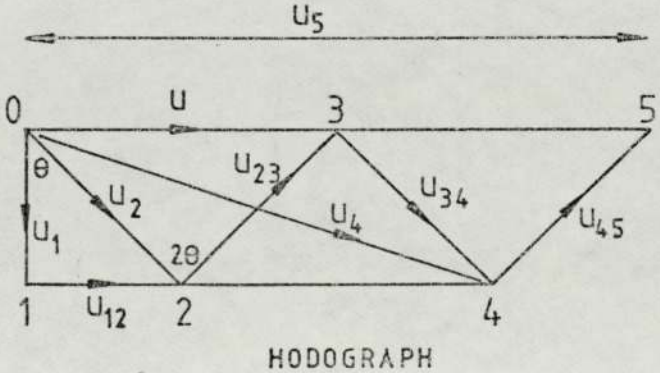

$$u_3 = 2u_1 \frac{w}{h} \qquad u_{34} = u_1 \frac{\sqrt{h^2 + w^2}}{h} \qquad u_{45} = u_1 \frac{\sqrt{h^2 + w^2}}{h}$$

$$u_{14} = 3u_1 \frac{w}{h} \qquad u_4 = u_1 \sqrt{1 + 9(w/h)^2} \qquad u_5 = 4u_1 \frac{w}{h}$$

$$\left\{\frac{dW}{dt}\right\}_{int} = k \sum U S = k\,(u_1\ AG + u_{12}\ HG + u_{14}\ HC + u_2\ GF + \ldots$$
$$\ldots + u_{23}\ HF + u_3\ FE + u_{34}\ HE + u_4\ HC + u_{45}\ CE)$$

$$\left\{\frac{dW}{dt}\right\}_{int} = \frac{k}{h}\left((H-h)h + 3wW + 4(h^2 + w^2) + \sqrt{h^2 + w^2}\ \sqrt{1 + 9\ (w/h)^2}\ \right)$$

Equating this to the externally applied work, P W,

$$\frac{P}{2k} = \frac{1}{2hW}\left((H-h)h + 3wW + 4(h^2 + w^2) + \sqrt{h^2 + w^2}\ \sqrt{1 + 9\ (w/h)^2}\ \right)$$

.... (A.7)

J.2.3. Calculation Of Ratio P/2k.

As stated in Section J.2.1, the most likely velocity field will be the one requiring the least load. The forming load can be calculated from the preceeding upper bound models.

Assuming, for example,

$$H = W = 1 \qquad \text{and} \qquad h = w = 0.05$$

..../over page

y	Model A P/2k	Model B P/2k	Model C P/2k	Model D P/2k	Model E P/2k
0	1.4763	1.4513	1.4763	10.075	4.4111
0.05	1.4806	1.4500	1.4526		
0.10	1.4882	1.4514	1.4304		
0.15	1.5000	1.4559	1.4097		
0.20	1.5167	1.4641	1.3907		
0.25	1.5393	1.4767	1.3735		
0.30	1.5692	1.4946	1.3583		

The table illustrates the variation of P/2k for the models considered as point C varies from y=0 to y=0.3, ie. y=0.3H. Model B shows a lower bound on the forming load when y=0.05. At this point, for this particular model when w=0.05, this may be expected since the inclination of the velocity discontinuity line will be 45 deg. In general, predictions from upper bound solutions become closer to the accurate value as the fields themselves resemble more closely the slip-line field.

REFERENCES

1. **Bessemer.H.** On the manufacture of continuous sheets of maleable iron and steel direct from fluid metal. JISI, p.23, 1891 II.

2. **Halliday.I.M.D.** Continuous casting at Barrow. JISI, v.191, p.121, 1959 I.

3. **Niyama.E, Kodama.H, Kimura.T. & Endo.M.** Belt-wheel type con-caster for steel billets. Iron & Steel Engineer, p.38, Aug. 1981.

4. **Metals Society, London.** Continuous Casting. Pub. Metals Society, 1982. 4th Int.Iron & Steel Congr, London, May 1982.

5. **Metals Society, London.** Hot Working And Forming Processes. Pub. Metals Society, 1980. Proc.Int.Conf.Hot Working and Forming Processes, Sheffield, July 1979.

6. **Lipton.J.** Concast News, p.3, v.19, n.3, 1980.

7. **Alberny.R, Bäcker.L, Birat.J-P, Gosselin.P. & Wanin.M.** Quality improvement of strand cast billets through electromagnetic stirring. Elec.Furn.Proc, p.237, v.31, Cincinnati, 1973.

8. **Perkins.A. & Irving.W.R.** Mathematical Process Models In Iron and Steel Making. p.187, Metals Society, 1975.

9. **British Iron & Steel Research Association.** Definitions and Causes Of Con-Casting Defects. ISI Pub. 106, 1967.

10. **Diehl.D.C, Rocchio.F.J. & Brown.J.J.**
In line reduction on a continuous billet caster. Iron and Steel Eng, p.39, March 1975.

11. **Gorecki.J.** The generation of internal cracks in ingots, blooms and slabs during rolling. Hutnik, v.6, p.228, 1957.

12. **Vater.M.** New results of research on the flow of material in the plastic deformation of metallic materials. Tech.Mitt, v.59, p.500, Oct.1966.

13. **Tagawa.H.** Effect of the rolling process on the pressing out and elimination of micro-porosities in large scale ingots. Tetsu-to-Hagane, v.62, n.13, p.1720, 1976.

14. **Tarmann.B.A.** High performance con-casting machines for the casting of small billets. Elec.Furn.Proc, Inovations & Materials, p.203, 1971.

15. **Baumann.H.G, Elsner.D.A. & Pirdzun.J.** External and internal quality of con-cast (steel) billets on strand reduction. Stahl und Eisen, v.91, n.3, p.139, 1971.

16. **Baumann.H.G.** Segregation in con-cast steel strands. Bander Bleche Rohre, v.12, n.6, p.239, 1971.

17. **Ushijima.K.** Working process and resulting properties of con-cast steel. Tetsu-to-Hagane, v.60, p.843, 1974.

18. **Pierce.W.B.** Status report on con-casting. Steel, v.183, n.15, p.256, 1953.

19. **Kosmider.H, Neuhaus.H. & Weyel.A.** Con-casting of rimmed basic Bessemer steel. Stahl und Eisen, v.76, n.11, p.668, 1956.

20. **Hofmaier.J.** Con-cast product for rolling and forging. Stahl und Eisen, v.77, n.2, p.69, 1957.

21. **Water.B.H.C, Pritchard.W.H, Braybrook.A. & Harris.G.T.** Con-casting of high speed steel. JISI, v.190, p.233, 1958 II.

22. **Fenton.G. & Pearson.J.** Con-casting on the BISRA experimental plant. JISI, v.189, p.160, 1958 II.

23. **Fenton.G, Littlewood.G. & Zaeytydt.A.** Con-casting research at BISRA and CNRM. Iron & Coal Trades Rev, v.182, p.681, 1961.

24. **Littlewood.G. & Pritchard.W.H.** Steel cast continuously in the Weybridge multiple mould. Iron and Coal Trades Rev, v.183, p.1381, 1961.

25. **Cabane.M.** Rolling of con-cast alloy steel billets. Steel and Coal, v.184, p.805, 1962.

26. **Takehara.E, Nishimura.O, Yamasaki.D, Tsunoi.M. & Akita.H** Production and properties of twin billet by a con-casting machine with reduction mill. Tetsu-to-Hagane, v.59, p.1925, 1973.

27. **Saigi.Y, Fukui.K, Tsunehisa.Y, Shioda.T.** Qualities of billets produced by con-casting with in-line reduction. Trans.ISIJ, v.15, n.3, p.153, 1975.

28. **Evteev.D.P. & Listopad.V.I.** Quality of con-cast strands on machines incorporating rolling with con-casting. Stal', v.6, n.11, p.602, 1976.

29. **Hawbolt.E.B, Weinberg.F. & Brimacombe.J.K.** Influence of hot working on internal cracks in con-cast steel billets. Met.Trans.B, v.10B, p.229, 1979.

30. **Kumazawa.M. & Sato.M.** Influence of hot grooved rolling on the mechanical properties of con-cast hot rolled steels. Trans.ISIJ, v.21, n.6, p.B-293, 1981.

31. **Hojas.H.** Hot working of con-cast billets in a continuous forging machine. Pub.Metals Society, 1976. Proc.Conf.Met.Society, p.182, Biarritz, June 1976.

32. **Hojas.H. & Garrett.N.I.** Design and application of forging rolling systems to produce bar steel. Pub. Metals Society, 1981. Proc.Conf.Met.Society, p.134, London, May 1981.

33. **Hill.R.** The Mathematical Theory Of Plasticity. Pub. Oxford University Press, 1950.

34. **Ford.H.** Advanced Mechanics Of Materials. Pub. Longmans, Green & Co, 1963.

35. **von Karman.T.** Contribution to the theory of rolling. Zeitschrift für Angewandte Mathematik und Mechanik, v.5, n.2, p.139, 1925.

36. **Siebel.E.** Stahl und Eisen, v.45, p.1563, 1925.

37. **Nadai.A.** Forces required for rolling steel strip under tension. J.Appl.Mech, ASME, p.4, 1939.

38. **Siebel.E. & Leug.W.** Measuring methods and equipment for investigating stress distribution in the gap between rolls. Stahl und Eisen, v.53, n.14, p.346, 1933.

39. **Ekelund.S.** The analysis of factors influencing rolling pressure in the hot rolling of steel. Steel, v.93, n.8, p.27, 1933 & issues 9,10,11,13 & 14.

40. **Tselikov.A.T.** Metallurgia, n.6, p.61, 1936.

41. **Orowan.E.** The calculation of roll pressure in hot and cold flat rolling. Proc.I.Mech.Eng, v.150, p.140, 1943.

42. **Prandtl.L.** Anwandungsbeispiele zu einem Henckyschen Satz über das plastische Gleichgewicht. Zeitschrift für Angewandte Mathematik und Mechanik, v.3, p.401, 1923.

43. **Nadai.A.** Plasticity - A Mechanics Of The Plastic State Of Matter. Pub. McGraw-Hill, London, 1931.

44. **Bland.D.R. & Ford.H.** The calculation of roll force and torque in cold strip rolling with tensions. Proc.I.Mech.Eng, v.159, p.144, 1948.

45. **Ford.H, Ellis.F. & Bland.D.R.** Cold strip rolling with tension. JISI, Pt.1, May 1951 & Pt's 2 & 3, July 1952.

46. **Orowan.E. & Pascoe.K.J.** Iron and Steel Inst. Special Report 34, 124, 1946.

47. **Sims.R.B.** The calculation of roll force and torque in hot rolling mills. Proc.I.Mech.Eng, v.168, p.191, 1954.

48. **Whitton.P.W. & Ford.H.** Surface friction and lubrication in cold strip rolling. Proc.I.Mech.Eng, v.169, p.123, 1955.

49. **Watts.A.B. & Ford.H.** An experimental investigation of the yielding of strip between smooth dies. Proc.I.Mech.Eng, 1B, p.448, 1952/3.

50. **Watts.A.B. & Ford.H.** On the basic yield stress curve for a metal. Proc.I.Mech.Eng, v.169, p.1141, 1955.

51. **Alder.J.F. & Philips.V.A.** Effect of strain rate and temperature on the resistance of aluminium, copper and steel to compression. J.I.Metals, v.83, p.80, 1954/5.

52. **Cook.P.M.** True stress-strain curves for steel in compression at high temperatures and strain rates. I.Mech.Eng, p.86, 1957.

53. **Cook.P.M. & McCrum.A.W.** The calculation of load and torque in hot flat rolling. BISRA, London, March 1958.

54. **Alexander.J.M.** On the theory of rolling. Proc.Royal Society London, A.326, p.525, 1972.

55. **Prager.W.** A geometrical discussion of the slip line field in plane plastic flow. Trans.Royal Inst.Tech, Stockholm, n.65, 1953.

56. **Alexander.J.M.** A slip line field for the hot rolling process. Proc.I.Mech.Eng, v.169, p.1021, 1955.

57. **Ford.H. & Alexander.J.M.** Simplified hot rolling calculations. J.I.Metals, v.92, p.397, 1963/4.

58. **Crane.F.A.A. & Alexander.J.M.** Slip line fields and deformation in hot rolling of strip. J.I.Metals, v.96, p.289, 1968.

59. **Druyanov.B.A.** Sheet rolling under maximum friction conditions. Plastic flow of metals, v.1, p.80, 1971.

60. **Dewhurst.P. & Collins.I.F.** A matrix technique for constructing slip line field solutions to a class of plane strain plasticity problems. Int.J.Num.Meth.Engng, v.7, p.357, 1973.

61. **Dewhurst.P, Collins.I.F. & Johnson.W.** A class of slip line field solutions for the hot rolling of strip. J.Mech.Eng.Sci, v.15, p.439, 1973.

62. **Potapkin.V.F. & Bobukh.J.A.** Stress state in the deformation zone in the hot rolling of thick and medium stock. Steel in the USSR, p.641, 1971.

63. **Filipov.E.L. & Klimenko.V.M.** Approximate formula for determining axial stresses during rolling of thick flat bars (ingots). Steel in the USSR, p.461, 1971.

64. **Pawelski.O. & Neüschutz.E.** Beitrag zu den Grundlagen des Walzens in Stekkalibern. Max Planck Inst, Eisenforsch, 1775, 1967.

65. **Ståhlberg.U.** Slip line field theory applied to rolling. Scand.J.Metallurgy, v.7, p.42, 1978.

66. **Ingham.P.M.** The mechanics of thick slab rolling. PhD Thesis, University of Aston in Birmingham, 1980.

67. **Pawelski.O. & Gopinathan.V.** Comparison of material flow and deformation resistance of HSLA steel deformed by hot rolling and by flat compression under simulated conditions. J.Mech.Work.Tech, v.5, n.3/4, p.267, 1981.

68. **Sparling.L.G.M.** Evaluation of loads and torque in hot flat rolling from slip line fields. Proc.I.Mech.Eng, v.197, Pt.A, p.277, 1983.

69. **Collins.I.F.** Slip line field analysis of forming processes in plane strain and axial symmetry. Proc. 1st Int.Conf.Tech.Plasticity, Advanced Tech.Plast--icity, Tokyo, v.II, p.1074, 1984.

70. **Ilyushin.A.A.** Prikladnaia Matematika i Mekhanika, v.9, p.207, 1945.

71. **Greenberg.H.J.** Complementary minimum principles for an elastic-plastic material. Q.J.Appl.Maths, v.7, n.1, p.85, 1949/50.

72. **Prandtl.L.** Spannungsverteilung in plastischen Körpern. Proc.1st Int.Congr.Appl.Mech, p.43, Delft 1924.

73. **Reuss.A.** Elastic deformation according to theory of plasticity. Zeitschrift für Angewandte Mathematik und Mechanik, v.10, n.3, p.266, 1930.

74. **Hodge.P. & Prager.W.** A variational principle for plastic materials with strain hardening. J.Maths.Phys, v.27, n.1, p.1, 1948.

75. **Hill.R.** A variational principle of maximum plastic work in classical plasticity. Q.J.Appl.Maths, v.1, n.1, p.18, 1948.

76. **Haar.A, & von Karman.T.** Zur Theorie der Spannungszustande in plastischen und sandartigen Medien. Göttinger Nachr, Maths-Phys.Kl, p.204, 1909.

77. **Hencky.H.** Über einige statisch bestimmte Fälle des Gleichgewichts in plastischen Körpern. Zeitschrift für Angewandte Mathematik und Mechanik, v.3, p.241, 1923.

78. **Hill.R.** A comparative study of some variational principles in the theory of plasticity. J.Appl.Mech, v.17, p.64, 1950.

79. **Markov.A.** On variational principles in the theory of plasticity. Prikladnaia Mathematika i Mekhanika, v.11, p.339, 1947.

80. **Hill.R.** A general method of analysis for metal working processes. J.Mech.Phys.Solids, v.11, p.305, 1963.

81. **Nagamatsu.A, Murota.T. & Jimma.T.** On the non-uniform deformation of block in plane strain compression caused by friction. Bull.JSME, v.13, p.1389, 1970.

82. **Murota.T, Jimma.T. & Nagamatsu.A.** Proc.16th Jap.Nat. Congr.Appl.Mech, p.141, 1966.

83. **Baraya.G.L. & Johnson.W.** Proc.5th Int.Mach.Tool Des. Res.Conf, p.449, 1964.

84. **Lahoti.G.D. & Kobayashi.S.** On Hill's general method of analaysis for metal working processes. Int.J.Mech.Sci, v.16, p.521, 1974.

85. **MacGregor.C.W. & Coffin.L.F.** The distribution of strains in the rolling process. Trans.ASME, J.Appl.Mech, v.65, p.13, 1943.

86. **Chitkara.N.R. & Johnson.W.** Some experimental results concerning spread in the rolling of lead. Trans.ASME, J.Basic Engng, v.88, p.489, 1966.

87. **Wusatowski.Z.** Hot rolling: study of draught spread and elongation. Iron & Steel, v.28, p.49, 1955.

88. **Wusatowski.Z.** Arch.Hutnictwa, v.3, p.161, 1958.

89. **Sparling.L.G.M.** Formula for spread in hot flat rolling. Proc.I.Mech.Eng, v.175, p.604, 1961.

90. **Geleji.A.** Spatial distribution of the flow of material and of the roll pressure within the roll gap. Archiv für das Eisenhuttenwesen, v.38, Pt.2, p.99, 1967.

91. **Gokyu.I, Kihara.J. & Mae.Y.** J.Jap.Soc.Tech.Plasticity, v.11, p.11, 1970.

92. **Polukhin.P.I.** Spread during the hot rolling of alloy steels. Stal', v.7, p.616, 1975.

93. **Oh.S.I. & Kobayashi.S.** An approximate method for a three dimensional analysis of rolling. Int.J.Mech.Sci, v.17, p.293, 1975.

94. **Washizu.K.** Variational Methods In Elasticity and Plasticity. Pub. Pergammon Press, p.515, 1982.

95. **Saito.Y.** Deformation analysis in shape rolling using an upper bound method. Proc.1st Int.Conf.Tech.Plasticity Advanced Tech.Plasticity, Tokyo, v.II, p.1190, 1984.

96. **Himmelblau.D.M.** Applied Non-Linear Programming, p.141. Pub. McGraw-Hill, 1972.

97. **Zienkiewicz.O.C.** The Finite Element Method. Pub. McGraw-Hill, 1977.

98. **Huebner.K.H.** The Finite Element Method For Engineers. Pub. John Willey & Sons, 1975.

99. **Lee.E.H, Mallet.R.L. & Yang.W.H.** Stress and deformation analysis of the metal extrusion process. Comp.Meth.Appl.Math.Engng, v.10, n.3, p.339, 1977.

100. **Rao.S.S. & Kumar.A.** Finite element analysis of cold strip rolling. Int.J.Mach.Tool Des.Res, v.17, p.159, 1977.

101. **Keifer.B.V.** Three dimensional prediction of material flow and strain distribution in rolled rectangular billets. Proc. 1st Int.Conf.Tech.Plasticity, Advanced Tech.Plasticity, Tokyo, v.II, p.1116, 1984.

102. **Yarita.I, Mallet.R.L. & Lee.E.H.** Stress and deformation analysis of metal rolling process. Proc. 1st Int.Conf.Tech.Plasticity, Advanced Tech.Plast--icity, Tokyo, v.II, p.1126, 1984.

103. **Mallet.R.L. & Lee.E.H.** Plasticity Of Metals At Finite Strain: Theory, Experiment and Computation. Pub. Div.Appl.Mech, Stanford Univ, Aug/July 1981.

104. **Lynch.F.D.** A finite element method of visco-elastic stress analysis with application to rolling contact problems. Int.J.Num.Meth.Engng, v.1, p.379, 1969.

105. **Batra.R.C.** Cold sheet rolling, the thermo-visco-elastic problem, a numerical solution. Int.J.Num.Meth. Engng, v.11, p.671, 1977.

106. **Webber.J.P.H.** Stress analysis in visco-elastic bodies using finite elements and a correspondence rule with elasticity. J.Strain Analysis, v.4, p.236, 1969.

107. **Gerstenkorn.G.F. & Kobayashi.S.** Application of the direct stiffness method to plane problems involving large, time dependant deformations. Trans.ASME, J.Basic Engng, v.88, p.771, 1966.

108. **Lung.M. & Marrenholtz.O.** Finite element procedure for analysis of metal forming processes. Trans.Canadian Soc.Mech,Eng, v.2, n.1, p.31, 1973/4.

109. **Kobayashi.S.** Rigid plastic finite element analysis of axisymmetric metal forming processes. Num.Model.Manuf Processes, ASME, PVP-PB-025, p.49, 1977.

110. **Zienkiewicz.O.C, Jain.P.C. & Oñate.E.** Flow of solids during forming and extrusion: some aspects of numerical solutions. Int.J.Solids & Structures, v.14, p.15, 1978.

111. **Dawson.P.R. & Thompson.E.G.** Finite element analysis of steady state elasto-visco-plastic flow by the initial stress rate method. Int.J.Num.Meth.Engng, v.12. p.47, 1978.

112. **Dawson.P.R.** Visco-plastic finite element analysis of steady state forming processes including strain history dependance. ASME AMD, PVP-PB-025, v.28, p.55, 1978.

113. **Altan.T, Lahoti.G.D. & Oh.S.I.** ALPID - a general purpose finite element method program for metal forming. SME Tech.paper, Serial No. MS 82-398, 1982.

114. **Kanazawa.M. & Marcal.P.V.** Finite element analysis of the steel rolling process. ASME AMD, PVP-PB-025, v.28, p.81, 1978.

115. **Li,Guo-Ji & Kobayashi.S.** Spread analysis in rolling by the rigid-plastic finite element method. Num.Meth.Ind.Form.Proc, p.777, 1977. Pub. Pineridge Press, 1982.

116. **Li,Guo-Ji & Kobayashi.S.** Rigid-plastic finite element analysis of plane strain rolling. ASME 81-WA/PROD-13, 15-20 Nov. 1981.

117. **Osakada.K, Nakano.T. & Mori.K.** Finite element method for rigid-plastic analysis of metal forming - formulation for finite deformation. Int.J.Mech.Sci, v.24, n.8, p.459, 1982.

118. **Mori.K, Osakada.K. & Oda.T.** Simulation of plane strain rolling by the rigid-plastic finite element method. Int.J.Mech.Sci, v.24, n.9, p.519, 1982.

119. **Mori.K, Osakada.K, Nakadoi.K. & Fukuda.M.** Simulation of three dimensional deformation in metal forming by the rigid-plastic finite element method. Proc. 1st Int.Conf.Tech.Plasticity, Advanced Tech.Plast--icity, Tokyo, v.II, p.1009, 1984.

120. **Mori.K. & Osakada.K.** Simulation of three dimensional deformation in metal forming by the rigid-plastic finite element method. Num.Meth.Ind.Form.Processes, p.747, 1977. Pub. Pineridge Press, 1982.

121. **Mori.K. & Osakada.K.** Simulation of three dimensional deformation in metal forming by the rigid-plastic finite element method. Int.J.Mech.Sci, v.26, n.9/10, p.515, 1984.

122. **Ståhlberg.U, Söderberg.J-O. & Wallerö.A.** Overlap at the back and front end in slab ingot rolling. Int.J.Mech.Sci, v.23, n.4, p.183, 1981.

123. **Hwang.S.M. & Kobayashi.S.** Preform design in plane strain rolling by the finite element method. Int.J.Mach.Tool Des.Res, v.24, n.4, p.253, 1984.

124. **Kobayashi.S.** Approximate solutions for preform design in rolling. Int.J.Mach.Tool Des.Res, v.24, n.3, p.215, 1984.

125. **Zienkiewicz.O.C, Oñate.E. & Heinrich.J.C.** ASME AMD, PVP-PB-025, v.28, p.107, 1978.

126. **Bishop.J.F.W.** An approximate method for determining the temperatures reached during motion problems of plane strain. Q.J.Mech.Appl.Maths, v.9, 1956.

127. **Altan.T. & Kobayashi.S.** A numerical method for estimating the temperature distribution in extrusion through conical dies. Trans. ASME, J.Engng.Ind, v.90, p.107, 1968.

128. **Dawson.P.R. & Thompson.E.G.** Steady state thermo-mechanical finite element analysis of elasto-visco-plastic metal forming processes. Num.Model.Forming Proc, ASME PVP-PB-025, p.167, 1977.

129. **Tseng.A.A.** A finite difference thermal model of flat rolling. Num.Meth.Ind.Form.Processes, p.767, 1977. Pub. Pineridge Press, 1982.

130. **Abhijit.C. & Subrata.M.** Finite element analysis of metal forming processes with thermo-mechanical coupling. Int.J.Mech.Sci, v.26, n.11/12, p.661, 1984.

131. **Tozawa.Y, Nakamura.M. & Ishikawa.T.** Method of three dimensional analysis & an applied example - analytical study in three dimensional deformation in strip rolling. J.Jap.Soc.Tech.Plasticity, v.17, n.108, p.37, 1976.

132. **Lahoti.G.D, Akgerman.N, Oh.S.I. & Altan.T.** Computer aided analysis of metal flow and stress in plate rolling. J.Mech.Work.Tech, v.4, n.2, p.105, 1980.

133. **Malinin.N.N.** Elementary theory of hot rolling. Int.J.Mech.Sci, v.27, n.1/2, p.39, 1985.

134. **Kobayashi.S.** A review on the finite element method & metal forming process modelling. J.Appl.Metalworking, v.2, n.3, p.163, 1982.

135. **Oh.S.I.** Finite element analysis of metal forming processes with arbitrarily shaped dies. Int.J.Mech.Sci, v.24, n.8, p.479, 1982.

136. **Rebelo.N.** Finite element modelling of metalworking processes for thermo-visco-plastic analysis. PhD thesis, University of California, Berkeley, 1980.

137. **Kobayashi.S.** The role of the finite element method in metal forming technology. Proc.1st Int.Conf.Tech. Plasticity, Advanced Tech.Plasticity, Tokyo, v.II, p.1035, 1984.

138. **Thomason.P.F.** A theory for ductile fracture by internal necking of cavities. J.I.Metals, v.96, p.360, 1968.

139. **Quasier.M.I.** The cold rolling of aluminium strip. MSc thesis, University of Aston in Birmingham, 1966.

140. **Afonja.A.A.** The sandwich rolling of thin hard strip. PhD thesis, University of Aston in Birmingham, 1969.

141. **Personal Communication.** Land Infrared, Land-Cyclops emissivity manual, TN 101, TN 202, TN 209.

142. **Altan.T, Henning.H.J. & Sabroff.A.M.** The use of model materials in predicting forming loads in metal working. Trans ASME, J.Basic Engng, p.444, May 1970.

143. **Wanheim.T, Maegaard.V. & Danckert.J.** The physical modelling of plastic working processes. Proc. 1st Int.Conf.Tech.Plasticity, Advanced Tech.Plast--icity, Tokyo, v.II, p.984, 1984.

144. **Loizou.N. & Sims.R.B.** The yield stress of pure lead in compression. J.Mech.Phys.Solids, v.1, p.234, 1953.

145. **Tsukamoto.H, Taura.Y. & Ibushi.J.** Simulation of hot steel in plastic working with plasticine and lead. Proc. 1st Int.Conf.Tech.Plasticity, Advanced Tech. Plasticity, Tokyo, v.II, p.984, 1984.

146. **Personal Communication.** Mr M C Gleave & Dr D Dulieu, BSC Rotherham.

147. **United Steel Co, Sheffield.** Roll Pass Design. Pub. P.Lund, Humphries & Co, p.72, 1960.

148. **American National Standard (ASTM).** Standard Methods For Estimating The Grain Size Of Metals. ANSI/ASTM E 112-80.

149. **Pickering.F.B.** The Basis Of Quantitative Metallography. Pub. Institute Of Metallurgical Technicians, 1976.

150. **Hearn.E.J.** Mechanics of Materials. Volume 1, p.343. Pub. Pergamon, 1980.

151. **Holmes.E.L. & Winegard.W.C.** J.I.Metals, v.88, p.468, 1959-60.

152. **Personal Communication.** Dr A P Hirst, BSC Rotherham.

153. **Stahlberg.U, Keife.H, Lundberg.M. & Melander.A.** A study of void closure during deformation. J.Mech.Work.Tech, v.4, n.1, p.51, April 1980.

NOMENCLATURE

a	$2\mu s/k$
a_i	width polynomial coefficients (i=1,2,3,4)
a', b', c', d'	correction factors in the spread formula of Wusatowski (87,88)
A	stiction coefficient in Hill's principle measured length of void principle axis
A1, A2	initial and final cross section area
B	friction coefficient in Hill's principle measured length of void priciple axis
c	specific heat
CV	coefficient of variation
d	linear intercept
$\bar{d}$	mean linear intercept
D	roll diameter
$\bar{D}$	average grain diameter
Dm	maximum grain diameter
D1	pre-roll pass void y-axis length
D2	post-roll pass void y-axis length
dA	area reduction = (1-A2/A1) x 100%
$\dot{E}d$	energy rate due to velocity discontinuity
$\dot{E}f$	friction energy rate
$\dot{E}p$	plastic deformation energy rate
E1	pre-roll pass void z-axis length
E2	post-roll pass void z-axis length
f	horizontal force per unit width
f_i	an externally applied normal stress system

F_i	prescribed traction
h, h1, h2	current, initial and final stock thickness
hc	vertical projection of entry plane slip line
2h	void height
H, H1	current and initial billet semi-width
Hm	mean stock thickness
J	mechanical equivalent of heat
k	yield stress in pure shear
lc	horizontal projection of entry plane slip line
l_j	direction cosines of outward normal to a surface
L	horizontal projection of roll contact length
m	friction shear factor ($0 \leq m \leq 1$)
n	number of traverse counts made
n_i	local unit outward normal
N	roll speed (rev/min)
	number of grain boundary intercepts measured along a traverse of length L (mm)
$\bar{N}$	mean number of grain intercepts counted
N_i	number of grain boundary intercepts measured along traverse i
p	horizontal pressure
	index of (h1/h2) in the spread formula of Wusatowski (87, 88)
Pc	mean hydrostatic pressure at entry point c
Pm	mean rolling load
q	vertical roll pressure
r	reduction (h1-h2)/h1 x 100%

r_c	reduction required for void closure
R	roll radius
RT	total reduction
s	normal roll contact pressure
	azimuthal pressure
S	length of velocity discontinuity line
	yield stress in plane strain
Sc	surface adjoining a tool or container
Sf	an unconstrained surface
Si	surface adjacent to a rigid zone
So	apparent standard deviation
t	time
T	temperature (deg.C)
	roll torque (Nm)
Tt	total roll torque (Nm)
u_i	flow velocity on body surface
u_i^*	any velocity distribution satisfying the boundary conditions and the condition of incompressibility
U	particle velocity in roll gap
Ur	roll peripheral velocity
$\dot{U}p$	power of deformation
v, v1, v2	current, initial and final velocity
v_x , v_y , v_z	particle velocity in x, y and z directions
$\|\Delta v\|$	relative velocity difference
V	volume
Vf	volume fraction of void
Vf_1	initial volume fraction of void

Vo	variance
V°	velocity discontinuity
Vx_r	relative velocity in x-direction
V1, V2	billet initial and final velocities
w, w1, w2	current, initial and final stock width
w(x)	width function
w'	inhomogeneity factor
w_j	a sub-class of virtual orthogonalizing motions
2w	void width
W, W1	current and initial billet semi-width
$\dot{W}$	rate of energy dissipation along a velocity discontinuity line
Y	yield stress in uniaxial tension or compression
Z	Zener-Holloman parameter
$\bar{\Phi}$	functional or upper bound on forming power
α	upper bound solution angle
	friction angle, $\tan^{-1}(\mu)$
β	upper bound solution angle
γ_{max}	maximum shear strain
$\dot{\gamma}$	shear strain rate
δ	draft (h1-h2)
ε_x , ε_y , ε_z	natural strain components in x, y and z directions
ε_{ij}	strain tensor
$\dot{\varepsilon}_x$, $\dot{\varepsilon}_y$, $\dot{\varepsilon}_z$	strain rate components in x, y and z directions
$\dot{\varepsilon}_{ij}$	strain rate tensor
$\dot{\varepsilon}^{*}_{ij}$	any strain rate distribution satisfying the boundary conditions and the condition of

	incompressibility
ε_p	peak strain
ε_c	strain for dynamic recrystallisation
$\dot{\varepsilon}_o$	initial strain rate
$\dot{\varepsilon}_v$	volumetric strain rate
$\dot{\bar{\varepsilon}}$	effective strain rate
ε_I , ε_{II}	strain on void principle axes
η	a large positive constant
θ	angular ordinate
	void axial rotation
λ	Lagrange multiplier
μ	coefficient of friction
ρ	density
ν	Poisson's ratio
π	uniform fluid pressure
σ_x , σ_y , σ_z	normal stress on planes perpendicular to the x, y and z axes
σ_{ij}	stress tensor
σ_{ij}^*	any stress distribution satisfying the yield criterion
σ_r	radial stress
$\bar{\sigma}$	equivalent stress or flow stress
τ	shear stress at interface
ϕ	angular coordinate measured from the exit plane
ϕ_N	angular position of the neutral plane measured from the exit plane
ω	roll angular velocity (rad/sec)